FLOOD ESTIMATION IN DEVELOPING COUNTRIES WITH CASE STUDIES IN ETHIOPIA

Zeinu Ahmed Rabba

University of KwaZulu-Natal

Submitted in fulfilment of the academic requirements for the degree of *Doctor of Philosophy* in Civil Engineering, College of Agriculture, Engineering and Science, University of KwaZulu-Natal, Durban, South Africa

Supervisor: Prof Derek D Stretch

2017, Durban, SA

COLLEGE OF AGRICULTURE, ENGINEERING AND SCIENCE

As the candidate's supervisor, I have agreed to the submission of this thesis.

Prof. Derek D Stretch ..... Date: .....

DECLARATION 1 - PLAGIARISM

I, Zeinu Ahmed Rabba, declare that:

1. The research work reported in this thesis, except where otherwise indicated, is my original research.
2. This thesis has not been submitted for any degree or examination at any other university.
3. This thesis does not contain other persons' data, pictures, graphs or other information, unless specifically acknowledged as being sourced from other persons.
4. This thesis does not contain other persons' writing, unless specifically acknowledged as being sourced from other researchers. Where other written sources have been quoted, then:
    - Their words have been re-written but the general information attributed to them has been referenced.
    - Where their exact words have been used, then their writing has been placed in italics and inside quotation marks, and referenced.
5. This thesis does not contain text, graphics or tables copied and pasted from the Internet, unless specifically acknowledged, and the source being detailed in the thesis and in the References sections.

Signed .....

COLLEGE OF AGRICULTURE, ENGINEERING AND SCIENCE

DECLARATION 2 - PUBLICATIONS

DETAILS OF CONTRIBUTION TO PUBLICATIONS that form part and/or include research presented in this thesis:

Publication 1
Rabba, Z. A., Fatoyinbo , B. S. and Stretch, D.D. (2017). Applications of PyTOPKAPI model in ungauged catchments (Water SA 3464 paper, accepted for publication).

Publication 2
Rabba, Z. A. and Stretch, D.D. (2016). Streamflow Modeling by PyTOPKAPI Model utilizing Remotely Sensed Rainfall Data: A Case Study of Gilgel Ghibe River Basin. In *the College of Agriculture, Engineering and Science annual Post-graduate Research Day 2016*, UKZN, November 29, Durban, South Africa. 69 pp.

Signed: .....

ACKNOWLEDGEMENTS

First and foremost, I would like to express my sincere appreciation and heartfelt thanks to my supervisor Professor Derek D. Stretch for his support, enthusiasm, and expertise. His enthusiastic supervision and scientific guidance have been decisive for timely and successful completion of this PhD study. I honestly believe that without him this study would have never been completed. I am grateful for his support both in technical and personal spheres of my life.

I am also deeply indebted to Dr. Scott Sinclair for his help and guidance. His input to this thesis was invaluable.

I am very much thankful to the following for data and other inputs:

- Ministry of Education of Ethiopia for sponsorship
- Ministry of Water, Irrigation and Electricity of Ethiopia for stream flow data
- Ethiopian National Meteorological Agency (ENMA) for Meteorological data
- Jimma Institute Technology, Jimma university for material support
- All my friends for appreciated suggestions, encouragement and consistent support.

My special thanks go to Mr. Jagema Keneni Hora and Mr. Murad Mohammed for their valuable support and encouragement.

My appreciations also go to the support staffs at Civil Engineering, UKZN: Oliver Sjah, Ooma Chetty and Logan Govender, for their kind help and administrative support.

Most importantly, I would like to forward my thanks to my helpful wife Amina Mohamud and my lovely daughters and son (Fenan Zamin Naniye Ifnan) for their concern, understanding, support and patience; without which this achievement would have never been possible. This success belongs to all of us.

Finally, I would like to thank the Almighty Allah for helping me throughout my life including in the realization of this Work.

Zeinu Ahmed Rabba

ABSTRACT

Extreme flood events have become more destructive in some parts of Ethiopia. Thus, accurate estimates of flood frequencies are vital for effective flood risk management. Yet, estimation of the peak flood is exceptionally complex requiring a wide range of methodologies. One of the approaches is the statistical (traditional) method, which determines the frequency of a flood value from the annual maximum discharge data. However, when such records are too short for flood frequency analysis, empirical formulae can be the option for peak flood estimation. But, most of these formulae are regional formulae based upon the statistical correlation of the recorded peak flood and one or two physical catchment characteristics, and they are unlikely to give reliable results of peak flood for other regions than those for which they were developed. On the other hand, when there are no streamflow observations at the site of interest, hydrological models such as PyTOPKAPI are another option for modelling stream flows for flood frequency analysis. Thus, the main component of this study involves statistical data analysis and hydrological modeling aimed at finding out an appropriate method of flood frequency analysis for Ethiopian rivers. In this study, a broad overview of practical design-flood-estimation methods in Ethiopia along with international practices was carried out. The results revealed very large gaps in knowledge and in current design flood practices. The application of the PyTOPKAPI model in numerous catchments of the world was likewise reviewed including how the model has been used for flood prediction, forecasting of hydrological responses, etc. In this study, it was implemented in Ethiopia on Gilgel Ghibe and Mojo catchments, and promising results were obtained. This model was also combined with remotely sensed precipitation products for simulating stream flows which showed that the general streamflow patterns were well reproduced. Most importantly, the PyTOPKAPI model was applied in ungauged Ethiopian catchments using the Schreiber runoff ratio in an alternative model calibration approach. This shows how the PyTOPKAPI model can be used to predict runoff responses in ungauged catchments for water resources applications and flood predictions in developing countries. In addition, various flood frequency methodologies were evaluated on two Ethiopian rivers (Awash and Gilgel Ghibe). The aim was to find the most approprite method that best represents the statistical characteristics of the streamflow observations. In this case, the annual maximum discharge data from 14 stations of the two rivers (6 in Gilgel Ghibe and 8 in Awash) with 23 to 54 years of records were used. Seven flood frequency methodologies (TSPT, LN, LPIII, EVI, Chow's, Stochastic and Weibull's plotting position formula) were fitted to those data. Comparison of the results were made based upon probability plot correlation coefficient, normalized root mean square deviation and Nash-Sutcliffe fitting coefficient. The results showed that the TSPT technique was the best fit followed by Weibull's Plotting Position formula, Chow's, LPIII, EVI and Stochastic methods, in descending order of performance. Therefore, the TSPT method can be used for flood frequency analysis in Ethiopia. Moreover, flood frequency analysis was carried out based on the PyTOPKAPI modelled daily stream flows from the two case study catchments. The results were then compared with those of the traditional ones. It was found that simulation-based flood frequency analysis showed very good agreement with those from the traditional methods for both the case study catchments. It was thus concluded that PyTOPKAPI model-based flood frequency analysis could also be one of the appropriate methods of flood frequency analysis and peak flood estimation for Ethiopian rivers.

Keywords: *Design flood estimation, flood frequency analysis, PyTOPKAPI model, Return period, Schreiber's runoff ratio, Ethiopia*

Table of Contents

List of Figures

List of Tables

Acronyms

AD	Anderson-Darling test
AM	Annual Maximum
ASCAT	Advanced Scatterometer instrument
asl	above mean sea level
BM^3	Billion cubic meters
CAPA	Catchment Parameter
CDF	Cumulative Distribution Function
CN	Run-off Curve Number
CSA	Central Statistical Agency [of Ethiopia]
CSM	Continuous Simulation Modeling
CV	Coefficient of Variation
DEM	Digital Elevation Model
DMIP2	Distributed Hydrologic Model Inter-comparison Project - Phase 2
EMA	Expected moments algorithm
ENMA	Ethiopian National Meteorological Agency
ERA	Ethiopian Road Authority
ERS	European Remote Sensing
ETa	Actual evapotranspiration
ETo	Potential evapotranspiration
ETr	Evapotranspiration of a definite crop
EVI	Extreme Value Type I distribution
FAO	Food and Agriculture Organization of the United Nations
FDC	Flow duration curve
FEH	Flood Estimation Handbook

GeoSFM	Geospatial Stream Flow Model
GES-DISC	NASA's Goddard Earth Sciences (GES) Data & Information Services Center (DISC)
GEV	Generalized Extreme Value
GIS	Geographic Information Systems
GLCC	Global Land Cover Characterization
GOF	Goodness-of-fit Tests
HMS	Hydrologic Modeling System
HRU	Hydrological Response Unit
HWSD	Harmonized World Soil Database
IDF	Rainfall Intensity Duration Frequency
IIASA	International Institute for Applied Systems Analysis
IPCC	Intergovernmental Panel on Climate Change
JPV	Joint Peak-Volume
K-S	Kolmogorov-Smirnov test
LN	Log Normal distribution
LPIII	Log-Pearson type III distribution
MAF	Mean Annual Maximum Flow
MIPI	Midgley Pitman
MK	Mann-Kendall test
MoM	Method of Moments
NASA	National Aeronautics and Space Administration
NRMSD	Normalized Root-Mean-Square-Deviation
NS	Nash-Sutcliffe coefficient
PDF	Probability Distribution Function
P-III	Pearson type III Distribution
PPCC	Probability-Plot-Correlation-Coefficient
PWM	Probability Weighted Moments
PyTOPKAPI	Python based TOPographic Kinematic APproximation and Integration model
Q-Q	Quantile-Quantile plot
RFFA	Regional Flood Frequency Analysis

RLMASI	Regional L-Moment Algorithm and Scale Invariance
RMSE	Root Mean Square Error
RoR	Run-off Ratio
RS	Satellite Remote Sensing
SANRAL	South African National Roads Agency Limited
SAWS	South African Weather Service
SBPP	Satellite Based Precipitation Products
SCS	Soil Conservation Service
SDF	Standard Design Flood
SFFA	At-Site Flood Frequency Analysis
SK	Seasonal Kendall test
SMA	Soil Moisture Accounting
SNNP	Southern Nations, Nationalities and Peoples region
SRTM	Shuttle Radar Topography Mission
SSI	Soil Saturation Index
SWI	Soil Wetness Index
T-20	Technical Release 20
T-55	Technical Release 55
TMPA	TRMM Multi satellite Precipitation Analysis
TRMM	Tropical Rainfall Measuring Mission
TRMM3B42	The post-real-time version of TRMM precipitation products
TRMM3B42R	The near-real-time version of TRMM precipitation products
TSPT	Two-Step-Power-Transformation techinique
UM	Unified Model
USA	United States of America
USDA	United States Department of Agriculture
USGS	United States Geological Survey

Chapter 1

Introduction

1.1 General

The story of man's progress is closely linked with the exploitation of rivers [259]. In Ethiopia, where the agricultural sector plays the important role in its economic growth, the management of water resources is an item of high priority constituting a critical input for economic planning in their developmental activities [110]. Water resources projects are often quite huge, require huge investiment and once they are built, they are to be operated efficiently and successfully for decades. Of the various characteristics strongly affecting the design of these projects, the most essential and commonly used parameter is the design flood. It is characterized as the momentary greatest flood used for designing a water/civil structures after considering the economic as well as the hydrological variables. Either it is a flood that the project can sustain with no substantial damage to the items that it protects or to its own structures [123]. The damages produced by floods with respect to loss of life and property are all well known. Huge amounts of resources are used each year in flood control.

The knowledge of magnitude of design flood/peak flood is therefore, one of the most crucial information required for management of flood in a basin and for the design of different hydraulic structures. At a specified area in a watercourse, flood peaks fluctuate from year to year, and their extent constitutes a hydrologic time series, which allows one to assign a frequency to a specified flood peak magnitude. In general, for designing every water driven structure, the peak flood that can be expected with an assigned frequency is of the key information to sufficiently proportion the structure to withstand the impact of it. The design of water structures such as bridges, water-ways and spill-ways of dams, and estimate of scour at water structures are a few cases where flood-peak qualities are required. Notwithstanding that, forecasting of floods ahead of time enables a warning to be given to the general population prone to be influenced and further enables civil defense measures to be organized. Thus, in planning, designing and operating water resources system like single or multipurpose river-valley development projects for irrigations, flood control, power generation, etc., an appropriate estimation of flood magnitude and its frequency of occurrence is mandatory. The frequency analysis of annual peak- flood is considered to be the most widely used method regarding the estimation the magnitude and the probability of peak- floods. Flood frequency analysis is the term used to describe the activity devoted to answering the question about how often the magnitude of some flood exceeds a certain amount. The main aim of frequency analysis in flood hydrology is primarily to estimate the frequencies or probabilities of future flood events based on the past recorded hydrological data.

A large number of methods for flood frequency analysis based on a standard probability functions

are popular for estimating peak flood of a particular return period. But, the methodology to be adopted for estimation of peak flood magnitude depends up on the significance of the projects, economic and safety considerations, availability of data and computational methods etc. In Ethiopia, although a number of methodologies exist to address this issue, none has been accepted universally or uniformly standardized. In addition to this, there are a number of published articles offering different approaches on the methods of estimation of peak flood and its return period. For example, the methods that are based on a standard probability functions, such as gamma, log-normal, extreme values, log-pearson type III, etc, are well known for estimating design flood of a particular return period from historic data. The assumption is that the annual maximum discharge data series at a certain location follows one of the standard probability distribution functions (PDF). This could be worked out by plotting the cumulative-distribution-function of the observed flood peaks over a period of years on various probability papers. However, the accuracy depends first on the availability of a large number of observations and secondly, on the chance of finding standard probability distribution functions close to the sample cumulative distribution functions. The applications of these methods in any particular case show widely varying results. Hence, it has been recognized by the researchers in this field that none of common probability distributions can describe the true inherent variability of flood peak occurrences. The methods are therefore, rarely applied to individual design problems.

Furthermore, whenever hydrological records are inadequate for flood frequency analysis, the empirical formulae are the alternative methods to provide an estimate of peak flood. Many empirical formulae have been developed so far for different regions and they are commonly the regional formulations based upon statistical relationship of the recorded flood peaks and the essential catchments as well as climatological characteristics. Most of these formulae involve only one or two physical characteristics for estimation of the peak floods and they would not give reliable results of peak floods for other regions than those for which they were developed. In Ethiopia, few internationally evolved empirical formulae have been in use for peak flood estimation.

Presently, estimation of design flood in Ethiopia is generally based on empirical formulae (eg Rational formula, SCS method, etc), the most commonly known PDFs (like Gumbel, Log Pearson III, and GEV), Run-off routing and Regional flood frequency approach (the so-called" Regression Equation"). Almost all of these design flood estimation methods are internationally developed [79]. While direct statistical analysis and regional techniques are encouraged by Alexander [9], little effort has been devoted to the use of regional information in most basins in Ethiopia. Estimation of flood values using the regional information in areas where very few or no recorded flow data are obtainable are becoming progressively very essential in Ethiopia because several projects which need such information are found in locations where the recorded flood data are not obtainable. However, according to ERA Manual [79], there are no universally accepted methods of regionalization because of complexity in understanding the factors that affect flood generation in Ethiopia. Furthermore, in Ethiopia, empirical methods of design flood estimation seem to dominate. However, these methods are often unsuitable for application in other regions or to catchments with differing characteristics. On the other hand, most catchments in Ethiopia are ungauged and direct stream flow observations are not available at most sites for which rainfall–runoff relationships are required [281].

The purpose of this study is therefore, to find out an appropriate method of flood frequency analysis for Ethiopian rivers with use of the hydro-meteorological data of the two Ethiopian rivers (Awash and Gigel Ghibe). In addition, the frequency distributions such as Normal, EV1, LPIII, etc which are commonly applied to the annual maximum dischage data series would be fitted to the data of

the two major Ethiopian rivers. The results of the analysis would be used to select an appropriate method for estimation of flood peak of a certain return period for Ethiopian rivers. It would be expected that the best fit method would fit the data more closely and would be able to predict the higher return period peak flood values in the series more accurately. The outcome of the research can be a guideline for design flood estimation & flood risk management in Ethiopia.

1.2 Problem Statement

Accurate estimates of the maginitudes and the frequencies of peak floods are basic for designing and operating of water resources projects, for flood risk management, and for designing transportation infrastructures such as bridges and highways [254]. But, one of the main problems in flood hydrology is interpreting past extreme flood events in terms of the future probabilities of occurrences. Water resources engineers often encounter difficulties in approximating the magnitudes of these extreme flood events and their frequencies of occurrences. In order to minimize such type of problem and plan water resources systems for future events, accurate estimation of the magnitude of peak flood and its probability of occurrence are mandatory. However, the methods available so far for flood frequency analysis in Ethiopia are in general vague. Those methods, which are based on standard probability functions, rarely are applied to individual design problems as the applications of these methods in any particular case can produce widely varying results.

Furthermore, as most of the international empirical formulae developed so far for peak flood estimation involve only one or two physical characteristics, they would not give reliable results of flood peaks for other regions than those for which they were developed. In Ethiopia, although a number of methodologies exist to deal with the issue of flood frequency analysis and peak flood estimation, none has been accepted universally or uniformly standardized. On the other hand, many rivers in Ethiopia are commonly poorly gauged or totally ungauged which hinders water resources management and flood predictions in the country for which stream flow modeling is essential. Therefore, the main research questions relating to these problems are the following:

- How far do the existing methods of flood frequency assessment go to address the issue of flood frequencies in Ethiopia?
- Can the existing methods accurately predict the flood magnitude of a given return period?
- What are the lessons learnt from the experience of the developed world and other developing countries for flood frequency analysis and design flood estimation?
- How to include prior knowledge on flood frequency analysis for Ethiopian rivers?
- Is it suitable to implement an appropriate hydrological model in Ethiopia for stream flow modeling in gauged and ungauged catchments?
- Is it possible to select best-fit flood frequency methodology for Ethiopia from among the common ones?

Therefore, the study intends to find out an appropriate method of flood frequency analysis for Ethiopian Rivers.

1.3 Objectives of the study

The overall objective of this study is to find an appropriate method of flood frequency analysis for Ethiopian rivers. The specific objectives include:

1. To assess the design flood estimation methods in Ethiopia.
2. To evaluate the hydro-meteorological data trends of the study area.
3. To implement PyTOPKAPI model to gauged and ungauged catchments for stream flow modeling in Ethiopia.
4. To evaluate the various methods of flood frequency analysis for Ethiopian rivers.
5. To analyze the flood frequencies based on the PyTOPKAPI model simulated stream flows.

1.4 Methodological Approach of the Research

The general approach and methods used in this PhD study are the combination of data collection, intensive statistical data analysis and hydrological modeling. In this research, a physically based fully distributed hydrologic model that can offer finer-resolution data regarding the hydrological condition of a basin, PyTOPKAPI (Python based TOPographic Kinematic Approximation and Integration) model would be implemented in Ethiopia for stream flow modeling. Furthermore, the study involves exhaustive additional fieldwork data collection and critical assessment having the following main procedures:

1. Relevant literature review would be carried out. The available studies and researches that are related to flood frequency examination, methods of design-flood-estimation, and implementation of the (Py)TOPKAPI hydrological model would be reviewed.
2. Collection of important data for this study such as hydrometeorological data, topographical and digitized map, etc of the study catchments would be conducted.
3. Trend analysis of the hydrometeorological data of the study catchment would be carried out.
4. The PyTOPKAPI model would be implemented in Ethiopia for streamflow modelling and peak flood estimation.
5. The commonly used methods of flood frequency analysis would be evaluated using the data of two Ethiopian rivers.
6. An appropriate method of flood frequency analysis would be selected for Ethiopian rivers.

Analysis and Interpretation of the Results:
The two parameters of flood frequency analysis are the flood peak and its return period. The relationship between these two parameters would be analyzed so that the method of design flood estimation would be more generally and uniformly standardized.

Tools (models) and software used in this research work are:
Python computer programming, GIS , Microsoft Excel, Probability distribution Model (PDM), PyTOPKAPI model , and other relevant tools.

1.5 Justification of the study

Extreme hydrological events —floods & droughts— have become more harmful in many zones of the globe [126]. The same is true for Ethiopia. Flooding is becoming a major disaster in Ethiopia. Usually, floods are very common in the nation during the main wet season which is from June to September when rains climax. In the previous years, different parts of the country have been affected by problems related to flooding. Many people died or were dislocated from their homes, government and private properties have been damaged causing huge impact on the country's economy [185]. The country faces two forms of floods: flash floods and river floods. Flash floods are that sort of floods formed from surplus rains dropping on upstream areas of the watersheds and spout downstream with gigantic concentration, speed and force. Regularly, such floods are unexpected and seem unnoticed. In this way, these floods usually lead to a significant toll and the damage becomes distressing when they go crosswise over or along human settlements and infrastructural concentrations. The occurrence that the DireDawa City faced was an example of flash flood. On the other hand, a great part of the flood catastrophes in Ethiopia are as a result of flood occurrences from waterways or bursting their banks and submerging downstream flood plains. The flood that occurred in Southern Omo Zone in 2006 is a typical example of river floods.

Furthermore, the topographic characteristics of Ethiopia consists of both a highland and a lowland, because of which some parts of the country face foremost flooding. The major ones comprise: parts of Oromia and Afar regions that constitute the mid and downstream plains of the Awash River, areas in Somali regions that fall mostly along downstream of the Wabishebelle, Genalle and Dawa Rivers, the lowland areas of Baro, Gilo and Akobo Rivers in Gambella region, the downstream parts of Omo-Ghibe River in the Southern Nations, Nationalities and Peoples(SNNP) region, the flood plain neighboring the Lake Tana, and Gumara & Rib Rivers in Amhara region. In west Shewa Zone of Oromia region, for example, flooding of the upper basin of Awash River affected 14 peasant associations (PAs) in Illu, Sebeta Awas and Ejere localities of the zone. It was reported to have affected 14,790 people out of which 2052 people were evacuated and forced to live in provisional shelters. On the other hand, heavy rainfall in the central highlands is treated as a main hazard nearby the main dams in the county (Koka, Ghibe and Melka Wakena) [214].

Recent studies revealed that the most severe flood hazard in the history of Ethiopia happened in the month August 2006 as a result of heavy rainfall in the country. During that time, most areas of the nation had faced flood events of a certain proportion. For instance, the Omo- Ghibe River in the south ran out of its banks and inundated the local communities. Several cases of flood incidences and flood hazards were also reported from north-western areas of the country [21]. The author also confirmed that bank - overflows in the lower Omo-Ghibe basin affected 364 people, inundated 14 villages, and destroyed 10s of thousands of hectares of farmlands. A study conducted in Ribb–Gumara catchment, one of the highly flood-prone parts in Ethiopia, also showed that rainfall in the area has slightly reduced while flood water levels have increased, and this can be as a result of landcover change particularly in the upper watershed of Ribb–Gumara [96].

The other rivers where substantial floods occur are Wabi-Shebelle River in south-eastern Ethiopia near the Somali-border and Baro Akobo River in western Ethiopia near the border of Sudan. In the Baro Akobo Plain (well-known as Gambella Plain), an area of around 300,000-350,000 hectares is prone to flooding during the rainy season and in the Wabi Shebelle Basin , more than 100,000 hectares has been inundated [141].

To sum up, large scale flooding is observed in the lowland areas of Ethiopia where major rivers

cross to neighboring countries. In addition, heavy rainfall in the highlands could also cause inundation of settlements nearby any stretch of the river course. So, the need of determination of an appropriate method of flood frequency analysis has arisen from the damage caused by the devastating flood events that occurred over almost the entire areas of Ethiopia, especially during the period from June to September, 2006. This was reported as the most severe humanitarian disaster experienced in Ethiopia. Neither the severity nor the widespread nature of these floods was expected. Thus, flood frequency analysis and accurate estimation of peak flood are the issues of great significance due to its economic and ecological impact in Ethiopia.

It is observed that one of the major Ethiopian river basins that has serious flood problems is the Awash River basin. Irrigated-agriculture in the river basin is highly advanced. That is to mean, extensive irrigated-agriculture in the nation is concentrated along the Awash River basin and is found in the flood-plains on either side of the river. Huge property destruction happens during flooding along the river basin. Flood mitigation practices and river training structures in this river basin are very limited. It was assessed that in the Awash basin, nearly all of the area demarcated for irrigated-agriculture is subject to flooding. An area of about 200,000-250,000 hectares of land of the Awash River is subject to flooding during rainy season [141, 174]. Likewise, Omo-Ghibe river basin is the basin where most of the current hydropower development has been taking place. It is the second biggest basin in terms of hydropower development potential in the country [20]. Thus, this study mainly focuses on these two river basins (Awash and Gigel Gihbe) as these basins support a high population whose livelihood is dependent on agriculture which is the foremost source of the fast economic growth accounting for about 43% of Ethiopian economy [110]. The rapid population growth in these basins has led to adverse human activities which greatly affect the hydrology of the catchment.

While a huge literature exists, no study has been conducted regarding the determination of an appropriate method on flood frequency assessment in Ethiopia for design-flood-estimation & flood risk management. In general, even though, an accurate design-flood-estimation is essential for planning, designing and operating water structures such as bridges, culverts, dam-spillways, drainage-canals, etc. and also for protecting the life of people and property [192, 206, 213] as the result of the occurrences floods, there is no consistently applied and universally acceptable method flood frequency analysis in Ethiopia. Therefore, this study is important as it further enhances the understanding of flood frequency analysis for Ethiopian rivers. Morover, it would help:

1. Produce a better awareness of design flood estimation methods in Ethiopia.
2. Provide a clear understanding of PyTOPKAPI model application for flood frequency anlysis.
3. Give a scientific evaluation of the various flood frequency methodologies in Ethiopia.
4. Provide an appropriate method of flood frequency analysis for Ethiopian rivers.
5. Contribute better understanding of flood risk management in Ethiopia.

1.6 Data Availability

In order to obtain realisic results regarding the flood frequency analysis, complete and reliable hydrometeorological data are essential. Most hydrometeorological data may be obtained from either synthetic data (data obtained from experiments/model simulations) or historic data (those data that can be collected from the natural phenomena). The hydrometeorological data in Ethiopia are

historic data that are observed and collected from natural meteorological and hydrological phenomena.

In Ethiopia, presently hydrological data are collected and managed regularly encompassing some areas of the Ethiopian river basins. The hydrological network comprises of about 560 stream flow monitoring stations in 12 river basins (Figure 1.1), of which roughly 454 are currently functional. The Hydrology Department in the Ethiopian water affairs Ministry is accountable for stream flow data gathering, and distribution to the users [29]. Both the meteorological and hydrological data that can be utilized for this study are available for the two river basins (Awash and Ghibe rivers), and could be obtained from the National Meterological Agency and Water affairs ministry of Ethiopia, respectively. Other additional data such as digital terrain model, soil-type grid and land-use data, etc. would be acquired from relevant websites.

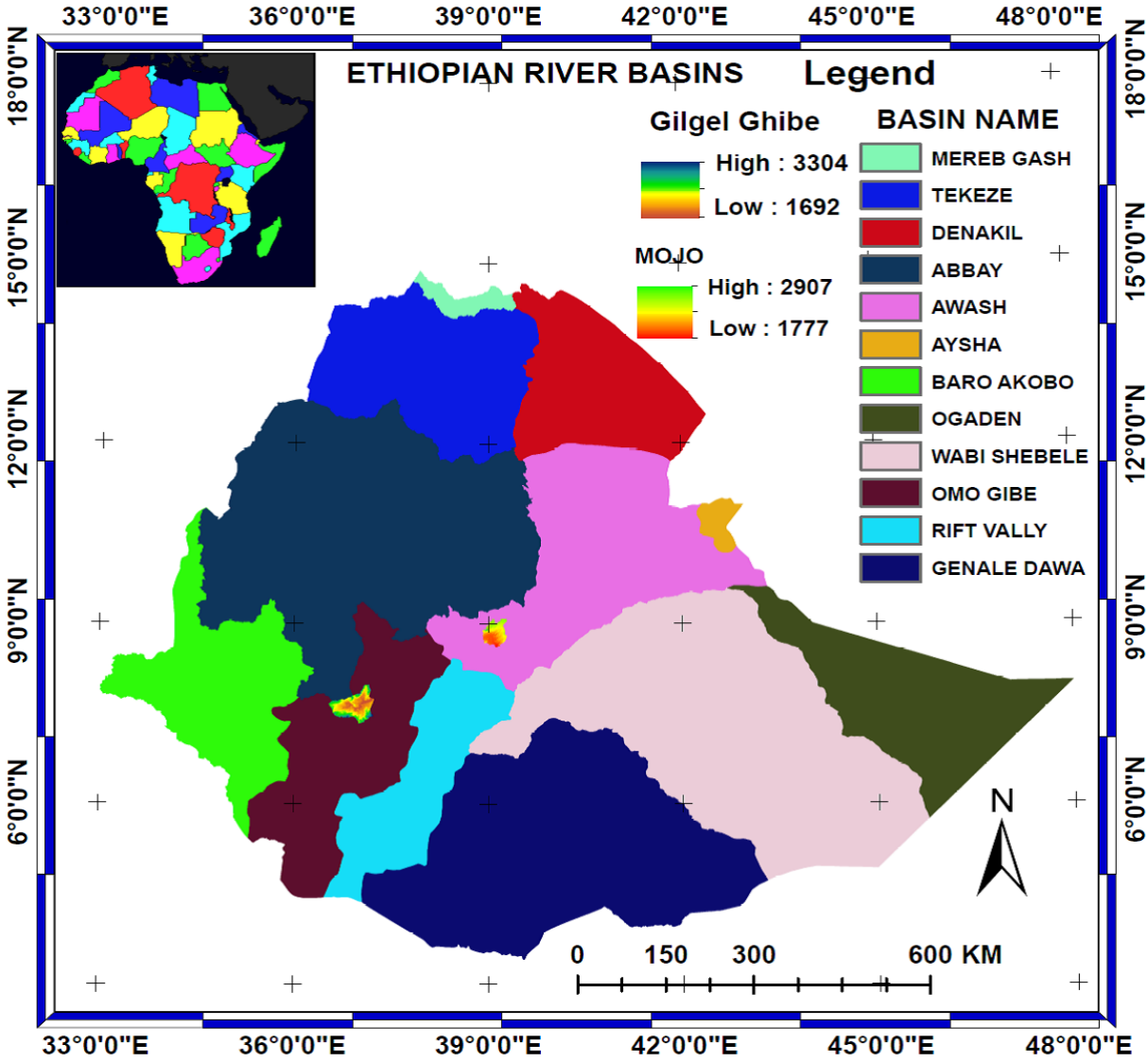

Figure 1.1: Ethiopian River Basins

1.7 Structure of the Thesis

This PhD thesis contains eight chapters including this one and is organized as follows.

Chapter 1: Introduction: This chapter discusses the general framework of the research-work, the problem statement, objectives, methodological approach, justification of the study and data availability.

Chapter 2: Literature review: This chapter summarizes the reviews of the literatures regarding state-of-the-art methods of design-flood-estimation in Ethiopia and presents a general overview on the application of the (Py)TOPKAPI hydrologic modeling.

Chapter 3: Study area and data: It describes the study area, which comprises the physical topographical characteristics and climatic situations of the area. The numerous data used for this study, and their sources are also concisely described.

Chapter 4: Trend analysis of hydrometeorological data: The chapter aims to indicate if there have been some substantial trends in hydro-meteorological data over the study-area as these would have some impact on PyTOPKAPI model simulated stream flows. Because, modelling requires rainfall and temperature data as the key inputs and then calibrated using observed stream flows. The results of the analysis can be used to show the trend changes in the basin in the future.

Chapter 5: Implementation of PyTOPKAPI Model in Ethiopia: This chapter discusses the implementation of PyTOPKAPI model in gauged catchments in Ethiopia for stream flow modeling. It also describes the preparation of the model input files, the setting up of the model, its calibration & validation.

Chapter 6: Implementation of PyTOPKAPI Model in ungauged catchments in Ethiopia: This chapter presents the implementation of PyTOPKAPI model in ungauged catchments in Ethiopia for stream flow modeling. It describes (1) how the PyTOPKAPI model can be used to predict runoff responses in ungauged catchments, and (2) the contribution of the satellite based precipitation products in streamflow modeling, for water resources applications and flood predictions in developing countries.

Chapter 7: Evaluation of the various methods of flood frequency analysis for Ethiopian Rivers: This chapter presents (1) evaluation of the various methods of flood frequency analysis using the data of two Ethiopian rivers (Awash and Gilgel Ghibe), (2) flood frequency analysis based on the PyTOPKAPI model simulated stream flows, and (3) the best fit method of flood frequency analysis in Ethiopia.

Chapter 8: Conclusion and Recommendations: This chapter summarizes the main outputs of the study regarding (1) the design flood estimation methods in Ethiopia and (2) the practical implementation of the PyTOPKAPI model in gauged and ungauged Ethiopian catchments for peak flood estimation, and (3) the summarized evaluation results of the various methods of flood frequency analysis for Ethiopian Rivers. It also outlines the contributions of this study and suggests recommendations for future research.

Chapter 2

Literature Review

2.1 General Summary

Estimate of design floods in Ethiopia is mostly based on empirical methods (e.g. Rational formula, SCS method, etc), the most commonly known PDFs (like EVI, Log Pearson III, GEV,etc.), Run-off routing and Regional flood frequency approach (the so-called" Regression Equation"). Almost all of these design flood estimation methods are the internationally developed. Other than these, there is no standardized Ethiopian guideline for design flood estimation procedures. The current procedures in Ethiopia for design flood estimation are majorly rainfall and rainfall frequency as the main input in place of flood frequency. Rainfall intensities are used to produce flood peaks by means of a simple classical rational method. In spite of the fact that the rational formula is proposed for small watersheds, its usage in bigger watersheds without any revision is also common practice in Ethiopia. Thus, accurate and reliable estimate of design floods remains one of the main challenges in project design where such information is required. Therefore, to refine the "international design flood estimation techniques that are in use in Ethiopia" and /or "update the existing flood estimation methods with additional hydro- meteorological data currently available in Ethiopia", it is crucial to review all the current methods of design flood estimation in Ethiopia together with the international best practice of design flood estimation methods. Thus, this review addresses the broad overview of the current-practical design flood estimation methods in Ethiopia.

On the other hand, many catchments in developing countries like Ethiopia are poorly gauged or totally ungauged. These situations restrict these areas to manage their water resources and hampers early flood warning arrangements leading to huge socioeconomic damages. In such cases, hydrological modeling is an appropriate and even the only option to obtain such information for data limited areas using hydrologic models. Such models are mostly fully distributed physically based type and are used for forecasting and understanding of hydrological processes. For example, given the precipitation data, they estimate flow at the outlet of a river basin with the help the recent advances like the geographic information systems (GIS) and remote sensing (RS), etc. so that forecasting extreme flood events can be done more easily and accurately. Based on a critical review of the ARNO and the TOPMODEL rainfall-runoff models, the distributed physically based TOPKAPI (TOPographic Kinematic APproximation and Integration) hydrological model had been developed recently for investigation of the hydrological processes [160]. The model combines the kinematic wave models with the topography of the basin and transmits the processes of rainfall-runoff into three structurally-similar -zero-dimension-non-linear reservoir equations to be solved in time. The model parameters are scale independent obtained from DEM, soil type and land use maps. Being physically based, TOPKAPI model is also appropriate for modeling ungauged catchments, with the use of literature, and existing thematic maps to create the values

of its parameters . It had already been successfully implemented as a research and operational hydrological model in several catchments of the world (Italy, Spain, France, Ukraine, China, South Africa, etc) [283]. This critical review therefore, presents a summarized practical implementation of the (Py)TOPKAPI model in numerous catchments of the world. It also highlights the capability of the model for use in stream flow simulation in gauged catchments and assesses its applicability to model ungauged Ethiopian catchments. This is the first attempt to implement the model in Ethiopia.

2.2 Review of Design-flood-estimation methods in Ethiopia

The hydrological data available in Ethiopia is very limited. So, the procedures that can be applied for design flood estimation are consequently imprecise. Hence, this review is intended: (a) to present an overview of the current design flood estimation methods in Ethiopia, including international best practices; (b) to identify the gaps and deficiencies in the techniques presently used to quantify design floods in Ethiopia; (c) to determine further research needs with respect to the estimate of design floods in Ethiopia. Therefore, the succeeding part describes a broad review of design-flood estimation methods in Ethiopia. The review includes both the situations where sufficient gauged stream flow data are available and the conditions where no or insufficient data are available. Until recently, no specific standards or definitive criteria for hydrological analysis are suitably recommended for design-flood estimation in Ethiopia. However, ERA Manual [79] presents the flowchart (Figure 2.1) for the general principles for hydrological analysis and selecting the appropriate methods of design-flood estimation.

The flow chart shows that the current design flood estimation methods in Ethiopia are empirical formulae (e.g. Rational formula, SCS method, etc), the most commonly known PDFs (like Gumbel, Log Pearson III, etc), Run-off routing and the out-dated Regional flood frequency approach (" Regression Equation"). The design flood estimation methods in Australia include empirical formulae, "At-site" or "Regional" frequency analysis and rainfall-based methods [246]; in South Africa are based on empirical techniques, deterministic and probabilistic methods [193, 277].

A study carried out by Campbell et al. (1986) showed that there is a lack of understanding of the numerous methods and the problem of getting sufficient recorded stream flow data [246] to consistently estimate the design flood .

Recent studies in general show that the approaches for design flood estimation are broadly categorized into two: (1) Statistical approach (analysis of stream flow data) and (2) Deterministic approach (rainfall based method) [16, 246]. Smithers and Schulze presents a systematized decision flowchart for the choice of the methods of design-flood estimation in South Africa [246]. This approach (Figure 2.2) was summarized by Smithers and Shulze (2001, 2003) and was adapted for international use [16].

Thus, the approach (Figure 2.2) was followed to review the design flood estimation methods in Ethiopia since it is generally acknowledged and acceptable by many researchers. Moreover, the approach encompasses all the current design flood estimation methods in Ethiopia.

2.2.1 Analysis of Stream Flow Data

Where long records of stream flow data are obtainable at the site of concern, in excess of the required return period, flood estimation based on an approach of stream flow analysis can be rela-

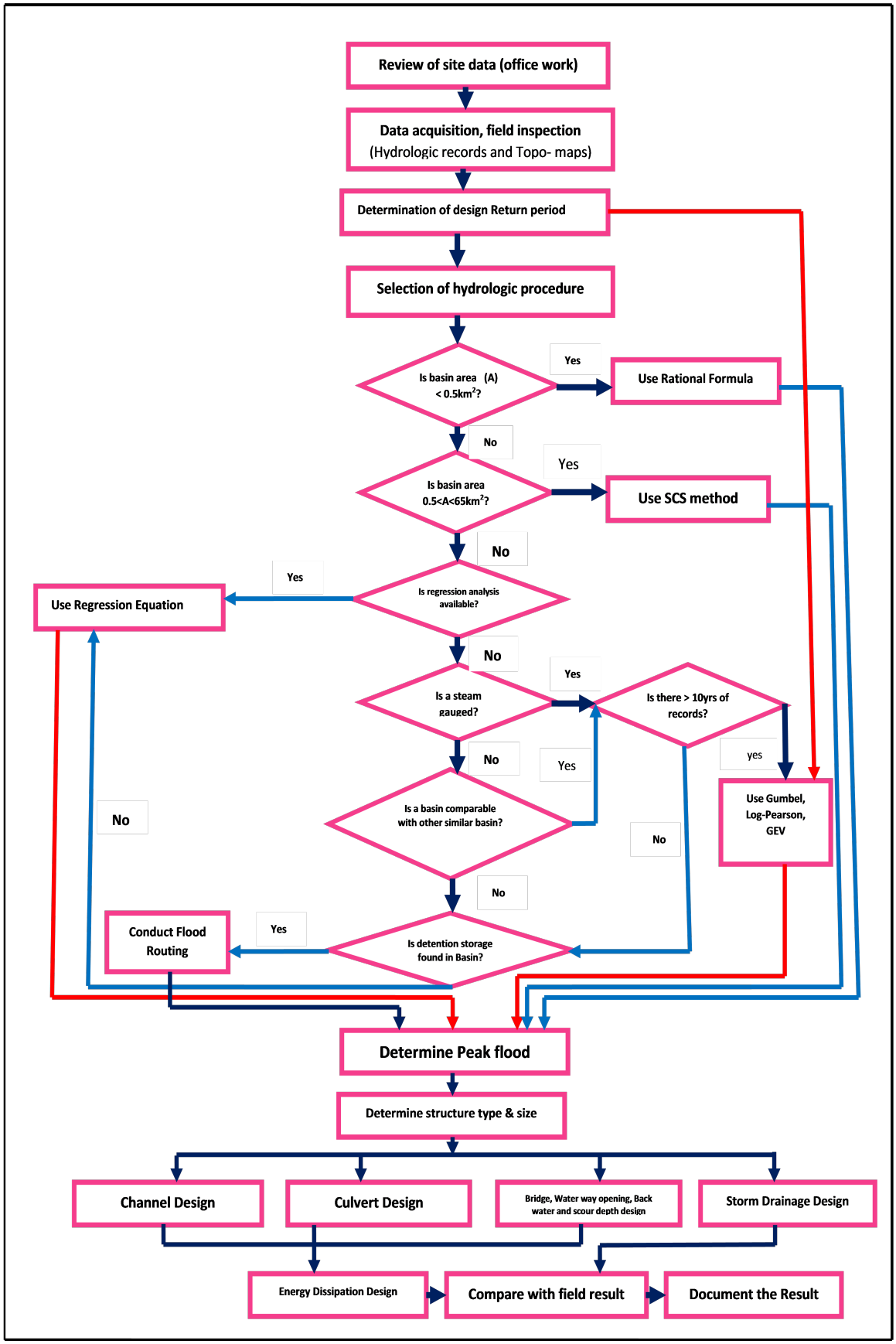

Figure 2.1: Flowchart of Hydrologic Analysis for Design flood Estimation in Ethiopia [79]

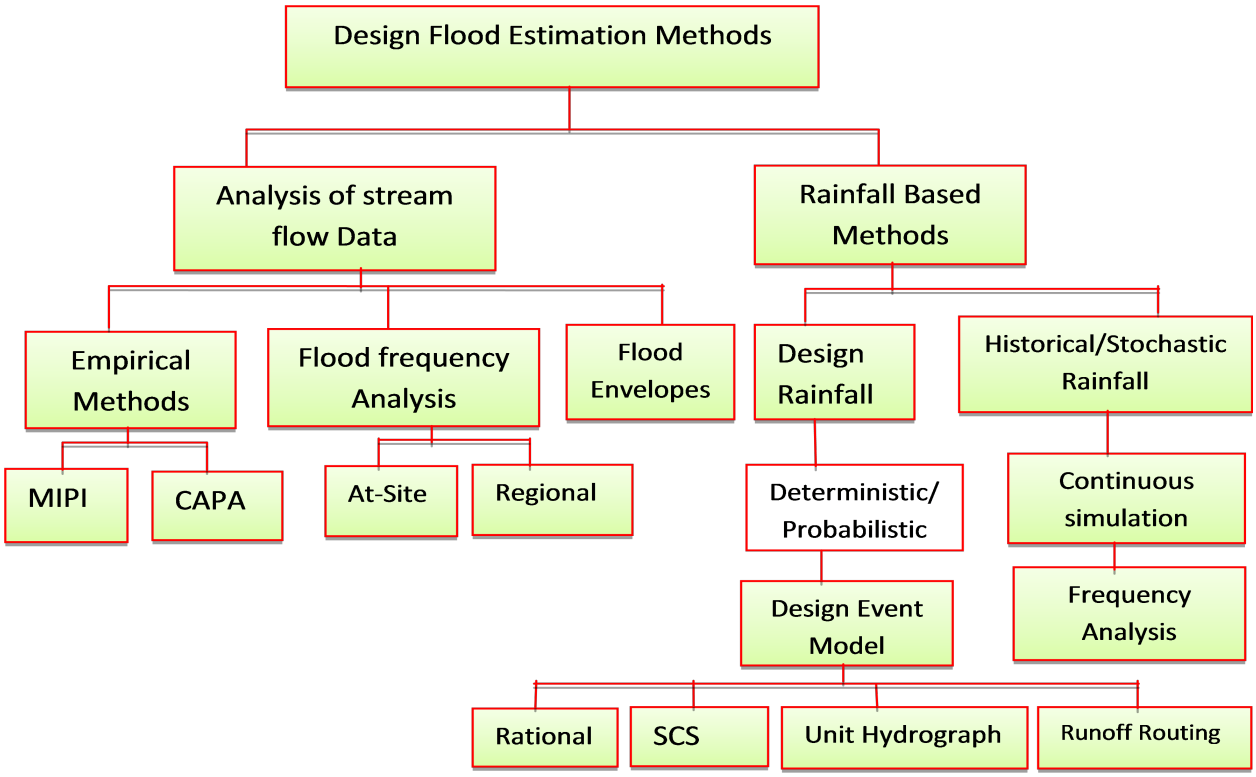

Figure 2.2: A modified form of decision tree of the design flood estimating methods [246]

tively straightforward [295]. Whereas, in areas where stream flow data are limited or not available at all (like the case of Ethiopia), rainfall based approaches can be used [246, 297]; but rainfall records should normally be longer, more plentiful and less variable over time. In Ethiopia, as the hydrological data is very limited, estimating peak floods for various return periods are very challenging. The current procedures in Ethiopia for design flood estimation are rainfall-frequency as the main input instead of flood-frequency. It is also generally expected that the 10-year extreme precipitation would give the 10-year flood. However, being dependent on prevailing soil moisture situations, and other hydrological variables, there is no such direct connection between rainfall-frequency and flood-frequency. A research conducted in UK in this regard revealed that, 140 years rainfall is expected to generate a 100 year flood [79].

2.2.1.1 Empirical formulae

Many empirical formulations have been established for the purpose of approximating peak discharges in different countries of the world. They can safely be applied in areas for which they were specifically derived, but some of them have found a wide application. These formulae must be used with great caution as no specific formula will offer accurate results for all the places. This is because the magnitude of flood of a given return period depends upon many factors, and no formula accounts for all those factors. Hence, a formula involving only two or three variables cannot be expected to give generalized precise results. Recent studies also revealed that empirical formulations are the systems that commonly correlate maximum discharge to catchment area and other physiographical and climatic features, and the usage of these formulae might be exceptionally unsafe, especially if they are not adjusted from the basin in question [246].

No standardized empirical formulae had been developed for Ethiopian catchments so far and few of the commonly used internationally evolved empirical flood formulae for design flood estimation

are listed below [204]. The application of those formulae in Ethiopia is actually very rare.

NB: - In all the formulae, Q_p is the flood peak in m^3/s and A is the drainage basin (km^2).

1. Dicken's formula: It is applicable on moderate size catchments in north and central India

$$Q_p = CA^{\frac{3}{4}} \tag{2.1}$$

where the Coefficient C varies from 11 to 35 depending upon the nature of the catchment and intensity of rainfall.

2. Ryve's formula: This formula is generally applicable to south Indian catchments.

$$Q_p = CA^{\frac{2}{3}} \tag{2.2}$$

where C varies from 6.8 to 10.0 (sometimes up to 40) depending on the location of the basin.

3. Inglis formula: Applicable in the locality of Maharashtra catchements, Bombay state, India

$$Q_p = \frac{124A}{\sqrt{A + 10.4}} \tag{2.3}$$

4. Myer's formula

$$Q_p = 175\sqrt{A} \tag{2.4}$$

5. Ali Nawab Jang Bahadur formula: This is for old Hyderabad state.

$$Q_p = CA^{0.93-\frac{1}{14}logA} \tag{2.5}$$

Where C varies from 48 to 60 with a maximum of 85 and A is area in square miles.

6. Fuller's formula (1914)

$$Q_p = CA^{0.8}(1 + 0.8logT)(1 + 2.67A^{-0.3}) \tag{2.6}$$

Where C varies from 0.026 to 2.77, T = return period in years.

7. Greager's formula for USA

$$Q_p = C(0.386A)^{0.894(0.386A)^{-0048}} \tag{2.7}$$

Where C $\approx$ 130 or 140.5 for localities with high floods.

8. Burkli Ziegler's formula for USA

$$Q_p = 412A^{\frac{3}{4}} \tag{2.8}$$

9. Pettis formula for USA

$$Q_p = C(P.B)^{\frac{5}{4}} \tag{2.9}$$

Where the coefficient C =1.5 for humid and 0.2 for desert areas= probable 100 year maximum 1 day rainfall in cm. B= average width of the basin in Kilometres.

2.2.1.2 Catchment Parameter (CAPA) and Midgley Pitman (MIPI) empirical design flood estimation methods

2.2.1.2.1 MIPI method The MIPI method, elaborated by Pitman and Midgley (1967) estimates flow peaks with four factors/variables: catchment area, return-period, locality, and peak flood [16]. It could best be expressed as an empirical-probabilistic design flood estimation procedure that takes the form illustrated by the equation :

$$Q_P = C.K_P.A^m \tag{2.10}$$

Where: Q_P - Design flood peak (m^3/s); C - Catchment coefficient; K_P - Constant derived from an assumed probability distribution ; A - Catchment area (km^2) ; m - Constant (≈ 0.5); $P - Probabilityofexceedance.$

The method is based on an earlier method called the Roberts Method (US, 2006) who assumed a value of 0.5 for m and derived K_P from the Hazen frequency distribution [243].

2.2.1.2.2 CAPA method This method was established by McPherson (1983) and stems from an analysis done on methods for estimating the average yearly and 1:2 year floods for South Africa. McPherson (1983) stated that a quick estimation of design flood peaks in an un-gauged catchment requires the following steps:

- Estimation of the mean annual flood (Q_S) or the 1:2 year flood (Q_2).
- The development of a regional flood frequency growth curves by means of statistical analyses of annual maximum flood peak records.
- The restriction of the upper limits of frequency curves by a "kind of" maximum flood peak.

According to Smal [243], McPherson (1983) attempted to solve the first three steps by collecting and analyzing hydrometeorological and physiographic data from more than 140 catchments in South Africa. The statistical analysis of the peak floods showed that it was better to use the average yearly flood, Q_S, in place of the 1:2 year flood, Q_2. It was found by McPherson (1983) that a graphical plot of the characteristics could be simplified by plotting the mean annual flood (Q_S) on the ordinate axis and the catchment area (A) on the abscissa. The other three characteristics were combined to form a single, lumped characteristic M. M is then defined as:

$$M = MAP\frac{SA\sqrt{A}}{L} \tag{2.11}$$

Where: MAP - mean annual precipitation (mm); SA - Mean Catchment Slope (m/m); A - Size of the catchment (km^2); L - Longest watercourse length (km). It is an index-flood type method dependent on five variables; basin area, slope, MAP, and shape-factor of a catchment [16]. The use of the CAPA method firstly requires the estimation of the drainage area (A), MAP, mean slope of a catchment (SA) and longest watercourse (L). The lumped parameter and catchment area are then used to estimate the mean annual flood, (Q_2). The mean yearly flood, (Q_S) is then multiplied by the constant, (K_P), to obtain (Q_P) [243].

Smal [243] then conducted a study on the evaluation and updating of the MIPI and the CAPA empirical design flood estimation methods by comparing design floods estimated by each method with more reliable probabilistic design floods derived from historical flow records of 53 gauging stations. The author [243] used the Log-Normal (LN) and Log-Pearson Type III (LP III) methods

to derive the probabilistic floods for each gauging station. The flow gauging stations were used to delineate catchments and to quantify catchment characteristics using GIS software. The formulae were derived by means of graphical plotting and fitting a trend line through the points and deriving a formula best describing the trend line. The derived formulae and the catchment characteristics were used to estimate the design floods for each method. A comparison was then done between the design flood results of the two methods and the probabilistic design floods. The results of these comparisons were used to derive correction factors which could potentially increase the reliability of the two methods used to quantify design floods.

It was proven that the correction factors decreased the difference between the "assumed and more reliable probabilistic design floods" and the methods' estimates. However, the increase in reliability of the methods through the use of the recommended correction factors is questionable due to factors such as the reliability of the flow data as well as the methods which had to be used to derive the correction factors. Moreover, the author strongly recommended that the findings of this research could be used as guide for subsequent research in this field of flood hydrology. However, these methods (MIPI and CAPA) are not utilized in Ethiopia for design flood estimation.

2.2.1.3 Flood frequency analysis

This approach is used to establish an association between flood value and the frequency of occurrence for the purpose of approximating the peak flood at a specified site of concern. The method may be applicable at a point ("At-Site" Flood Frequency Analysis, SFFA) or regionally ("Regional" Flood Frequency Analysis, RFFA) for forecasting the flooding situations at locations where no historical data are obtainable [49, 246]. Here, according to Salas and Obeysekera [219] and also Smithers [246], the existing practice of using probabilistic approaches for designing water related structures, extreme events are commonly assumed stationary. But, such records exhibit some type of non- stationary like trends and shifts. Human activities in basins, the effect of climate change because of an amplified green house gases in the atmosphere have been considered to be the principal causes of changes in the hydrologic cycle of the basins besides changes in the value and frequency of extreme floods. Nonetheless, several researches revealed that a RFFA leads to more reliable design flood estimates and; therefore, in virtually all real-world applications, a RFFA will be more effective than the SFFA [246]. Both SFFA and RFFA sub-approaches of flood frequency analysis, even though the methods are not mature enough in application in Ethiopia, are studied accordingly in the next sections.

2.2.1.3.1 At-site analysis The development of all design flood estimation procedures begins with the direct statistical analysis of recorded data at the gauged sites [9, 69]. All direct statistical analysis methods are data fitting procedures. The purpose of the statistical analysis is to figure out the flood magnitude – frequency (Q-T) relationship at the site [9] by selecting theoretically the best fit probability distributions [58, 261]. Here, the problem of choosing a suitable distribution has received great attention with differing suggestions articulated by different researchers if a specified probability function can be chosen, given that the best probability function varies with rainfall type, rainfall duration and regional differences or not. Due to this reason, Beven [32] identified the succeeding restrictions of a direct statistical approach. These are also acknowledged by Smithers [246].

- The precise probability function of the peak flood is basically not known as dissimilar probability functions might offer satisfactory fits to the obtainable data, but the results of design floods may be considerably different when extrapolated.

- The adjustment at the gauging stations may not be very robust as the recorded stream flows are commonly short and the best fit probability function may be more biased by recording inaccuracies.
- The rainfall and land use features that can produce flood may have altered in the duration of data records.
- The fitted probability function does not clearly reflect any alterations in the run-off generation procedures.

In areas where lengthy records of stream flow are obtainable at a site, a frequency assessment of recorded data can be accomplished. Here, Gedefa [98] investigated "At-site" flood frequency evaluation in the upper Omo-Gibe sub-basin using 27 years annual maximum stream flood data of 19 gauged stations in that basin of Ethiopia. Four distributions; (i) Generalized Extreme Value (GEV), (ii) Lognormal (LN), (iii) Lognormal with three parameters (LN3) and (iv) Log-pearson three(LP3) were fitted to the regional data. For selection of best-fit methods for "At-site" Flood Frequency evaluation, EASY FIT software was employed. The results show that three parameters Lognormal (LN3) and GEV distributions gave best fit by Probability Weighted Moments (PWM) were selected for most of the stations.

2.2.1.3.2 Regional analysis Regionalization is still a favorite method in approximating parameters in hydrology recompensing the lack of long hydrological information. The purpose of regional analysis is to improve the estimate of the distribution parameters used in single site analysis. This in turn assumes that the catchments are exposed to similar flood- causative hydrological phenomena [9]. Regionalization is; therefore, the generally accepted term to explain the transfer of information about flood peaks to one catchment from other hydrologically similar catchments. It was observed from the literature that the approach of a regional frequency analysis for design flood estimation has advantages [246] particularly in the estimation of frequencies for higher flood magnitudes with limited data at site. In Ethiopia, the use of regional data to quantify the design flood values in areas with little or no recorded data has become progressively central as several projects which might need such data are found in areas where stream flow data are either absent or insufficient.

Tadesse et al. [261] also found that estimation of a specified return period (T) flood magnitude (Q) is complicated in Ethiopia due to lack of a physical basis for determining the form of the underlying flood frequency function and the necessity of evaluating flood event for return periods that exceed the observation period. In order to advance the estimation of the "Q-T" relationship, the need to use regional information arises so that stabilizing site specific estimates based on limited data can be handled. Tadesse et al. [261] informed that, the RFFA procedure involves the definition and identification of homogeneous regions.

Yirefu [304] investigated RFFA for gauged catchments in the upper and middle Awash sub-basin (u/s of Kesem) through the application of index flood method with the objective of testing the homogeneity of the stations and regions in the sub-basin. Statistically, he had got five regions; the first region includes the Berga, Holeta, Teji, Ginchi, and Awash-Bello station and the second region have Akaki, Melka-hombola, Melka-kunture and Mojo stations; the third Awash-below koka, Wonji, Kelata and Nura-Hera; the fourth Methara,Awash-at Awash-Station,Arba-Abomsa, and Awash Melka-Sedi; and the fifth Kesem-Baka and Kesem at Awara Melka. Homogeneity test was applied and the result obtained from the tests indicates that all the five regions satisfied the homogeneity test applied. In addition, the Goodness-Of-Fit was also employed for selecting the best

fit distributions. Finally, the quantiles estimated obtained for region one was GEV/MoM, region two Gama/MoM, region three P-III/MoM, region four Gama/MoM and region five P-III/MoM. This shows that MoM found to be an appropriate method for estimation of parameter. Regression analyses have also been applied to develop regression models to predict mean annual flood from ungauged catchment so as to predict quantiles for various return periods with the help of standardized frequency curve.

Gedefa [98] has also carried out an investigation to develop a relationship between (Q_T/Q_{mean}) and return period T (a growth curve) for use in the upper Omo-Gibe sub-basin. In this study, at-site and RFFA are applied to the selected annual maximum stream flood observed at 19 gauged stations with a record period of 27 years in upper Omo-Gibe sub-basin using index flood estimation procedure. Statistical homogeneity tests (convectional and L-moment based tests) have been used to identify the homogeneity of the regions. Accordingly, upper Omo-Gibe sub-basin has been divided into two homogeneous (Region 1 and Region 2) regions. Region 1 includes the Wabe, Warabessa, Kuliti, Derghe, Wegecha, Gogheb, Gibe-Bako, and Walga stations and Region 2 compresses Gojeb-Shebe ,Gilgel Gibe-Asandabo, Gilgel Gibe-Seka , Great Gibe-Abelti , Kitto-Jimma and Bulbulo-Serbo stations. L-Moment method has been used for selection of appropriate probability distribution for identified homogeneous regions. The result indicated that three parameters Log-normal (LN3) and GEV distributions are most appropriate probability distribution for Region-1 and Region-2 respectively. Finally, the growth curves were developed using the estimated at site and regional quantiles for all stations and identified regions.

Willems et al. [293] accomplished a study on RFFA for the Nile basin based on the data of 56 gauging stations distributed over 5 nations (Egypt, Sudan, Tanzania, Kenya and Ethiopia) encompassing the Nile basin, and they created regional flood frequency curves for Nile (Abbay) Ethiopia basin. This was done by "at-site-calibration" of flood frequency curves to the yearly maximum observations based on regression in quantile-quantile plots (Q-Q plots). They identified homogeneous regions based on resemblance in the properties of these curves, and the consistency in the relationships between these properties and the upstream sub basin characteristics. These relationships produce the basis of the regional curves, which permit flood frequency and quantile estimates to be done at any location along the Nile basin's systems. Finally, the "at-site" flood frequency distributions can be defined by: the growth curve (the flood frequency distribution for the yearly maximum flows after rescaling by the mean annual maximum flow, MAF); and the MAF value. The growth curve was found to be roughly uniform for Blue Nile sub basin; Atbara sub basin; Awash sub basin; Sobat region; Sudd region; Tanzanian sub basins upstream of lake Victoria; and Kenyan sub basins upstream of lake Victoria.

Tadesse et al. [261] in turn revealed that in the current frequency investigation, the usage of index-flood RFFA is regarded as one of the tools in overcoming difficulties of ungauged catchments or catchments with short records. For this purpose, the upper sub-basin of Awash River with 8 gauged streams consisting of stream flow records varying from 15 to 33 years has been analyzed. The result of the study showed that an extreme value distribution 1 (EV1) is chosen as the best fit distribution for the sub-basin and this is also exhibited by other similar analysis in the Nile basin nations (Kenya, Tanzania and the Sudan). However, caution must be taken [246] to warrant that the method may not be practicable outside of the area for which it was developed, or beyond the range of data employed to develop it.

ERA Manual [79] recommended that regional regression equations are the most universally recognized technique for correlating peak flows at ungauged or poorly gauged sites in Ethiopia. Here,

the regression equations, which relate peak discharge of a particular return period to the physiography, hydro-meteorology of the catchment, had been developed by Gebeyehu [97] for Ethiopia. However, these out-dated regression equations should be up-dated with additional data (more than 25 years data) currently available in Ethiopia. It was also stated in ERA Manual [79] that though the regression equations and the common probability distribution functions (Gumbel, Log Pearson, and General Extreme Value) are preferable for design flood estimation in Ethiopia, only the rational and the SCS methods are widely applicable to the whole country at the present time. But, no reason has been documented why only the rational and the SCS methods are widely applicable in Ethiopia presently.

2.2.1.3.3 Probability Distribution Fitting The choice of an appropriate flood frequency procedure to model flood flows for a particular site or region can be made by applying a series of tests. Both SFFA and RFFA approaches need the fitting of an suitable probability distribution to the data. According to Smithers [246], the available approaches for fitting an appropriate probability function to the data are the method of moments, maximum likelihood procedure , probability weighted moments , L-moments , bayesian inference and non-parametric methods. The author informed that the usage of L-moments has received widespread exposure for fitting the distributions.

Haktanir and Horlacher [114] also carried out a study for evaluating the goodness of estimates of the extreme events using the flow data of 11 rivers in the Rhine Basin in Southern Germany having a record period of $>$ 30 years. They also took the yearly flood peak data series of two other streams in Scotland for comparison. They then conducted the assessment by all the methods through exhaustive studies of lengthy synthetic data and found out that the GEV and 3-parameter lognormal (LN3) methods were found better fit for estimating floods of return period's 100 years. The GEV 2 and the Log-pearson type 3 (LPIII) would generally give slightly conservative peaks when skewness is positive.

According to Stedinger [254], the U.S. flood management community has implemented the expected moments algorithm (EMA) as it offers a direct fit to the LP-III method by means of the entire data set. Bobée and Ashkar [40] observed that since the official implementation of the LPIII method in USA and Australia, its applications for flood investigations have been widespread. This opinion was also indicated in Bulletin 17B [109]. So, LPIII is still the suggested method for flood frequency investigations in USA and Australia.

Moreover, Alexander [8] proposes the usage of the LPIII methodology for design flood estimation in South Africa. While Görgens suggested both the LPIII and GEV methods to be applicable in South Africa in 2007 [246, 277]. Mkhandi et al. [176] also conducted replication experiments for selecting the most suitable flood frequency technique by means of the yearly extreme flood data encompassing 407 places from 11 nations of southern Africa. They found that the most suitable flood frequency procedure(s) for modeling flood flows for homogeneous regions in southern Africa are LP-III distribution fitted by MOM and/or P3 distribution fitted by PWM.

Tadesse et al. [261] report their findings with regard to probability distribution fitting for Ethiopia. Using the annual flood maximum data series of the upper Awash gauging sites (Berga- Addis Alem , Holeta, Awash-Bello, Teji- Asgori, Akaki , Awash-Melka Kunture, Awash- Hombole, Mojo river @ Mojo Village), they applied the most common probability distributions (PDF) such as Extreme value type I; 2 parameter Gamma distribution; 2- and 3-parameter Log-Normal distributions; and Pearson type III. They also used two parameter estimation methods, method of moments and method of maximum like-lihood, for fitting these distributions. By conducting the Goodness-Of-

Fit tests, they selected the best method for each set of annual Maximum data series and found out that although there remain researchable topics in development and application of regionalization methods, the performance of regional EV1 (Extreme Value 1) distribution is found to be highly satisfactory and can be widely applied in Ethiopia.

According to ERA Manual [79], the most commonly used PDFs for estimating the peak flood in Ethiopia is LP-III distribution. However, as the record length increases, the Log-Normal distribution or General Extreme Value (GEV) distribution could be used. The recent data analysis demonstrated that GEV can best be used to estimate the peak flow in Ethiopia. But, the ERA Manual [79] recommended lastly that the PDF which gives the best fit to the record data should be used. Other than these, there is no Ethiopian guideline for fitting a suitable method to hydrological data to estimate design flood flows.

2.2.1.4 Flood Envelopes and Regional Maximum Flood (RMF)

Areas with similar climatic conditions and topographic features are assembled together. All obtainable discharge data are also assembled with their respective drainage areas, and these data are then plotted to produce envelope curves. Such curves are mainly used for comparison only as the design floods acquired by other methods are higher than that from these curves [204]. But, according to Smithers [246], in this method, the largest observed discharges are plotted against catchment areas. An envelope curve is plotted comprising all the data points and the peak floods can then be determined at ungauged sites with the help of these envelope curves.

In these curves, as the flood data has been associated with the drainage area only, the result that could be obtained will not be precise. However, they can be used for preliminary guidance for determining peak flood better than the empirical formulae, in a sense that here the selection of coefficients based on judgement is not required. The essential constraint of these curves lies in the fact that they are based on the past records obtainable up to the time the curves are plotted. Furthermore, such curves can tell us nothing about the future probabilities of the occurrence the peak flood [95]. So, as no comprehensive flood envelope curves have been available in Ethiopia for flood estimation, further research is vital for wide applicability of the method in Ethiopia.

2.2.1.5 Run-Hydrograph and Joint Peak-Volume method

According to Pegram and Parak [193], the method was established by Hiemstra and Francis in 1979 from the previous work done by Hiemstra in 1972 and onwards. The authors [193] also informed that this was applied on the basis of the joint probability assessment of same-event flood peak and flood volume pairs of observed data of 43 catchments in South Africa. Alexander [8] suggested that though the run-hydrograph method is advantageous when compared with the unit hydrograph method, it is not recommendable for universal use in South Africa as no additional assessment of the technique has been recorded since its establishment. Alexander [8] lastly concluded that the run-hydrograph technique needs additional refinement. However, Smithers [246] agreed with the recommendation of the technique for use in South Africa by Pegram in 1994.

Görgens [104] has additionally advanced the run-hydrograph method for South Africa considering the joint probability of hydrograph volumes and the Joint Peak-Volume (JPV) design flood method. The approach allows the estimate of the exceedance probability of a design flood by means of a regionally-pooled procedure. The outcomes indicated that the wide-pool GEV have been observed superior to either the wide- pooled LPIII or the unit hydrograph results in over estimation in few

catchments. This method is not known in Ethiopia for design flood estimation and further research is required for its applicability in Ethiopia.

2.2.2 Rainfall-Based methods

In areas where there is no, or inadequate stream flow data at a site of interest, rainfall-based techniques are used to estimate the design flood. The current methods are on the basis of the design event technique that use a probabilistic precipitation data in incorporation with representative values of other inputs, and then assume that the subsequent flood has identical recurrence interval as that of the input precipitation value. However, such assumption is irrational [206]. The peak discharge response of a catchment to rainfall is dependent on several factors including rainfall rate, space-time variability, and catchment characteristics such as soil moisture and infiltration capacity, groundwater storage, land use/land cover, and geomorphology [88, 99, 246]. The available approaches in such cases are either to use design event models (rational formula, SCS or unit hydrograph) or continuous simulation methods. Smithers summarized the benefits of rainfall-runoff approches for design-flood estimation follows [246].

- Generally longer and better quality rainfall data at more sites could possibly be obtainable for assessment compared to stream flow data.
- Recording errors, irregularities in the data and non-homogeneity of the stream flows might make the infornation unacceptable for frequency investigation.
- Likewise, non-stationary discharge data because of altering catchment situations can make the discharge data unacceptable for frequency investigation.
- Areal extrapolation of precipitation data may be attained more effortlessly than streamflow records.
- Physical catchment characterstics may be combined into a hydrological model.
- The past, the present or the future land use situations within a basin could possibly be modeled.

Rainfall-runoff approches are used to, and can best estimate peak discharge from rainfall data when longer rainfall data are available or when precipitation can be more reliably estimated from surrounding stations [297]. They furthermore allow the estimation of the (PMF) probable maximum flood [88].

2.2.2.1 Design Event Models

The ‘design event’ method implicates producing a design rainfall from the Flood Estimation Handbook (FEH) TRKjeldsen2005 precipitation frequency statistics and running it through a simple catchment model to produce a design flood. The main benefit of the method over statistical investigation is that this method gives a full hydrograph rather than a peak flood. Since, precipitation records are more abundant and generally lengthier than streamflow records, flood approximation is achieved ultimately by means of a hydrological model. This method is commonly used for the design of flood storage areas or reservoir spillways [146]. In addition, the design-event models are associated by grouping of various complex catchment processes into a single one. The event-based method thus streamlines the estimate of catchment situations before the incidence of an

extreme event, even when hydrological modeling is accomplished for estimating the flood hydrograph [246].

Most of these models need, however, to be locally calibrated based on precipitation, temperature (which will eventually be converted to ETo) and runoff records. Only models where the parameters can be estimated by other means can therefore be applied to ungauged sites. The difficulty in applying rainfall-runoff models to small catchments is the case when better quality–longer rainfall data are not available. This is due to the fact that the quality of the flood estimates derived using hydrological models mainly depends on the quality of the estimated rainfall data input and its representativeness of areal precipitation in the catchment of interest. Event-based models typically apply intensity-duration-frequency curves for the estimation of extreme precipitation events, one of the simplest examples being the unit hydrograph. The drawback of this approach is that similar return periods for design rainfall and discharge are frequently assumed. But a precipitation event of a certain return period does not necessarily lead to a flood event of the same return-period [88]. Thus, the design event methods, which are widely used in Ethiopia, are as presented below.

2.2.2.2 Rational Formula Method

The rational formula is the commonly used flood estimation method for small watersheds especially for urban drainage design. The characteristics which describe a small watershed are; (1) rainfall can be assumed to be uniformly distributed in time and space, (2) storm duration usually exceeds concentration time, (3) runoff is primarily by overland flow, and (4) channel storage processes are negligible. Watersheds having either the concentration time of less than 1 hr or areas less than 2.5-10 km^2 has been defined as a small watershed. The method is an approximate deterministic model giving the peak flood from an assumed precipitation value [234].

ERA Manual [79] also indicated that the rational formula method offers estimations of peak runoff for small watersheds of areas less than 50 hectares ($0.5km^2$). It is the best suited for the design of urban storm drainage systems, highway side ditches, and culverts. But, it needs to be used with caution if the time of concentration is greater than 30 minutes.

Therefore, it can be concluded that the rational method is generally suited for design flood estimation for small watersheds of areas less than 50 hectares (0.5 km^2) where natural or man-made storage is small or negligible.

In the traditional form of the rational method, the peak discharge (Q), is determined as a linear relationship of the form stated below [79, 88, 121, 234, 246].

$$Q = 0.278CiA \tag{2.12}$$

where: Q = the peak discharge for the required return period (m^3/s), C = the coefficient of runoff, i = the intensity of rainfall for a required return period of duration that is equal to critical storm duration (mm/hr), A = the Drainage watershed area (km^2).

For application of the method in flood estimation, the rainfall intensity and runoff coefficient are chosen for an event of a specified return-period. The rainfall intensity is taken to be the average over the critical storm duration, which is supposed to be equal to the time of concentration of the catchment. The time of concentration is the time it takes from the start of a rainfall event until the whole catchment is providing flow to the catchment outlet. The basic assumption here is that the whole catchment is more or less uniformly covered by a rainfall event of constant intensity,

which limits its application for larger catchments. On the other hand, the rational formula method is recommended for catchments with areas up to 15 km^2 (HRU, 1972) in South Africa or to larger catchment sizes than conventionally acceptable [246].

Basic assumptions the rational formula method:

1. The rate of run-off resulting from any intensity of rainfall is maximum when the duration of the intensity of rainfall greater than the time of concentration.
2. The frequency of rainfall intensity is the same as that of the peak discharge for the assumed time of concentration.
3. The portion of rainfall that becomes run-off (C) is not dependent on rainfall intensity. This is rational for impervious areas only. Thus, the usage of the rational formula needs the choice of a coefficient that is relevant for the storm, soil, and land use situations.
4. The peak run-off is an adequate information for the design.

Many different modifications of the rational formula have been developed for use [88]. Accurate and reliable estimation of the runoff coefficient is mainly crucial for successful application of the rational formula method, as it has to account for all factors influencing the relation of peak flow to the mean rainfall intensity other than area and response time. Hence, the two catchment parameters, i.e. the run-off-coefficient and the time of concentration, have to be estimated for application in ungauged catchments. Both are usually estimated from empirical formulae or tabulated values.

The average intensity of rainfall , i, has a duration equal to the critical storm duration, generally taken as the time of concentration (t_c). For design purpose, the mean rainfall intensity, i, is estimated from the rainfall intensity duration frequency (IDF) data for the area considered, with its frequency the same as that designated for the design flood.

Determination of the time of concentration (t_c) and estimation of coefficient of runoff(C) in Ethiopia

For urban areas, values of t_c in minutes are basically calculated as length divided by velocity determined by hydraulic formulas. For rural drainage basins, t_c is generally estimated by means of an empirical formula such as Kirpich's equation [234]:

$$t_c = 3.976 L^{0.77} S^{-0.385} \tag{2.13}$$

where: L = channel length from divide to outlet (km); S = average channel slope (m/m).

Estimating the value of the runoff-coefficient is the utmost difficulty and the key source of uncertainty in the usage of the rational method. A better estimate would be obtained from measurements of runoff volume at the flow outlet and rainfall volume over the watershed. Indicative runoff coefficients (Tables 2.1 & 2.2) presently in use in Ethiopia for urban and rural areas are given [234].

Precautions to be considered while applying the rational formula method in Ethiopia [79] are:

- Having a topographic map that defines the boundaries of the catchment, a field inspection should be conducted to see if the watersheds have been changed.

Table 2.1: Average runoff coefficients for urban areas: 5-year & 10-year design frequency [166]

Description of area		**Runoff coefficient**	**Characteristics of surface**	**Runoff coefficient**
Business	Downtown areas	0.70 to 0.95	Streets: Asphalt	0.70 to 0.95
	Neighborhood areas	0.50 to 0.70	Streets: Concrete	0.80 to 0.95
Residential	Single-family areas	0.30 to 0.50	Streets: Brick	0.70 to 0.85
	Multiple units, detached	0.40 to 0.60	Drives and walks	0.70 to 0.85
	Multiple units, attached	0.60 to 0.75	Roofs	0.75 to 0.95
	Residential (suburban)	0.25 to 0.40	Lawns, sandy soil: Flat (2 %)	0.05 to 0.10
	Apartment –dwelling area	0.50 to 0.70	Lawns, sandy soil: Average (2 to 7 %)	0.10 to 0.15
Industrial	Light areas	0.50 to 0.80	Lawns, sandy soil: Steep (7%)	0.15 to 0.20
	Heavy areas	0.60 to 0.90	Lawns, heavy soil: Flat (2 %)	0.13 to 0.17
	Parks, cemeteries	0.10 to 0.25	Lawns, heavy soil: Average (2 to 7 %)	0.18 to 0.22
	Playgrounds	0.10 to 0.25	Lawns, heavy soil: Steep (7%)	0.25 to 0.35
	Railroad yard areas	0.20 to 0.40		
	Unimproved areas	0.10 to 0.30		

Table 2.2: Average runoff coefficients for rural areas [228]

Vegetation	Topography	Runoff coefficient based on Soil Texture		
		Open Sandy Loam	Clay and Silt Loam	Tight Clay
Woodland	Flat(0–5% slope)	0.1	0.25	0.3
	Rolling(5–10% slope)	0.3	0.35	0.5
	Hilly(10–30% slope)	0.4	0.5	0.6
Pasture	Flat(0–5% slope)	0.1	0.16	0.22
	Rolling(5–10% slope)	0.3	0.36	0.42
	Hilly(10–30% slope)	0.4	0.55	0.6
Cultivated land	Flat(0–5% slope)	0.3	0.4	0.52
	Rolling(5–10% slope)	0.5	0.6	0.72
	Hilly(10–30% slope)	0.6	0.7	0.8

- In obtaining the C value for the catchment area, consideration shall be given to future land use alterations that might occur in the basin under consideration.
- Existing constraints to the natural flow (e.g. highway crossings,etc) in the catchment shall be investigated.
- The charts, the tables and the illustrative graphs encompassed in ERA Manual [79] are not envisioned to substitute the practical engineering judgment in the process of designing.

According to ERA Manual [79], the rational formula method has been still widely used in Ethiopia. Though it has been criticized for its simplistic approach, no other design flood estimation method has achieved such widespread use in Ethiopia. So, further research is required to fine tune the method for Ethiopia.

2.2.2.3 Unit Hydrographs

This method signifies the response of a basin to a unit depth of preciptation excess for specific duration distributed uniformly over the catchment [58, 190]. Basically, the method considers a characteristic linear response from a basin. The consideration of the linear response of a watershed to rainfall has two implications; the concepts of proportionality and superposition. The unit hydrograph has to be defined for each catchment separately from rainfall and runoff observations. Alternatively, empirical formulae can be used to derive the unit hydrograph from physiographic catchment data for ungauged catchments [187, 246]. However, careful use of the method can provide better estimation of floods. A constraint of a unit hydrograph technique is the supposition of spatial regularity of rainfall [58] as the use of the method is only recommended for catchments in the regions for which they were developed.

Investigation conducted by Smithers [246] concluded that unit hydrograph techniques are broadly utilized internationally for design-flood estimation. For instance, in the UK it is contained within in the Flood Estimation Handbook (FEH) and is generally used owing to its simplicity for mostly being derived at any site. The author [246] also informed that the method is a reliable technique of peak flood estimation for basins size from 15 to 5 000 km^2 (SANRAL, 1986; HRU, 1972) in South Africa. The above explanation indicates that the unit hydrograph technique is a useful technique for design-flood estimation even when only a few observations are obtainable. However, no standard unit hydrographs are developed in Ethiopia and thus further work is essential to develop the method.

2.2.2.4 SCS Method

The SCS method is a technique established by the US Soil Conservation Service for estimation of flood discharge. It requires similar key data as the rational formula method: a catchment area, a run-off coefficient, a time of concentration, and the rainfall. Boughton and Droop [42] stated that it is the most widely used model all over the world. It is broadly utilized for design flood estimation in the USA [246]. According to Fleig Wilison [88], the SCS method relates runoff depth and rainfall during a flood event by the run-off curve number; CN. Peak flow is then estimated using the runoff depth, the catchment lag time, the concentration time and the rainfall duration. For the estimation of a flood event of a certain return period, the rainfall event of the same return period is chosen. Tabulated empirical values for the runoff curve number, CN, are available for different antecedent moisture conditions, soil type and land cover (which also considers the differing hydrological surface properties of vegetation in good and poor condition). Antecedent moisture conditions are specified by three classes (dry, average, wet) and soil type by four characters (high,

moderate, slow, very slow infiltration). The time of concentration can be estimated by various general procedures, which are not developed particularly for the SCS method. Some evaluation studies suggest; however, that the method does not perform equally well under all conditions. It seems, for instance, to be more suitable for bare soil and sparse vegetation than dense vegetation. The estimate of the time of concentration can be more relevant than the influence of CN and catchment characteristics. Furthermore, the effect of the assumed antecedent moisture conditions on the results can be large and care is therefore required in its application. Smithers [246] also mentioned irregularities in the usage of the SCS technique are because of the choice of the procedures for approximating the concentration time and in selecting a relevant CN.

According to ERA Manual [79], the technique is more explicitly known in Ethiopia by the name "NRCS- Run-off Curve Number Methods". The Technical Release 20 (T-20) [264] , which uses "the Curve Number Method" and a "dimensionless unit hydrograph" for peak discharge estimate, can be used for designing culverts, bridges as well as detention ponds; for adjustment of waterways; and for investigation of flood protection reservoirs in Ethiopia. Technical Release 55 (T-55) [265], simplified form of TR -20 , is also in use for estimating flood peaks for small watersheds whose concentration time is $\leq$ 10 hours.

The unit hydrograph employed by the SCS technique is based on an investigation of a number of natural unit hydrographs from dissimilar geographic locations and hydrologic regions in USA. The SCS technique is therefore, a technique for estimating direct run-off from 24-hour rainfall value. The equation is as shown below [79].

$$Q = \frac{(P - I_a)^2}{P - I_a + S} \tag{2.14}$$

where: Q = accumulated direct runoff (mm), P = accumulated rainfall(mm), I_a = initial abstraction like surface storage, interception and infiltration prior to runoff (mm), S = potential maximum retention (mm).

The relation between Ia & S was established from experimental catchment area data and it is; $I_a = 0.2 * S$, and thus making the SCS equation to be:

$$Q = \frac{(P - I_a)^2}{P + 0.8S} \tag{2.15}$$

S is associated with the soil and land use conditions of the catchment area by the CN which varies from of 0 to 100 as:

$$S = \frac{25400}{CN + 254} \tag{2.16}$$

ERA Manual [79] has provided a concluding remark that the SCS method is applicable in Ethiopia to small catchments (up to 6,500 ha) with a time of concentration within 0.1 – 10 hours, when the CN $\geq$ 50, the computed value of Ia/P is in between 0.1 and 0.5 and when the watershed has one main waterway or when there are two main waterways that have roughly equal concentration times. It was; however, suggested by Smithers [246] that the current improved computing capacity and existing better quality precipitation data, land use and soil type databases could be exploited to refine the technique. So, the SCS method should further be updated in Ethiopian context for its wide applicability to estimate the design flood.

2.2.2.5 Run-off Routing

In addition to peak discharges, hydrologists/engineers are occasionally attentive to the flood volume and time distribution of run-off. This is a requirement to implement the usage of flood hydrographs to route floods through bridges, culverts, flood storage and other roadway structures. It is especially important when an embankment is to be built across a floodplain and flood compensation storage area that is required to be provided to compensate the lost natural floodplain storage area due to the construction of the road embankment and to mitigate the flood risk to the upstream areas. In Ethiopia, the peak flood is adequately used for designing conveyance structures like storm water drainages, open canals, culverts, and bridges. Nonetheless, if the design requires routing of flood through such areas, a flood hydrograph is essential. This is the case in the Afar and Somali region of Ethiopia where flash flood occurs for a limited period of time [79, 234]. Thus, this Run-off routing techniques should widely be practiced in Ethiopia wherever the applicability of the technique is necessary.

2.2.2.6 Probabilistic Rational Method (Standard Design Flood-SDF)

According to Alexander [9], the SDF procedure is the calibrated rational formula method. Alexander [9] established an SDF technique by allocating rain gauges to 29 typical basins in South Africa that have recorded stream flows. He then calibrated the runoff-coefficient till the design flood estimated with the use of design rainfall magnitudes equaled the value determined directly from the recorded flow information. The result showed that the SDF exceeded the "At-Site" values by 60%.

Smithers [246] found that on the average, the ratio of Q_{50} estimated by SDF method to that by LPIII method is observed to be approximately 210% and hence the SDF method may give rise to substantial over-design (uneconomical) of water structures like spillways. SANRAL Report [221] noted some significant differences between the design–flood calculated from at-site data using SDF technique after assessing the SDF method at 5 stations. The report showed that no clear trends were observed. So, Van Bladeren (2005) suggested that, the SDF practice must be advanced in the following ways [246]:

- Enhanced regionalization incorporating more locations.
- Re approximation of basin features.
- The improvement of lower and upper growth curves to evaluate the outcomes of the SDF technique.
- Additional approaches to assess the design floods need be employed in combination with the technique.

Pegram and Parak [193] standardized the rational formula technique runoff-coefficient by means of design rainfall maginitudes approximated by the Regional L-Moment Algorithm and Scale Invariance (RLMASI) technique and peak floods values from 29 catchments approximated with the use of the run-hydrograph technique. They observed that the runoff-coefficients should be connected to time of concentration, land use, slope and return-period. They additionally found that the calibrated runoff-coefficients were mostly smaller than that of the literature values. Finally, they concluded that the calibrated rational formula technique may be applicable for all catchments, but recommended that it must be used with other approaches. Researches conducted in Australia revealed the better efficiency of the probabilistic rational formula method compared to the deterministic approach as the former is used for catchments area up to $250km^2$ and the later has shown

very poor performance in application to flood estimation. However, this approach requires further investigation and refinement as the approach has a room for subjectivity of adjustment, combination of variability within regions, and incorporating method of regionalization in to it [246].

The SDF method is not currently used in Ethiopia. Researchers are encouraged to conduct studies with regard to the applicability of the SDF method in Ethiopia for design flood estimation.

2.2.2.7 Continuous Simulation Modeling (CSM) and Joint Probabilities

The present rainfall-based design-flood estimation procedures (e.g. the Design Event method) do not account the probabilistic character of the key factors except the peciptation depth that can lead to irregularities and substantial bias in flood estimations for a particular return-period [205]. Simple concept models like the rational formula and more sophisticated derivatives of it involve some considerations concerning the most appropriate procedures, but are criticized for encompassing factors that are challenging to approximate (e.g. runoff coefficient) or for being based on unreliable assumptions (e.g. identical return-period for rainfall and the peak flow). However, the approaches were broadly utilized in the past and confirmed productive for average situations. Smithers [246] summarized the opinions of several authors and concluded that CSM and joint-probability methods were suggested to minimize the key constraints of the event models.

2.2.2.7.1 Continuous Simulation Modeling(CSM) The key goal of this method is to get flood hydrographs without recording the discharges for a catchment. Subsequently, these hydrographs help estimate the appropriate flood values [206]. That is to mean CSM attempt to represent the major processes responsible for providing stream flow from the input catchment rainfall , the potential evapo-transpiration and other climatological and catchment variables [54]. A wide-range of review of CSM for design-flood estimation is available in [42]. The CSM to design-flood estimation has numerous benefits and has a capacity to minimize the limitations of the design event model. For instance, the hydrologic processes like interception, depression storage, infiltration, percolation, etc. can be considered in CSM [25].

Bashar and Zaki [25] conducted Soil Moisture Accounting (SMA) based Continuous Hydrologic Simulation investigation on Abay basin in Ethiopian, in which the Hydrologic Modeling System (HMS) model was employed for CSM of the Abay basin. The model encompasses the SMA algorithm to predict the long-term association between run-off, rainfall, storage, evapotranspiration, and soil losses in the basin. It is to assess the efficacy and capacity of the HMS with the SMA algorithm on the Blue Nile basin. The result of the study indicated that the HMS application produced satisfactory performance. However, the development of model parameterization methodology using GIS is highly recommended. More hydrological data and satellite images are needed to take into account the climatic, hydrological and spatial variability of soil characteristics for better modeling of the hydrological processes in the catchment.

Viviroli [284] also conducted a study to an innovative flood estimation methods by using CSM at hourly resolution for ungauged mesoscale catchments in Switzerland. Consequently, the stream flows were evaluated using extreme value statistics to estimate of flood peak maginitude of a specified return period. The appropriateness of the modeling process is verified comprehensively, by considering a large number (n = 140) of catchments. The outcomes showed that the CSM is suitable for application in ungauged catchments of Switzerland. They finally concluded that the technique is a deterministic and process-oriented substitute for estimation of floods in ungauged catchments.

Smithers [248] carried out a study regarding application of the CSM system for design-flood approximation in ungauged catchments. The study includes an analysis of the suitable spatial scale of model structure, the temporal disaggregation of daily precipitation, flood routing and the usage of radar & gauged data for improving catchment rainfall. Results of the study were used for design-flood assessment in the catchment of Thukela in South Africa. The author concluded that an appropriate estimation of design floods in the Thukela catchment can be achieved using the ACRU (Agricultural Catchments Research Unit) model.

But, as was reviewed by Smithers [246], Schulze (1989) argued for using the CSM method in design-flood estimation, since: (1) lengthy record data are required for precise estimation, (2) such lengthy data are mostly not obtainable for calibration, (3) the exceedance probability of floods is not associated with that of rainfall, as presumed in simple event-based approaches.

Moreover, Chetty and Smithers [54] also investigated the use of the CSM method to evaluate design floods in South Africa on Thukela basin . The pattern of the replicated peak floods mostly agreed well with that of the observed ones for the smaller basins of areas $< 150km^2$ only. They therefore suggested that the translation of the run-off volume into a hydrograph and the subsequent peak flood needs additional improvement. Consequently, Smithers [246] summarized the suggestions of different authors regarding the advantages & disadvantates of the CSM approach as follows:

Advantages:

- A complete hydrograph is generated.
- As real storm records are used, no artificial storms are required and the critical storm duration is not a problem.
- The assumptions about losses can be avoided with the usage of calibrated rainfall-runoff model.
- It is possible to model the antecedent moisture conditions and hence any inaccuacies in trying to account for it is avoidable.
- The statistical investigation of output proposes that the return-period of the run-off is not supposed to be identical with that of the precipitation.

Disadvantages:

- The complications in effectively representing the soil moisture balance and gaining input information at the specified time-based and spatial scale.
- Numerious parameters might be calibrated.
- The loss of 'sharp' events if the modeling is performed with coarser time scales.
- The widespread data necessities that lead to substantial time and effort to acquire and organize the input information.
- The experience needed to determine parameter values that satisfactorily replicate observed hydrohraphs.

Therefore, the advantages of a CSM to design-flood estimation is evident [246] as numerous constraints of event-based procedures can be minimized [248]. This approach would be one of the best solutions for design flood estimation in Ethiopia.

2.2.2.7.2 Joint Probabilities This approach considers that any peak flow could be as a result of an assortment of groupings of flood producing factors. Thus, it seems that the approach will lead to an improved approximation of design flow [206]. Hence, subjectivity of the choice of input variables is removed by taking-into-account the inputs as random variables [246]. By using identical component models as the existing design event method but considering the input variables to the design as random variables, the method evidently removes biased criteria in specifying input values. Therefore, the method is theoretically better than the design event approach and is considered as an attractive method [206, 246]. Flood frequency assessment in basins of Victoria state in Australia were well assessed by this approach [205]. This approach could be helpful for design flood estimation in Ethiopia with further research.

2.2.3 Impacts of Climate Change on Design Floods

Climate change is expected to disturb rainfall and evapo-transpiration patterns as well as other variables such water availability, streamflow, and the periodical availability of water supply [150]. According to IPCC [127], there is indication that several natural configurations are being impacted by climate changes, e.g. temperature. Smithers [246] also stated that the alterations in the character and pattern of the rainfall and runoff would influence the estimation of design floods. He further suggested that the impact of climate change on design-rainfall should be evaluated to know its impact on the estimated design-flood.

Zhao et al. [311] carried out a study that examines the spatial distribution and temporal variation of precipitation, potential evapotranspiration, temperature and stream flow by using hydro-climatic series from the 1950s to 2010 in the MRYRB, the middle reaches of the Yellow River basin in China. They investigated individual impacts of climate variability and human activities and identified potential causes for the stream flow changes. The result of the study showed that a general decrease in the annual precipitation and a rising temperature trend have been detected in the MRYRB. The average annual stream flow shows a significant decrease and abrupt changes in stream flow occurred in the mid-1980s and around 1999 in the tributaries, which may have resulted from the application of soil and water preservation processes. Stream flow at mainstream stations showed abrupt changes in 1985 that were evidently due to the trapping effects of reservoirs. In general, the overall results show that climate change had shown huge impact on stream flows, while human undertakings accounted for an extra impact on streamflow variability in tributaries of MRYRB over the last six decades.

Kim et al. [144] conducted an assessment to evaluate the impacts of climate change on hydrological processes of the upper Abbay basin in Ethiopia. The results suggest that (1) the climate in the basin is likely becoming wetter and warmer in the 2050s (2040-2069) and (2) low flows may become higher and severe droughts are probably to become less frequent throughout in the basin.

Bates et al. [26] found that at the global scale, trends in run-off do not essentially follow the trend in rainfall that are being influenced by climate change. Moreover, according to results obtained by Knoesen in 2011, both of the design rainfall and design flood are anticipated to increase in South Africa due to climate change [246]. Therefore, as the natural hydrologic systems are being impacted by local climate changes, such impacts on design flood should investigated and incorporated into design flood estimation for future climate change impacts.

2.2.4 Results and Discussions

The above literature review showed that fine-tuning and updating the existing design flood estimation methods in Ethiopia are required to keep up with the state-of-the-art of the design flood estimation methods. It is also an appropriate time to look-for another reliable alternative design flood estimation methods for Ethiopian catchments based on long records and improved information currently available. Meanwhile, it is a good opportunity to introduce additional international flood estimation techniques to Ethiopia. The summarized results of this review are presented below:

1. Estimation of design flood is accomplished by flood frequency assessment of the recorded flows data where such data can be obtained adequately and in good quality. Alexander [9] stated that the development of design flood estimation procedures begins with the direct statistical analysis of recorded data at the gauged sites. It was also detected from the literatures reviewed that RFFA results in more consistent design flood estimates in approximately all real-world applications than the implementation of an "at-site" investigation [246]. Regionalization approach design flood estimation technique should be investigated in Ethiopia, especially index-flood approach should be further developed for practical use in Ethiopia.

2. Flood frequency analysis is applied in determining flood magnitudes of defined return periods by fitting the data to the best probability models [58, 261]. But, the precise fitting models of the flood peaks is not known [246] as dissimilar probability functions may offer acceptable fits to the obtainable data, and result in expressively dissimilar approximations of design floods when projected. This should be re-evaluated and further developed in the context of Ethiopia.

3. In Ethiopia, the use of regional information to evaluate flood magnitudes at ungauged sites has become progressively important since numerous projects which need such data are found in areas where recorded flood data are either absent or insufficient. On the other hand, Tadesse et al. [261] found that estimation flood magnitude (Q) corresponding to a specified return period (T) is complicated in Ethiopia due to lack of sufficient data at the site of concern. The author also agreed that, to tackle such complexity of estimation of the Q-T relationship for Ethiopian case, regional approach to frequency analysis is the best alternative. So, this approach should be re-refined.

4. The regression flood equations, which relate peak discharge of a given return-period to the physiography, hydro-meteorology of the basin, was developed by Gebeyehu [97] for Ethiopia 25 years ago. These outdated regression equations should be revised and updated using the extra data presently obtainable in Ethiopia.

5. It has been observed from ERA Manual [79] that though the regression equations and the common PDFs (Gumbel, Log Pearson, and General Extreme Value) are preferable for estimation of design flood in Ethiopia, only the rational formula and the SCS method are widely applicable in the country presently. So, researchers need to investigate, verify and update the usage of these methods.

6. The run-hydrograph technique summarizes the family of characteristic volume and peak of stream flows for a specified return period in a catchment. However, this method is not known in Ethiopia and further research work is required to assess its applicability in Ethiopia.

7. According to ERA Manual [79], the PDF method for estimating peak discharges in Ethiopia is Log-Pearson Type III. The manual additionally verified that a Log-Normal distribution or

General Extreme Value (GEV) distribution could be used if long records are available at a site of interest. EV1 can be also the best to estimate the peak flow in Ethiopia [261]. ERA Manual [79] lastly recommended that the PDF methods which give a best fit to the record data should be used. These diverging opinions expressed by various authors and reports must be verified to consistently estimate the design flood in Ethiopia.

8. The envelope curves are usually employed for preliminary comparison of the design floods as such floods acquired by other approaches are higher than that from envelope curves [204]. In this approach, the flood peak has been correlated to the drainage area only, others basin features have been ignored. However, they are better than Empirical formulae, in a sense that here the selection of coefficients based on judgment is not required, as is required in the empirical formulae [95]. So, further development, refinement and standardization of flood envelope curves should be conducted for Ethiopia catchments.

9. Smithers [246] stated that at sites with very limited observed stream flow data, the suggested approaches for design-flood estimation in South Africa comprise rational formula, the unit hydrograph, and the SCS methods. The possibility of using this suggestion has to be refined for Ethiopia.

10. The rational formula method is commonly used for flood estimation in the world on small watersheds. In Ethiopia, it could be used for watersheds with either the concentration time less than 1 hr or areas less than 2.5 - 10 km^2 [234]. ERA Manual [79] ; however, reported that the method can be applied to small watersheds of areas less than 50 hectares (0.5 km^2). It is also suggested to be used on basins with areas up to 15 km^2 (HRU, 1972) or much bigger catchment sizes than conventionally acceptable in South Africa [246]. These differing suggestions should be investigated to consistently and suitably use the method in Ethiopia.

11. A modified probabilistic rational method has also been proposed for design flood estimation in South Africa [192, 193]. The observed discharge data necessary for this approach could be complemented with the result of the CSM approach. For example, Alexander [9] has developed an SDF using this approach, even though it demands additional fine-tuning. Thus, the probabilistic technique should also be investigated for use in Ethiopia.

12. ERA Manual [79] indicated that the unit hydrograph employed by the SCS technique was developed based on the comprehensive analysis the natural unit hydrographs obtained from different catchments in USA. Other than this, no development of the unit hydrograph method for Ethiopian catchments has been reported and is used in practice in Ethiopia. So, it is essential to develop and refine the unit hydrograph approach of design flood estimation in Ethiopia.

13. The SCS method requires similar basic catchment data as that of the rational formula method for estimation of design flood. It is extensively used as a substitute of the rational formula method in the USA. However, Sileshi [234] argued that it is more sophisticated as it considers the temporal distribution of the precipitation, the initial precipitation losses that might decrease during the course of a storm. Smithers [246] also informed that there are irregularities in the usage of the method as due to the choice of the techniques for approximating the concentration time and in selecting a appropriate CN. ERA Manual [79] has provided a concluding remark that the SCS method is applicable in Ethiopia to small catchments (up to 6,500 ha) with a time of concentration within 0.1 – 10 hours, the CN 50, the I_a/P value in between 0.1 and 0.5 and when the catchment has only one main channel or when two main waterways having closely equal concentration times are available in a catchment. It was

however, suggested by Smithers [246] that the current improved computing capacity and the existing better quality rainfall, land use and soil type data could be exploited to improve the technique. So, the SCS method should further be updated in Ethiopian context for its wide applicability to estimate the design flood.

14. According to Alexander [9], SDF method is the adjusted rational formula method (Probabilistic based approach). Alexander [9] developed an SDF method by assigning rain gauges to twenty-nine typical catchments in South Africa that have recorded flow data. He then calibrated the run-off coefficient with the use of the design rainfall based design flood expected and the value calculated directly from the recorded flow data. The result showed that on average the SDF exceeded the "At-Site" magnitudes by 60%. Smithers [246] reviewed that on the average, the proportion of Q_{50} estimated by SDF method to that by LPIII method is observed to be approximately 210% and hence the SDF method may lead to considerable over-design (uneconomical) of water structures like spillways. So, it is not recommendable to use this approach in Ethiopia for design flood estimation currently unless this method is further developed in the context of Ethiopia.

15. In Ethiopia, since usually lengthier rainfall records are obtainable at some sites for analysis compared to stream flow records, rainfall-runoff models is desirable to estimate peak discharge using rainfall data as input. Hydrological models furthermore allow the estimation of the (PMF) probable maximum flood [88]. So, it is vital to expand the rainfall-runoff models for design-flood estimation in Ethiopia.

16. Specifically, the CSM technique to design-flood estimation has numerous benefits and has a capacity to minimize the constraints of the design event model. The key objective of the technique is to get discharge hydrographs for any catchment without measuring the discharges. Consequently, the appropriate flood estimations are to be derived from these hydrographs [206]. That is to mean CSMs try to signify the chief processes accountable for transforming the input catchment precipitation data into streamflow information and hence flood hydrographs are produced over lengthy period of time from the input of past precipitation data, potential evapo-transpiration and other climatological as well as catchment factors [54]. Therefore, CSM method should be developed, elaborated and then used for design flood estimation in Ethiopia as the approach can take account of the current and projected catchment conditions like expected land use.

17. The joint probability technique combines a deterministic hydrological model with stochastic inputs as the probability function [206]. Using the same concept models as the present design event technique but considering the inputs variables as random, the method noticeably can eradicate subjective criteria in stipulating input values. The flood outcome, consequently, will also have a probability distribution in place of a single value. Therefore, the method seems theoretically better than the design event method [206, 246]. Flood frequency investigations for the catchmentsin in Victoria state in Australia were, for example, well done by a joint probability technique [205]. This technique should be practiced for Design flood estimation in Ethiopia if further research so provides.

18. Climate change is anticipated to affect rainfall and evapo-transpiration patterns and other variables such as water availability, streamflow, and the seasonal variations of water supply [150]. According to IPCC 2007 [127], there is an indication that numerous natural processes are being impacted by local climate changes, especially by temperature changes. Smithers [246] also reviewed that the changes in the character and pattern of the rainfall and the resulting run-off would have an impact on the estimation of design floods. He finally

suggested that the impact of climate change on design-rainfall should be firstly assessed to know its impact on the design-flood. So, impact of climate change on design flood has to be investigated in Ethiopia to make some allowances for such impact on design flood.

19. The review of the current and the practical design flood estimation methods in Ethiopia emphasized that there was very lagre gap between flood analysis and flood estimation practice in that it currently requires urgent attention and further researches are necessary to advance the estimates of peak floods in the country. This can be carried out by re-refining the existing methods and/or developing, introducing as well as evaluating new approaches which have been accepted for design flood assessment in other nations like South Africa, USA, Australia, European countries, etc.

2.2.5 Conclusions and Recommendations

The review of the current and the practical methods of design flood estimation in Ethiopia revealed very large gaps between flood researches and the current design flood practices. It can therefore be concluded that further research works are required to enhance the estimates of design floods in Ethiopia by making use of longer recorded data and improved information currently available.Thus, the following recommendations have been made for further research to design flood estimation in Ethiopia.

1. Evaluating and fine-tuning outdated regression flood equations with more than 25 years of supplementary data presently available in Ethiopia.
2. Development of regionalized index-flood method of design flood estimation.
3. Improvement of the methods for regionalization and pooling techniques for design flood estimation.
4. Further imprvement for the selection and appropriate use of the suitable probability distribution for design flood estimation in Ethiopia.
5. Updating and fine-tuning of the rational method especially in estimation of Coefficient of run-off (c) and time of concentration (tc).
6. Updating and refinement of rainfall Intensity- duration- frequency curves.
7. Refinement of the estimate of design rainfall for Ethiopian catchments.
8. Establishment of reliable methodologies for the standardization of data and estimation of catchment feedback characteristics.
9. Investigating the applicability of the joint probability method for flood estimation in Ethiopia.
10. Introducing CAPA and MIPI empirical design flood estimation methods to Ethiopia
11. Comprehensively reviewing and refining the SCS technique for design flood estimation on small watersheds by taking into account antecedent soil conditions and land use/cover information presently available and the appropriate design rainfall values.
12. Conducting further research work for wide applicability of the run-hydrograph technique in Ethiopia

13. Developing and standardizing of unit hydrograph procedure for design flood estimation for Ethiopian catchments.
14. Evolving Ethiopian context-regional Empirical formulae for design flood assessment.
15. Refining and updating the probable maximum precipitation (PMP) envelopes for Ethiopia and spatial distribution of extreme rainfall events.
16. Development of the SDF practice for Design flood estimation in Ethiopia.
17. Establishment of watershed-based regression relations to approximate the runoff-coefficients to implement the technique in ungauged watersheds.
18. In addition, the following recommendations are suggested for enhancing design flood estimation in Ethiopia:
    (a) Compiling the entire obtainable stream flow records and the assessment of design events by means of modernized databases.
    (b) Using an appropriate probability distributions for assessment of design floods.
    (c) Development of updated precipitation database for Ethiopia.

2.3 A general overview of (Py)TOPKAPI hydrologic modeling

Catchment hydrologic models have been developed with the objective to provide a better understanding of the hydrologic phenomena operating in catchments. They are intended for generation of synthetic sequences of hydrologic data for facility design or for use in forecasting. Such models are also helpful in providing valuable information on the potential impacts of land use or climate changes [57]. The historical development of hydrological modeling ranges from the rational formula method to present distributed physically based models [272]. The hydrological models are conceptual and simplified demonstrations of a part of the water cycle. They are basically used for forecasting and understanding of hydrological processes: given the precipitation data, they estimate flow at the outlet of a river basin [66, 152]. Some of such models are physically based, as they are inherited from the physical hydrologic processes which affect the response of a basin. The physically based models are essentially of the distributed type, since the equations defining them usually involve one or more spatial coordinates. They have therefore the capacity of predicting the spatial trend of the hydrological conditions of the basin [13, 57]. Recent advances in remote sensing (RS), Geographic information systems (GIS), and computer technology make the use of physically based distributed hydrologic models more attractive approach to simulate the stream flow. The connection of a distributed hydrologic model with the spatial data handling capacities of digital elevation model (DEMs) provides advantages related to the full usage of spatially distributed data to investigate hydrologic processes [59]. In 1995, a new physically based fully-distributed TOPKAPI (TOPographic Kinematic APproximation and Integration) model, was developed by Liu and Todini [157, 160] based on the critical analysis of two popular hydrological models (ARNO and TOPMODEL) for the purpose of realization of the hydrological models on a strong physical base and a parsimonious number of physically meaningful parameters; and for applying them at increasing spatial scale without losing the physical based meaning of the model parameters. Since its advent in 1995, the TOPKAPI model has been successfully applied to numerous catchments of the countries in the world like Italy, Spain, France, Ukraine, China, South Africa, USA , and many more; in both small and large catchments including mountainous areas, sub-tropical climate regions and dry areas for various uses such as for flood prediction, for extreme

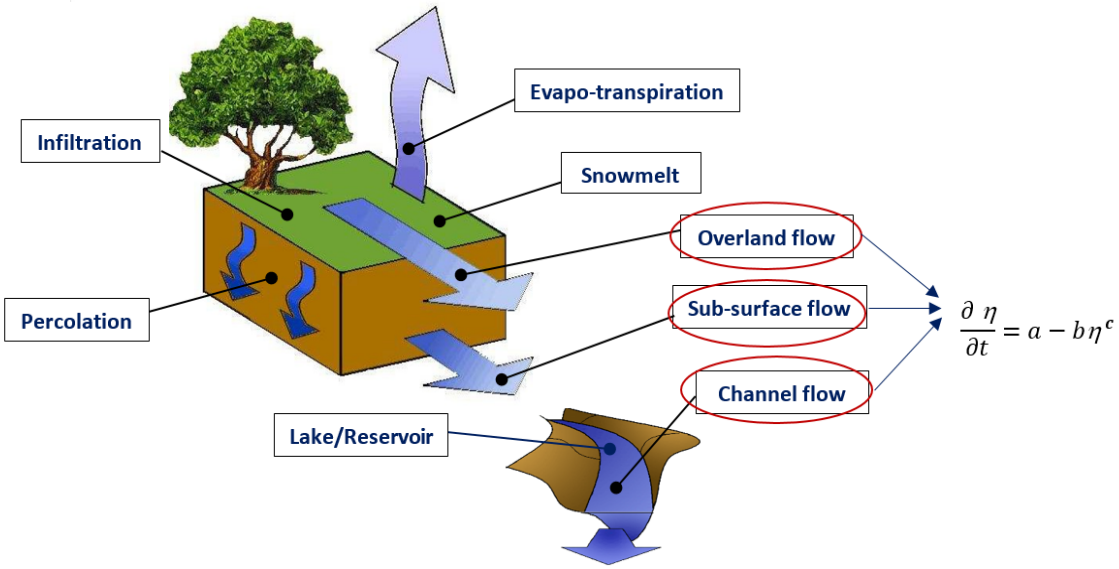

Figure 2.3: Schematic representation of the (Py)TOPKAPI model [152, 272]

flood investigation, and for forecasting hydrological response to land use/cover change caused by human activities [160, 283].

It is well known that most of the catchments in Ethiopia are ungauged and direct stream flow observations are not available at most sites for which rainfall–runoff modeling are required [22]. In this study, the TOPKAPI model, initially developed by Liu and Todini in 1995 [157, 160], is to be applied to Ethiopian catchments for which this critical review of the implementation of the model is required. It is the first attempt to implement the model in Ethiopia. The summarized details of the practical applications of the model to catchments of the world are presented below.

2.3.1 Review of Implementation of the (Py)TOPKAPI model

TOPKAPI hydrological model is a distributed physically-based hydrological model comprising of 5 main modules (Figure 2.3); namely soil, overland, channel, and evapotranspiration and snow modules [160]. The first three take the form of non-linear reservoirs regulating the horizontal flows (flow in the soil, flow over the land and flow in the channel). The model [59, 60, 156, 160] combines the kinematic wave models with the topography of the basin defined by means of a network of cells and then transfers the hydrological processes into three 'structurally-similar' zero-dimension non-linear reservoir equations. The non-linear reservoir equations are resulting from the integration in space of the non-linear kinematic models that represents the soil drainage, the flow over the land and the flow in the channel. The flow directions and slopes are estimated from the DEM in accordance with a neighborhood relationship derived from the principle of minimum energy, i.e, the maximum elevation difference. Due to the finite difference method underpinning the model, the active cell is supposed to be connected to a single downstream cell, while it can receive from up to three upstream contributing cells. Being a physically based model, the parameter values of the model are scale independent and are obtainable from DEM, soil type and land use maps [160].

Moreover, the TOPKAPI model meets most of the requirements of both operational and research hydrology in the sense that:

- It is a fully distributed model, and the dimension of the grid cell up to which the model is valid is 1 km

- It is physically-based: it clearly represents the hydrological processes based the fluid mechanics and soil physics, while the input parameters may be truly acquired from prevailing spatial datasets.
- There are comparatively few (about 15) input parameters of the model from which only three or four naturally need calibration [156, 160]

To sum up, the TOPKAPI model is structured into three main components [157] which represent the sub-surface, the overland and the channel flows components. These three essential components of the model can be articulated by non-linear kinematic wave equations and the integration in space of these equations results in three 'structurally-similar' non-linear reservoir equations in each grid cell [60, 147, 157, 161]. The model is a grid-based spatially distributed procedure in which all of its components are conceivably activated on an individual grid cell of the DEM [156, 157].

Various authors have informed that the TOPKAPI model is a promising tool for hydrological modeling. In this regard, Liu and Todini [160] conducted a case study aiming at demonstrating the suitability of TOPKAPI approach by applying the model on to the Upper Reno river basin of an area of 1051 km^2 at 200 m DEM grid scale. In addition, they implemented the model on the Arno river basin of an area of 8135 km^2 at 1000 m DEM grid scale for real-time flood forecasting in the catchment. Their results revealed that the model demonstrated good agreement between the recorded and the simulated catchment responses that encourages further usage of the model.

Liu et al. [156] performed a study of flood estimation on the upper Xixian catchment of the Huaihe river having an area of 1000km^2 in China and developed another version of TOPKAPI model in which inception, infiltration, percolation, ground water flow and lake/ reservoir routing were included. They lastly confirmed that the model performed well in predicting flood and low flows.

Vischel et al. [283] applied the TOPKAPI model to the Liebenbergsvlei catchment of an area of 4 625 km^2 in South Africa for the first time. In this application, they slightly modified the evapotranspiration module [157] and ignored the snow component as the influence of snow-falls on runoff is negligible in the Liebenbergsvlei catchment. Finally, they concluded that apart from obtaining good results in modeling the river discharges of Liebenbergsvlei catchment, the physical basis of the equations, the fine-scale representation of the spatial catchment features, the parsimonious parameterization linked to field/catchment information, the good computation time performance, the modularity of the processes, and the-ease-use-of the model make the TOPKAPI model a promising tool for hydrological modeling of catchments in South Africa.

Liu et al. [161] applied the TOPKAPI model on three flood prone sites in China to predict floods in those catchments. The case study sites are the upper Longmenzhen sub basin of Yihe River in Yellow River with an area of 5,318 km^2 found in a semi humid zone, the upper Xixian basin in Huaihe River having 10,000 km^2 area located in the humid zone and the Qingjiang basin in the upper Yangtze river of an area 15,500 km^2 located in an extremely humid zone. They tested the model on theses catchments at 1 km by 1 km grid scales and by varying 1 to 24 hours time steps. The results showed that the model achieved well in predicting floods for the time steps considered: hourly, 6 hourly, and daily and they finally concluded that the model is a wide-ranging ability for flood prediction applications. They also suggested that the model has a clear potential for flood forecasting in ungauged basins.

Peng et al. [197] conducted a study for assessing the quality of the general numerical algorithm of distributed TOPKAPI model by applying the model to the Buliu river basin in China, which has an

area of 3 310 km^2, at 1 km DEM grid resolution. They used a variable-step fourth-order Runge-Kutta algorithm numerical solution for TOPKAPI equations. The results show that the usage the mentioned algorithm for nonlinear reservoir equations has shown a good approximation of the flow in the soil, over the land, and in the channel, allowing for the retention of the physical properties of the original equations at finite scales ranging from a few meters to 1 km. In this method, the distribution of water mass over one grid cell is assumed uniform. When the grid scale is large, the variation of water storage in each grid cell cannot be ignored. This application has used a model with 1-Km-grid cell resolution; the scale is moderate for an assumption that the grid is uniform in space. They added that when the grid scale is large, it is necessary to use a new model structure that better corresponds to practical physical laws, or probe the solution of the above equation to set up the model.

Vischel et al. [282] conducted a case study comparing two independent procedures for assessing soil moisture at local level in a Liebenbergsvlei basin of an area of 4625 km^2 in South Africa. The first is from the TOPKAPI model and the second is from the European Remote Sensing (ERS). They compared the modeled humidity estimates of soil detection and calculating the soil Water Index (SWI) that is the soil moisture relative to the long depth of the soil. Since the satellite provides ground soil moisture (the first 5 cms), a conceptual infiltration model developed [290] estimates soil moisture from the detected surface to estimate a SWI. The results showed that the comparison between modeling and SWI remote sensor has shown good agreement with a regression coefficient of 0.678 to 0.923. Although a bias of about 19% has been detected, the dynamic behavior of soil moisture is very constant between the two approaches. Finally, they concluded that the two approaches are very promising for for assessing soil moisture in this region.

Amengual et al. [11] implemented two different hydrological models (HEC-HMS and TOPKAPI) over river Rino basin in Italy, measuring an area of 4,930 km^2 to analyze the performance of the two hydrological models. In this, firstly, stream-flow replications acquired by using rainfall input data were assessed. Then, the models were forced with rainfall forecast fields provided by mesoscale atmospheric model simulations to assess the dependability of the discharge forecasts resulting by the one-way coupling. In this application, the grid resolution of 500 m by 500 m was used. The result of the study indicated that the modelling results by TOPKAPI show quite alike with the recorded peak discharges. Furthermore, they observed that as TOPKAPI model is continuous promising run model,and that the lengthier is the calibration time used, the more reliable were the simulated flows.

The physically based and fully distributed TOPKAPI hydrological model was applied by Coccia et al. [60] to the Sierra Nevada basins within the DMIP 2 Project (the Distributed Hydrologic Model Intercomparison Project - Phase 2) on two river basins in USA: Carson River basin and American River basin. These two basins are quite dissimilar: Carson River basin is found at a high altitude and its hydrological condition is mainly affected by the snow melting process where as American River basin is located at lower altitude and has a more complex hydrological condition with numerous flood events throughout the year and snow melt is less significant. The simulation showed well the river behavior. However, in this application, a comparison of calibrated and non-calibrated simulations showed that the use of literature parameter values in the application of the model results in poor performance. This is mainly because of the low values of the soil conductivity. Because of this reason, flood events are always overestimated. Therefore, they suggested that it is reasonable to use the higher horizontal and vertical hydraulic conductivity values than those of literature. In addition, the comparison between the calibrated and calibrated model parameters for the two basins showed that the calibrated parameters are higher than the literature values. Therefore, they

concluded that it is often adequate to increase values such parameters without calibrating them to get rational outcomes.

Sinclair and Pegram [236] compared two independent soil moisture estimations over South Africa: the first is a Soil Saturation Index (SSI) obtained by automated real-time computations of the Py-TOPKAPI model, and the second is the remotely sensed ASCAT (Advanced Scatterometer instrument) Surface Soil Moisture product, temporally filtered to yield a Soil Wetness Index (SWI). They used "TRMM 3B42RT" product [274] for the rainfall forcing, while the ETo forcing is based up on a modification of the FAO56 reference crop ETo. They computed ETo by means of forecast fields of meteorological variables from the Unified Model (UM) runs done by the South African Weather Service (SAWS). They validated these ETo values comparing them with those obtained by means of observed data and the result was found to be unbiased with acceptable form. Using the rainfall and the ETo forcing data, the percent saturation of the TOPKAPI soil store was determined as an SSI for all of un-calibrated TOPKAPI model cells at 3 hours time-steps. These SSI values were then associated with the SWI values acquired from ASCAT. They lastly argued that the linear agreement in dynamic behavior for these independent soil moisture estimates proposes that both are suitably showing the soil moisture dynamics in South Africa, and could possibly be combined to produce a best estimate of soil moisture field.

Sinclair and Pegram [238] also carried out a study to extend the efficacy of the TOPKAPI model by adding the model of Green and Ampt [108] as the infiltration module because of the fact that the original TOPKAPI model [157] formulation does not contain an infiltration process and to make the model and source code freely available on the internet as PyTOPKAPI model. The key aim of their study was to find out the model input variables and parameters that have the major effect on the dynamics of the soil store as this information is very vital for model application in ungauged basins. They then examined the sensitivity of the PyTOPKAPI model to systematic bias in the variables rainfall and evapotranspiration, as well as the physically based soil properties that describe the model behavior by determining the model sensitivity at 7200 locations in South Africa, for a 2.5 year simulation period with a time-step of 3 hours. The outcomes show that the sensitivity of the model comes out to be a closely linear function of the forcing/parameter bias. They also stated that the model is robust to errors in forcing/parameters.

Ragettli and Pellicciotti [203] used the TOPKAPI model to examine the exchange between climate and glaciers in the upper Aconcagua River Basin of the Dry Andes in central Chile in the summer season. This study was also to detect the model parameters that are robust more dependent on calibration. They evaluated the parameters' transferability in time and space by applying the model at two spatial scales. They also tested the TOPKAPI model's capacity to simulate the relevant processes against the data. The model was finally applied effectively in the Dry Andes after its parameters were determined. They found a clear difference between parameters that are stable in time and those that need calibration.

Birsan [36] carried out the first effort to simulate streamflow in Romania using the TOPKAPI model. The model was applied to the upper basin of Someşul Mare having an area of 4328 km^2 for the period of 2000-2006. Precipitation and temperature data from 8 weather stations were used. The model was calibrated by trial-and-error procedure without losing the physically meaningful values of the model parameters. The result indicated that the model replicated the behavior of the catchment well. The author finally concluded that the modeling results were very satisfactory.

Sinclair and Pegram [240] currently introduced PyTOPKAPI package (BSD licensed -`http://`

opensource.org/licenses/bsd-3-clause/), which is an open-source BSD licensed implementation of the TOPKAPI hydrological model that can be operated on most popular operating systems. This PyTOPKAPI package includes tools to help in the extraction of model parameters from GIS data on soil properties, elevation and land-use characteristics in a semi-automated way. They also provided details on where to obtain the model source code, along with typical installation requirements. In addition, example code snippets are provided showing how easy it is to apply the PyTOPKAPI Python library for new modeling tasks. They also described the process of constructing new catchment models in detail.So, PyTOPKAPI is an open-source improvement of the earlier TOPKAPI model. The model code is freely available under an open source license at http://sahg.github.com/PyTOPKAPI/.

Liu et al. [161] also pointed out by examining the suitability of the TOPKAPI model and the possibility of using the model in ungauged basins by applying the model on three case study Chinese catchments. In this case, they verified that the TOPKAPI model performed well for flow reproduction. So, they lastly concluded that the model represents an all-inclusive hydro-local model, which offers a strong capability for predicting flood flows, and has shown fitness to use in ungauged catchments.

2.3.2 Results and Discussions

The above literature review showed that the (Py)TOPKAPI model is a distributed physically-based model that combines the continuity equation with the soil and surface dynamic equations, resulting in a set of three structurally similar nonlinear kinematic wave equations applied to the soil, the overland and the channel reservoirs within each cell. Its implementation is mainly based on elevation data (Digital Elevation Model) along with the information about catchment surface properties and land use. That is to mean, the model [157] uses a physical representation of catchment features. Thus, the required data for the application the model comprise the terrain or the DEM, the land use and the soil type data as well as the geographical coordinates along with the hydro meteorological data (such as rainfall, streamflow and evapo-transpiration). These data can be obtained from Internet and/or concerned local government agencies. The model can be used both as a separate program and inside real-time operative flood predicting systems. It is generally a powerful tool for: flood forecasting and flood studies, impact studies for changes in land use and climate, watershed management, and extreme value analysis for design purposes. Therefore, this review can be used as a quick reference for the application the PyTOPKAPI model in Ethiopia, which is the first application of the model on the Ethiopian catchments, as the performance of the model had already been confirmed in several catchments of the world. It is now to implement the model on Gilgel Ghibe catchment ($2943km^2$) of Omo-Ghibe Basin and Mojo catchment ($1496km^2$) of Awash Basin in Ethiopia.

2.3.3 Conclusion

PyTOPKAPI model is the improved version the earlier TOPKAPI model. TOPKAPI is the acronym of: TOPographic Kinematic APproximation and Integration and is a distributed physically-based model that combines the kinematic approaches with the topography of the basin and transmits the hydrological processes into three 'structurally-similar' zero-dimension non-linear reservoir equations representing different hydrological processes. A precise integration of these differential equations can fundamentally produce comparatively scale independent models that preserve the physical based meaning of the model parameters. The parameters of the PyTOPKAPI model are perceived to be scale independent and obtainable from DEM, soil type and land-use maps.

With the benefit of being a physically-based model by a simple and parsimonious parameterization, the PyTOPKAPI model can have several applications ranging from flood predicting, extreme flood investigation and forecasting hydrological response due to land use changes caused by human activities. This review has therefore, provided a significant knowledge and an understanding of the PyTOPKAPI model and its application to a research and operational hydrological processes. From this review, it can be concluded that PyTOPKAPI is a very promising hydrological model for modeling the river behavior of gauged and ungauged catchments in the following ways.

- Because of its simple and highly comprehensive reservoir structure, its parsimonious parameterization and the direct physical linkage between the catchment data and the model parameters, the PyTOPKAPI model is very easy to use.
- Combining the representation of the rapid flows associated with flash flood events and the fast computation time, PyTOPKAPI is a suitable tool for operational hydrology.
- The option to have predictions in ungauged inner parts of the basin is one of the benefits of the model.
- Additional advantage of the model is its capability to replicate streamflow in ungauged basins, using the parameters value obtainable from literature.
- Because of its "physically based", the parameters can be assigned according to field data obtained from in-situ measurements or remotely sensed data or literature.
- The configuration of the model is based on the connection of independent cell entities that allows the easy addition of external flows or some other hydrological processes that might alter the hydrological response of the catchment.

It is, in general, a useful tool for scientific and research hydrology. Nonetheless, good skills and experience on calibrating the model helps gaining better model efficiency when applied to ungauged catchments. In Summary, while using the PyTOPKAPI model one can:

1. Have reduced implementation times appropriate for the model calibration and real-time operational applications.
2. Easily calibrate the model due to the physically based meaning of the model parameters whose values might be gained from DEM, soil type grids, and land use maps.
3. Track the spatial variability of runoff conditions in the catchment getting flow predictions at any point of the channel network.
4. Fully make use of spatial variability in rainfall estimations from RADAR systems.
5. Resolve basin hydrologic feedback at very fine temporal (few minutes) and areal (100m-1000m) scales in both small and big basins.
6. Run the model at dis-similar scales, up to 24-hour time steps.

2.4 Overall Summary of Literature Review

The hydrological data available in Ethiopia is very limited. So, the procedures that can be applied for design flood estimation are consequently imprecise. For that reason, the above review of the design flood estimation methods was conducted to identify the gaps in the techniques presently used to estimate design floods and to determine further research needs with respect to the estimation of design floods. This is essential for fine-tuning and updating the existing design flood estimation methods in Ethiopia in order to keep up with the state-of-the-art of the design flood estimation methods. The review is in general important to looking for an alternative method of peak flood estimation and flood frequency analysis for the country. The overall summary of the above literature review thus showed very large gaps between the flood researches and the current design flood estimation practices in Ethiopia. Moreover, many Ethiopian rivers are totally ungauged. This situation limits the nation to manage its water resources and hinders early flood-warning systems resulting in massive socioeconomic damages. Due to this, rainfall-runoff models like PyTOPKAPI are crucial for simulating stream flows. The simulated stream flows would ultimately be used for flood frequency analysis and peak flood estimation in the region for water resources planning and flood risk management.

Chapter 3

The study area and Data

3.1 Description of the Study area

3.1.1 General

Ethiopia is found in North-East part of Africa in between 3^o and 15^o North latitude, 33^o, and 48^o East longitude. It is the 2^{nd} most populous nation in Africa with a population of about 86 million people [80] and the 9^{th} biggest in Africa having an area of 1.13 million km^2 of which 1.12 million km^2 (99.3 %) is land area and the remaining 7444 km^2 is water area (rivers, lakes, ponds etc.) It has 12 river basins with (Abbay, Tekeze, Awash, Wabi Shebele, Ogaden, Genale Dawa, Rift Vally, Omo Ghibe, Baro- Akobo, Mereb Gash, Aysha And Denakil) an annual total runoff volume of 122 Billion cubic meters (BM^3). Most of this water volume flows across to other countries; and only about 1% is utilized for power generation and 1.5% is used for irrigation. Presently, the hydrological network consists of around 560 gaging stations in those12 basins of which about 454 are functional [29]. The estimated renewable ground water potential of the country is nearly 2.6 BM^3 [179]. The country also has 3.73 Million hectares (Mha) of irrigable land from which only 4.3% of it has been developed. The aggregate hydropower capability of the country is assessed at 650 Terra Watt Hour (TWh)/year, out of which, around 160 TWh/year is technically and economically utilizable [20]. There is also various assortment of climatic, bio-physical and socio-economic settings in Ethiopia. The atmosphere changes from central rainforest in the south and southwest, which is depicted by overpowering precipitation and moisture to afro-high on the summits of the Semien and Bale mountains and dry areas of the Northeastern, Eastern and Southeastern marshes. Rainfall is the main source of Ethiopia's renewable water resources. The rainy season in the nation is concentrated in four months of the year (June - September) during which about 80% of the rains are received [141]. Average yearly precipitation of the nation is 848 mm, shifting from under 100 mm over the Afar lowlands in the northeast to 2,000 mm in the southwest highlands. However, rainfall in many areas of Ethiopia is highly erratic with very high rainfall intensity and extreme spatial and temporal variability [29]. Elevation gradient ranges from 125 metres below sea level (in Dallol depression) at which the temperature is greater than 60^0c to about 4620 metres above sea level (asl) at Ras Dajen-Semien mountains having icing temperature throughout the year [20]. The socioeconomic activities in the nation varies from booming industrial development and agribusiness in/around Metropolitan urban areas to moving ranchers and wandering pastoralists in the fringes. The allotment of infrastructures and amenities is also similarly very variable with a few sections of the nation modestly all around served and others barely reached.

The country is of great topographical assortment with high and rough mountains, level topped plateaus, deep gorges,, etched stream valleys, and undulating fields (**http://ethiopiamountain.**

com/topography/). The geophysical setting of the nation is dome fashioned nature of the panorama characterized through highlands within the center surrounded by the lowlands. Excessive rising mountain chains with flat and steep aspects are widely recognized features of the Ethiopian highlands. The lowlands are flat with common incision via gorges and valleys. The transition from highlands to lowlands may be very abrupt with sharp water falls. The basins of Ethiopia show a big elevation gradient with the very highest being inside the Danakil Basin except the Ogaden and Aysha Basins are totally located in the lowland areas. The Ethiopian Rift Valley that divided the highland plateau from Northeast to Southwest, which inclines from the center in the Northeasterly and Southwesterly path, is also accountable for presenting the Lakes Basin and defining the path of flows of some rivers that end in the Rift-Valley system. The upper basins of the Ethiopia are relatively endowed with a better rainfall exceeding evaporation and seepage and resulting in ample surface run-off that feed the neighboring lowland areas in all directions. The early settlement within the highlands associated with rapid population growth and general dependency on herbal sources in the basins, brought about the sever land degradation of the highland regions. The extensive range of topographic difference together with its climatic variety makes the variability in the country's land and water resources [30]. These complicated interactions between climate, biophysical and socio-economic situations led to excessive spatio-temporal variation of stream flow, huge amount turbidity, and outstanding capability water power generation in the highlands and irrigation development in the lowlands and sceneries along the most important gorges.

3.1.2 River Basins of Ethiopia

The land of Ethiopia is hydrologically divided into 12 basins, 8 of which are river basins, 1 lake basin and the remaining 3 are dry basins with no or minor flow out of the drainage system. Five basins (Omo-Ghibe, Awash, Rift-valley Lakes, Denakil and Aysha) are regarded as the Rift-valley basin because all of them feed the Great East African Rift-valley. Four basins (Abbay, BaroAkobo, Mereb and Tekeze) are part of Nile basin, flowing generally towards the west direction to Sudan and then ending in the Mediterranean Sea. The other three (Genale-Dawa, Wabishebelle and Ogaden) are part of the eastern Ethiopian basins that usually flow in the southeasterly direction towards Somalia. Nearly all the basins start flowing from the central ridges that separate the Rift Valley from the highlands of Ethiopia, to all directions out of the country. The map of Ethiopian river basins is shown in Figure 1.1. This study is concentrated on parts of Omo-Ghibe and Awash basins and these basins are briefly described hereunder.

3.1.3 Omo-Ghibe Basin

The Omo-Ghibe Basin is found in south western Ethiopia covering parts of the Southern Nations, Nationalities, and Peoples Region (SNNPR) and Oromia regional states. It has an area of 79,000 Km^2. The overall average yearly flow from the basin is about 16.6 BM^3. Its altitude ranges from 350m to 3610m amsl. With regard to the development potential of hydropower, it is the second largest, and is the basin within which most of the present hydropower construction is going on [20]. The highlands of this basin have cool to moderate temperature and sufficient rainfall while the lowlands have high temperature and low to medium rainfall. Yearly precipitation varies from 400 mm in the extreme south lowlands to 1900 mm in the highlands with the average being 1140 mm. The mean annual temperature in the basin varies from less than 17^0C in the west highlands to over 29^0C in the south lowlands. The soils in the highland areas of the basin are dominated by very deep red, and reddish-brown-clay-loam overlaying clays. The majority of these soils have moderate fertility and are very good for cultivation. The lowland soils are coarse textured with moderate to high fertility. The land use/land cover of the basin consists of fallow (29%), forestlands (14%),

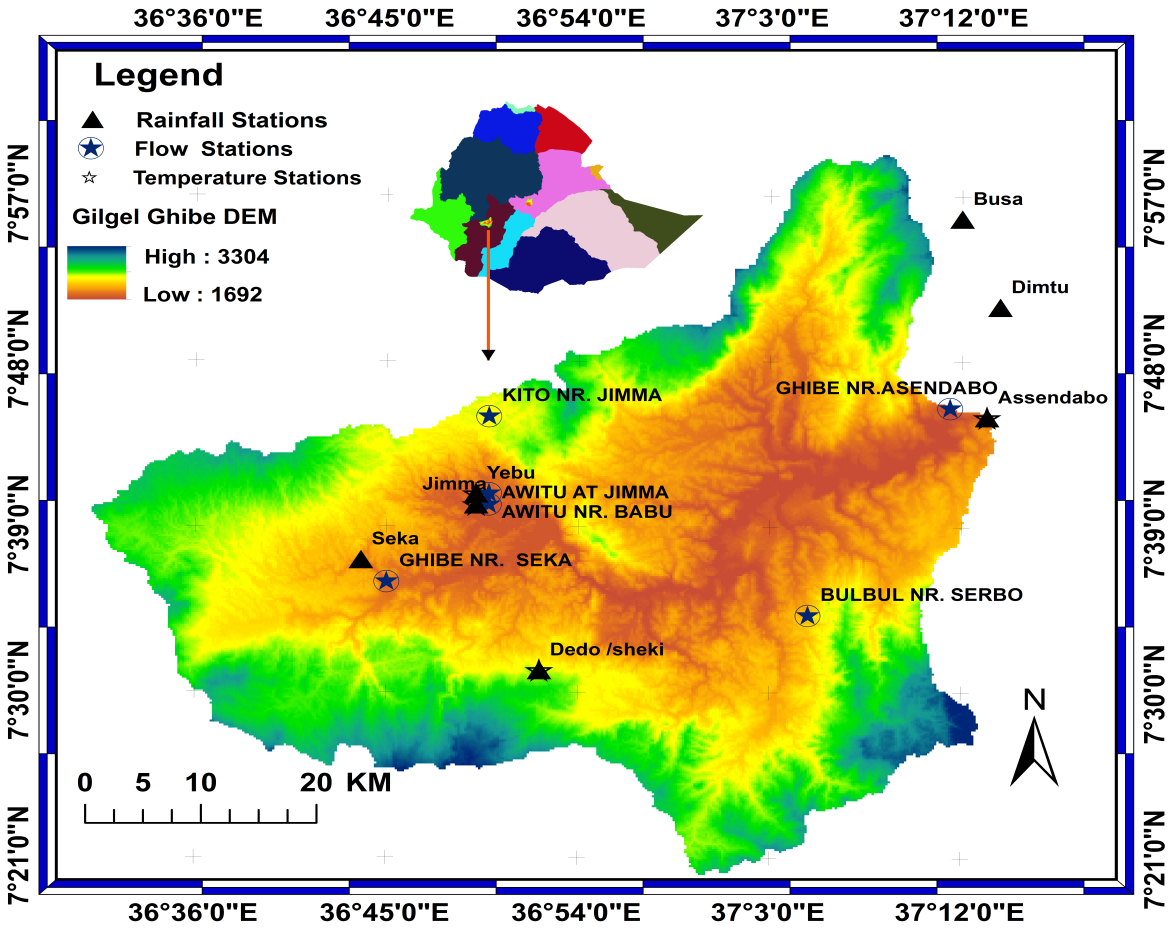

Figure 3.1: Location map of Gilgel Ghibe catchment for PyTOPKAPI model implementation

woodlands (29%), grasslands (15%), and bush and shrub lands (13%) [66].

The study area Gilgel Ghibe catchment (Figure 3.1) is a catchment of Gilgel Ghibe river (in Omo-Ghibe Basin), which feeds the Ghibe river that is found in southwest Ethiopia (**http://en.wikipedia.org/wiki/Gilgel_Gibe_River**). It is geographically located in between $7^0 20' 01.58"$N & $7^0 59' 15.32"$N latitudes; and $36^0 31' 04.91"$E & $37^0 13' 31.07"$E longitudes. It has a catchment area of about 2943 km^2, and is commonly characterized by high mountains having an average elevation of about 1700 m asl. The catchment is characterized by wet climate (sub-humid, warm to hot) with an average yearly precipitation of 1550 mm and average temperature of 19^0C. The precipitation pattern during the long rainy season is mono-modal rainfall pattern (June-September) which is called summer during which about 50-80% of annual rainfall totals are received. The main socio-economic undertakings in the catchment are plantation agriculture and cattle breeding [66].

3.1.4 Awash Basin

This is one of the major Ethiopian river basins having a total area of 112,696 km^2, of which about 64,000 km^2 drains to the main river. The remaining area drains to dry land in the locality and does not feed the main river course [20, 185]. The river basin has an elevation that ranges from the lowest 210m to the highest 4195m. The overall average yearly flow from the basin is estimated to

be about 4.92BM^3. It is 1,200 km long, 60 m wide and 1.2 m deep in the dry season [20]. The average yearly rainfall of the basin is in thr range of 1,600 mm at Ankober in the highlands and 160 mm at Asayita in the lowlands. The mean annual temperatures range from 20.8^0C at Koka to 29^0C at Dubti, with the maximum mean monthly temperatures at these stations happening in June, at 23.8^0C and 33.6^0C, respectively [185]. Of the total mean annual water resources of the Awash basin (4.9 BM^3), 3.85 BM^3 is currently utilizable, the balance being lost to Gedebassa swamp and elsewhere in the river system [185]. The land use condition in the basin includes mainly of cultivated agricultural land, grassland, and forestland, rural and urban settlements. It is estimated that 67% is intensively cultivated, 25.5% is moderately cultivated, 4.5% is bush land or shrub land or wooded grassland, and 3% is urban area and alpine vegetation [65]. Strictly speaking, the land use within the sub catchment is diverse. In the upper most part where there is high rainfall, land is used for cultivation. Steeper slopes are heavily wooded with natural acacia and eucalyptus. On the lower most part, however, rainfall is too unreliable and the sparse dry acacia scrub gives way to wide stretches of bare ground with clumps of coarse grass and occasional thickets of acacia. The soil-type grid in the study area is also variable. The most common soil types are Clay, Sand, Clay-Loam, Silt-Clay -Loam, Sand-Clay, Silt-Clay [65]. The net area currently commanded for irrigation schemes in the Upper, Middle, and Lower valleys of Awash basin is estimated to be about 69,000 hectars which is fairly distributed between the three zones, with slightly less in the Middle Valley. Cereals, e.g. teff, maize, wheat, barley are the most important agricultural output (80%) of the basin. The principal cash crops are coffee (grown mainly in the Awash valley), fruit and vegetables. Goats and camels dominate the livestock populations in the area [185].

Relatively, Awash basin is the most utilized basin in the country due to its strategic location, access roads, available good land and water resources. It has an estimated irrigation potential of 134,121 hectares [20]. However, the basin is highly vulnarable to flooding [65]. Presently, the government of Ethiopia has organized flood control administration to minimalize the flood risk in the basin. However, the problems associated with flood hazard are still prevailing in the area [174]. The study area covers the total area of 19,251 km^2 catchment located in upper and middle part of Awash River (Table 7.5) where flooding is common during the rainy season. On the other hand, extensive irrigated agriculture of the nation is concentrated alongside of the Awash basin. Irrigated agriculture is highly advanced in this river basin and is found in the flood zones on either side of the Awash River. During the floods, the water depth of the river rises up to 15 to 20 meters above low-water mark, thus submerging the plains for many miles along its both banks. Unlike many other Ethiopian rivers, the alluvial plains adjacent to the Awash River are relatively wide extending over 25 km (**http://en.wikipedia.org/wiki/Awash_River#cite_note-1**). This makes the river more vulnerable for flooding. Therefore, high economic loss occurs during flooding alongside this river for which this study should give due attention.

The other study area where PyTOPKAPI model was implemented in Awash basin is the Mojo river catchment (Figure 3.2). It was purposefully selected for this PyTOPKAPI model application as it is found in lower in elevation in dry climate. It is geographically located in central Ethiopia in between $8^0 36' 59.86" N$ and $9^0 04' 38.06" N$ latitudes and $38^0 54' 18.01"$ E and $39^0 17' 03.83" E$ longitudes having an area of 1496 km^2. The mean annual preciptation & temperature in the catchment are 959 mm & 19.73^0C. It is generally characterized by flat land with an undulation of some ridges and mountains around the eastern part of the catchment. The elevations of the catchment range in between 1777 m asl at Mojo town and 2903 m asl at the eastern part of the catchment. The catchment mainly comprises of cultivation of rain based cereal crops, livestock rearing and vegetables along ridges and banks of the river.

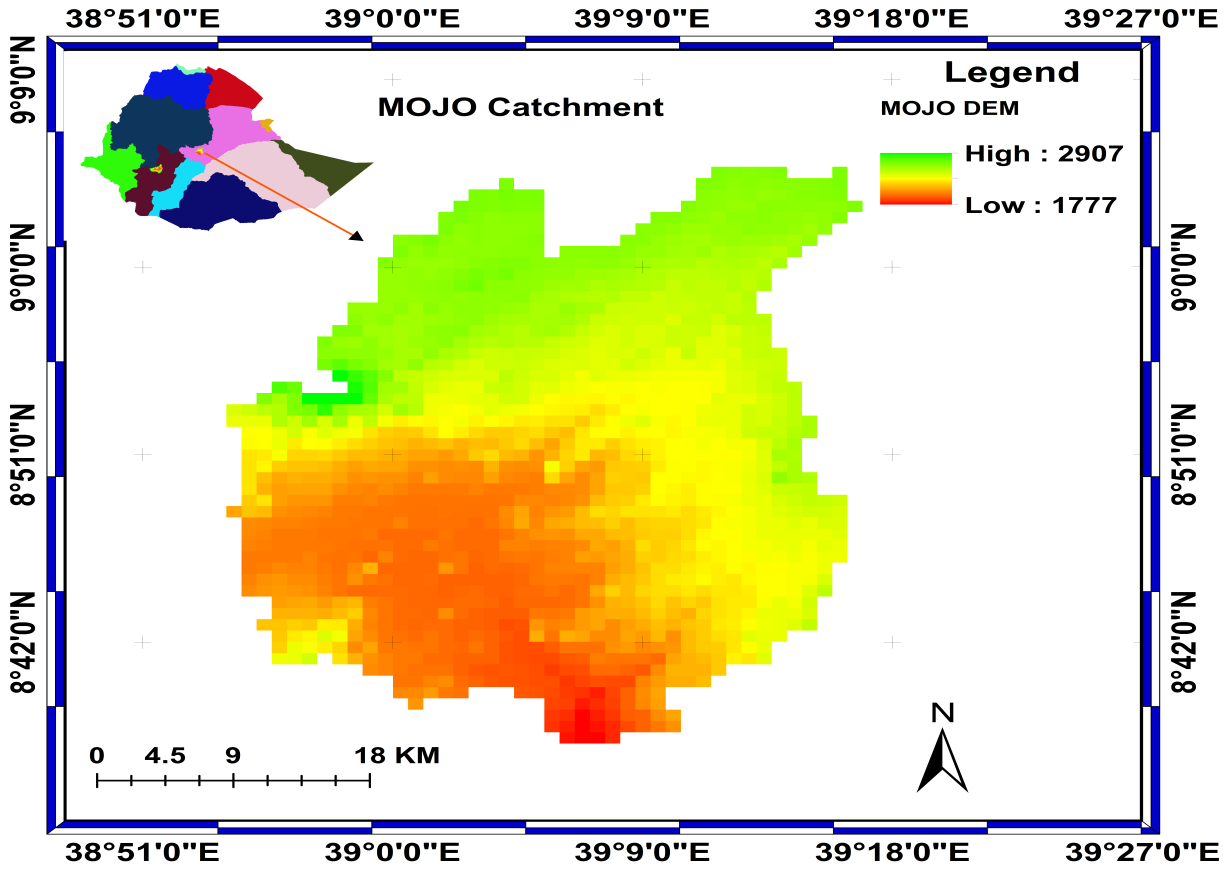

Figure 3.2: Location map of Mojo catchment for PyTOPKAPI model implementation

3.2 Data collection and Data processing

Complete and reliable data are required for this research work. These data include a hydrometeorological data, a soil type grid, a land cover, and a digital elevation data (DEM). These datasets were obtained from Ethiopian government agencies (Ethiopian National Meteorological Agency and Ministry of Water affairs) and were downloaded from internet. Description of each of them is as given below.

3.2.1 Hydrometeorological data

Hydrometeorological data are important for various water resouces applications such as hydrologic modeling, planning and designing of water resources projects, flood risk management, etc. The meterological data such as daily rainfall and temperatures were acquired from the Ethiopian National Meteorological Agency (ENMA) for the most important stations in and around the boundaries of the two river basins (Awash and Omo-Ghibe). Here, in Omo-Ghibe river basin, the rainfall data were obtained for 12 stations (Jimma, Limmu Genet, Sekoru Assendabo, Busa, Dimtu, Cheka, Kumbi, Meteso, Dedo-Sheki, Seka and Yebu) and the temperature data for 6 stations (Assendabo, Dedo Sheki, Jimma, Limu Genet, Sokoru and Yebu). In similar fashion, the streamflow information were collected from Ethiopian Ministry of Water affairs for 8 stations of Omo-Ghibe Basin (Gilgel Ghibe Nr Assendabo, Ghibe Nr. Seka, Aweitu Nr. Babu, Aweitu Nr. Jimma, Bulbul Nr. Serbo, Kitto Nr. Jimma, Bidru Awana Nr. Sekoru, and Ghibe Nr. Limu Genet) and for another 8 stations in Awash River catchment part (Akaki @ Melka Kuntire, Akaki, Mojo @ Mojo Village, Awash below Koka Dam,Berga Nr. Addis Alem,Holota Nr. Holota, Bello Nr. Guder and Teji Nr. Asgory).

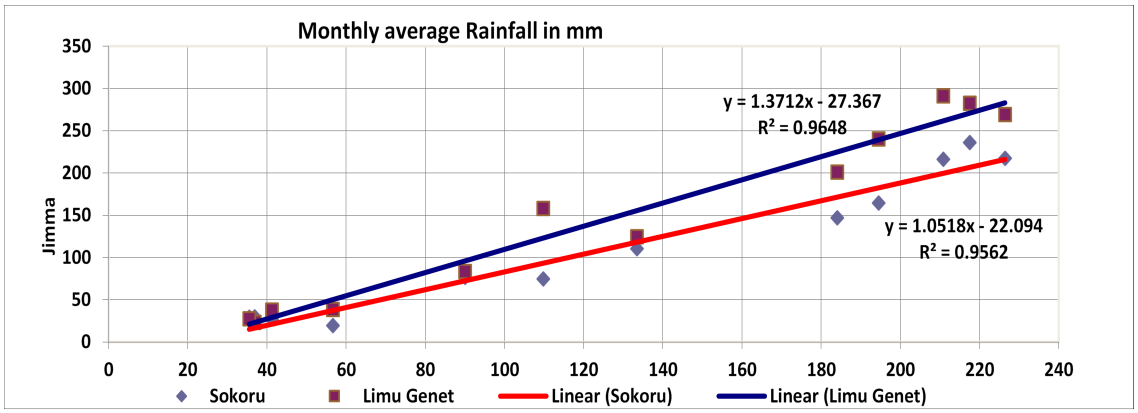

Figure 3.3: Sample: Rainfall-Rainfall relationship at Sekoru/Limu Genet and Jimma Stations

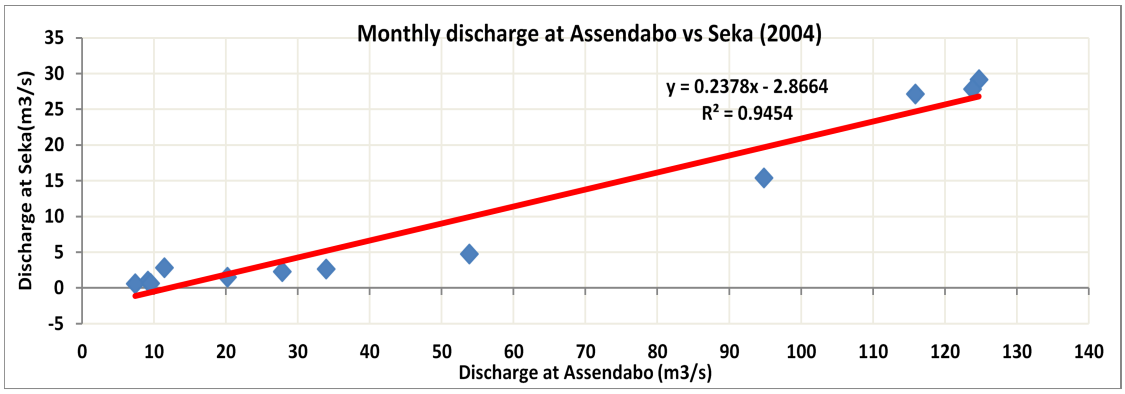

Figure 3.4: Sample: Discharge –Discharge relationship at Seka and Asendabo stations

3.2.1.1 Estimating the missing Hydrometeorological data

It was observed that there were some missing values in these hydro-meteorological data. The missed rainfall data were estimated by establishing linear regression equation between the station where missed data was seen and the other nearest station rainfall data. Here, the periods (years) with complete data set were chosen, and these data values were used to establish the regression equation between the stations. By using the established regression equation, the missed values the rainfall and the stream flow data were computed using the data of the corresponding station. The missed temperature data have been filled by taking the average of the data before and after the missed value. The sample linear regression equations used for estimating the missed rainfall data and discharge data are shown in Figures 3.3 and 3.4.

The bar graphs and the time series of the rainfall data at those 12 weather stations (Jimma, Limmu Genet, Sekoru Asendabo, Busa, Dimtu, Cheka, Kumbi, Meteso, Dedo-Sheki, Seka and Yebu); the temperature data at the 6 stations (Assendabo, Dedo Sheki, Jimma, Limu Genet, Sokoru and Yebu); and the stream flow data at the 8 flow gauging stations (Gilgel Ghibe Nr Assendabo, Ghibe Nr. Seka, Aweitu Nr. Babu, Aweitu Nr. Jimma, Bulbul Nr. Serbo, Kitto Nr. Jimma, Bidru Awana Nr. Sekoru, and Ghibe Nr. Limu Genet) in Omo-Ghibe river basin are given in Figures 3.5, 3.6, 3.7, 3.8 and 3.9. Similarly, the time series for the stream flow data at the 12 flow gauging stations (Akaki Melka Kuntire, Akaki, MojoMojo Village, Awash below Koka Dam, Berga Nr. Addis Alem, Holota Nr. Holota, Bello Nr. Guder and Teji Nr. Asgory) in Awash Basin is presented in Figure 3.10.

The monthly values of the rainfall data, the temperature data and the stream flow data at those

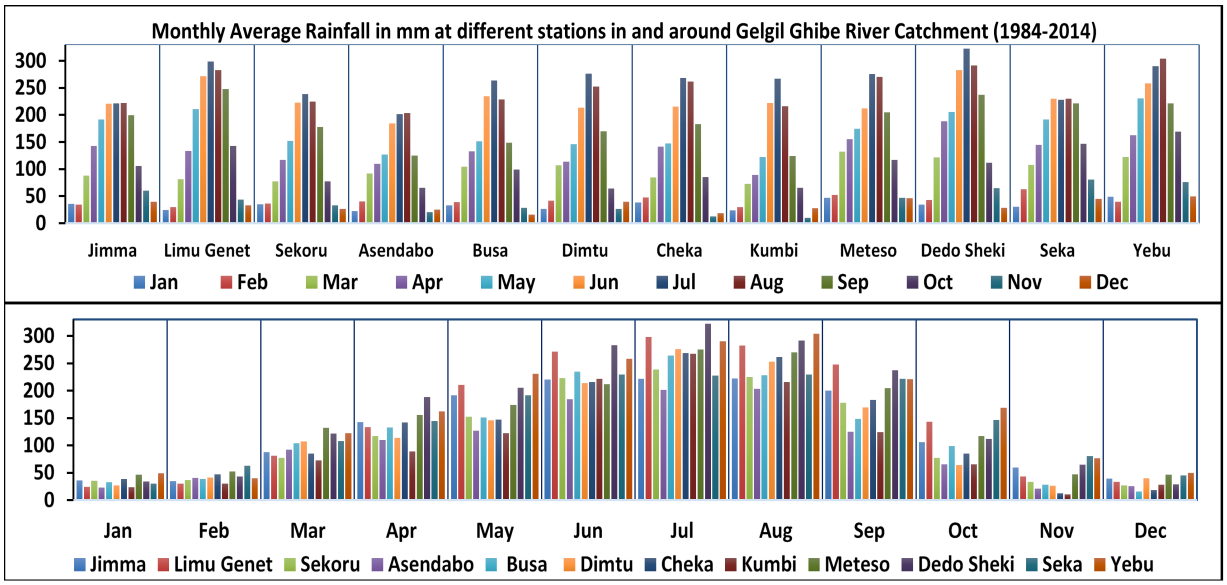

Figure 3.5: Rainfall (Bar graphs) at the stations in /around Gilgel Ghibe catchment.

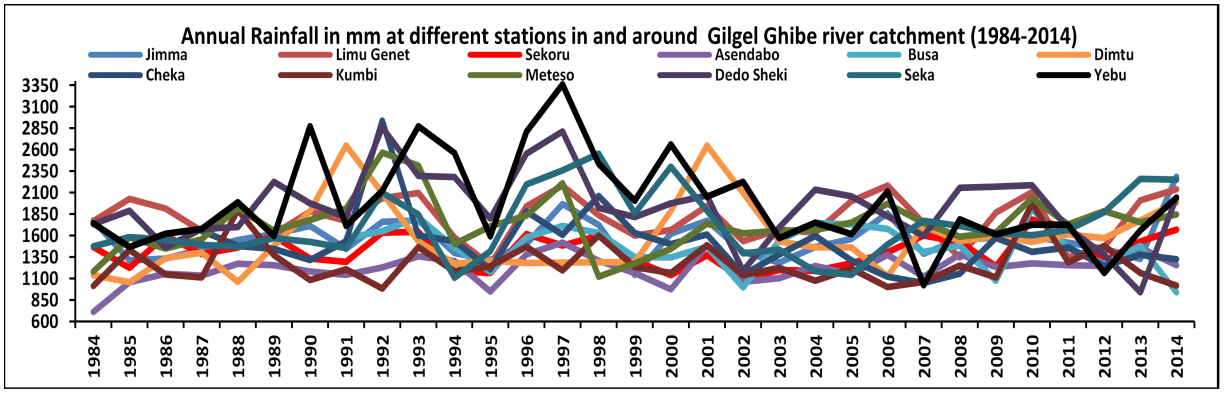

Figure 3.6: Time series of annual rainfall at 12 stations in /around Gilgel Ghibe catchment.

respective stations in Gilgel Ghibe catchment are given in Appendix A.1 (Tables A.1.1 - A.1.12), Appendix A.2 (Tables A.2.1 & A.2.2) and Appendix A.3 (Tables A.3.1 - A.3.8), respectively. The annual maximum discharge for the stations in the Gilgel Ghibe catchment and in the Awash catchment are presented in Appendix A.4 (Tables A.4.1 & A.4.2), respectively.

3.2.1.2 Asessment of the consistency of Hydrometeorological data

Meteorological data at a meteorological station administered over a period of numerous years might not be consistent, i.e, the dataset representing a particular meteorological factor might have a unexpected change in mean and variance compared to the original values. This situation may be because of a number of causes, some of which are connected to alterations in instrumentation and recording practices, and others are related to alterations of the site's environmental situations such as urbanization or, conversely, expansion of irrigation. Therefore, it is essential to put on a suitable procedure to assess if a specified dataset can be regarded consistent or not. In this case, double mass curve was used to check the consistency of the hydrometololgical datasets and some of the datasets were accordingly adjusted.

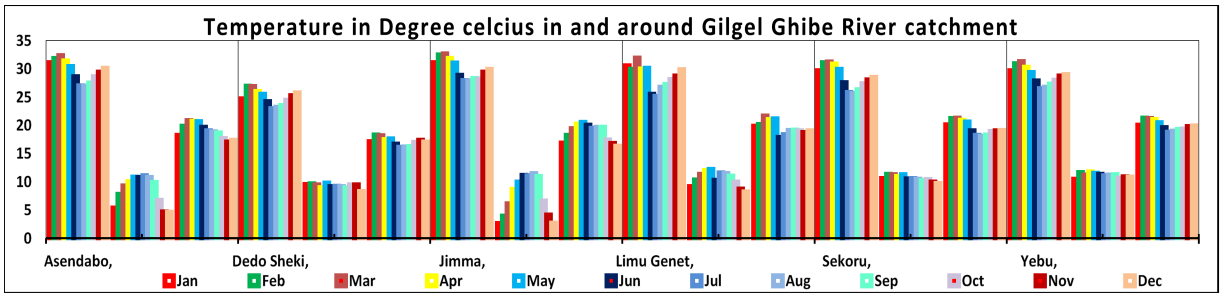

Figure 3.7: Temperature (max/min/average) at six stations in /around Gilgel Ghibe catchment.

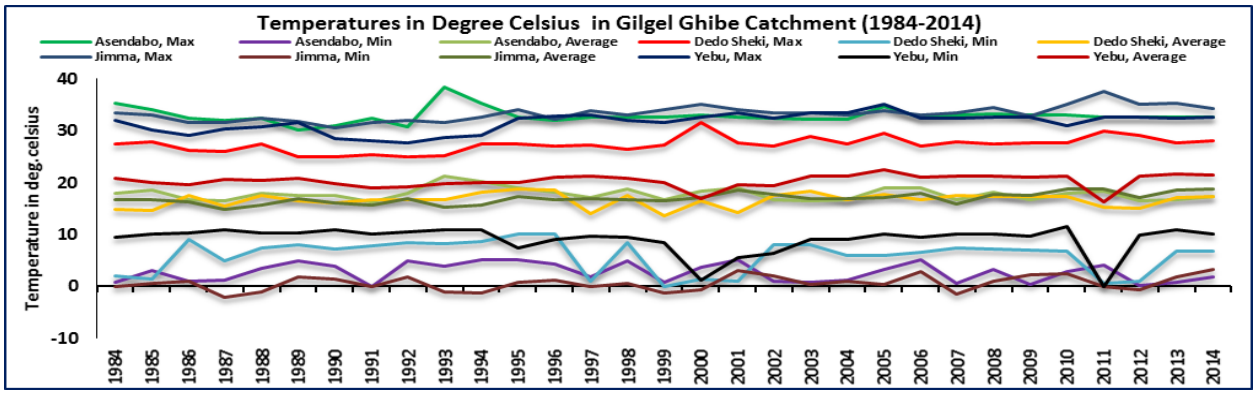

Figure 3.8: Time series of temperatures (Max /Min/Average) for stations in /around Gilgel Ghibe catchment.

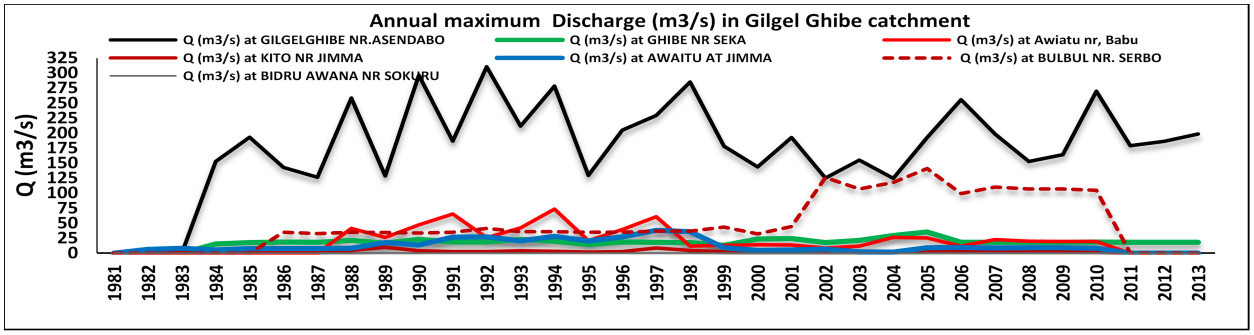

Figure 3.9: Stream flow time series for stations in /around Gilgel Ghibe catchment.

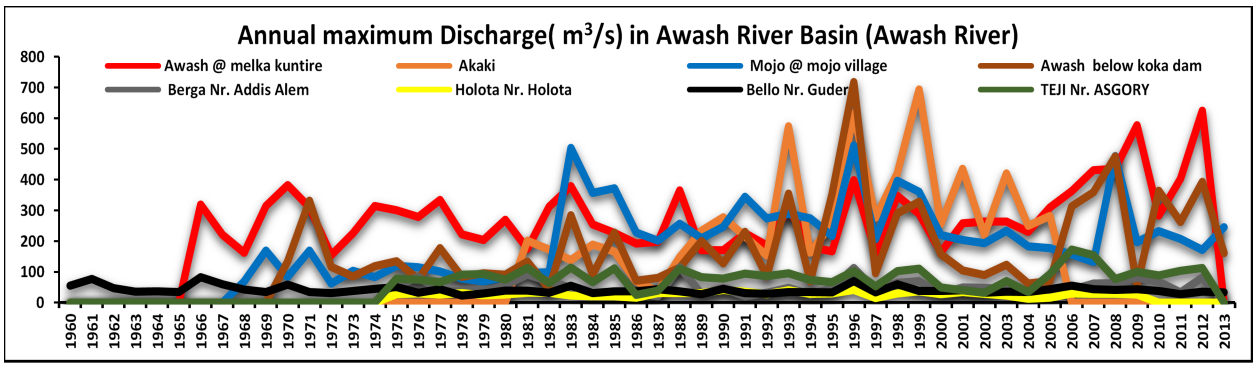

Figure 3.10: Time series for the streamflow data for stations in Awash River Basin.

3.2.2 Evapotranspiration Data

Evapotranspiration is the other essential data required for this research work. It is the amalgamation of evaporation from the land surface and transpiration from plants. Potential-evapotranspiration often refers to the evapotranspiration of a definite crop (ETr). The potential-evapotranspiration of a different crop (ETo) growing under identical situations as the benchmarked crop is determined by multiplying the evapotranspiration of the benchmarked crop (ETr) by crop coefficient Kc (0.2 <Kc <1.3) the value of which changes with the phase of growth of the crop. The actual evapotranspiration (ETa) is found by multiplying the potential evapotranspiration by a soil coefficient Ks (0 <Ks <1).

$$ETa = Ks * Kc * ETo \tag{3.1}$$

However, the evapotranspiration data was not obtained for the study area. The correlation equations developed for the purpose of estimating the monthly potential evapotranspiration (ETo) over the Awash and Rift Valley and Omo-Ghibe basins by Sileshi [234] [Appendix A.5 (Tables A.5.1 & A.5.2)] along with the methods of Bleney-Criddle [37] and Thornthwaite [268] were used to estimate the monthly ETo, from which ETa can be obtained.

3.2.3 Soil data

Recognizing the crucial necessity for a better-quality world soil data, in particular in the framework of the Convention on Climate Change and the Kyoto Protocol for soil carbon measurements, the Food and Agriculture Organization of the United Nations (FAO) and the International Institute for Applied Systems Analysis (IIASA) have taken the initiative to combine the lately composed huge sizes of regional and national updates of soil data with the data previously enclosed within the 1:5,000,000 scale FAO-UNESCO Digital Soil Map of the World, into a new wide-ranging Harmonized World Soil Database (HWSD). The European Soil Database (ESDB), the 1:1 million soil map of China, various regional SOTER databases (SOTWIS Database), and the Soil Map of the World are the four source databases that were used to compile the HWSD [84]. The synchronization and data encoding in a GIS was ascertained at IIASA and confirmed by all partners. The soil properties offered in HWSD were obtained from the examined soil profile data from several countries and sources. These variables (soil properties presented in HWSD) have been obtained in several laboratories in the world. The subsequent raster database contains of 21,600 rows and 43,200 columns that are connected to synchronized soil property data. The resulting digital online obtainable soil data will help soil scientists, managers, and other specialists in overcoming some of the shortages of data obtainability to address the problems related to food production and food safety and plan for innovative climate change problems and enhanced natural resources degradation [84]. Thus, we used the HWSD for obtaining soil data. It is a 30 arc-second raster database with over 16,000 dissimilar soil mapping units and composed of a raster image file and a linked attribute database. The grids contain the main soil texture class for each of the 13 standard soil layers by means of the USDA (US Department of Agriculture) soil texture category index by referring to the HWSD attribute table.

3.2.4 Land use Data

The land use classes of the study locality was acquired from the United States Geological Survey (USGS) Global Land Cover Characterization (GLCC) database (**http://edcsns17.cr.usgs.gov/glcc/glcc.html**) provided by Dr Karim Abbaspour of Eawng and made available on the WaterBase web site (www.waterbase.org). These maps are available in two spa-

tial resolutions, the original at approximately 400 meters (at the equator) and the resampled at 800 meters, for each continent/region. For this study, we used the first one (the 400m resolution) as it is relatively finer and more accurate.

3.2.5 Digital Elevation Model (DEM) data

Topography is fundamental for numerous earth surface processes. It is used for analyses of hydrology, agriculture, climatology, geology, geomorphology, ecology, etc. It can also be used as a means for clearing up of the processes and for predicting them via modeling. Understanding and processing of models therefore depends on the quality of the topographic data that are available. In hydrological modeling, finer-resolution DEM data is essential. Most countries have much of the surfaces covered by cartographic maps at different scales and different accuracies. In most humid countries, these maps are created through manual elucidation of stereo pairs of aerial photos, and in some cases the topographic data can be inaccurate or missing where cloud was present. With the commencement of satellite imagery covering the globe, various global datasets of topography have been produced, of progressively better resolution, from 10 arc-minutes (approximately 18 km at the equator) to 30 arc-seconds (approximately 1 km at the equator) using the United States Geological Survey (USGS) product, GTOPO30. This topography dataset was extensively used for almost a decade, essentially for broad scale assessments. However, the 1-km spatial resolution prohibited its use in modeling more detailed earth surface processes, particularly in fields such as hydrology, pedology, or small-scale geomorphology [133].

In 2003, the National Aeronautics and Space Administration (NASA) released the Shuttle Radar Topography Mission (SRTM) dataset for some areas, with 3 arc-second resolution for the world, and 1 arc-second for the United States. This huge leap forward in spatial resolution for DEMs with global coverage is likely to alter the way in which associated study can be accomplished and applied, bringing local catchment and sub-catchment scale modeling into the realm of worldwide applicability. The SRTM DEM which is obtained from (**http://srtm.csi.cgiar.org**) has a 90 by 90 m ground resolution [131, 133].

Jarvis et al [133] concluded by the study they conducted regarding usage of the SRTM DEM data in tropical areas comparing with DEM produced from cartographic data that the SRTM DEM can be more promising for hydrological modeling. But, improved outcomes may be expected by interpolating and then digitizing the cartographic data of scale 1:25,000 and below, if obtainable. Thus, the SRTM DEMs of the study catchments were used to obtain the physical features of the areas that are required for PyTOPKAPI modeling.

Chapter 4

Trend analysis of Hydrometeorological Data of Gilgel Ghibe catchment

4.1 General Summary

Trend analysis of hydro-meteorological data is vital for the proper water-resources management. This chapter examines the trends of the hydrometeorological data in Gilgel Ghibe catchment and whether or not they are significant. Daily rainfall, temperature and steam flow data of the stations in/nearby the catchment for a period longer than 25 years were analyzed to detect the variability and the changes in trend. The non parametric Mann-Kendall test was utilized for detection of the monotonic trends of the data series. The results show that on average, the rainfall exhibits a slight increasing tendency. We also observed that there is an increasing tendency in temperature in the study locality. The analysis of the stream flows indicated that only one station (Bulbul Nr. Sebo) showed a positive slope at 5% significance level. Two stations (Aweitu Nr. Babu and Ghibe Nr. Seka) revealed a slight increase in stream flow. Whereas the remaining 3 stations (Ghibe Nr. Assendabo, Aweitu at Jimma, and Kitto Nr. Jimma) indicated an infinitesimal decreasing trend in stream flow. The stream flow of the catchment in general showed insignificant decreasing tendency (0.007% per year) at its outlet.

4.2 Introduction

For a series of hydro-meteorological observations (rainfall, temperature or stream flow) over time, it is vital to know whether the values are increasing, decreasing, or remaining the same. For example, the knowledge of the rainfall behaviors especially its variability and trend are important for the proper water resources management [251]. The stream flow time series almost constantly show seasonality owing to the seasonality of rainfall and other meteorological variables [66]. It is also recognized to reproduce a combined reaction of the total catchment while rainfall can be used as one of the key input into the run-off developments. Trend analysis of the hydrometerological data thus provides evidence that shows such variability and trends. It can also indicate the extent of the apparent components such as trends, jumps and seasonality in hydro-climatic variables. It is comprehensively employed to evaluate the probable effects of climate change and irregularity on streamflow data in numerous zones of the globe for the past decades.

A lot of researches have been conducted for detection significant tendencies in hydro-meteorological data in several tropical and temperate regions. In this case, the widely used non parametric Mann–Kendall trend test was employed to detect the trends of those hydro-meteorological time

series. Few of them are the rainfall and the temperature trends in the upper and middle parts of the Ganga basin in northern India [148], the seasonal rainfall trend in peninsula Malaysia [260], the trend in rainfall data for Ipoh, Perak conducted by Hashim et al. in 2010 [70], the trend in extreme precipitation indices in order to estimate the impacts of global climate change on the water source area of the middle route of South-North Water Transfer Project [314], the spatio-temporal trend of precipitation in Iran [251], the trends of the Canadian stream flows [46, 306], the trends of stream flows in western Britain [72], the trends and variability of rainfall series at Seonath River basin in Chhattisgarh in India [51], the temperature trends variation over the northern and southern part of Bangeladesh [183], the trends in the mean surface air temperatures over the southern parts of Ontario Quebec in Canada [181], the trends of pre-monsoon precipitation in Nepal [77], the trends in the spatio-temporal variation of the air temperature, precipitation and runoff in Xinjiang in China [155], the trend of pre-monsoon rainfall data for western India [182], the trend of the Assam precipitation variation in India [106], the relationship between hydro-climatic trends and their impacts on water resources in Italian and Swiss Alps [15], the trend analysis of streamflow in Turkey [138], the long term meteorological trends in the Indus Basin of Pakistan [5], the precipitation trend in the Upper Tennessee Valley in the vicinity of Chattanooga [130], the trends in hydro-climatic variables in the Wei River Basin in China [312], the rainfall trend in the Onkaparinga catchment in South Australia [209], the precipitation trend of in Slovakia [308], the spatial and temporal trends of precipitation and temperature in eastern India [232], the temporal trend in the mean of flood peaks in Quebec in Canada [93], the rainfall trends and their fluctuations over time in northern Bangladesh [24], the trends in Japanese precipitation [301], the long-term tendency of the hydrological data series (temperatures, rainfall, and stream flows) in the Tarim River basin, west China [300] and the trends of the hydro-climatic variables in the Te^t River in the South of France [163]. These are few of the recent studies.

This chapter thus examines and evaluates the trends of the hydro-meteorological data in the Gilgel Ghibe catchment to see if the data is following some trend, if the trend is increasing or decreasing with time and if or not they are significant. It determines the rate of that change (if any), with respect to some principal value of the distribution such as the average or the middle value. The non parametric Mann-Kendall test, which had been commonly employed to detect monotonic trends in series of environmental data, climate data or hydrological data, was used. Non-parametric tests are generally distribution-free. They are very valuable since most hydrometeorological time series are not normally distributed [55].The purpose of the test is to test for monotonic trend with the concept that the null hypothesis: H_0 is rejected indicating that the data come from a population with independent realizations and are identically distributed. The alternative hypothesis, H_A, is that the data follow a monotonic trend. That is to say, if H_0 is rejected at a specified significant level, we conclude that there is a monotonic trend in data over time. In this study, daily rainfall, temperature and steam flow data of the stations in/nearby Gilgel Ghibe catchment have been collected and aggregated into monthly annual totals and then were assessed to detect the variability and the changes in trend.

4.3 Methodology

4.3.1 Mann-Kendall test

The non-parametric Mann-Kendall (MK) test is the widely used test for detection of the anticipated trends in different fields of research including hydrology and climatology [14, 94, 115, 3 10]. It is used for identifying trends in hydro-climatic data. Every data value is compared with all subsequent data values. It is a simple test for trend and as such, it is not dependent upon: the size of

data, assumptions of distribution (does not have to have a normal / bell shape distribution), missing data or haphazardly spaced observing periods. It helps assess if a data series shows an increasing or a decreasing trend at a specified significance level. [48].

Alternatively, Seasonal Kendall (SK) test for trend [120] was established by the U.S. Geological Survey (USGS) in the 1980s to study trends in surface-water quality all over the USA. It uses the Mann-Kendall (MK) trend examination for different seasons of the year, where season is defined by the user. It then combines the separate results into one overall test for if the dependent (Y) variable changes constantly over time [118]. Since then, it has become the mostly utilized test for trends in environmental engineering and has been applied for variety of realted purposes in numerous dissimilar spaces. The applications of this test have encompassed tests for tendency in biologic community structure, estuarine salinity , lake water quality and atmospheric chemistry (Cortes and Hites, 2000) [118].

So, the Seasonal Kendall test [120] considers for seasonality by determining the Mann-Kendall test for each of m seasons (in our case, m denotes months) distinctly, and then uniting the results in to one general form. This means that January data are associated only with January, February month is with February merely, etc. No associations are made crosswise the seasons or the months [66]. The statistical Kendall S measures the monotonic dependence of Y on T and is determined by equation 4.1.

$$S = P\text{-}M \tag{4.1}$$

where P = the no. of times the $Y^{'}$s rise as T's rise; M = the no. of times the $Y^{'}$s fall as the $T^{'}$s rise. When S is a big positive number, later measured values tend to be bigger than former values and a rising trend is showed. When S is a big negative number, later values tend to be less than former values and a descending tendency is specified. When the value of S is insignificant, no trend is showed. But, it is necessary to check if the trend is significantly different from zero or not. Taking the variable Y, (in our case rainfall, temperature and stream flow) and time T, S is determined with the use of the equation (4.1) and considering that there are $\frac{n(n-1)}{2}$ possible comparisons for n data pairs. If the entire Y values increase with the T values, $S = \frac{n(n-1)}{2}$, in which case the coefficient of correlation τ should be equal +1. Whereas, if the entire Y values decrease with rising T, $S = \frac{n(n-1)}{2}$ and the τ shall be equal -1. Thus, by dividing S by $\frac{n(n-1)}{2}$ shall provide a value commonly falling between -1 and +1. This is known to be the tau (τ) value quantifying the power of the monotonic association between two variables. Hence the definition of tau (τ) is:

$$\tau = \frac{S}{\left(\frac{n(n-1)}{2}\right)} \tag{4.2}$$

where: S is Kendall overall statistics, n = number of data. If the number of years of records is adequately big (>25), the Z value may be compared to standard normal tables for testing a statistically significant trend [172]. The pattern of S can therefore, be estimated well by a normal distribution procedure with expectation (μ_S) equal to the sum of the individual S_i, and variance equal to the sum of their variances. S is standardized using Equations (4.3) and the outcome, Z_S, is compared with a table of the standard normal curve [115].

$$Z_S = \begin{cases} \frac{S\text{-}1}{\sigma_s}, \text{if S >0} \\ \frac{S+1}{\sigma_s}, \text{if S <0} \\ 0, \text{if S = 0} \end{cases} \tag{4.3}$$

where: the variance σ_s^2 is given by,

$$\sigma_s^2 = \frac{n(n-1)(2n+5) - \sum_{j=1}^{p} t_j(t_j-1)(2t_j+5)}{18} \tag{4.4}$$

where, p is the no. of the tied groups in the data and t_j is the size in the j^{th} tied group.

For sample size < 10, the S test can be employed and for sample size ≥ 10, the normal approximation can be applied [269]. Now, it is to investigate the null hypothesis of no trend, H_O, i.e. the recorded data Y_i are randomly ordered in time, against the alternate hypothesis, H_A, where there may be some monotonic trend at a specified significance level, α (say 0.001, 0.01, 0.05 or 0.1). For example, α = 0.001 indicates that there may be a 0.1 % probability that the values Y_i are from a random sample and that the presence of a monotonic trend is very likely [55, 269].

The existence of a statistically significant trend is assessed by means of the value of Z_S . A (+) or a (-) value of Z_S specifies a rising or (a falling) trend. The Z_S has a normal distribution. To investigate for a rising or (a falling) monotone trend at α significance level, H_O is rejected if the Z_S value is more than $Z_{1-\frac{\alpha}{2}}$, where $Z_{1-\frac{\alpha}{2}}$ is obtained from the table of standard normal curve. If a significant trend is acquired, the rate of change can also be measured with the use of the Sen's slope approximate [269].

4.3.2 Sen's method

To evaluate the slope of a prevailing trend, the Sen's non-parametric technique was utilized [269]. That is to mean:

$$f(t) = Qt + B \tag{4.5}$$

where Q is the required slope and B is a linear constant .

To find out Q in expression (4.5), we should first compute the slopes of all data pairs. Here, if there are n values x_j in the data series, we get as many as $N = \frac{n(n-1)}{2}$ slope Q_i. The Sen's slope is the medium of these N values of Q_i. The N values of Q_i are arranged in ascending order of magnitude and the Sen's slope is;

$$Q = \begin{cases} Q_{\frac{(N+1)}{2}}, \text{if N is odd} \\ \frac{1}{2}(Q_{\frac{N}{2}} + Q_{\frac{N+2}{2}}), \text{if N is even} \end{cases} \tag{4.6}$$

The confidence limits of the median slope were determined at α =0.05, with the use of the two-sided confidence limit about the slope estimate. For larger data size, the critical value $Z_{1-\frac{\alpha}{2}}$ from a table of standard normal curve gives the upper and lower ranked values of the slopes corresponding to the end values of the confidence limit [48, 66, 269]. The value of Z at α =0.05 is 1.96. Using Equation (4.7), Ml and Mu are calculated as [52];

$$Ml = \frac{(N\text{-}1.96\sigma_s)}{2} \tag{4.7}$$

$$Mu = \frac{(N + 1.96\sigma_s)}{2} \tag{4.8}$$

where: N is the over-all number of slope approximations, and σ_s as given in equations (4.3). The upper and lower limits of the confidence interval of the slope are the Ml^{th} and the $(Mu+1)^{th}$.

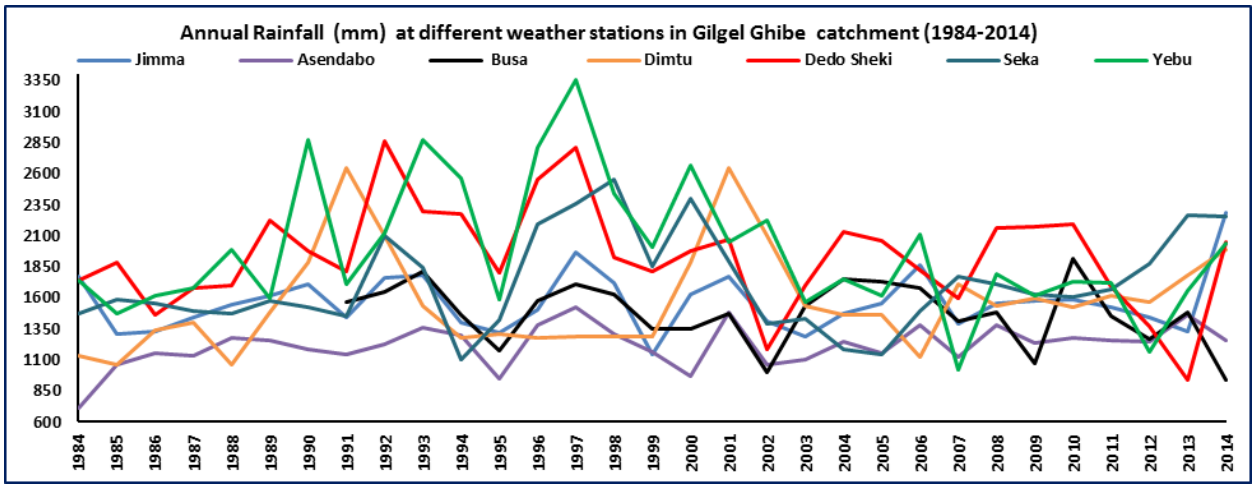

Figure 4.1: Time series for rainfall data

In this study, the MAKESENS tools were used to detect the trends in data [269]. The values of Kendall's tau, the Kendall score(S), its variance and its two-sided p-value along with alpha value are displayed. These values are computed separately for each month and each year at each station. The MAKESENS technique calculates the confidence limits at two dissimilar significance levels: α= 0.05 & α= 0.01 [48].

In the beginning we compute [52],

$$C_\alpha = (Z_{1-\frac{\alpha}{2}})\sigma_s \tag{4.9}$$

where σ_s is as in equations (4.3), and $Z_{1-\frac{\alpha}{2}}$ is found from the standard normal table. Then after, $M1 = \frac{(N-C_\alpha)}{2}$ and $M2 = \frac{(N+C_\alpha)}{2}$ are determined. The lower and upper confidence limits, Q_{min} & Q_{max}, are the $M1^{th}$ biggest and the $(M2+1)^{th}$ biggest of the N ordered slope estimates Q_i. If M2 is not a whole number, the upper limit is interpolated. Similarly, if M1 is not a whole number, the lower limit is interpolated.

To obtain the value of the linear constant B in equation (4.5), the n values of differences x_i - Q_{ti} are determined. The meddle of the values offers an estimation of B [269]. The estimations of B for lines of the 99% and 95% confidence limits are computed following the same steps.

4.4 Results and Discussion

4.4.1 Trend analysis of rainfall

Daily preciptation data of seven (7) stations in/nearby Gilgel Ghibe catchment have been summed into monthly and annual totals. Here, the daily rainfall data of Jimma, Asendabo, Dimtu, DedoSheki, Seka & Yebu stations for the period 1984-2014 were used. Likewise, the available rainfall data for the period of 1991-2014 for BUSA rainfall station was utilized. The data of the yearly rainfall of those stations is shown by Figure 4.1. The trend analysis of rainfall was carried out and the results of the assessment are presented in Table 4.1 and by their successive graphical representations as indicated in Figures 4.2 and 4.3. The summary of the true slopes of the existing trend (change per year) for annual rainfall data of seven stations in Gilgel Ghibe Catchment estimated by the Sen's non-parametric method was also shown in Table 4.2.

Table 4.1: Summaried results of trend test for rainfall data

Station/ years	Mean (mm)	STD (mm)	tau	MKS (S)	Var (S)	p- value	Alpha	Z	Sen's slope	Trend	Statis. signif
Jimma (1984-2014)	2288.0	1562.0	0.0	19	666.3	0.50	0.05	0.31	1.089	Increase	No
Assendabo(1984-2014)	1217.3	166.8	0.2	115	1785.5	0.007	0.05	1.94	5.668	Increase	Yes
Busa (1991-2014)	1478.2	252.5	-0.2	-52	1625.3	0.206	0.05	-1.27	-9.999	Decrease	No
Dimtu (1984-2014)	1576.6	401.2	0.3	140	4299.2	0.034	0.05	2.36	15.412	Increase	Yes
DedoSheki(1984-2014)	1932.9	414.1	0.0	-19	3461.7	0.76	0.05	-0.31	-2.053	Decrease	No
Seka (1984-2014)	1718.2	378.8	0.2	77	6606.3	0.35	0.05	1.29	7.517	Increase	No
Yebu (1984-2014)	1419.7	193.2	-0.1	-55	2763.3	0.304	0.05	-0.92	-6.85	Decrease	No

Table 4.2: Summary of the true slopes of the existing trend for rainfall data

Station/ years	Obs (years)	Mean (mm)	Std.dev (mm)	Sen's slope	B in Sen's Equation	Change per year (%)	Status
Jimma (1984-2014)	31	2288.0	1562.0	1.089	1524.77	0.071	Increase
Assendabo (1984-2014)	31	1217.3	166.8	5.668	1129.60	0.502	Increase
Busa (1991-2014)	24	1478.2	252.5	-9.999	1641.00	-0.609	Decrease
Dimtu (1984-2014)	31	1576.6	401.2	15.412	1197.30	1.287	Increase
DedoSheki (1984-2014)	31	1932.9	414.1	-2.053	1951.14	-0.105	Decrease
Seka (1984-2014)	31	1718.2	378.8	7.517	1532.10	0.491	Increase
Yebu (1984-2014)	31	1419.7	193.2	-6.850	1908.90	-0.359	Decrease

The results show that, out of the 7 rainfall stations, 2 stations (Asendabo and Dimtu) showed an increasing trend at 5% significance level. The remaining 5 stations (Jimma, DedoSheki, Seka, Yebu and BusaA) did not show any significant trend at 5% significance level. But, stations Jimma and Seka exhibited a slight increment in trend whereas stations DedoSheki, Yebu and Busa showed a decreasing trend. Generally, the Gilgel Gibe river catchment has been receiving more or less an increasing magnitude of annual rainfall though not significant. This finding, which is based on rainfall data of few stations, is in agreement with other studies conducted at the national level in Ethiopia. For example, Africa Climate Change Resilience Alliance (ACCRA) report [4] and McSweeney et al. [170] specified that there is no a statistically substantial trend in observed mean precipitation in any season in Ethiopia between 1960 and 2006. Similarly, Cheung te al (2008) concluded in their study that, in the nationwide and basin-level investigation, neither the basins nor the nation was found to be facing any major changes with yearly precipitation for the time period covered by their study [66].

4.4.2 Trend analysis of temperature

By the same token, the yearly average monthly maximum/minimum temperatures as well as average annual temperature data of Asendabo, DedoSheki, Jimma, & Yebu weather stations for the period of 1984-2014 were analyzed for trend. The time series of the temperatures (Maximum /Minimum/Average) at those stations is indicated (Figure 4.4) and the results of the trend analysis is also presented in Table 4.3 & by the successive graphical representations of the results of trend analysis (Figure 4.5). The summary of the true slopes of the existing trend (change per year) for average annual temperature data of those four stations estimated by the Sen's non-parametric method was also presented in Table 4.4.

Trend analysis for temperature data by the Mann Kendall method indicates that the temperatures (maximum, minimum annual average) at Jimma station, the annual average temperature at Yebu

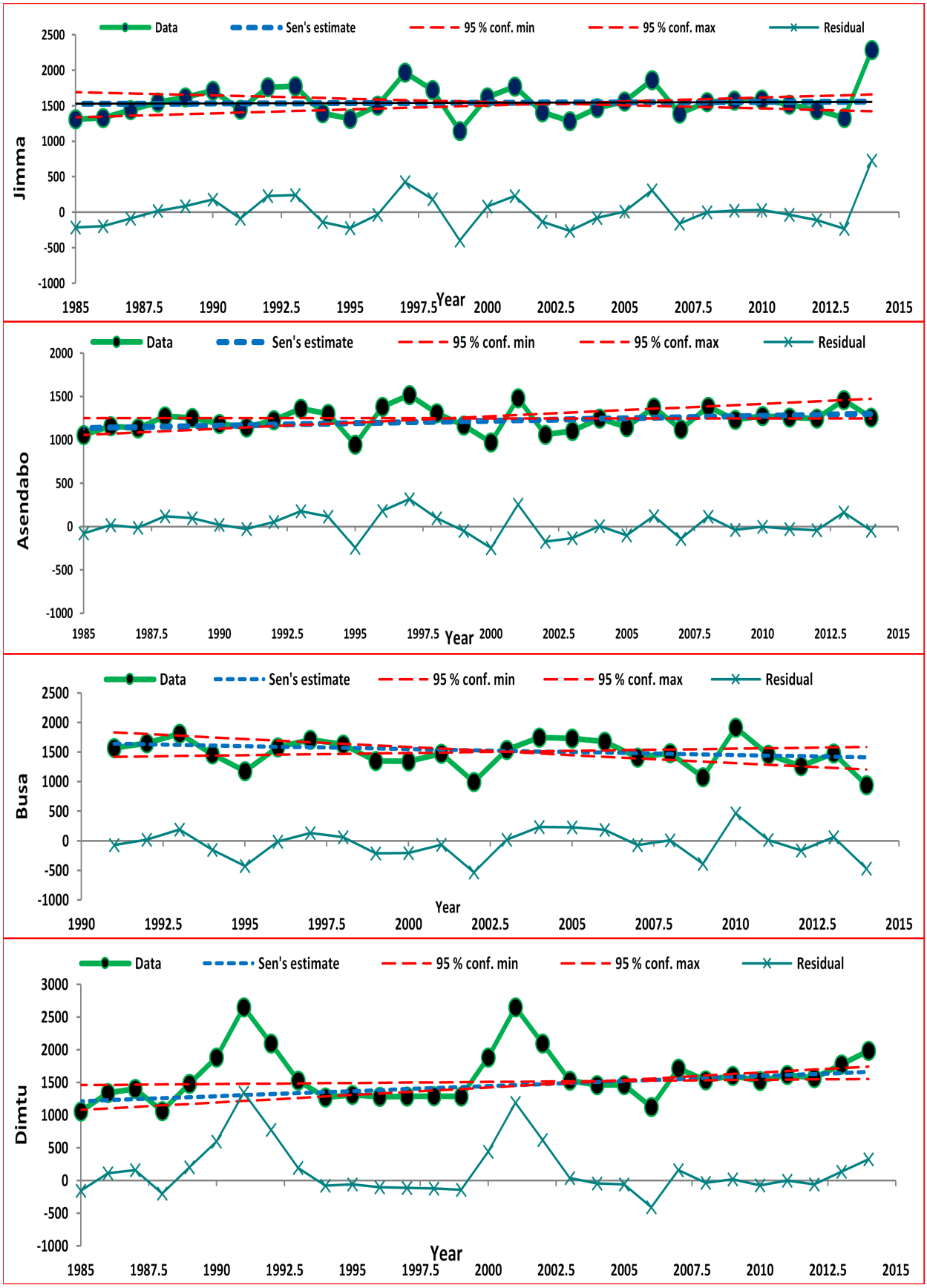

Figure 4.2: Graphical representations of trend analysis for rainfall data (Plate 1)

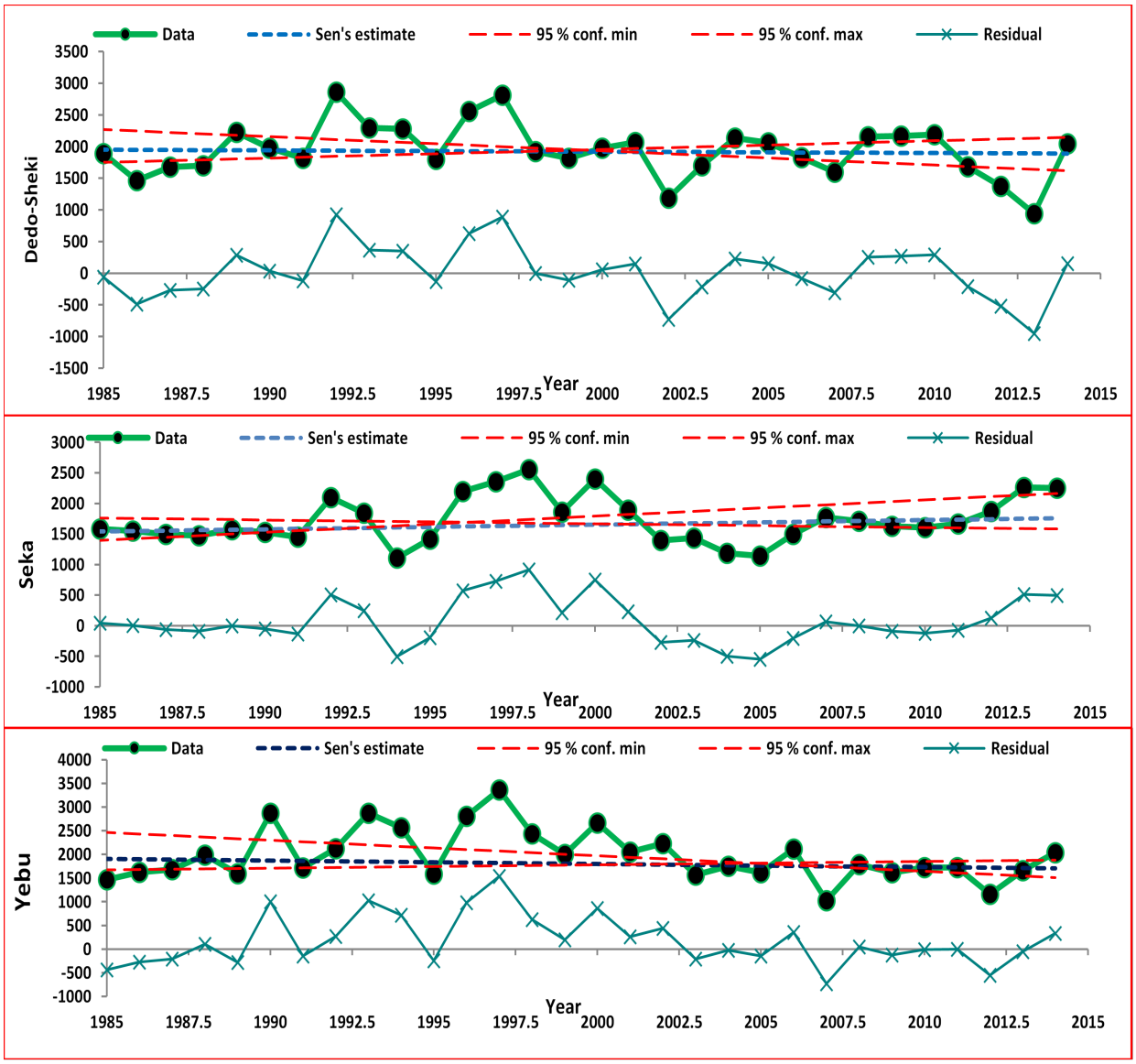

Figure 4.3: Graphical representations of trend analysis for rainfall data (Plate 2)

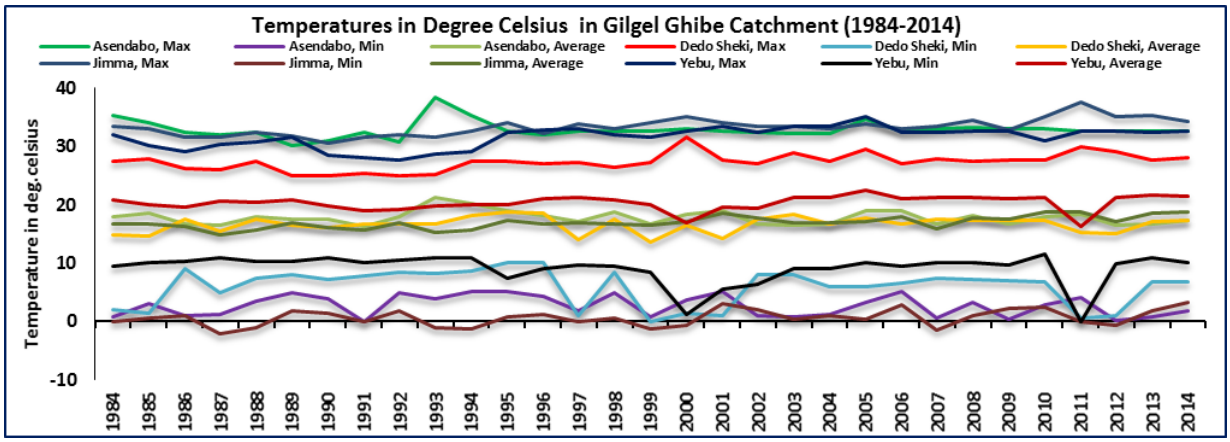

Figure 4.4: Time series for temperatures (Maximum /Minimum/Average)

Table 4.3: Summaried results of trend test for temperatures

Station/years	Variable	Mean (^{0}C)	St.dev (^{0}C)	tau	MKs (S)	Var(S)	p-value	Alpha	Z	Sen's slope	Trend	Statis. signif
Asendabo (1984-2014)	Average	19.0	0.6	-0.1	-53	6484.1	0.500	0.05	-0.90	-0.008	Decrease	No
	Min	8.4	1.3	-0.1	-58	6756.0	0.500	0.05	-1.00	-0.034	Decrease	No
	Max	29.5	0.5	0.3	150	3460.7	0.000	0.05	2.50	0.035	Increase	Yes
DedoSheki (1984-2014)	Average	17.0	0.9	0.2	85	5684.0	0.300	0.05	1.43	0.025	Increase	No
	Min	9.2	1.7	-0.1	-39	3459.7	0.500	0.05	-0.65	-0.009	Decrease	No
	Max	24.9	0.8	0.2	80	4377.0	0.200	0.05	1.34	0.024	Increase	No
Jimma (1984-2014)	Average	18.6	0.5	0.6	270	5826.6	0.000	0.05	4.57	0.046	Increase	Yes
	Min	7.4	0.8	0.4	175	3461.7	0.003	0.05	2.96	0.049	Increase	Yes
	Max	29.9	0.6	0.4	187	5913.8	0.016	0.05	3.16	0.045	Increase	Yes
Yebu (1987-2014)	Average	20.4	1.3	0.4	179	3461.7	0.000	0.05	2.64	0.038	Increase	Yes
	Min	9.1	2.6	0.00	15	2498.6	0.800	0.05	0.92	0.074	Increase	No
	Max	31.60	1.8	0.4	169	7759.9	0.100	0.05	3.14	0.089	Increase	No

Table 4.4: Summary of the true slopes of the existing trend for temperatures

Station/years	Obs (years)	Mean (^{0}C)	Std.dev (^{0}C)	Sen's slope	B in Sen's Equation	Change per year (%)	Status
Asendabo (1984-2014)	31	19.00	0.60	-0.008	18.98	-0.04	Decrease
DedoSheki (1984-2014)	31	17.00	0.90	0.025	16.77	0.15	Increase
Jimma (1984-2014)	31	18.60	0.50	0.046	17.82	0.26	Increase
Yebu (1987-2014)	31	20.35	1.29	0.038	20.19	0.19	Increase

station and the maximum temperature at Asendabo station show an increasing trend at 5% significance level. In addition, the annual average & the maximum temperatures at Dedo Sheki station, the temperatures (maximum minimum) at Yebu station indicate an increasing trend though they are not substantial at 5% significance level. Similarly, the minimum and annual average temperatures at Asendabo station, and the minimum temperature at Dedo Sheki station show an immaterial decreasing trend at 5% significance level. Generally, there is a rising tendency in temperature in the study area. McSweeney et al. [170] also confirmed that the average yearly temperature in Ethiopia has rised by 1.3^0C from 1960 to 2006, with the average increment rate of 0.28^0C per decade. The increment in temperature in Ethiopia has been most prompt in the months of July, August and September ('JAS'), which was @ a rate of 0.32^0C per decade. The national picture regarding climate change in Ethiopia also indicate that a range of studies of national climate trends since the 1960s show that mean yearly temperatures in Ethiopia have rised by between 0.5^0Cand 1.3^0C [4].

4.4.3 Trend analysis of stream flows

Likewise, the stream flow data at six (6) gauging stations (Ghibe Nr. Assendabo, Ghibe Nr. Seka, Aweitu Nr. Babu, Aweitu at Jimma, Bulbul Nr. Serbo and Kitto Nr. Jimma) in the catchment were analyzed for trends. Figure 4.5 shows the time series of the annual maximum (AM) discharge in

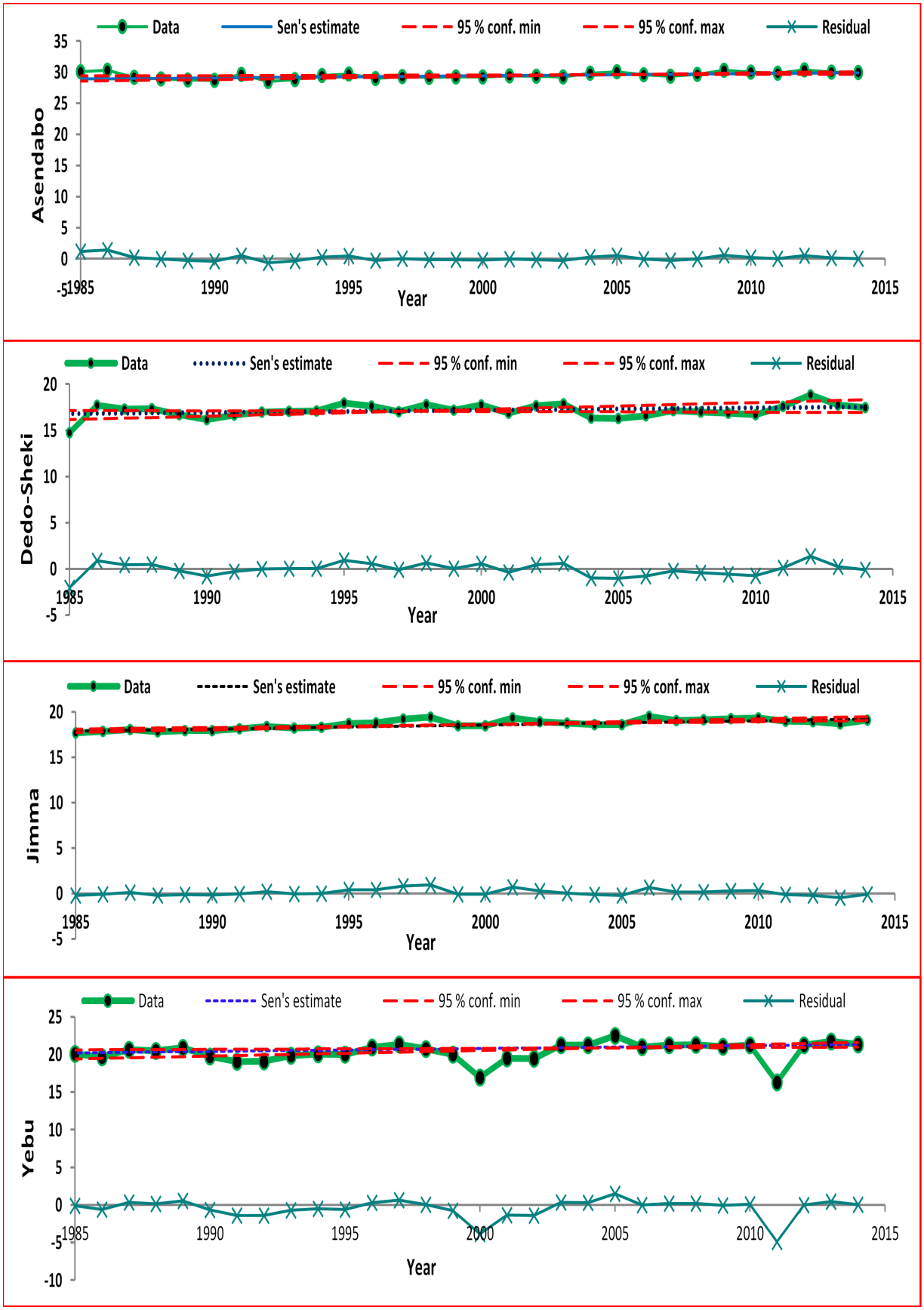

Figure 4.5: Graphical representations of trend analysis for temperatures

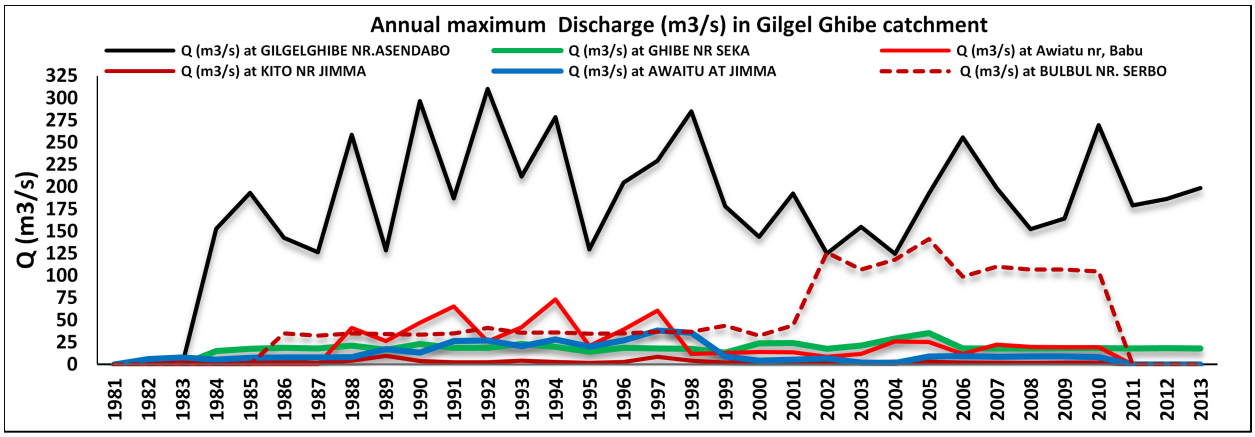

Figure 4.6: Time series for stream flows

Table 4.5: Summaried results of the trend test for stream flows

Station/ years	Mean (m^3/s)	St.dev (m^3/s)	tau	MKS (S)	Var (S)	p- value	Alpha	Z	Sen's slope	Trend	Statis. signif
GhibeNrAssendabo(1984-2013)	195.0	55.4	0.2	-36	3068.2	0.186	0.05	-0.02	-0.013	Decrease	No
GhibeNrSeka(1984-2013)	19.6	4.3	0.2	46	18.7	0.897	0.05	0.68	0.026	Increase	No
AweituNrBabu(1988-2010)	26.8	22.5	0.4	44	491.3	0.056	0.05	0.81	7.132	Increase	No
Aweitu@Jimma(1982-2010)	13.9	10.9	0.0	-6	5502.6	0.946	0.05	-0.12	-0.044	Decrease	No
BulbulNrSerbo(1986-2010)	51.7	37.8	0.6	102	1632.7	0.012	0.05	3.28	1.108	Increase	Yes
KittoNrJimma(1982-2010)	3.5	2.0	0.0	-8	429.3	0.735	0.05	-0.18	-0.011	Decrease	No

m^3/s at those gauging stations. The summary of the trend test results by the Mann Kendall method for AM stream flows are given in Table 4.5 and by the subsequent graphical representations of the results of trend analysis (Figure 4.7). The summary of the true slopes of the prevailing trend (change per year) for the AM stream flow data of the six stations estimated by the Sen's method was also specified in Table 4.6.

The results of the trend assessment of the stream flows highlighted that only one station (Bulbul Nr. Serbo) showed a positive slope at 5% significance level which is a jump. Two Stations (Aweitu Nr. Babu and Ghibe Nr. Seka) indicated a slight increment in streamflow. This could be due to the increment of rainfall over the catchment as explained earlier. In addition, the increase in recorded temperature experienced in the catchment could not significantly reduce the surface water due to evaporation. Other activities, such as river water abstractions/diversions for agricultural purposes that could possibly reduce the stream flow amounts are not so significant within and around the catchment. Whereas, the remaining 3 stations (Ghibe Nr Assendabo, Aweitu at Jimma and Kitto Nr. Jimma) indicated a very little decreasing trend. The changes in stream flow records might be on account of land use change besides the annual and seasonal distribution of rainfall. However, impact of landuse alteration on stream flow in the catchment is not considered in this study.

4.5 Conclusion and Recommendation

The issue of trend assessment in hydrometrological data has received a pronounced attention recently, particularly in association with the expected alterations in worldwide climate [115]. The knowledge of the precipitation behaviors especially the variability and trends are vital for the prop-

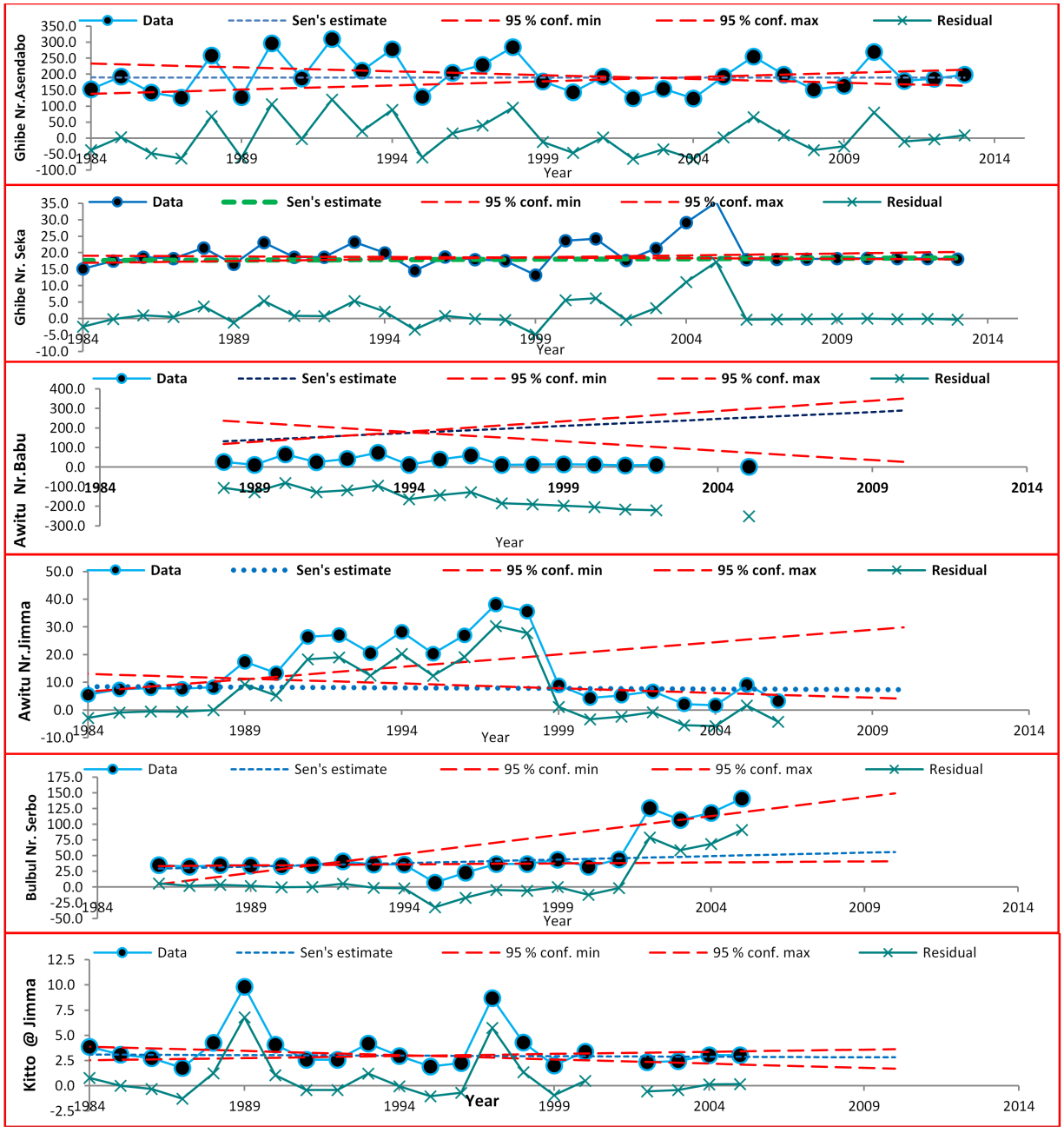

Figure 4.7: Graphical representations of trend analysis for stream flows

Table 4.6: Summary of the true slopes of the existing trend for stream flows

Station/ years	Obs (years)	Mean (m^3/s)	Std.dev (m^3/s)	Sen's slope	B in Sen's Equation	Change per year (%)	Status
GhibeNrAssendabo(1984-2013)	30	195.0	55.4	-0.013	189.85	-0.007	Decrease
GhibeNrSeka(1984-2013)	30	19.6	4.3	0.026	17.61	0.150	Increase
AweituNrBabu(1988-2010)	23	26.8	22.5	7.132	131.84	5.410	Increase
Aweitu@Jimma(1982-2010)	29	13.9	10.9	-0.044	8.53	-0.516	Decrease
BulbulNrSerbo(1986-2010)	25	51.7	37.8	1.108	29.25	3.788	Increase
KittoNrJimma(1982-2010)	29	3.5	2.0	-0.011	3.11	-0.353	Decrease

erly designing water related structures for which estimation of design flood is required. Time series examination may illustrate the extent of the apparent elements such as trends, jumps and seasonality of such hydro-climatic information. The hydrologic data series virtually constantly show seasonality due to the periodicity [165] of the weather in that climatic variability, which is replicated in hydrologic data, can unfavorably impact trend test outcomes [115]. This study examines the trends of the hydrometeorological data in Gilgel Ghibe catchment and whether or not they are significant. Daily rainfall, temperature and stream flow data of the stations in/nearby the catchment for a period longer than 25 years were analyzed to detect the variability and the changes in trend by using the non parametric Mann-Kendall test. The outcomes of the investigation showed that there is minor increasing trend in annual precipitation data in the study area. However, the results indicate no significant trend in monthly and seasonal rainfall data. In general, on average, the rainfall data series shows a slight increasing tendency in the study catchment. But, the stream flow shows an infinitesimal decreasing tendency (0.007% per year) at the outlet (Ghibe Nr. Asendabo gauging station). An increasing trend in temperature was observed in the study area as well. The results of this study are also in agreement with the study conducted earlier in Ethiopia [170] which confirmed that the mean yearly temperature in Ethiopia has rised by 1.3^0C in between 1960 and 2006, at an average increment rate of 0.28^0C per decade. The results of trend change in general were insignificant. Similar results could also be obtained for the other catchment/basin (Mojo). Although, the Mann-Kendall method that uses skewed, cyclic and serially interrelated data was employed to examine the extents of trend, better quality lengthier data series is suggested for a more reliable indication of the presence and the extents of the trend.

Chapter 5

Implementation of PyTOPKAPI Model in Ethiopia

5.1 General Summary

Rainfall–runoff models are valuable tools for water resources management. They are mostly physically based distributed and are used for forecasting and understanding of hydrological processes of a catchment/basin. For example, given precipitation data, the models can estimate flow at the outlet of a river basin. The PyTOPKAPI (Python based TOPographic Kinematic APproximation and Integration) model, an improved version of the earlier TOPKAPI model, is a physically based fully-distributed rainfall-runoff model which combines the kinematic wave approaches with the topography of the basin and transmits the hydrological processes into three kinematic non-linear-reservoir wave models applied to the flows in the soil, over the land and in the channel system. The present study demonstrates the practical implementation of the PyTOPKAPI model on two case study Ethiopian (Gilgel Ghibe and Mojo) catchments to test its suitability for simulating stream flows from the catchments. It also outlines the physical processes captured in the model to address the issue of stream flow simulation at the specified catchments presenting the details of the application of the model to the Gilgel Ghibe catchment ($2943km^2$) and the Mojo catchment ($1496km^2$) in Ethiopia. In this work, the physical basis of the model, the fine-scale representation of the spatial catchment features, the parsimonious parameterization linked to field/catchment information, the good computation time performance, and finally the good results obtained from simulation, made the PyTOPKAPI model a promising tool for forecasting stream flows from the catchments. This is the first effort to put the model into practice in Ethiopia.

5.2 Introduction

The development of a new rainfall-run-off model has arisen by gathering information regarding the hydrological modeling, and matching them with the different growing needs both in the applied research and operational fields [59, 156]. Such models are valuable tools for hydrological investigation, water resources engineering and ecological applications [169]. PyTOPKAPI model is one of such models that has been employed to numerous catchments of the world for diffrent uses like flood prediction, extreme flood investigation, and forecasting of hydrological response under altered landscape situations caused by human activities since its advent in 1995 [160, 283]. It has now been applied to the catchments in Ethiopia (Gilgel Ghibe and Mojo catchments). These two catchments are geographically located in different hydrological regimes: the Gilgel Ghibe catchment (Figure 3.1) is found at a high altitude in wet zone while the Mojo catchment (Figure

3.2) is located in areas that is relatively lower in elevation. The reviewed literatures regarding the practical implementation of the (Py)TOPKAPI model in numerious catchments of world (section 2.3) was the entry point to apply the model on Ethiopian catchments. This chapter then presents the main structure of the model, its principle and physical concepts as well as the realistic application of the model for simulating stream flows in Ethiopia.

5.3 Description of the PyTOPKAPI model

The PyTOPKAPI model is an improved version of the earlier TOPKAPI model [239, 240]. TOPKAPI is the acronym of: TOPographic Kinematic APproximation and Integration and is a distributed physically-based model implementable at different spatial scale, ranging from the hill slope to the basin scale without missing the physically based meaning of the model parameters. The model is developed based on the combination of a kinematic assumptions of flows in the soil, over the land and in the channel [59], and resulted in converting the rainfall-runoff processes into three 'structurally-similar' zero-dimension non-linear reservoir differential equations describing the dissimilar hydrological processes [160]. The model parameterization is relatively simple and parsimonious [160, 161]. Moreover, the model parameters are scale independent obtainable from DEM, soil type & land use maps [160].

The fundamental assumptions of the (Py)TOPKAPI model are [157, 160]:

1. Precipitation is constant over the domain cell in space and time. This assumption simply means that the model is lumped at the grid scale.
2. All precipitation falling on the soil infiltrates, unless the soil is previously saturated.
3. The slope of the ground water table is expected to coincide with the slope of the ground unless the latter is very small (less than 0.01%).
4. The soil conductivity at saturation is considered constant with depth of soil layer but much larger than that of the deeper layers.
5. The integral of the soil conductivity over the vertical in the unsaturated zone can be rationally expressed as a function of the overall water content of the soil.
6. During the transition phase, the variation of water content with time is constant over elementary cell.

An accurate integration of the differential equations offers a comparatively scale-independent physically-based model which preserves the physical meaning of the model parameters. The geometry of the basin is expressed by the pixels of a DEM over which the equations are integrated to feed into a cascade of non-linear reservoirs. It is assumed that the non-linear cascade aggregates into a unique non-linear reservoir at the basin level whose parameter values can be estimated directly without missing the physical meaning of them [160]. Each grid cell of the DEM is allocated a value for each of the physical features represented in the model. The flow directions and slopes are assessed beginning from the DEM, consistent with a neighborhood association based on the principle of minimum energy. The active cell is supposed to be linked with a single downstream cell, while it can receive from up to three upstream contributing cells [59, 160]. Since its parameters have physical meaning, it can be likewise appropriate for modeling ungauged catchments with the use of the literature and prevailing thematic maps for obtaining the parameter values [36].

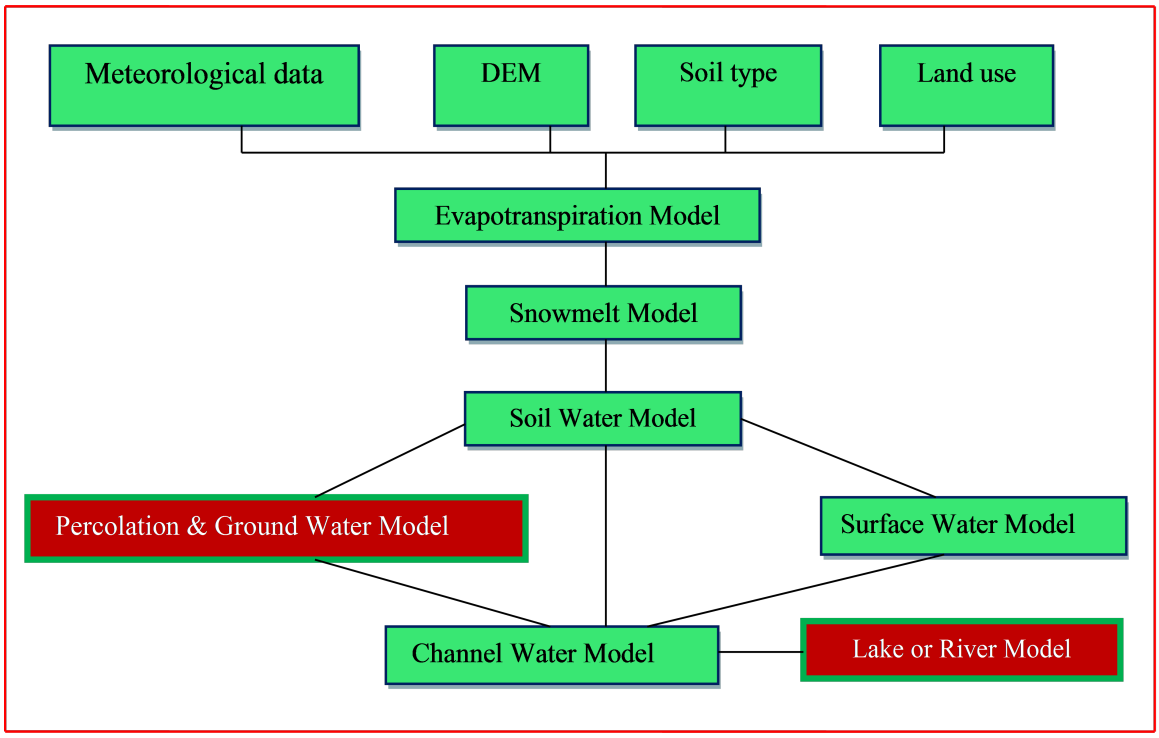

Figure 5.1: A flow chart indicating the components of the (Py)TOPKAPI model [160]

The following sections describe the general structure and methodology of the model, the model input data and parameters, the setting up of the model, its calibration and validation.

5.3.1 Structure and Methodology of the Model

The model comprises of five key components (Figure 2.3) namely soil, overland, channel, evapotranspiration, and snow modules [160, 161]. The graphical representation of the (Py)TOPKAPI model is also presented in Figure 5.1. The first three take the form of non-linear reservoir equations controlling the horizontal flows. This mechanism plays a key role in the model, both as a direct contribution to the flow into the channel network and as a factor regulating the soil moisture balance. Overland flow is produced by the excess rainfall on the different cells while the total run-off (surface plus sub-surface) is then drained by the drainage system. The evapotranspiration plays a key role not only in its direct influence, but also in its cumulative temporal consequence on the soil moisture volume depletion on condition that its total effect is well preserved [60]. In the current PyTOPKAPI modeling, evapo-transpiration was added directly as an input to the model, while the snow module part was totally ignored since there are no snowfalls in the study catchments. In the flow prediction, on the basis of the soil situation and actual-evapotranspiration, the rainfall onto the catchment is divided into direct run-off and infiltration, which reflects the nonlinear relationship between the soil water storage and the saturated contributing area in the basin. The infiltration and direct run-off are input into the soil and surface reservoirs, respectively. Outflows from the two reservoirs as interflow and overland-flow are then drained into the channel reservoir creating the channel flow [160].

In summary, the model has been structured into three reservoirs (soil, overland and channel) [59, 156, 160] that can be expressed with the help of non-linear kinematic wave models, the integration in space of which results in three ‘structurally-similar’ zero-dimension-non-linear reservoir equations in each grid cell [60, 147, 156, 160, 161] to be solved in time.

The improved PyTOPKAPI model is coded in the python programming language and accessed directly through an interactive Python environment. It is open-source with BSD license, and runs on most popular operating systems [239]. The model was previously tested on the Liebenbergsvlei gauged catchment in South Africa to simulate river discharge at 6-hour time-steps and showed good performance [283]. Sinclair and Pegram [240] also applied the model to estimate soil water volume across South Africa. The result shows that the model is also capable for estimating soil water volume upon improvement of bias in model forcing parameters such as rainfall and the physically-based soil properties that define the model.

5.3.2 PyTOPKAPI Model input Data

Basically, the PyTOPKAPI model input comprises gridded data including: (1) a Digital Elevation Model (DEM); (2) a soil type classification; (3) a land use classification; and (4) hydro-meteorological data, such as rainfall, observed streamflow and temperature data. Descriptions of these data are presented hereunder.

5.3.2.1 DEM

The SRTM (Shuttle Radar Topographic Mission) DEM was obtained from (`http://srtm.csi.cgiar.org`) [253] following Step by Step Geo-Processing [131], and was pre-processed for the current study. The SRTM DEM data, created by NASA initially, is a main development in digital mapping of the world, and offers a major improvement in the obtainability of high quality elevation data for large portions of the tropics and other zones of the developing world. The NASA SRTM has provided digital elevation data (DEMs) for over 80% of the world. This data is presently disseminated free of charge by USGS [131, 132]. The DEM pre-processing comprises finding and adjusting bowls and false outlets in the basin, detecting the networks amongst the cells thus proving the flow directions, computing the steepness, and finding cumulative drained area by the automatic detection of the stream network with the help of the spatial analyst toolbox (Hydrology tool) of ArcGIS [160].

The resolution of the DEM was set to 1km for the two study catchments (Figures 5.2 and 5.3). This resolution has been employed for all the other maps also. As indicated above, the DEM was then treated to eradicate eadicate the unwanted basin closure and the bowls in the basin. The unwanted basin closure cells are the cells in the periphery of the basin with lower elevation than all the other adjacent cells that are dissimilar from the real basin closure cell. The bowls are the cells inside of the basin having elevation lower than the adjacent cells which is not allowed as each cell should have its own single outflow path. In both these cases, the cell elevation is set to the lowest elevation the neighboring cell such that the flow path and the basin closure cell are exceptionally identified [60].

5.3.2.2 Soil Type Data

The soil data was acquired from the Harmonized World Soil Database, HWSD [116]. The soil categories can be defined by the data established by the soil type grid (HWSD_RASTER) [84,116]. The HWSD is consisted of a raster image file and a linked attribute database. The grids comprise the main soil texture class for each of the 13 standard soil layers by means of the USDA soil texture class index with reference to the HWSD attribute table [267]. Table 5.1 shows the identified USDA soil texture class index and USDA Soil texture class name and code for Gilgel Ghibe and Mojo catchments. Figures 5.4 and 5.5 show the soil maps of the two catchments, respectively.

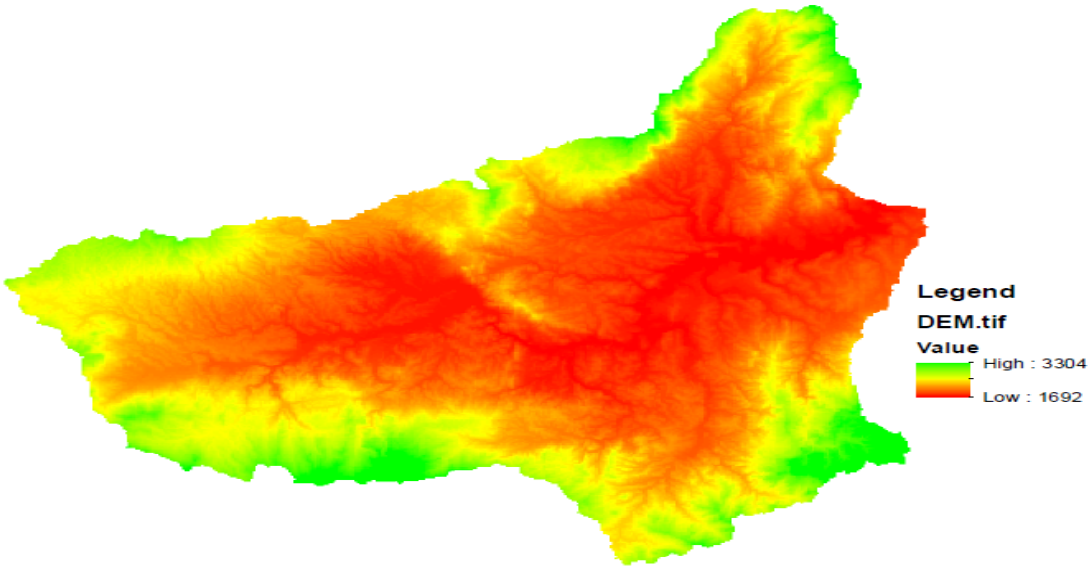

Figure 5.2: DEM grid of Gilgel Ghibe River

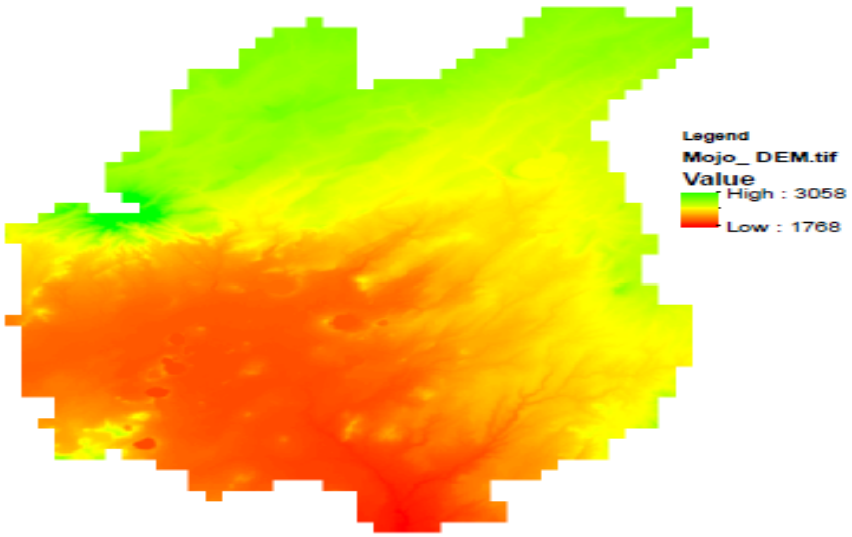

Figure 5.3: DEM grid of Mojo River

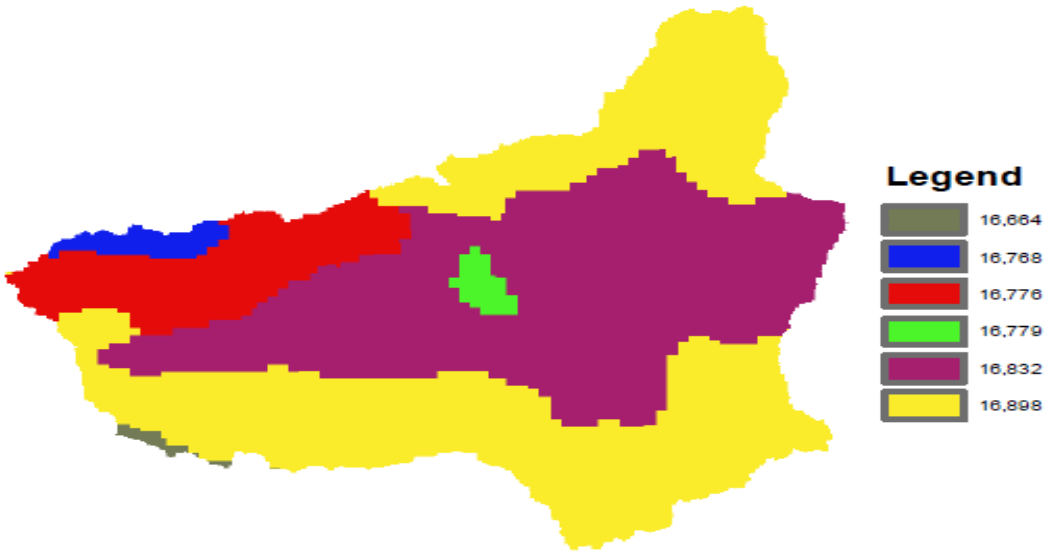

Figure 5.4: Soil category grid of Gilgel Ghibe catchment

Figure 5.5: Soil category grid of Mojo River

Table 5.1: Identified USDA soil texture class(index), code, name & the corresponding soil depth

		Identified Soil ID, Soil Depth and USDA Soil texture class code & name (According to HWSD table)							
	Soil ID	16664	16768	16776	16779	16832	16898	-	-
	Soil depth(L), m	0.3	1	1	1	1	1	-	-
	USDA Soil Texture Code	9	3	3	10	3	5	-	-
	USDA Soil texture class	Loam	Clay	Clay	Sandy clay loam	Clay	Clay loam	-	-
	Soil ID	16651	16664	16714	16724	16739	16841	16842	16963
	Soil depth(L), m	0.1	0.3	1	1	1	1	1	1
	USDA Soil Texture Code	5	9	10	3	10	3	3	3
	USDA Soil texture class	Clay loam	Loam	Sandy clay loam	Clay	Sandy clay loam	Clay	Clay	Clay

5.3.2.3 Land Use

The land use maps of the study catchments were acquired from the United States Geological Survey (USGS) Global Land Cover Characterization (GLCC) database and is accessible through the WaterBase web site [291]. These maps are available in the form of tiles for each continent/region. They are in two resolutions: the original at approximately 400 meters (at the equator) and resampled versions at 800 meters. For this study, the first one (the 400 meters resolution map) was used as it is finer and more accurate. Table 5.2 shows the identified ID value of land use classes for Gilgel Ghibe and Mojo catchments.

Table 5.2: Identified code of land use classes [101]

Catchment	**Identified Id value of land use classes (According to GLCC)**					
Gilgel Ghibe	2	6	7	10	13	15
Mojo	1	2	7	10	-	-

The PyTOPKAPI model needs the values of the Manning$'$s roughness coefficient for every grid cells for each land use class. These parameters were obtained from the land use gridded data in the USGS Land Use/Land Cover System Legend-Modified Level 2 [101] and Manning's roughness coefficient utilized for different land cover categories in GeoSFM [19]. Figures 5.6 and 5.7 show the land use grids of the two river catchments. Table 5.5 also shows the identified land use classes and Manning's coefficient (n_o) values for the two river catchments.

5.3.2.4 Hydro-Meteorological Data

The available meterological information (1) for Gilgel Ghibe catchment comprised daily rainfall and temperature records from Jimma, Asendabo and Yebu weather stations for the period 01/01/1986 and 31/12/2010, and (2) Mojo weather station between 01/01/1984 and 31/10/2014 for Mojo catchment acquired from the Ethiopia National Meterological Agency (ENMA). For the Gigel Ghibe River, the discharge data were the observed stream flows at Ghibe Nr Asendabo gauging station, between 01/01/1984 and 31/12/2013. For the Mojo catchment, the discharge data were the recorded stream flows at Mojo @ Mojo village gauging station, between 01/10/1968 and 31/12/2013 acquired from water affairs Ministry in Ethiopia.

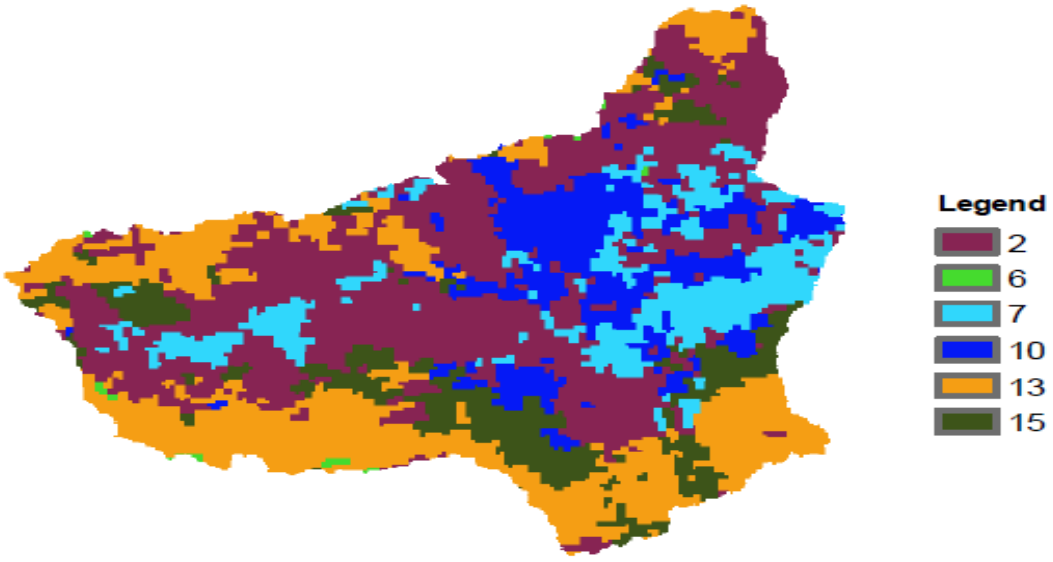

Figure 5.6: Land Use grid of Gilgel Ghibe River

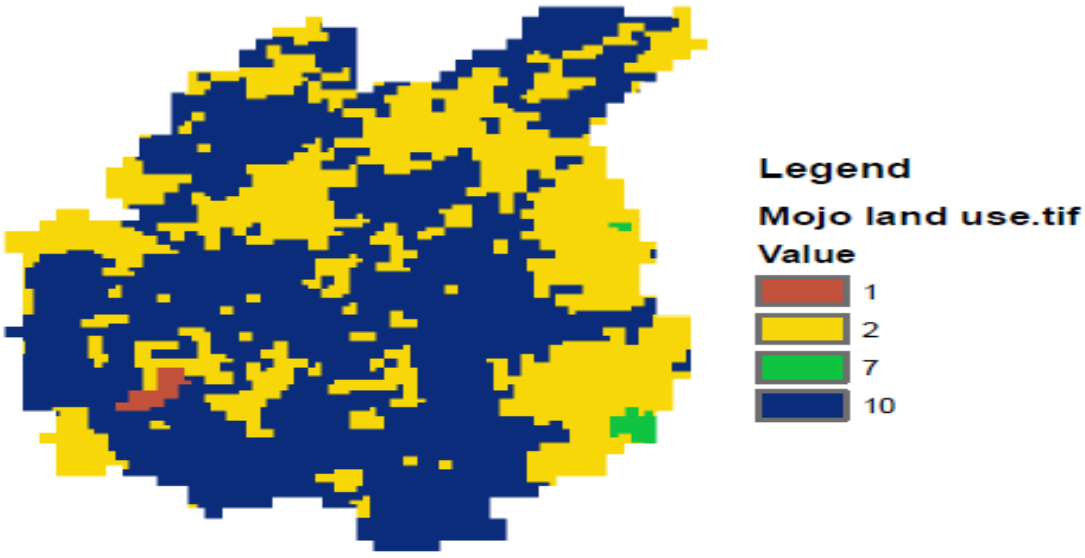

Figure 5.7: Land Use grid of Mojo River

5.3.2.5 Potential Evapotranspiration (ETo)

Evapotranspiration is a key variable of the global water budget and is central to agriculture and water management [23]. In PyTOPKAPI modeling, the evapo-transpiration is assessed at the DEM grid scale. Many methods of estimating evapotranspiration, whether for hydrologic models or irrigation scheduling, have been developed [57]. The most difficult but physically convincing model for finding the actual evapo-transpiration is the Penman-Monteith method that is commonly utilized for numerous hydrological models like SHE, DHSVM [160, 292]. However, a simplified method is mostly indispensable since the required historic data for Penman-Monteith method may not be comprehensively obtainable for many developing nations of the world because limited weather stations. In addition to that, it is almost not possible to obtain the actual required data for flood prediction applications in developing countries [1, 160]. So, as reliable data have not been obtained from Ethiopia, the simplified techniques were used to compute the evapo-transpiration data using the temperature and additional topo-geographic and climatic data.

One empirical equation to compute the benchmarked monthly potential evapo-transpiration is the one due to Thornthwaite and Mather [268]. This equation estimates the average monthly potential evapotranspiration by the following expression.

$$ET_{om}(i) = 16a(i)\left[10\frac{T(i)}{b}\right]^{c} \tag{5.1}$$

where,

$$a(i) = \frac{n(i)}{30}\frac{N(i)}{12}\text{ , }b = \sum_{1}^{12}\left[\frac{T(i)}{5}\right]^{1.514}\textbf{ and }c = 0.49239{+}1792{*}10^{-5}b{-}771{*}10^{-7}b^2{+}675{*}10^{-9}b^3 \tag{5.2}$$

where, ET_{om}(i) = mean potential evapotranspiration [mm/month], T(i) = average temperature for i^{th} month [^0C], n(i) = no. of days in month i, N(i) = average daily maximum sunshine hours [82, 83].

The second simplified empirical equation for estimates of the mean monthly potential evapotranspiration is the one according to Blaney and Criddle [37]. In particular situations, such as in a region at very high elevations, it was found that the Thorntwaite formula largely underestimates potential evapotranspiration due to climatic conditions. In these cases, it is possible to compute the potential reference evapotranspiration using Blaney-Criddle formula. The Blaney-Criddle technique basically denotes to mean monthly values, both for the temperature and the ET_0. If, for instance, it is obtained that the average temperature in June is 28^0C, it denotes that throughout the whole days of June month, the average temperature is 28^0C.

The following equation can be used:

$$ET_{om}(i) = n(i) * k * p(i) * (0.46 * T(i) + 8) - 2 \tag{5.3}$$

where ET_{0m} (i) = mean monthly potential evapotranspiration for month i [mm/month], T(i) = mean air temperature for i^{th} month [^0C], n(i) = no. of days in month i, k = Blaney-Criddle coefficient (=1.11 in PyTOPKAPI model), p(i) = average daily percentage of annual daytime hours=N(i)*100/(12*365), N(i) = average daily maximum sunshine hours [82].

Here, this method is simple as it uses the recorded temperature data only. However, it should also be noted that this method is not very precise. It offers an approximation or "order of magnitude" of the ET_0 only particularly for dry climatic conditions.

The third is the regression equations developed for estimating the monthly potential evapotranspiration (ET_r or most commonly called as PET) over the Awash Rift Valley, and Omo-Ghibe Basins by Sileshi [234] as described in section 3.2.2, from which ETo could be obtained. The potential evapotranspiration so obtained (as indicated in Chapter 3) often refers to the evapotranspiration of a specific crop (ET_r). The potential evapotranspiration of different crop (ETo) growing under the identical situations like the benchmarked crop is determined by multiplying the benchmarked crop evapotranspiration (ETr) by coefficient of crop (Kc), the value of which varies with the level of the crop growth, i.e., ET_o= Kc * ET_r. The values of the crop coefficient (Kc) varies within the range of 0.2 < Kc < 1.3 [234].

The average value of the evapotranspiration estimates obtained by the above three estimation methods has been used as the input data of the evapotranspiration for this PyTOPKAPI model application.

Table 5.3: Monthly potential evapotranspiration (ETo) estimates by different methods

(a) Gilgel Ghibe catchment

Method	Daily ETo in mm/day of the month											
	Jan	Feb	Mar	Apr	May	Jun	Jul	Aug	Sep	Oct	Nov	Dec
Blaney-Criddle	4.762	5.000	5.143	5.243	5.323	5.246	5.113	5.079	4.981	4.812	4.735	4.683
Thornthwaite and Mather	2.071	2.408	2.564	2.607	2.633	2.448	2.273	2.267	2.235	2.055	2.008	1.969
Yilma Seleshi	5.268	3.941	3.972	3.814	3.340	2.902	2.567	2.420	2.876	3.288	3.389	3.462
Average ETo	4.034	3.783	3.893	3.888	3.765	3.532	3.318	3.255	3.364	3.385	3.377	3.372

(b) Mojo catchment

Method	Daily ETo in mm/day of the month											
	Jan	Feb	Mar	Apr	May	Jun	Jul	Aug	Sep	Oct	Nov	Dec
Blaney-Criddle	4.718	5.035	5.305	5.527	5.664	5.693	5.413	5.264	5.145	4.913	4.742	4.612
Thornthwaite and Mather	1.893	2.360	2.754	3.023	3.132	3.125	2.635	2.447	2.392	2.115	1.921	1.757
Yilma Seleshi	3.775	4.289	4.538	4.313	4.133	4.052	3.306	3.419	3.625	3.650	3.943	3.944
Average ETo	3.462	3.894	4.199	4.287	4.310	4.290	3.784	3.710	3.721	3.559	3.535	3.438

The potential evapotranspiration is adjusted with the use of the actual soil water content for obtaining ETa, the actual evapotranspiration by the expression indicated below, in which Ks is a soil coefficient whose value is (0 < Ks < 1). [234].

$$ETa = Ks * ETo \tag{5.4}$$

where Ks = (0 , 1)

5.3.3 Model Performance Assessment Tools

The behavioral and performance assessment of a hydrologic model is commonly made by comparisons of simulated and observed variables [35, 38, 151]. In this case, this was carried out by using a series of performance measuring criteria incorporating the observed discharge data into the modeling process and matching the outlets of the modeled catchments with the physical locations

of the flow gauging stations of the modeled rivers. In this regard, comparisons of simulated discharge data (Q_{sim}) with the observed discharge data (Q_{obs}) for the identical set of conditions over a given period of time N (in our case, daily time steps) are conducted. The statistical tools that were utilized in these investigates for evaluating the efficacy of the model are as described below.

5.3.3.1 Root Mean Square Error (RMSE)

The RMSE has been used as a standard statistical metric to measure model performance. It is also known as the Root Mean Square Deviation (RMSD) that is commonly used to quantify of the variance between the model forecasted magnitudes and the truly recorded values of the basin [50]. These specific differences are also called residuals, and the RMSE helps to combine them into a single measure of predictive power [61, 154].

It is determined using the expression given below [3]:

$$\mathbf{RMSE} = \sqrt{\frac{\sum_{i=1}^{N} (\boldsymbol{Q}_{sim} - \boldsymbol{Q}_{obs})^2}{\boldsymbol{N}}} \tag{5.5}$$

$0 \leq \text{RMSE} \leq \infty$

A smaller value indicates better model performance.

5.3.3.2 Coefficient of Determination (R^2)

It is a measure that assists us conclude how confident one can be in making forecasts from a certain model/graph. It signifies the percent of the data that is closest to the line of finest fit. That is to say, if the regression line passed accurately through all the points on the scatter plot, it would be able to enlighten all of the variation. R^2 ranges from 0 to 1, with higher values representing less error variance. The closer R^2 is to one, the better the model explains the data. In the case of a precise fit, R^2=1 and naturally values greater than 0.5 are considered suitable [154, 178]. In general, it is a pointer of the linear association amongst the recorded and predicted stream flow quantities. It is given by:

$$\boldsymbol{R^2} = \frac{\left[\sum_{i=1}^{N} (\boldsymbol{Q}^{sim} - \boldsymbol{Q}_{mean}{}^{sim})(\boldsymbol{Q}^{obs} - \boldsymbol{Q}_{mean}{}^{obs})\right]^2}{\sum_{i=1}^{N} (\boldsymbol{Q}^{sim} - \boldsymbol{Q}_{mean}{}^{sim})^2 \sum_{i=1}^{N} (\boldsymbol{Q}^{obs} - \boldsymbol{Q}_{mean}{}^{obs})^2} \tag{5.6}$$

$0 \leq \text{R}^2 \leq \mathbf{1}$

where: $\boldsymbol{Q}^{obs}$ is recorded streamflow in m^3/s, $\boldsymbol{Q}^{sim}$ is simulated streamflow in m^3/s, $\boldsymbol{Q}^{sim}{}_{mean}$ is mean of simulated values, $\boldsymbol{Q}^{obs}{}_{mean}$ *is* mean of recorded values, and $\boldsymbol{N}$ sample size.

5.3.3.3 Nash-Sutcliffe Coefficient of Efficiency (NS)

The NS performance measure has been extensively utilized to assess the efficiency of hydrologic models [153, 225]. Nash and Sutcliffe described the NS, which varies from -∞ (poor fit) to 1.0 (perfect fit), as follows [67, 154]:

$$\mathbf{NS} = 1 - \frac{\sum_{i=1}^{N} (\boldsymbol{Q}^{obs} - \boldsymbol{Q}^{sim})^2}{\sum_{i=1}^{N} (\boldsymbol{Q}^{obs} - \boldsymbol{Q}_{mean}{}^{obs})^2} \tag{5.7}$$

$-\infty \leq \text{NS} \leq \mathbf{1}$

It is the ratio of the Mean Square Error to the variance in the recorded data, deducted from 1. For example, if the square of the variances between the predicted values and the recorded values is as big as the variability in the observed data, then NS = 0.0 and if it surpasses it, then NS < 0.0 (i.e., the recorded mean is a well predictor than Qsim). This means that an NS value = 1.0 specifies the model accurately simulates the target output (perfect model performance), an NS value = 0 specifies that the model is acting out only as good as the use of the average target value as prediction. An NS value < 0 designates choice of model is questionable. Thus, it is good idea to have the NS values to be larger than 0·0 and approaching 1·0 [113, 225]. The simulation outcomes are considered to be good if $NS \geq 0.75$, and satisfactory if $0.36 \leq NS \leq 0.75$ [68, 117, 278]. Otherwise, it is considered as unsatisfactory.

5.3.4 Model parameters

In PyTOPKAPI model applications, the model parameters would be linked with the catchment characteristics. This is the greatest advantage of the model [160, 194]. These parameters were generated from the DEM, the soil and the land use data of the study catchments. This is automated in the PyTOPKAPI model which needs numerically gridded and interconnected square pixel cells of the catchment area to transfer the flows (surface and subsurface) within the catchment. The main base map used was the DEM of the respective catchment from which the grid definition, the setting of the spatial resolution of the model and delineation of the stream network were carried out.

The spatial resolution of the model (the parameter X of the pixel) is usually governed by the resolution of the DEM. In this study, the DEM was purposely re-sampled to a resolution of 1 km from its original fine resolution of 90m for both the study catchments. Then, the 1 km resolution DEM was used to define the stream flow directions. A problem of availability of sinks in the DEMs was also corrected. A sink (a depression or pit) is a cell or an area surrounded by higher elevation cells that prevents the down-slope flow of water (unless it is some sort of natural case like a lake or swamp) which in turn creates an error in the data-set. So, to make a precise representation of the flow direction, the DEM was treated in such a way to get a depression less DEM.

For DEM treatment to define the flow direction, Liu and Todini [160] suggested to consider only 4 drainage directions (D4). However, limiting the drainage path to only 4 directions can lead to an impracticable representation of the relief variability. For this purpose, the PyTOPKAPI model was reformed to well-match with D8 (8-flow-direction) where 4 additional diagonal pixels are included [195]. Thus, the sink in the DEM Raster was filled in D8 to define the flow direction by the hydrology toolbox of the ArcGIS software for both of the study catchments.

For delineation of stream networks, the number of flow contributing upslope cells was determined by using the "Flow Accumulation" tool from the hydrology toolbox of the ArcGIS. A threshold area ($A_{threshold}$), i.e., the area of the minimum number of upstream cells that are essential to create flow to an active cell, was ultimately set to $25km^2$ on the flow accumulation raster for both the catchments. Setting $A_{threshold}$ equal to $25km^2$ is in accordance with Todini's (1996) recommendation that the ratio between the number of cells containing channels and the total number of cells of the respective catchment shall have a value ranging between 5% and 15% of the total catchment area [195]. This $A_{threshold}$ defined a total channel length of 173 km by 1 km pixel width (5.96%) of the total Gilgel Ghibe catchmet area of $2943km^2$ and 198km by 1km (13.41%) of the total Mojo catchment area of $1496km^2$.

Different dataset and appropriate tables from the literature were utilized to obtain the appropriate

Table 5.4: Hydrologic soil properties classified by Soil Texture [210]

Texture class	Sample size	Total porosity (θ), cm^3/cm^3	Residual saturation (θ_r) cm^3/cm^3	Effective porosity (θ_e), cm^3/cm^3	Bubbling pressure (ψ b) Arithmetic, cm	Bubbling pressure (ψ b) Geometric,† cm	Pore size distribution (λ) Arithmetic	Pore size distribution (λ) Geometric‡	Water retained at −0.33 bar tension, cm^3/cm^3	Water retained at −15 bar tension, cm^3/cm^3	Saturated Hydraulic Conductivity‡ (K_s) cm/h
Sand	762	0.437** (0.374 0.500)	0.020 (0.001 0.039)	0.417 (0.354–0.480)	15.98 (0.24–31.72)	7.26 (1.36–38.74)	0.694 (0.298 1.090)	0.592 (0.334–1.051)	0.091 (0.018 0.164)	0.033 (0.007–0.059)	21.00
Loamy sand	338	0.437 (0.368–0.506)	0.035 (0.003 0.067)	0.401 (0.329–0.473)	20.58 (0.0 45.20)	8.69 (1.80 41.85)	0.553 (0.234–0.872)	0.474 (0.271 0.827)	0.125 (0.060 0.190)	0.055 (0.019 0.091)	6.11
Sandy loam	666	0.453 (0.351–0.555)	0.041 (0.0–0.106)	0.412 (0.283–0.541)	30.20 (0.0–64.01)	14.66 (3.45 62.24)	0.378 (0.140–0.616)	0.322 (0.186 0.558)	0.207 (0.126 0.288)	0.095 (0.031–0.159)	2.59
Loam	383	0.463 (0.375–0.551)	0.027 (0.0 0.074)	0.434 (0.334 0.534)	40.12 (0.0 100.3)	11.15 (1.63–76.40)	0.252 (0.086–0.418)	0.220 (0.137 0.355)	0.270 (0.195–0.345)	0.117 (0.069 0.165)	1.32
Silt loam	1206	0.501 (0.420 0.582)	0.015 (0.0–0.058)	0.486 (0.394 0.578)	50.87 (0.0 109.4)	20.76 (3.58 120.4)	0.234 (0.105–0.363)	0.211 (0.136 0.326)	0.330 (0.258–0.402)	0.133 (0.078 0.188)	0.68
Sandy clay loam	498	0.398 (0.332–0.464)	0.068 (0.0 0.137)	0.330 (0.235 0.425)	59.41 (0.0 123.4)	28.08 (5.57 141.5)	0.319 (0.079–0.559)	0.250 (0.125 0.502)	0.255 (0.186 0.324)	0.148 (0.085–0.211)	0.43
Clay loam	366	0.464 (0.409 0.519)	0.075 (0.0 0.174)	0.390 (0.279–0.501)	56.43 (0.0–124.3)	25.89 (5.80 115.7)	0.242 (0.070–0.414)	0.194 (0.100–0.377)	0.318 (0.250–0.386)	0.197 (0.115 0.279)	0.23
Silty clay loam	689	0.471 (0.418 0.524)	0.040 (0.0 0.118)	0.432 (0.347–0.517)	70.33 (0.0 143.9)	32.56 (6.68 158.7)	0.177 (0.039–0.315)	0.151 (0.090–0.253)	0.366 (0.304 0.428)	0.208 (0.138–0.278)	0.15
Sandy clay	45	0.430 (0.370 0.490)	0.109 (0.0 0.205)	0.321 (0.207 0.435)	79.48 (0.0 179.1)	29.17 (4.96 171.6)	0.223 (0.048 0.398)	0.168 (0.078–0.364)	0.339 (0.245 0.433)	0.239 (0.162–0.316)	0.12
Silty clay	127	0.479 (0.425 0.533)	0.056 (0.0–0.136)	0.423 (0.334–0.512)	76.54 (0.0 159.6)	34.19 (7.04 166.2)	0.150 (0.040–0.260)	0.127 (0.074 0.219)	0.387 (0.332 0.442)	0.250 (0.193–0.307)	0.09
Clay	291	0.475 (0.427 0.523)	0.090 (0.0 0.195)	0.385 (0.269 0.501)	85.60 (0.0 176.1)	37.30 (7.43 187.2)	0.165 (0.037–0.293)	0.131 (0.068 0.253)	0.396 (0.326 0.466)	0.272 (0.208 0.336)	0.06

* First line is the mean value
Second line is + one standard deviation about the mean
† Antilog of the log mean
‡ Obtained from Fig. 2

values of the initial PyTOPKAPI model parameters. The initial values model parameters are taken from literature based up on the category of soil, and land use. The initial values of the soil depth L, the residual soil moisture θr, saturated soil moisture, Θs, the soil conductivity Ks, the bubbling pressure and the pore size distribution index λ for each soil class were taken from Harmonized World Soil Database [116] and the report paper by Rawls et.al [210] as indicated in Table 5.4. The values of these parameters are therefore illustrated in Tables 5.6 and 5.7 for Gilgel Ghibe and Mojo catchments, respectively. The initial values for the parameter (n_o) are selected referring to Table 5.5 of USGS Land Use/ Land Cover System Legend; and Table 5.5 of Manning's roughness values in the USGS Land Use/Land Cover System Legend (Modified Level 2) and in the Technical Manual for the Geospatial Stream Flow Model (GeoSFM), Open-File Report 2007–1441 [19], and are presented by Table 5.8.

The Strahler order [102, 199] was employed for defining the Manning's roughness coefficient n_c values for channel flow and accordingly, therefore, the Manning's coefficient values of 0.045, 0.04, 0.035 and 0.035 were assigned to channel orders of 1, 2, 3 and 4, respectively [160, 195].

The value of the pore-size distribution parameter (α_s), which is dependent on the soil property, was constantly set to 2.5 for all the cells. Using the value of (α_s) within its representative values in between 2 & 4 (Brooks & Corey, 1964) was observed to have a little influence on the results of the simulations [160, 195].

In addition, a constant value of $\frac{5}{3}$ is also used for both of the well-known power coefficients α_o and α_c (the nonlinear exponents of overland and channel flows) originating from the Manning$'$s equation for overland and channel flows, respectively. As a first approximation, the Kc (crop factor) was set to 1 uniformly over the basin. This is so because the evapotranspiration forcing files applied in the simulations is assumed to be the actual ETa.

Consequently, maps of the soil depth (L), the saturated soil water content (Θs), the residual soil water content (Θr), the hydraulic conductivity (Ks), the bubbling pressure (Ψ_b), the pore size distri-

Table 5.5: USGS Land Use/Land Cover System Legend (Modified Level 2) and Manning's roughness values used for various land cover classes in GeoSFM

USGS Land Use/Land Cover System Legend (Modified Level 2) (http://edc2.usgs.gov/glcc/globdoc1_2.php)			Manning's roughness coefficients used for various land cover classes in GeoSFM. [19]	
Value	Code	Description	Anderson Code	Manning Roughness
1	100	Urban and Built-Up Land	100	0.03
2	211	Dryland Cropland and Pasture	211	0.03
3	212	Irrigated Cropland and Pasture	212	0.035
4	213	Mixed Dryland/Irrigated Cropland and Pasture	213	0.033
5	280	Cropland/Grassland Mosaic	280	0.035
6	290	Cropland/Woodland Mosaic	290	0.04
7	311	Grassland	311	0.05
8	321	Shrubland	321	0.05
9	330	Mixed Shrubland/Grassland	330	0.05
10	332	Savanna	332	0.06
11	411	Deciduous Broadleaf Forest	411	0.1
12	412	Deciduous Needleleaf Forest	412	0.1
13	421	Evergreen Broadleaf Forest	421	0.12
14	422	Evergreen Needleleaf Forest	422	0.12
15	430	Mixed Forest	430	0.1
16	500	Water Bodies	500	0.035
17	620	Herbaceous Wetland	620	0.05
18	610	Wooded Wetland	610	0.05
19	770	Barren or Sparsely Vegetated	770	0.03
20	820	Herbaceous Tundra	>800	0.05
21	810	Wooded Tundra		
22	850	Mixed Tundra		
23	830	Bare Ground Tundra		
24	900	Snow or Ice		

Table 5.6: Parameters value assigned to the HWSD soil texture classes for Gilgel Ghibe river catchment(Uncalibrated values of soil parameters)

Soil ID	Soil Texture class	Description	Depth (m)	Hyd.cond. Ks[mm/s]	Res.soil moisture (Θr)	Sat.soil moisture (Θs)	Bub. pressure (mm)	Pore size dist. index(λ)
16664	**9**	Loam	0.3	0.00367	0.027	0.434	111.5	0.22
16678	**3**	Clay	1	0.000167	0.09	0.385	373	0.131
16776	**3**	Clay	1	0.000167	0.09	0.385	373	0.131
16779	**10**	Sandy clay loam	1	0.000417	0.04	0.432	325.6	0.151
16832	**3**	Clay	1	0.000167	0.09	0.385	373	0.131
16898	**5**	Clay loam	1	0.000639	0.075	0.39	258.9	0.194

Table 5.7: Parameters value assigned to the HWSD soil texture classes for Mojo river catchment(Uncalibrated values of soil parameters)

Soil ID	Soil Texture class	Description	Depth (m)	Hyd.cond. Ks[mm/s]	Res.soil moisture (Θr)	Sat.soil moisture (Θs)	Bub. pressure (mm)	Pore size dist. index(λ)
16651	**5**	Clay Loam	0.1	0.000639	0.075	0.39	258.9	0.194
16664	**9**	Loam	0.3	0.00367	0.027	0.434	111.5	0.22
16714	**10**	Sandy clay loam	1	0.000417	0.04	0.432	325.6	0.151
16724	**3**	Clay	1	0.000167	0.09	0.385	373	0.131
16739	**10**	Sandy clay loam	1	0.000417	0.04	0.432	325.6	0.151
16841	**3**	Clay	1	0.000167	0.09	0.385	373	0.131
16842	**3**	Clay	1	0.000167	0.09	0.385	373	0.131
16963	**3**	Clay	1	0.000167	0.09	0.385	373	0.131

Table 5.8: Manning roughness coefficient (n_o) values used for the two river catchment(According to the USGS Land Use/ Land Cover System Legend and Manning's roughness values in GeoSFM)

Land use ID value	**1**	**2**	**6**	**7**	**10**	**13**	**15**
Code	**100**	**211**	**280**	**311**	**332**	**421**	**430**
Gilgel Ghibe Catchment	**-**	**0.03**	**0.04**	**0.05**	**0.06**	**0.12**	**0.1**
Mojo Catchment	**0.03**	**0.03**	**-**	**0.05**	**0.06**	**-**	**-**

bution index (λ) and the Manning$^{'}$s roughness coefficient for overland (n_o) were generated using ArcGIS software. The slopes of the ground $tan\beta$ (for flows in the soil and over the land) were obtained from the DEM. This was accomplished by using the "slope" tool in the ArcGIS toolbox. The slopes used for the transmission the flows of the channel network $tan\beta_c$ had been determined by means of differences in elevation from cell to cell in the downstream direction .

Table 5.9 provides the summary of the model parameters and the sources where the parameter values are obtained. Generally, a total of about 17 parameters are to be used in the PyTOPKAPI model application, as listed in the Table 5.9 out of which, 13 ($tan\beta$, $tan\beta_c$, L, K_s, Θ_r, Θ_s, n_o, n_c, α_s, K_c, Ψ_b, λ, W) are cell specific (spatially variable with a specific cell) and they mainly refer to physical characteristics of the cells. The remaining 4 parameters (X, $A_{threshold}$, the minimum channel width W_{min}, and the maximum channel width W_{max}) are constant representing the geometric characteristics of the channel or grid cell [195]. Moreover, according to Liu and Todini [160], from among the parameters of PyTOPKAPI model, the soil depth L (m), the soil conductivity Ks (mm/s), the residual soil water content,$\Theta_r(cm^3/cm^3)$, the saturated soil water content, $\Theta_s(cm^3/cm^3)$ and the power of the transmissivity law for the soil component αs relate to the soil and regulate runoff production; whilst the surface roughness coefficient n_o ($m^{-\frac{1}{3}}/s$) and the coefficient roughness for the channel n_c ($m^{-\frac{1}{3}}/s$) are routing parameters.

The parameter X and $A_{threshold}$ have been defined by the DEM pre-processing as described above and their individual values are 1 km and $25km^2$ for both the study catchments. The W_{min} and W_{max} were respectively set at 5m and 38m for Gilgel Ghibe (obtained from surveying data) and at 3m and 20m for Mojo catchment (estimated from Google map).

The width (W_i) of each channel cell was determined by the relation shown below [160, 195].

$$\boldsymbol{W_i = W_{max} + \left[\frac{W_{max} - W_{min}}{\sqrt{A_{tot}} - \sqrt{A_{th}}}\right]\left(\sqrt{A_i} - \sqrt{A_{tot}}\right)} \tag{5.8}$$

where, W_{max} is the maximum width at the basin outlet, $\boldsymbol{W_{min}}$ is the minimum width corresponding to the $A_{threshold}$ area, $\boldsymbol{A_{th}}$ is the threshold area which is the smallest up-stream area necessary to create a channel, $\boldsymbol{A_{tot}}$ is the total area and $\boldsymbol{A_i}$ is the area drained by the $\boldsymbol{i^{th}}$ cell.

Table 5.9: Summary of the initial PyTOPKAPI model parameter values estimated from (DEM, Soil and land use) maps and literature.

Parameter	Initial values		**References**
	Gilgel Ghibe	**Mojo**	
Cell Specific			
tan(β), gradient of the ground slope angle	5.00E-4 – 2.84E-1	1.77E-4 – 3.38E-1	SRTM DEM [253]
tan(βc), tangent of the channel slope angle	7.70E-5 – 7.00E-2	4.30E-5 – 6.08E-2	SRTM DEM [253]
L, soil depth (m)	0.30 – 1.00	0.10 – 1.00	Soil Type [84, 116, 210, 267]
K_s, saturated hydraulic conductivity(mm/s)	1.67E-4 – 3.67E-3	1.67E-4 – 3.67E-3	Soil Type [84, 116, 210, 267]
Θ_r, residual soil moisture content (cm^3/cm^3)	0.027 – 0.09	0.027 – 0.09	Soil Type [84, 116, 210, 267]
Θ_s, saturated soil moisture content (cm^3/cm^3)	0.385 – 0.434	0.385 – 0.434	Soil Type [84, 116, 210, 267]
n_o, Manning's roughness coeffi. for overland flow, $\frac{m^{-1}}{s^{-1}}$	0.03 – 0.10	0.03 – 0.06	Land use [19, 101, 291]
n_c, Manning's roughness coeffi. for the channel flow, $\frac{m^{-1}}{s^{-1}}$	0.035 – 0.045	0.035 – 0.045	Strahler order method [160]
α_s, a dimensionless pore-size distribution parameter	2.5	2.5	As per Brooks and Corey(1964) [195, 210]
α_c & α_o, Power coefficients of Manning's roughness	1.667	1.667	As per Brooks and Corey(1964) [195, 210]
K_c ,the crop coefficient	1	1	Land use [19, 101, 291]
Ψb, bubbling pressure (mm)	111.5 – 373.0	111.5 – 373.0	Soil Type [84, 116, 210, 267]
λ, pore size distribution index	0.131–0.220	0.131–0.220	Soil Type [84, 116, 210, 267]
W, Channel width (m)	Equation 5.8	Equation 5.8	[160]
Constant			
X, lateral dimension of the grid-cell (m).	1000	1000	SRTM DEM [253]
$A_{threshold}$, area over which a cell is assumed to create a channel (m^2)	25000000	25000000	As per Todini [195]
W_{min}, minimum width of channel at outlet (m)	5	3	Collected by fieldwork surveying (Ghibe); Estimated from Google Map (Mojo)
W_{max}, maximum width of channel at outlet (m)	38	20	Collected by fieldwork surveying (Ghibe); Estimated from Google Map (Mojo)

In general, it was observed that the model parameters' values are in the range of : L =0.10 $\sim$ 1.00 m, the bubbling pressure(Ψ_b) =111.5 $\sim$ 373 mm, the pore size distribution index (λ) = 0.131 $\sim$ 0.220, Ks = 1.67x10-4 $\sim$ 3.67x10^{-3} mm/s, Θ_s = 0.385 $\sim$ 0.434 cm^3/cm^3, Θ_r = 0.027 $\sim$ 0.09

cm^3/cm^3, n_c = 0.035 $\sim$ 0.045 $m^{-\frac{1}{3}}/s$, and n_o =0.03 $\sim$ 0.12 $m^{-\frac{1}{3}}/s$.

These values are the appropriate initial values to create the model parameters of the study catchments. Hence, the values of the cell specific parameters (cell_param) for all the cells were generated from the extracted thematic maps by using Python scripts. Adjusting of some parameters to account for the uncertainties in the parameter estimation procedures was also carried out to obtain better performance of the model. Once the model parameters have been generated, the implementation of the model additionally requires fixing the simulation periods, setting the simulation time-step and preparing the forcing files (variables) matching with spatial scale and time-step of the simulation.

5.3.5 Simulation periods

The selection of the simulation periods depends on the coincident availability of rainfall and streamflow data. In the process of defining the simulation periods, it is imperative to consider that the minimum requirement to evaluate a model is to have two independent simulation periods that can be used for calibration and validation. Moreover, the calibration and validation are highly affected by the quality of the data. Klemes proposes a hierarchical scheme for the systematic testing of hydrological simulation models. These are :(1) the split-sample test (SS): consists of taking two periods, calibrating the model in the first period, validating (or verifying) the model on the second period; (2) the differential split-sample test (DSS): applied under non-stationary climatic forcing conditions; (3) the proxy-basin test (PB): as for example, the model is calibrated on the basin A and applied on the basin B. Then the model is calibrated on the basin B and applied on the basin A. If the test is satisfactory, the model can be reliably applied to ungauged catchments; (4) the proxy-basin differential split-sample test (PB-DSS): applied under non stationary climatic forcing conditions [56]. The classical split-sample test was used for this study as it is the most widely used procedure to evaluate models in hydrological modeling studies [195]. This means that two periods of some suitable length must be available where both precipitation and flow data are continuous and of good quality to be used as a point of reference for appraisal of the model efficiency. For that reason, the rainfall and flow data were first analyzed separately as shown below.

Analysis of rainfall and streamflow data

As the densities of rain gauges and steamflow gauges are very low in Ethiopia, defining the simulation periods is not easy task since the required data have some missing values, and the periods with available stream flow and rainfall records are not always concurrent.

The flow outlet was chosen at station “Ghibe Nr.Asendabo” for Gilgel Ghibe catchment, and “Mojo @ Mojo village” for Mojo catchment. The observed streamflow data were available at Ghibe Nr.Asendabo gauging station since January 1, 1984 up to December 31, 2013 and at Mojo @ Mojo village flow gauging station since January 1, 1968 up to December 31, 2013. The streamflow data availability at those stations are presented in Figures 5.8 and 5.9, respectively in which the hydrographs of the flow gauges were plotted for the whole period of available records at monthly time steps.

Note that, though the hydrographs in Figures 5.8 & 5.9 are on monthly basis, the streamflow data were analyzed at a daily time step since the model is to run at a 24-hour time step. This computation was subsequently done for the calibration and validation.

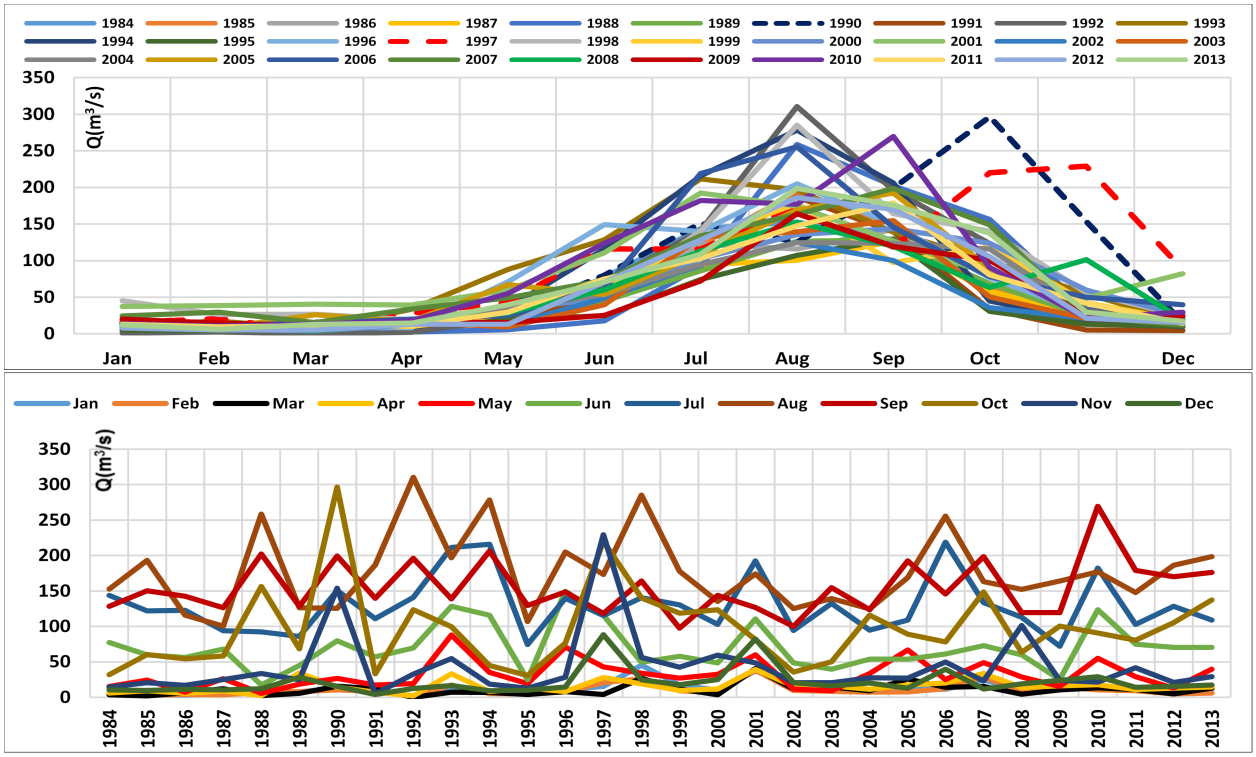

Figure 5.8: The graphs of streamflow data availability for Gilgel Ghibe catchment.

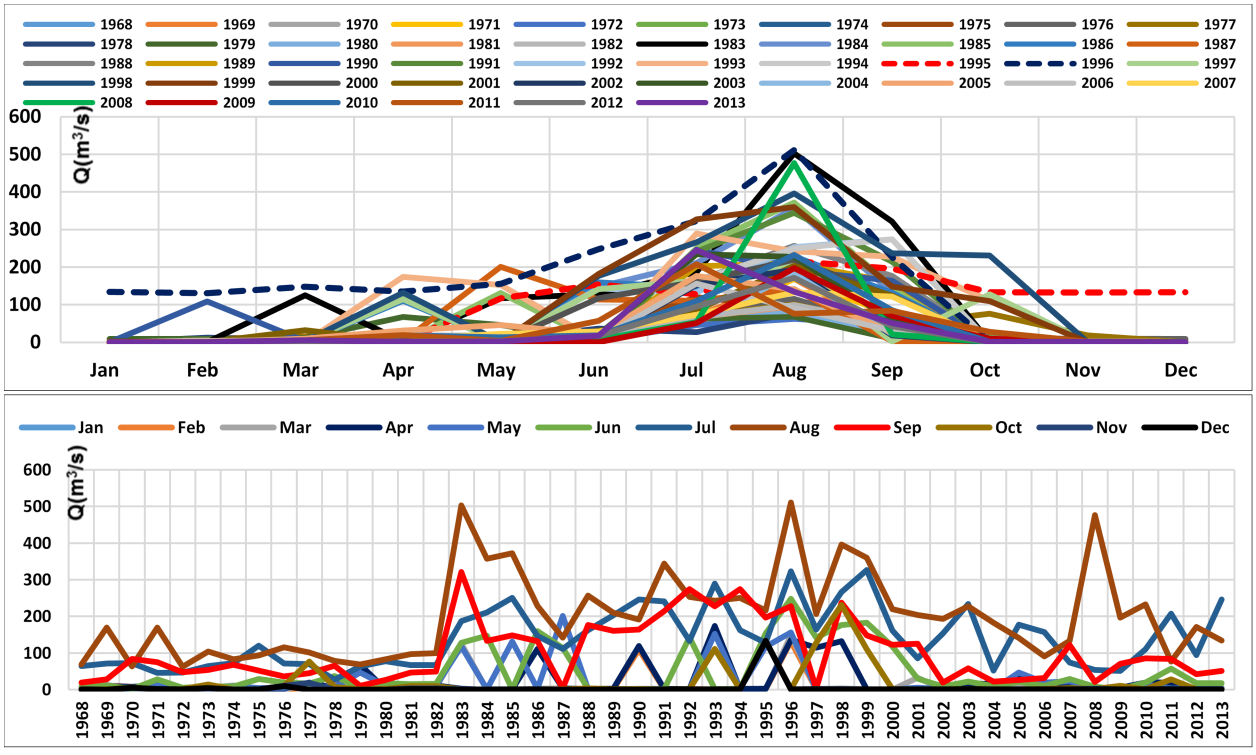

Figure 5.9: The graphs of streamflow data availability for Mojo catchment

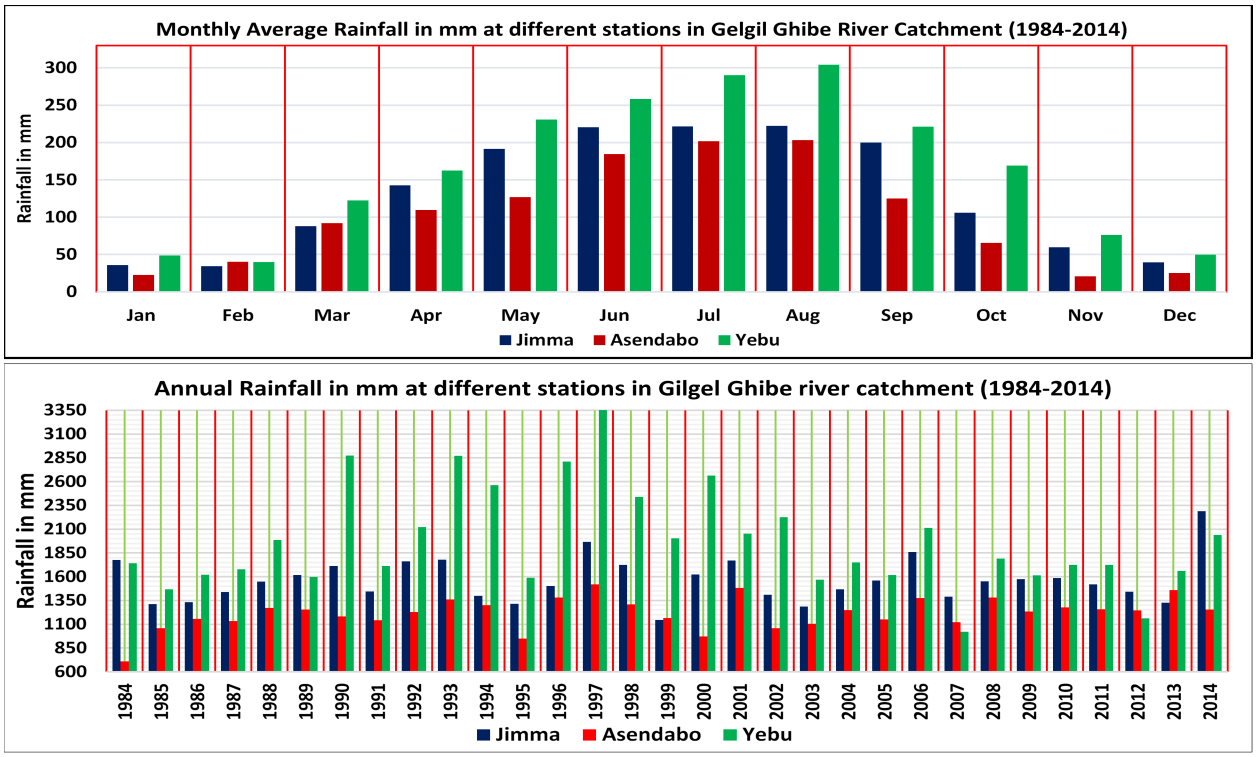

Figure 5.10: Rainfall data availability for Gilgel Ghibe catchment

The rain gauge network of Gilgel Ghibe catchment is composed of 5 rain- gauge stations namely Jimma, Asendabo, Seka, DedoSheki and Yebu (Figure 3.1). Jimma, Asendabo and Yebu rain gauges have a recorded data from January 1984 to December 2014 with very few missing data. The data availability of these network are relatively good during the period of 1985-2013 though the density of data decreases for few months from the year 2011 to 2014. The remaining two rain gauging stations (Seka and DedoSheki) were not used for this study as the recorded data have a lot of missing values. Only one rain gauge station (Mojo rain gauge) is available for Mojo catchment with recorded length of 31 years (1984-2014) and very few missing values. The quality of the recorded rainfall data of this station is uniformly good. That rainfall data has been utilized for flow simulation of Mojo catchment. The graphs of the period of availability rainfall data for each station of each catchment are as shown by the figures 5.10 and 5.11.

Thus, for fixing the simulation periods for Gilgel Ghibe and Mojo catchments, it is now possible to

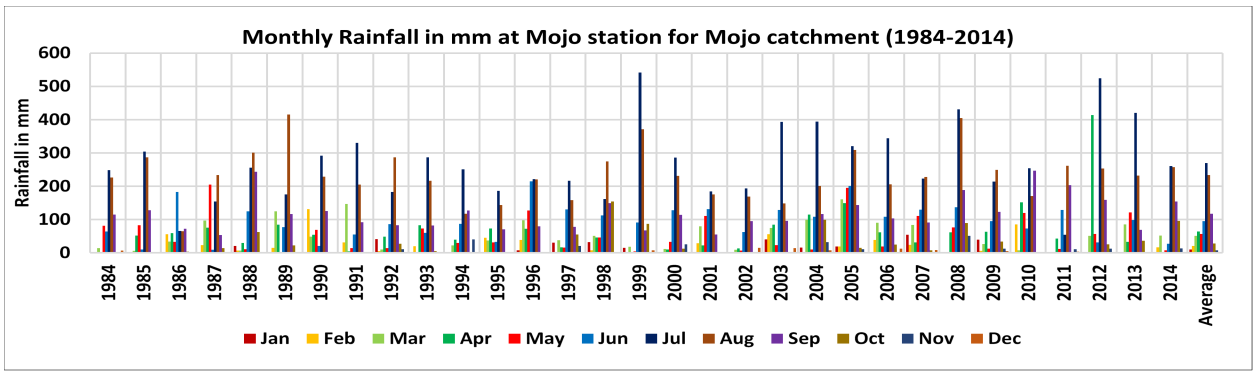

Figure 5.11: Rainfall data availability for Mojo catchment

carefully observe the periods that contain both continuous and good quality rainfall and flow data. Note that the period laid within 1986-2010 for Gilgel Ghibe catchment and 1999-2013 for Mojo catchment that corresponds to the period of simultaneous availability of stream flow and rainfall data from which selection of the two independent simulation periods have been carried out. This duration of time has concurrent: (i) streamflow data at the outlet station ("Ghibe Nr.Asenbdabo" for Gilgel Ghibe and "Mojo @ Mojo village" for Mojo), (iii) the complete rainfall station with few missing data during the most of these periods.

Thus, the data series in the range of 1986-2000 can be used for calibration and the data in between 2001 and 2010 can be used for validation of the model for Gilgel Ghibe catchment. Similarly, the data within the period of 1999-2008 is utilized for calibration and the dataset within 2009-2013 can be used for validation the model for Mojo catchment. The simulations were started at the beginning of every calendar year when the dependable flow of the rivers are almost constant (overland flow nearly equal to zero) for both catchments.

5.3.6 Model Time-Step

Based up on the availability of the essential data, the simulation time was chosen to be a 24-hour time step, which is observed to be very appropriate to simulate the main discharge variations of the study areas. It is also worth noting that, at this time step, approximately 60-150 minutes computing duration is required to simulate the entire catchment (2901 cells of 1 km for Gilgel Ghibe and 1476 cells of 1km for Mojo) by present day Personal Computer.

5.3.7 Forcing variables

For Gilgel Ghibe catchment, the average of the daily rainfall data of Jimma, Asendabo and Yebu gauging stations computed by "Theissen polygon method", were used to create the "rain-fields" forcing files. Similarly, the rainfall data of Mojo station was used for Mojo catchment. The respective evapotranspiration data, which were separately calculated in section 5.3.2.5 were used for both the catchments. These data were then prepared in HDF5 format using the python scripts as the forcing variables.

5.4 Model setup, calibration and validation

The PyTOPKAPI model was set-up to simulate steam flows from the case study Ethiopian catchments using the essential data described above. The model was then calibrated by a trial and error fine-tuning of grouped key parameters [195] to match the simulated with the observed stream flows. The performance of the model was further analyzed using the NS efficiency coefficient and the R^2 correlation and finally validation of model calibration was done with simulations over a few years of the data. Details of these are as given below.

5.4.1 Model setup

The PyTOPKAPI rainfall-runoff modeling starts with pre-processing of the DEM and preparation of model input parameters and then applies them into the model to simulate the realistic stream flow data along the drainage system. The model setup steps are briefly summarized below.

1. The DEM of the study areas were loaded to the GIS and were treated by pre-processors that help eradicate the false outlets & the sinks so that the flow direction and the basin closure cell are uniquely identified.

2. The stream-network was created by defining a minimum (threshold) area that initiates a stream. In this case, $25km^2$ (2500 ha) was used as the threshold area to define the stream network as per the recommendation of Todini [195].

3. The location of the outlet was carefully selected and then the entire watershed of the respective catchment was delineated.

4. Similarly, the land use and the soil maps were loaded to GIS and then extracted by the defined watershed as a mask. The attribute table for each map was edited with the values of the literature parameters.

5. The different thematic maps (the GIS files to generate parameter files) were created.

6. The cell parameters were generated and consequently modified to eliminate zero slopes with help of the relevant python scripts.

7. The rainfall and the ETo data were prepared as the forcing files in HDF5 format.

8. In the final step, after the input files were successfully prepared and introduced to the model, the model simulated the stream flows for the simulation periods.

5.4.2 Calibration

Basically, a physically based model such as the PyTOPKAPI model should require no calibration since its parameters can be estimated from catchment data such as morphology and hydraulic catchment properties, soil, vegetation, literature and experience [60]. Even though the PyTOPKAPI model is a physically based model, as in every physically distributed model, it may be subject to several uncertainties associated with the data on topography, soil characteristics and land uses and on the approximations introduced by the scale of the parameter representations. For these reasons, Liu and Todini [160] suggest that the calibration of parameters is still necessary for fine tuning the model. Here, all studies dealing with the PyTOPKAPI model indicated that the calibration of the model is more of a fine-tuning than conventional calibration which can be achieved by a simple trial and error adjustment of grouped key parameters to match the simulated stream flows with the observed flows [195].

According to a sensitivity analysis conducted by researchers, the most sensitive parameters controlling the runoff production are the soil depth and the soil conductivity, while the Manning roughness of channel n_c and overland n_o are the primary routing parameters [156, 200]. The adjusting factors implementable for calibration were $f_{ac}Ks$ (for soil conductivity), $f_{ac}L$ (for soil depth), $f_{ac}nc$ (for channel roughness) and $f_{ac}no$ (for overland roughness) [195]. The initial soil moisture (Vs_$_i nitial$), which has a strong impact on the simulation results, was firstly calibrated. Then after, the triplets ($f_{ac}L$, $f_{ac}Ks$, Vs_initial) were adjusted to minimize the RMSE by comparing the modeled and observed stream flows. Once the optimum triplet was established, the pair ($f_{ac}no$, $f_{ac}nc$) was adjusted with the help of the R^2 criteria as a controlling measure. Note that the initial parameters are not individually calibrated for each cell as that would lead to an extreme over-parameterization of the model and create inconsistent combinations of parameter values [195].

In view of that, calibration was conducted using the streamflow observations at station Ghibe Nr.Asendabo (u/S drainage area of $2943km^2$) for Gilgel Ghibe catchment and Mojo @ Mojo village flow gauging station (u/s drainage area of $1496km^2$) for Mojo catchment for their respective calibration periods. Here, firstly the preliminary soil saturation percent was fixed to 80% and 50% for entire cells at the commencement of the calibration period for both the study catchments. So, at the commencement of the calibration period, it is rational to accept that the replicated basin state was a descriptive of the actual state. Then, the PyTOPKAPI model was operated for getting the saturation condition of the soil at a designated period. This process offers representative values for the preliminary situation, mainly regarding the areal distribution of the soil wetness proportion. At the initial condition, it was assumed that no surface water was over the slopes and the depth of water in a generic channel cell increases linearly with the channel width of the cell [160, 195].

"Goodness of fit" by the NS efficiency and the R^2 correlation were quantified between the observed and the final simulated discharges. As it can be seen from the Figures 5.12 ,5.13 and 5.14 and the calculated performance efficiency values of NS and R^2 (Table 5.10), the simulated daily flows closely matched the observed values. Therefore, the calibration results show that there is a good agreement between observed and demonstrated hydrographs that is supported by high values of the overall NS's of 0.699 for Gilgel Ghibe catchment and 0.748 for Mojo catchment. A very good correlation was also observed in which the overall coefficient of determination R^2 values are 0.913 for Gilgel Ghibe catchment and 0.865 for Mojo catchment as indicated in Table 5.10.

Table 5.10: Summaried values the performance criteria of model calibration.

Gilgel Ghibe Catchment	Year	1986	1987	1988	1989	1990	1991	1992	1993
	R^2	0.943	0.935	0.949	0.977	0.833	0.875	0.953	0.921
	RMSE	24.72	25.10	25.17	29.28	39.74	25.64	25.69	34.27
	NS	0.688	0.539	0.861	0.679	0.529	0.676	0.874	0.658
	Year	1994	1995	1996	1997	1998	1999	2000	Overall
	R^2	0.952	0.950	0.921	0.922	0.944	0.928	0.963	0.913
	RMSE	25.98	22.21	34.14	40.44	25.66	29.98	31.49	31.98
	NS	0.876	0.677	0.641	0.618	0.833	0.642	0.627	0.699
Mojo Catchment	Year	1999	2000	2001	2002	2003	2004	2005	
	R^2	0.913	0.850	0.828	0.854	0.849	0.939	0.948	
	RMSE	18.314	13.402	5.483	4.413	8.430	5.688	6.463	
	NS	0.751	0.608	0.680	0.722	0.715	0.795	0.784	
	Year	2006		2007		2008		Overall	
	R^2	0.940		0.894		0.903		0.865	
	RMSE	4.274		4.805		9.598		9.186	
	NS	0.855		0.799		0.781		0.748	

The calibration results indicated that all the initial estimated quantities of the model parameters were reasonably suitable with the exception of the hydraulic conductivity which have been altered by suitable multiplying factors ($f_{ac}Ks$=0.70, & $f_{ac}L$=1.0 for Gilgel Ghibe catchment and $f_{ac}Ks$=0.73, & $f_{ac}L$=1.0 for Mojo catchment) for satisfactory model performance.

5.4.3 Evaluation of the calibration

As a confirmation for the relevance of the calibration on the entire catchment, the predicted and observed discharges at the outlets of the catchments (Gilgel Ghibe and Mojo) for the years calibration are plotted in Figures 5.12 and 5.13. Generally, there is good agreement that was observed

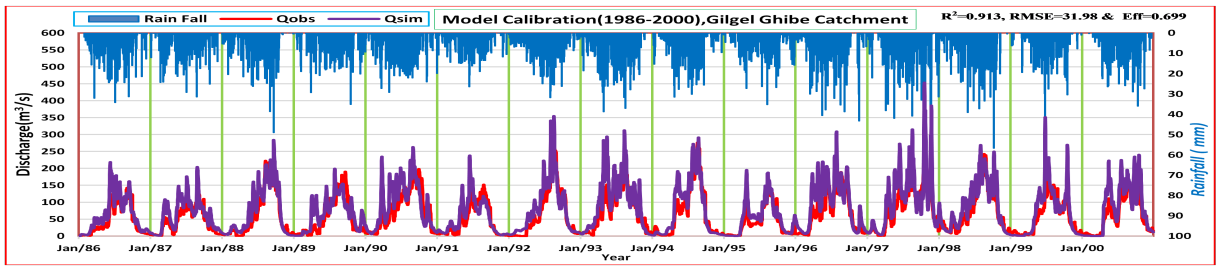

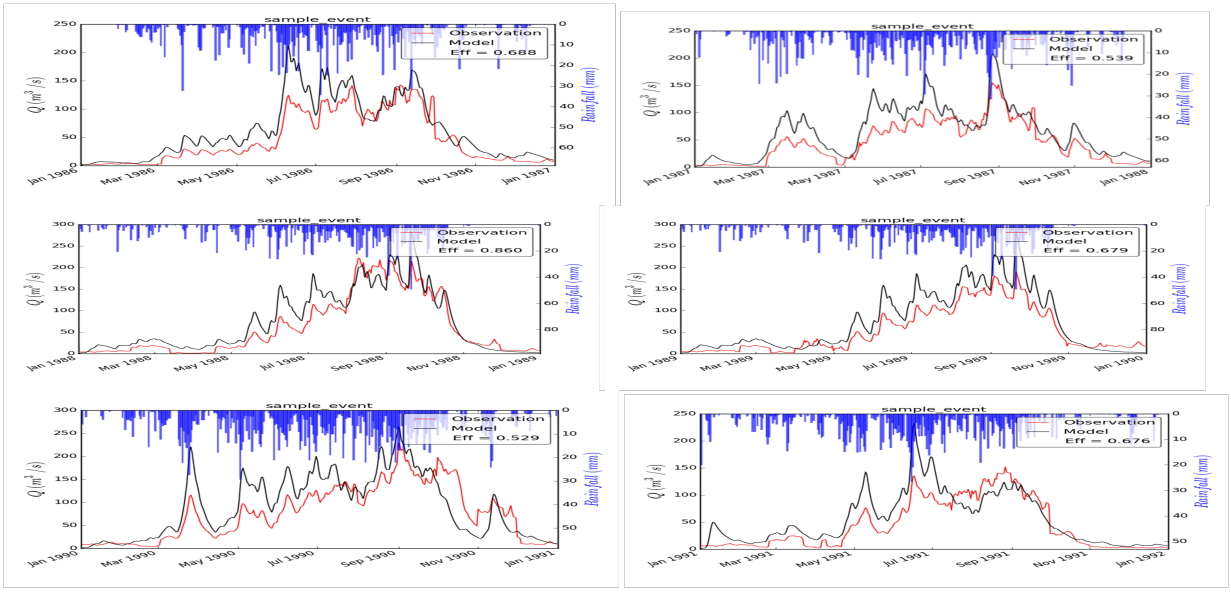

(a) Plate 1

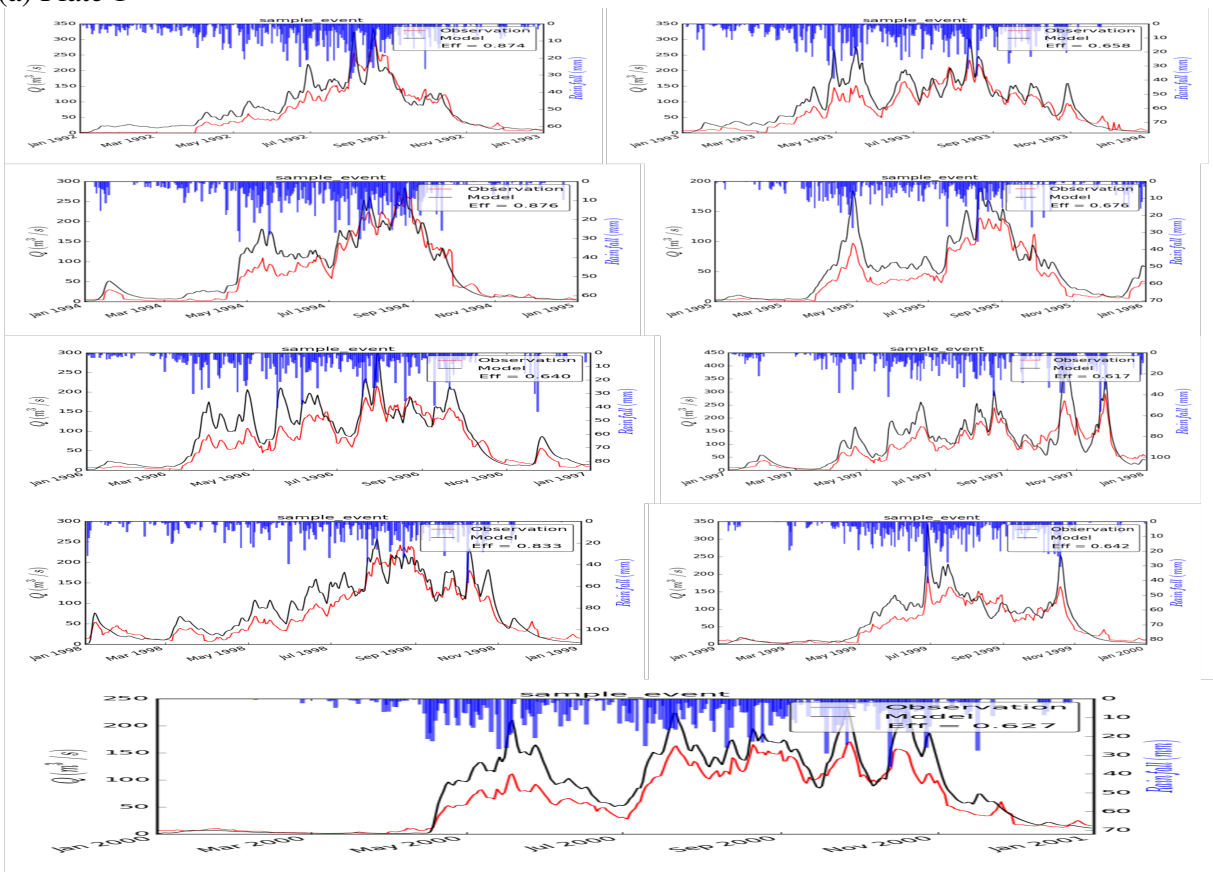

(b)Plate 2

Figure 5.12: Graphs of simulated and observed discharges for Gilgel Ghibe catchment (calibration)

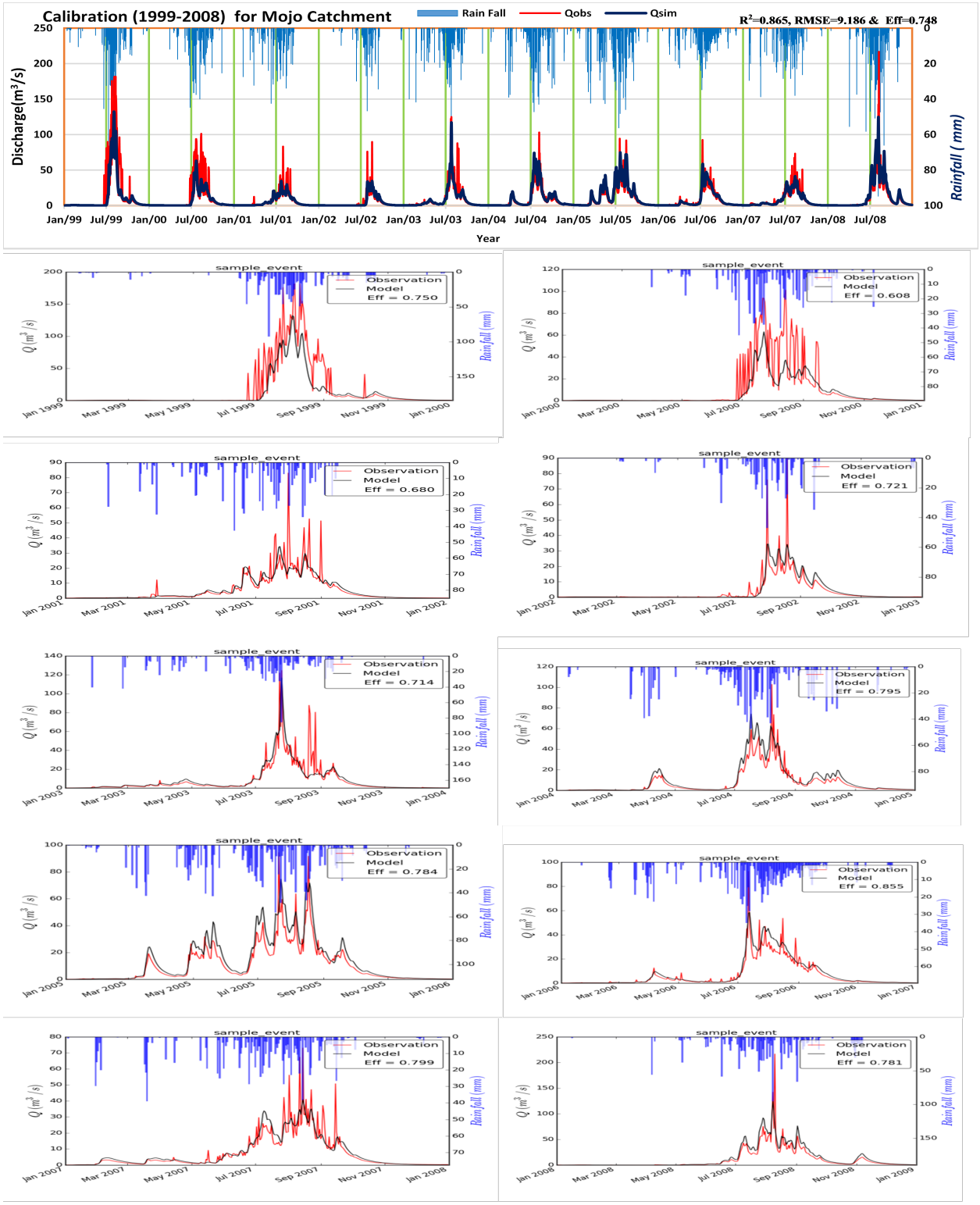

Figure 5.13: Graphs of simulated and observed stream flows for Mojo catchment (calibration)

between recorded and predicted flows, though at few of the data points, the recorded data appear unrealistic as few peak flow observed at "gauging" stations did not emerge in the stream flow simulation results specially for Mojo catchment. As can be seen from Figures 5.14 b and 5.15 b, the scatter plots of simulated versus observed discharge values showed an over estimation of the simulated discharge at a value of 10-20 m^3/s from the observed discharges.

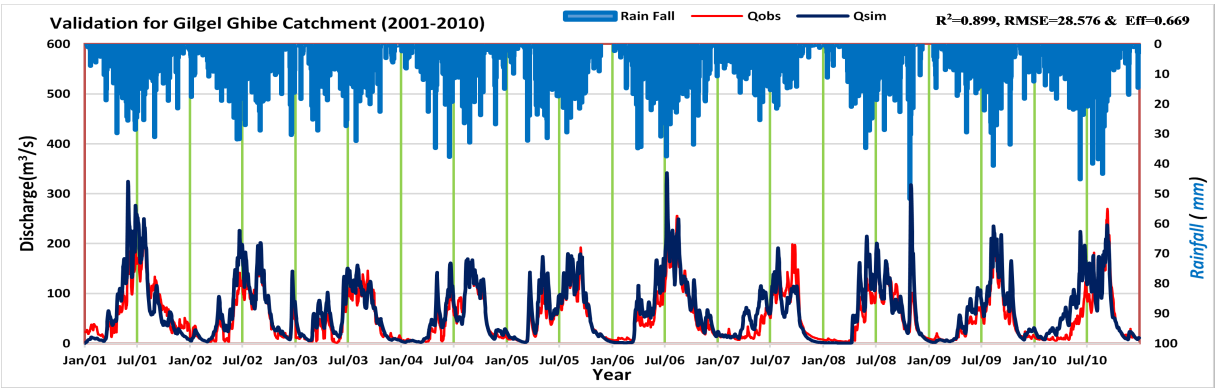

(a) Hydrographs

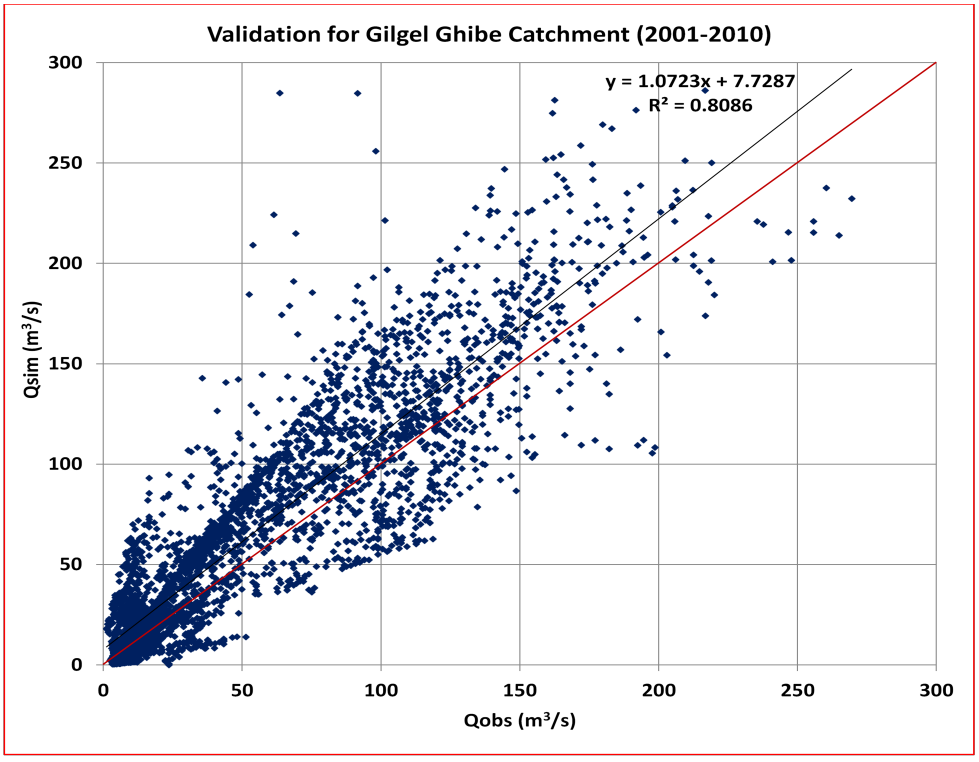

(b) Scatter plots

Figure 5.14: Graphs of simulated and observed discharges for Gilgel Ghibe catchment (validation)

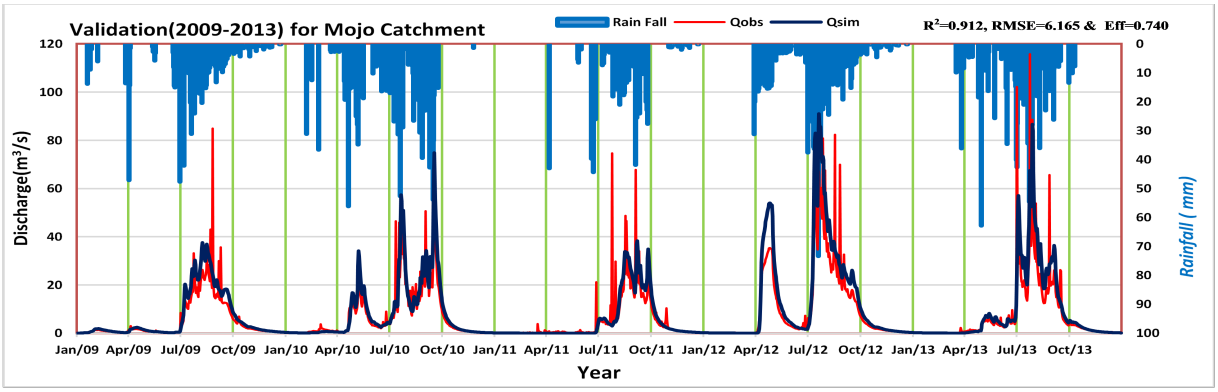

(a) Hydrographs

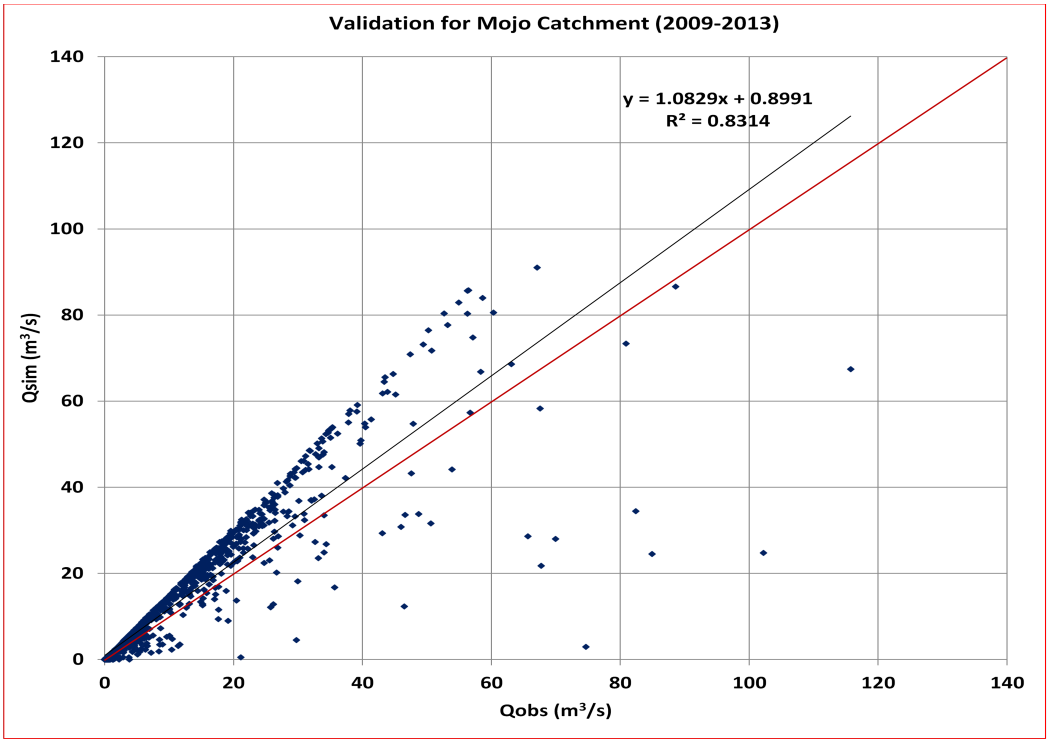

(b) Scatter plots

Figure 5.15: Graphs of observed versus simulated stream flows for Mojo catchment (validation)

5.4.4 Validation

In order to approve the effectiveness of the PyTOPKAPI model calibration, the model was operated on additional data of the other year's data using the same parameter values as for data of calibration period for both the catchments. Thus, utilizing the calibrated values of the model parameters, the model was validated with the use of the hydro-meteorological dataset within the time duration of: (a) Jan. 1, 2001 and Dec. 31, 2010 for Gilgel Ghibe catchment and (b) Jan. 1, 2009 and Dec. 31, 2013 for Mojo catchment. The hydrographs are plotted in Figures 5.14 a and 5.15 a, and the scatter plots of observed versus simulated discharges are illustrated in Figures 5.14 b and 5.15 b. Good simulation results were acquired even if some peak discharges simulated by the model were slightly overestimated.

5.5 Results and Discussions

PyTOPKAPI model was used to simulate stream flows from two Ethiopian case study catchments with the area of (1) $2943km^2$ defined by the flow outlet at "Ghibe Nr.Asendabo" gauging station of the Gilgel Ghibe catchment and (2) $1496km^2$ defined by flow outlet station at "Mojo @ Mojo village" gauging station for Mojo catchment. The simulations were achieved at a 24-hour time-step and a resolution of 1 km along with other spatial data of each catchment. The model was then calibrated as indicated above by a trial and error procedure. The efficiency of the model was analyzed using RMSE, NS and R^2 and finally validation for the model was done using continuous simulations over a few years of the data of the validation periods.

In this PyTOPKAPI application, the assessment of the simulation results from the calibrated and un-calibrated parameters show that the usage of literature value offers somewhat poor model performance. Here, the simulated flood events were slightly overestimated which was mainly because of the inappropriate values of the firstly assigned soil conductivities. Moreover, the calibration results showed that calibration was mainly concerned with the hydraulic conductivities. Rather than these, the overall model performance evaluations for both catchments were satisfactory. These simulations replicated the rivers' behavior well on both catchments. The observed results indicated that, the PyTOPKAPI model is efficient for replicating the river behavior.

5.6 Conclusions and recommendations

Hydrological modeling offers a way for examining of the relations between streamflow and climate [13]. The physically based fully distributed PyTOPKAPI hydrological model [59, 156, 160] has been applied successfully to two case study Ethiopian catchments (Gilgel Ghibe and Mojo) that are located 300km distance apart in different hydrologic regimes. This is the first implementation of the model in Ethiopia. Applied on the Gilgel Ghibe catchment ($2943km^2$, in Omo-Ghibe River Basin) and Mojo catchment ($1496km^2$, in Awash River Basin) on daily basis using 1km pixels with very few modification of the parameters and low computation times, it was observed that the model showed good capacity in modeling the river discharges. This has provided a significant knowledge and a further understanding of the model. Finally, it was concluded that PyTOPKAPI model is a very promising tool for modeling the behavior of river.

Chapter 6

Implementation of PyTOPKAPI Model in ungauged catchments in Ethiopia

6.1 General Summary

Many catchments in developing countries are poorly gauged or totally ungauged which hinders water resources management and flood predictions in these countries. In this study, the application of the PyTOPKAPI model to ungauged Ethiopian case study catchment (Gilgel Ghibe, Figure 3.1) was explored. The aim was to extend the model application to poorly gauged/totally ungauged catchments in developing countries. To generate reliable stream flows, models generally need to be calibrated which typically relies on the availability of reliable stream flow data. Previous application of the PyTOPKAPI model (Chapter 5) was accomplished in that satisfactory model performance was achieved by simple trial and error adjustment of grouped key parameters to match observed streamflow. This is not the option for ungauged catchments (catchments without stream flows). The model calibration in this case would use rainfall and potential evapotranspiration data to give a runoff ratio by means of Schreiber's formula, and then the runoff ratio value so obtained was used to calibrate the model. This was achieved without stream flow data unlike the standard calibration process of the catchment models. So, this study showed how application of simple lumped models for average runoff ratios, such as that proposed by Schreiber, can be used as an alternative to detailed calibration with gauged flows. This shows how the PyTOPKAPI model can be used to predict runoff responses in ungauged catchments for water resources applications and flood forecasting in developing countries.

On the other hand, reliable streamflow information is the main input for flood frequency analysis and peak flood estimation. Such information is directly measured through ground-based hydrological monitoring gauges installed at monitoring stations. However, in many developing countries like Ethiopia, ground-based stream flow monitoring networks are either sparse or nonexistent, which hinders the management of water resources and hampers early flood-warning arrangements. In such cases, satellite remote sensing is an alternative means to acquire such information via stream flow modelling. This particular study discusses the application of remotely sensed rainfall data for streamflow modeling with a case study in Gilgel Ghibe basin in Ethiopia. Ten years (2001-2010) of two satellite-based precipitation products (SBPP), TRMM & WaterBase, were used. These products were combined with the PyTOPKAPI hydrological model to generate daily stream flows. The results were then compared with streamflow observations at Gilgel Ghibe Nr, Assendabo gauging station (Figure 3.1) using four statistical tools (Bias, R^2, NS and RMSE). The statistical evaluation suggests that the bias-adjusted SBPPs agree well with gauged rainfall compared to bias-unadjusted ones. The SBPPs with no bias-adjustment tend to overestimate (high Bias and high RMSE) the ex-

treme precipitation events and the corresponding simulated streamflow outputs, during wet months (June-September) and underestimate during few dry months (January and February). This shows that bias-adjustment can be important for improving the performance of the SBPPs in streamflow modelling. The overall results indicated that the general streamflow patterns were well captured at daily time scales using bias-adjusted SBPPs. These results, however, demonstrate that the simulated stream flows using the gauged rainfall is superior to those obtained from the SBPPs including bias-adjusted ones. This shows how remote sensing gives valuable information to streamflow estimations.

6.2 Introduction

Natural disasters are considered to be an increasing threat for sustainable development and the security of humankind [74]. Floods are one example that can often lead to loss of life and property [279]. Accurate and reliable streamflow forecasting is a key for effective flood management [139, 159, 218, 299, 313] and is vital for effective water resources planning and management [39, 215, 220]. Traditionally, stream flow is directly measured with the use of ground based gauges installed at monitoring stations. However, in numerous countries, especially in developing nations [262] like Ethiopia, hydrological monitoring networks are sparse or non-exist. Because of these facts, estimation of streamflow time series in ungauged catchments remains a challenge. Thus, streamflow modelling is the only option for reliable quantification of stream flows. However, to generate reliable stream flows, models generally need to be calibrated which typically relies on the availability of reliable stream flow data. This is not the option for ungauged (non-streamflow) catchments.

Early attempts to estimate stream flows from ungauged catchments employed calibrated model parameters from nearby gauged catchments where streamflow data were available. However, the modelled streamflow from ungauged catchments may be uncertain when basin features such as geography, vegetation and soil character, are significantly different from those of gauged catchments [135, 281]. While the estimation of model parameters for ungauged catchments is challenging, it is important to evaluate whether simulated time series preserve critical aspects of the streamflow hydrograph [281]. The present study thus demonstrates the practical implementation of PyTOPKAPI model [240, 283] on an Ethiopian (Gilgel Ghibe, 2943km^2) ungauged catchment, in a sense that there was rainfall data but little/no streamflow data, for streamflow modelling. However, it is difficult to calibrate the model for quantification of a reliable streamflow time series from such catchments. Efforts are made to investigate the use of runoff ratio formula proposed by Schreiber [18, 90–92] as an alternative model calibration procedure. Thus, this study showed how application of simple lumped models for average runoff ratios, such as that proposed by Schreiber, can be used as an alternative to detailed calibration with gauged flows. This approach seems to be new in this context as an alternative model calibration procedure for streamflow simulation from ungauged catchments. In Schreiber's work, the runoff ratio is the (time averaged) ratio of volume of runoff to volume of rainfall in a catchment. It illustrates the average excess rainfall for a catchment [92]. Consequently, the runoff ratios were computed from the simulated stream flows and the rainfall data of the study catchment. The model was then calibrated using the simulated runoff ratio with that predicted by the Schreiber formula in that it generated a realistic daily stream flows for the catchment.

Conversely, it is evident that precipitation is a key input for streamflow modeling. Nevertheless, in developing countries, ground-based monitoring gauges for rainfall (radars or rain gauges) are also either sparse or totally absent. These circumstances limit the management of water resources and

hamper early flood warning systems in these regions as well and consequently can lead to substantial socio-economic losses. In such cases, satellite remote sensing (RS) is an alternative source of information for data limited zones. In this study, the contribution of RS to streamflow modeling using remotely sensed rainfall data for data scarce areas was assessed, the results of which would ultimately be used for flood frequency analysis and peak flood estimation. The PyTOPKAPI hydrological model was used to convert remotely sensed rainfall data into useful streamflow information.

To sum up, this study in general shows how the PyTOPKAPI model can be used to predict runoff responses in ungauged catchments for water resources applications and flood predictions in developing countries.

6.3 Application of PyTOPKAPI Model in ungauged catchments

6.3.1 PyTOPKAPI Model Application

As indicated in section 5.3.2 of Chapter 5, the PyTOPKAPI model requires gridded data including: (1) a Digital Elevation Model (DEM); (2) a soil type classification; (3) a land use classification; and (4) hydro-meteorological data (rainfall, and temperature). The observed streamflow data were also utilized for testing the suitability of the calibration approach. Brief descriptions of these data were presented hereunder.

6.3.1.1 Digital Elevation Model (DEM)

As shown in section 5.3.2.1 of Chapter 5, the SRTM DEM obtained from (`http://srtm.csi.cgiar.org`) was used. The resolution of the DEM were set to 1km for this study also. All other terrain maps were set to this resolution. The DEM was pre-processed to eradicate the false outlets and the sinks so that the flow system and the basin outlet unit are exceptionally identified.

6.3.1.2 Soil Type Data

The soil type grid data was obtained from the Harmonized World Soil Database (HWSD) [84,116]. This is clearly indicated in section 5.3.2.2 of Chapter 5. The HWSD contains of a raster image file and an associated characteristic database. The grids comprise the main soil texture class for each of the 13 standard soil layers by means of the USDA soil texture class index with reference to the HWSD attribute table.

6.3.1.3 Land Use

The Land use maps for the study catchment was obtained from the USGS (United States Geological Survey) Global Land Cover Characterization (GLCC) database and made accessible using the WaterBase web site [291] as shown in section 5.3.2.3 of Chapter 5. The required values of the Manning roughness coefficient for all grid cells forevery land use class were obtained from the land use grids data of USGS Land Use/Land Cover System Legend-Modified Level 2 [276] and Manning's roughness values indicated for different land cover classes in GeoSFM [19].

6.3.1.4 Hydro-Meteorological Data

As described in section 5.3.2.4 of Chapter 5, the meteorological utilized in this study were daily rainfall and temperature records of Jimma, Asendabo and Yebu weather stations between 01/01/1986 and 31/12/2010 collected from the Ethiopia National Meteorological Agency. We also utilized the

daily discharge observation data (1986 - 2010) at the Gilgel Ghibe catchment's outlet acquired from Ministry of Water affairs in Ethiopia to confirm the suitability of the Schreiber's run-off ratio for model calibration.

6.3.1.5 Potential Evapotranspiration (ETo)

The ETo data used were obtained by taking the average value of ETo computed by the methods of Bleney-Criddle [37], Thornthwaite [268] and the ETo regression equations developed by Sileshi for Ethiopian case [234]. These computations were shown in section 5.3.2.5 of Chapter 5.

6.3.2 Model Calibration and Validation

6.3.2.1 Model Calibration

As explained in section 5.4.2 of Chapter 5, a physically based model like the PyTOPKAPI model should require no calibration. Because, its parameters are estimated from catchment data such as morphology and hydraulic catchment properties, soil, vegetation, literature and experience [60]. In spite of this fact, it may be subject to several uncertainties associated with the data on topography, soil characteristics and land use and on the approximations introduced by the scale of the parameter representations. Due to these reasons, Liu and Todini [160] suggest that the calibration of the parameters is still necessary for fine tuning the model.

Previous studies using the PyTOPKAPI model indicated that satisfactory model performance could be achieved by simple trial and error adjustment of grouped key parameters [195] to match observed streamflow. This is not an option in the case of ungauged ungauged catchments. Thus, the use of the runoff ratio formula proposed by Schreiber [91] was investigated as an alternative to detailed model calibration procedure. The runoff ratio shows the percentage of precipitation that appears as runoff by taking other basin characteristics (e.g., soil, slope, vegetation) into account. It is used to describe the overall water balance of a basin and is an indication of how well the model is simulating the water balance of the basin based on the primary input information [92, 234].

Schreiber examined data of the mean annual run-off R versus the annual rainfall totals P of continental European river basins and fitted them to a polynomial curve. He developed the formula: $R = Pexp(-N/P)$ where N is potential evapotranspiration and the expression (N/P) is defined an aridity index (ϕ) or a Dryness index (D) [90–92].

The functional form of the Schreiber formula is based on the aridity index (ϕ), defined as the ratio between the ETo and precipitation (P), is a reasonable first-order approximation of the actual evapotranspiration (ETa) [18, 103]. Thus, it may be called as an integrated runoff rainfall ratio calculated using the functional form of ϕ. The formula can also be extended to determine the ratio between the actual evapotranspiration (ETa) the precipitation (P) through the balance of water as shown below.

Water balance refers to the quantitative description of the hydrologic cycle. Water is supplied by precipitation, and is balanced by runoff and evapotranspiration [73, 92]. This gives the basic Water balance equation:

$$R = P\text{-}ETa \tag{6.1}$$

From which, the evapotranspiration ratio is expressed as [18, 92];

$$\frac{ETa}{P} = 1 - e^{-\phi} \tag{6.2}$$

Where $\phi = \frac{ETa}{P}$=Aridity index= Dryness index (D) =N/P

Thereby yielding the value of the mean annual runoff (R) as a function of the dryness index and precipitation (P) [103].

$$R = P(1\text{-}f(\phi)) \tag{6.3}$$

This implies, the runoff- ratio, $\frac{R}{P} = e^{-\phi}$

Accordingly, the above integrated Schreiber's runoff ratio formula was used for computation of the runoff ratios to calibrate the model. In this case, the monthly average potential evapotraspiration (ETo) value of the catchment is 109 mm (see section 5.3.2.5 of Chapter 5) and that of the precipitation (P) is 120 mm. Based on these data, the calculated runoff ratio by the Schreiber's formula was shown in Table 6.1.

Table 6.1: Calculated run-off ratio by the Schreiber's formula

Catchment	Potential Evapotranspiration, ETo (mm/month)	Precipitation, P (mm/month)	Aridity index, $\phi = ETo/P$	Run-off ratio, R/P=exp(-ϕ)
Gilgel Ghibe	109	120	0.908	0.403

Table 6.1 shows that the Schreiber's runoff ratio for the study catchment is 40%. If observed streamflow data is available, the runoff ratio can also be obtained from the plot of cumulative volumes of precipitation versus the cumulative volume of observed discharge data. Consequently, the runoff ratio based on 10 years (2001-2010) data for Gilgel Ghibe catchment was 39% (Figure 6.1). Similarly, the runoff ratio for Mojo catchment, both by Schreiber's formula and runoff verus rainfall observations, was found as 17%. Therefore, the generally good agreement between the observed values and those predicted by the Schreiber's runoff ratio formula indicated that the Schreiber's formula can be used in this regions to predict average runoff coefficients for use in calibrating the PyTOPKAPI model.

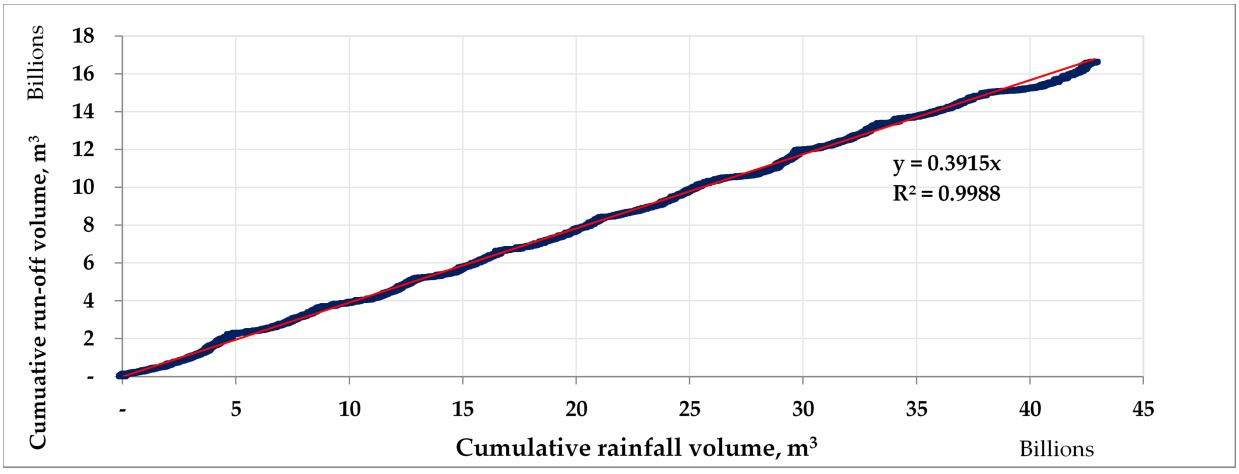

Figure 6.1: Plot of cumulative volumes of precipitation and observed discharge (2001-2010)

Hence, the model could possibly be calibrated by comparing the simulated run-off ratio with the Schreiber's runoff ratio. According to a sensitivity analysis conducted by researchers, the most sensitive parameters controlling runoff production by PyTOPKAPI are the soil conductivity (K_{sat}) and the soil depth (L), whereas the Manning roughness of channel (n_c) and overland (n_o) are the primary routing parameters [156, 200]. While calibrating the model, it was also observed that the most sensitive model parameter was the soil conductivity (K_{sat}), followed by the soil depth (L). These parameters are then described as shown below.

The first and the most sensitive parameter is the Ksat. It is the most important soil hydraulic parameter for flow in soil. Direct measurement of this parameter is "very challenging, laborious, and expensive" [210] under field or laboratory situations, and even "sometimes unfeasible for numerous hydrological assessments" [222]. Due to that, soil scientists and engineers have intensively investigated its estimation over the past several decades. Consequently, numerous models/ pedotransfer functions (PTFs) were developed to estimate the representative Ksat values with readily obtainable soil data [222] such as soil texture, soil organic matter, and soil bulk density [129, 210, 222, 223, 244]. However, the accuracy and the reliability of each of them are very variable [47, 75, 175, 180, 210, 211, 222, 223, 244, 250, 257]. Large errors in some cases and good accuracy in the other cases were observed. That is to say, the accuracy of using the indirect methods for Ksat estimation was relatively low. Conversely, direct estimation of Ksat is a difficult task involving testing, measurement and judgment. Hence, it advisable to adequately asses a representative Ksat value balancing between cost and accuracy. With these inferences, we used the Ksat value provided in Table 2 of Rawls et al. [210] for the current study as it provides an adequate estimate for applications where more detailed data are not available and direct Ksat measurements are not feasible.

The second sensitive model parameter is the soil depth. The soil depth that the PyTOPKAPI model uses is the sum of the depths for the A and B horizons [195]. It is the important parameter but is the most challenging to estimate. In this study, we used the uniform "Reference soil depth" presented in the Harmonized World Soil Database (HWSD) [84]. In this case, the 'Reference soil depth' of all soil units are uniformly set at 100 cm, except for Rendzinas and Rankers of FAO-74 and Leptosols of FAO-90, in which it is set at 30 cm, and for Lithosols of FAO-74 and Lithic Leptosols of FAO-90, where the same is set at 10 cm. The soil characteristics in the HWSD represent data from real soil profiles for surface (0 to 30 cm) and deeper (30 to 100 cm) soil horizons. An estimate of the real soil depth can be obtained by considering applicable depth restricting soil stages, interferences to roots and event of impervious layers. We expected that the 'Reference soil depth' contained in the HWSD can provide an appropriate estimate of the soil depth for the current PyTOPKAPI applications since more detailed data of soil depth are not available in the study areas and is eventually adjustable by calibration.

These two sensitive parameters were then optimized (Table 6.2) by assuming the soil depth from within the range of its realistic values that would provide the target runoff ratio (basically, fL=1.0) and finding the corresponding value of the soil conductivity since the accuracy of the soil depth is relatively low. Table 6.3 subsequently shows the final optimum (unique) calibrated model parameters. To check the streamflow variability, the coefficient of variation (CV) of the flows was employed. The CV provides a temporal variability of runoff estimation in a catchment [31, 53]. In this case, the CV of the observed stream flows of the catchment was found as 0.793.

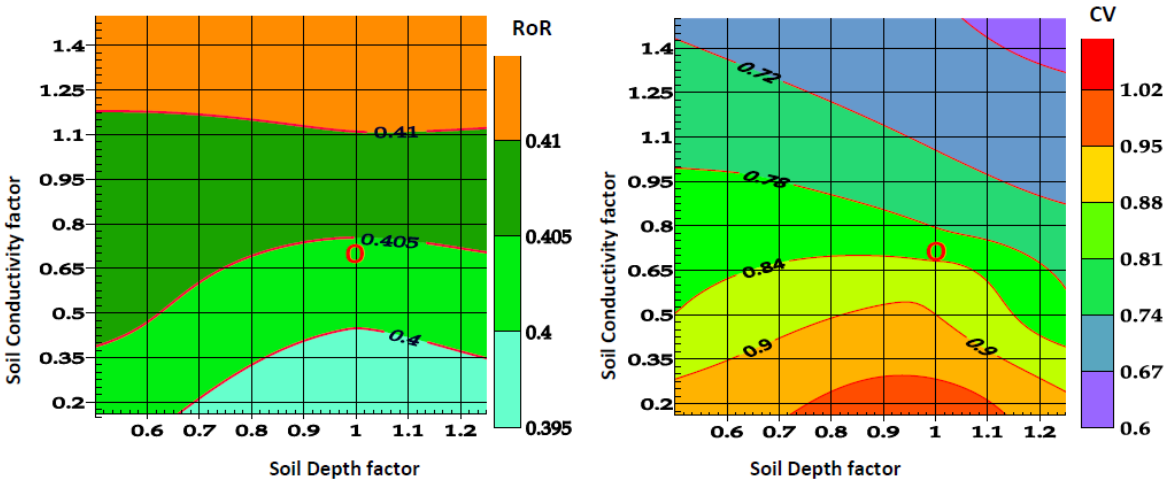

Figure 6.2: Contour plot of different combinations of the model parameters with the resulting RoRs and CVs wherein the red rings indicate the combination that provided the satisfactory RoR compared with target ones.

Table 6.3: The calibrated sensitive model parameters

Calibrated Multiplying factor		Q/AR	Q mean (m^3/s)	SD (m^3/s)	CV
Soil Depth (fL)	Hyd. Conductivity (fK)				
1.00	0.70	0.404	65.82	53.40	0.81

Table 6.2: Parameters obtained from simulated stream flows (Schreiber's Runoff ratio is 40%)

Multiplying factor		RoR (Q/AR)	Q mean (m^3/s)	SD (m^3/s)	CV
Soil Depth (fL)	Hyd. Conductivity (fK)				
0.50	0.50	0.407	61.40	51.43	0.84
0.63	0.93	0.408	67.82	53.33	0.79
1.00	0.16	0.395	58.31	58.93	1.01
1.00	0.45	0.400	61.97	54.46	0.91
1.00	0.65	0.403	62.71	55.81	0.89
1.00	**0.70**	**0.404**	**65.82**	**53.40**	**0.81**
1.00	1.00	0.409	71.50	51.93	0.73

Figure 6.2 also shows the contour plot of different combinations of the model parameters with the resulting runoff-ratios (RoRs) and CVs in which the red rings indicate the combination that gave the satisfactory RoR. The correcsponding CV value from this contour plot was found as 0.81. It was identified that the parameter adjustment factors were essentially identical for two the case study Ethiopian catchments (Gilgel Ghibe [fL=1.0, fK=0.7] and Mojo [fL=1.0, fK=0.73]) as shown in section 5.4.2 of Chapter 5. Moreover, this approach was also tested on very small catchment (Mhlanga, 80km^2) in South Africa and identical results were obtained [85, 202]. This suggests the generality of the results in that it would work for other catchments as well with the same parameter adjustment factors [fL=1.0, fK=0.7]. This further supports the use of PyTOPKAPI model for ungauged catchments.

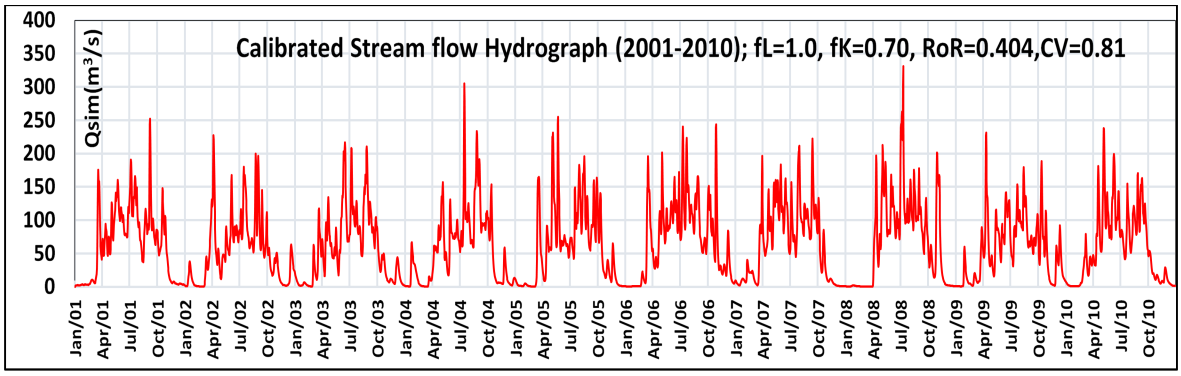

Figure 6.3: Simulated streamflow hydrograph of the catchment (calibration)

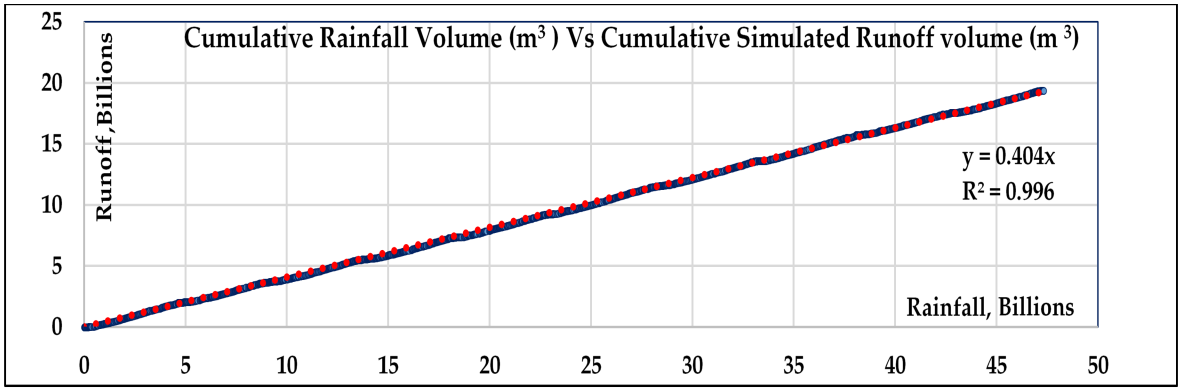

Figure 6.4: Plot of simulated runoff ratio for the catchment (calibration)

6.3.2.2 Evaluation of the calibration

As a confirmation of the relevance of the calibration, the simulated stream flows of the catchment for the years of calibration are plotted in Figure 6.3. The CV value obtained from the simulated results agreed with the estimated CV value of the catchment. It was also observed from scatter plot of cumulative rainfall volume and cumulative simulated runoff volume (Figure 6.4) that there is, in general, good agreement between Schreiber's runoff ratio and simulated runoff ratio. To further realize the flow characteristics, comparison between observed and simulated stream flows was also done using flow duration curves (Figure 6.5). The flow-duration curve is an aggregate frequency curve that demonstrates the percentage of time during which the predefined stream flows were equaled or exceeded in a given period. It consolidates the flow components of a stream all through the scope of discharge in one curve, deprived of the sequence of occurrence. It also offers a suitable means for studying the flow characteristics of streams and can be used to compare streams in dissimilar geomorphic settings. Subsequently, the overall comparisons in this perspective revealed that the model reasonably captured stream flows including extreme discharges and their timings (Figure 6.5). This further proves the capability of PyTOPKAPI model, together with the Schreiber's runoff ratio, in modeling the stream flows from ungauged catchments.

6.3.2.3 Validation of the calibration

In order to validate the PyTOPKAPI model calibration on more reliable data, the model was applied to a different period of data, using the calibrated model parameter values and the hydrometeorological dataset of the period between January 1, 1986 and December 31, 2000. The simulated hydrograph is given in Figure 6.6, and scatter plot of cumulative rainfall volume and simulated runoff volume is illustrated in Figure 6.7. In this validation period, the simulated run-off

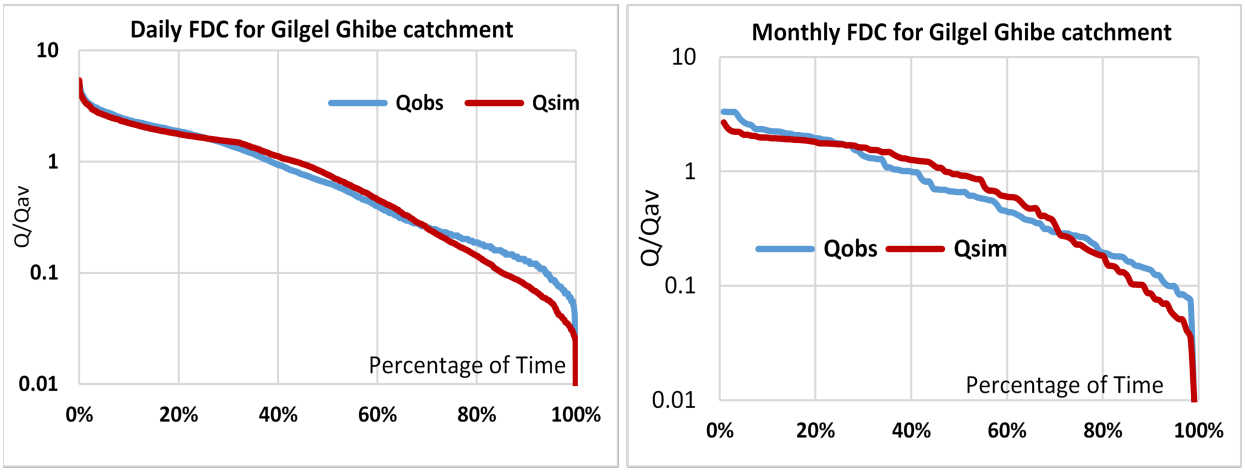

Figure 6.5: Flow duration curves (FDC) of observed and simulated flows

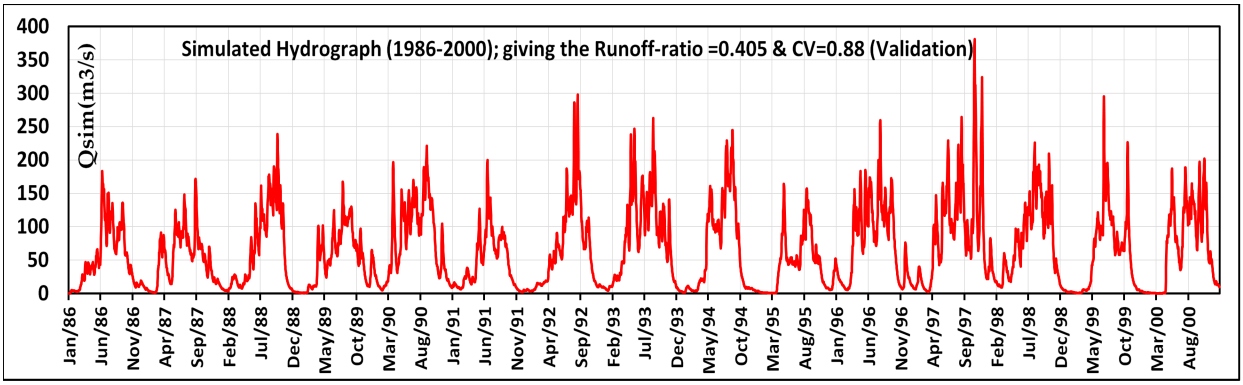

Figure 6.6: Simulated streamflow hydrograph of the catchment (Validation)

ratios and the CV value were also observed to be in a good agreement with the target ones. In general, good simulation results were obtained.

6.3.3 Conclusion and recommendations

Water resources are of great value as they are deeply connected with the well-being of man-kind. Hydrological processes of a specified area are often known by studying river catchments [41] for which sophisticated rainfall-runoff models are essential to assess climatic and hydrometerological conditions, as they influence the sustainability of water resources and water availability [41, 89, 136]. These rainfall-runoff models are powerful tools used in various water resources applications for simulating stream flows. However, most rivers of developing countries are poorly gauged or totally ungauged thereby resulting in limited data for calibration of models such as the PyTOPKAPI model. In this study, we examined the possibility of using the physically based PyTOPKAPI model together with the Schreiber run-off ratio formula for application to ungauged catchments. This method is a new approach to model calibration in this context. The results suggest this approach can produce acceptable streamflow predictions. The optimum values of the sensitive model parameters were established by assuming the soil depth from within a range of its realistic values (thus retaining its physical meaning) and then finding the corresponding values of saturated hydraulic conductivity to match the predicted run-off ratio. Stream flow variability was also used by matching the coefficient of variation of the simulated flows to what is predicted by regression onto the runoff-ratio. In summary; our results suggest that the PyTOPKAPI model,

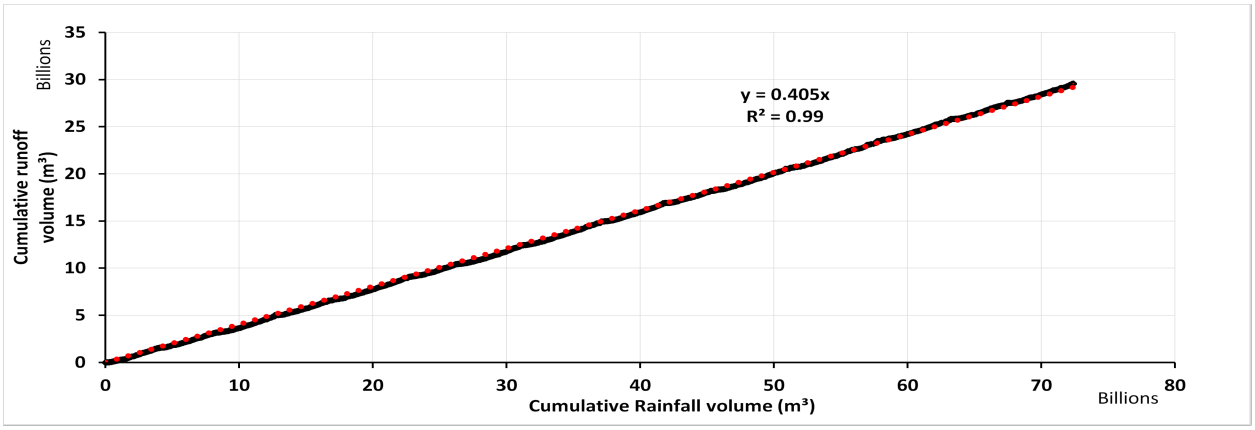

Figure 6.7: Plot of simulated run-off ratio for the catchment (Validation)

with our simplified calibration approach, can be used to predict run-off responses from ungauged catchments for water resources applications and flood predictions in developing countries. Further refinement of the approach is recommended by implementing and testing it on additional catchments.

6.4 Application of PyTOPKAPI model with Remotely Sensed Rainfall Data on Gilgel Ghibe Catchment

The role of RS in giving subdaily, uninterrupted and economical hydro-meteorological datasets has been widely recognized. Basically, the role of RS in obtaining stream flow information are in (1) streamflow modeling – remotely sensed data as "input" for a hydrological model [7, 208] ; (2) stream flow estimation – estimation of stream flow by RS data alone deprived of the usage of any hydrological model [245] as shown in figure 6.8.

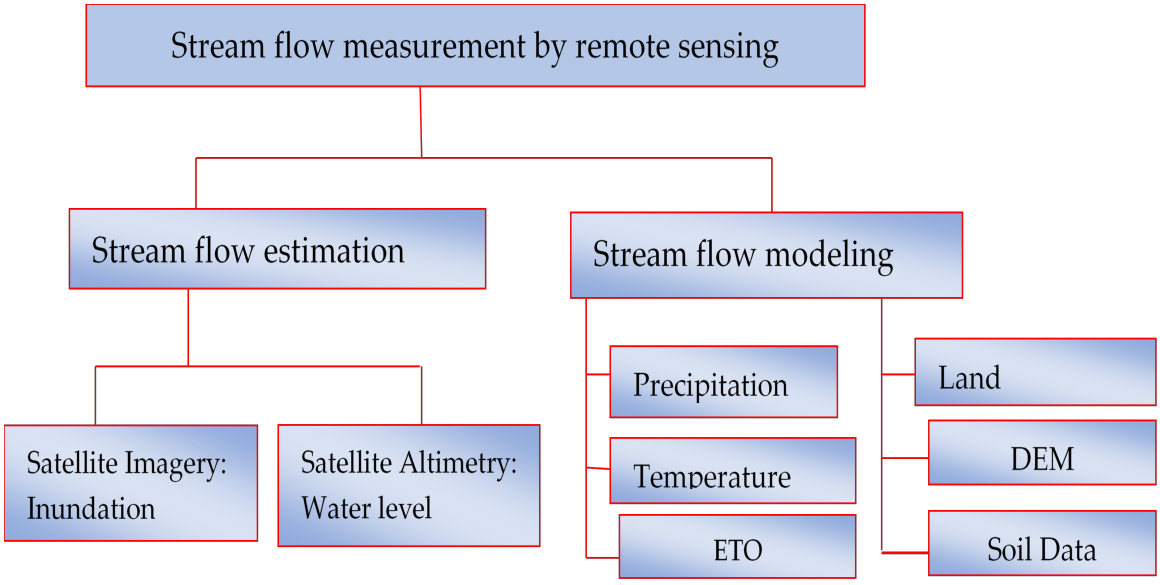

Figure 6.8: Role of RS in stream flow measurement [262]

6.4.1 PyTOPKAPI model Application

As shown in section 5.3.2 of Chapter 5, the required input data to PyTOPKAPI model are: (1) a Digital Elevation Model (DEM); (2) a soil type classification; (3) a land use classification; and (4) hydro-meteorological data (rainfall [in this case, remotely sensed rainfall data], and temperature). The observed streamflow data were also utilized for testing the suitability of the remotely sensed rainfall data for stream flow modeling. Brief descriptions of these data are presented hereunder.

6.4.1.1 Remotely Sensed Rainfall Data

Precipitation data is a key "input" to a hydrological model [145, 158]. In areas of sparse or nonexistent rain gauge distribution, satellite RS is an alternative way for providing precipitation data to carry out streamflow modelling. It is also an appropriate tool to help alleviate some of the hydrometric data collection and management problems facing many of the developing nations [145]. Generally, RS offers the components of such information in digital form for streamflow forecasting with the benefit of giving uninterrupted, vast coverage and free for data users. Provided that precipitation is the key input that directly impacts the outcome of simulation [145, 263], this section concerns the aspects of rainfall in the streamflow modeling. There are numerous freely available global SBPPs that can be used for stream flow modeling [263]. In this study, we used two SBPPs (TRMM & Waterbase) as "input" for the model. A brief description of each of them is given below.

6.4.1.1.1 Tropical Rainfall Measuring Mission (TRMM): The TRMM, a joint NASA (US)-Japanese satellite mission, was launched in 1997 [122] with aim of providing global rainfall observations that can be used for enhanced scientific studies. The TRMM Multi satellite Precipitation Analysis ("TMPA") is a new SBPP dataset designed to combine precipitation estimates from various satellite systems, as well as land surface precipitation gauging stations when possible and provides a calibration-based precipitation estimates at finer spatio-temporal scales ($0.25^0 X 0.25^0$ & 3 hourly) [10, 122]. The "TMPA" products are obtainable in two types: post-real-time version (3B42) and near-real-time version (3B42RT). The post-real-time version (3B42) only integrates gauge data presently [262]. These data are available for the period from 1998 to the late present covering the latitude of $50^0 N$ to $50^0 S$. Finer-scale "TMPA" is fruitful for approximately replicating the surface observation–based variation of precipitation, as well as rationally identifying huge day-to-day happenings [122].

Various authors have described TRMM rainfall dataset is a promising way for obtaining the precipitation data to perform streamflow modelling. Duan and Bastiaanssen [76] found that TRMM3B43 and TRMM3B42 data were reliable in Iran in the Caspian Sea Region for most months of years in the period 1999-2003. Dinku et al. [71] also assessed efficiency of 10 dissimilar SBPPs over Ethiopia in Africa and found out that TRMM-3B43 & TRMM-3B42 performed realistically well. Similarly, Behrangi et al. [27] appraised the performance of numerous SBPPs [TMPA real time (TMPA-RT); TMPA bias adj. (TMPA-V6); PERSIANN; PERSIANN bias adj. (PERSIANN-adj); and Climate Prediction Center morphing algorithm (CMORPH)] for streamflow modeling over Illinpis River Basin in USA. The results pointed out that all SBPPs gave good replication at sub-daily and monthly time steps.

According to Huffman et al. [122] the "near–real time" product makes the estimates useful to several new classes of users. Consequently, we used the daily 0.25^0X0.25^0 near-real-time version of TRMM precipitation products (TRMM3B42RT) [128, 226] that can freely be assessed and obtainable through the GES-DISC : Giovanni as part of the NASA's Goddard Earth Sciences (GES) Data & Information Services Center (DISC) [125].

6.4.1.1.2 Satellite- precipitation products from Waterbase Web Site: This is the second SBPP which could be obtained with other weather datasets such as Temperature (^0C), Wind speed (m/s), Relative Humidity (fraction) and solar radiation (MJ/m^2) which are collectively available at Waterbase Web Site (http://globalweather.tamu.edu/). These weather data are available from January, 1979 to August, 2014. For this study, the remotely sensed rainfall data for period of 10 years (2001-2010) obtained from this Waterbase web site were used.

6.4.1.2 Hydro-meterorological data

As indicated in section 5.3.2.4 of Chapter 5, the reference daily observed precipitation data were obtained from Ethiopia National Meterological Agency from 1986 to 2010 for the 3 rain gauging stations (Jimma, Asendabo and Yebu) located within the Gilgel Ghibe basin. The daily streamflow recorded data at the basin's outlet (Ghibe Nr Assendabo) was also obtained from Water affairs Ministry in Ethiopia.

6.4.1.3 Evapotranspiration(ETo)

The ETo data used were obtained by taking the average value of ETo computed by the methods of Bleney-Criddle [37], Thornthwaite [268] and the ETo regression equations developed by Sileshi for Ethiopia [234]. These computations were shown in section 5.3.2.5 of Chapter 5.

6.4.1.4 Land use/land cover

The Land use maps used for this part of the study is obtained from WaterBase web site [291] as shown in section 5.3.2.3 of Chapter 5. The Manning roughness coefficient, which are required by the model for every grid cells of the land use class, were obtained from the land use grids data of USGS Land Use/Land Cover System Legend-Modified Level 2 [276] and Manning's coefficient values used for various land cover classes in GeoSFM [19].

6.4.1.5 Soil data

The soil type grid was obtained from the Harmonized World Soil Database (HWSD) [84, 116]. This is clearly indicated in section 5.3.2.2 of Chapter 5. The soil type classes can be defined by the data established by the soil type grid (HWSD_RASTER) acquired from Harmonized World Soil Database. The HWSD is consisted of a raster image file connected with attribute database.

6.4.1.6 Digital Elevation Model (DEM)

As shown in section 5.3.2.1 of Chapter 5, the DEM data obtained from SRTM at (http://srtm.csi.cgiar.org) was used. The NASA SRTM has provided the DEMs data for the entire globe (over 80% coverage). This data is presently disseminated cost free by USGS [131, 132].

6.4.2 Performance Evaluation Criteria

To quantitatively analyze the reliability of the two SBPPs against gauged rain observation and their effect on streamflow simulation, four widely used performance evaluation statistical tools (Bias, RMSE, R^2 and NS) were employed. In this case, the relative Bias (Rel.Bias (%)) was used to additionally measure the agreement between the averaged value of simulated rainfall data (we used "Rsim" for both satellite precipitation products as "simulated rainfall data") and observed

rainfall (gauged rainfall) data ("Robs" was used in the formula). Moreover, the adjustment of the bias was done using the simple ratios of the respective SBPP data and the gauged rainfall data.

$$Rel.Bias(\%) = \left[\frac{\sum_{i=1}^{n} Rsim_i - \sum_{i=1}^{n} Robs_i}{\sum_{i=1}^{n} Robs_i}\right] X100 \tag{6.4}$$

6.4.3 Model Calibration & Validation

The modeling starts with pre-processing of the DEM and preparation of model input parameters and then incorporates them into the model to generate reliable streamflow data along the drainage system. The streamflow modelling was performed using 10 years SBPPs data (2001–2010) over the study basin located upstream of Gilgel Ghibe Nr, Assendabo gauging station. So as to generate a more dependable streamflow information, the model parameters required calibration. In this case, calibration was performed using 15 years gauged rainfall data (1986–2000) as indicated in section 5.4.2 of Chapter 5. The remaining dataset (2001–2010) of the gauged rainfall was used for verification of the results. Subsequently, the PyTOPKAPI model generated daily streamflow similar to the daily collected streamflow observation at the basin's outlet.

6.4.4 Results and Discussion

So as to examine the performance of the SBPPs for streamflow predicting, it is vital to assess the effect of the distinct SBPP compared to the gauged rainfall information. Consequently, the assessments are accomplished for both the rainfall involved and the matching simulated stream flow outputs. The rainfall/streamflow assessments are conducted at daily scales with the help of visual examination of the simulation results along with the statistical procedures mentioned above. Details are as given below.

6.4.4.1 Comparison of precipitation inputs

To better realize the effect of rainfall inputs on the model, the accuracy of the SBPPs against the gauged rain observations should be assessed first. This section compares the SBPPs and gauged rain observations from 2001 to 2010. Figure 6.9 shows the daily basin averaged precipitation time series (2001–2010) for reference gauged rainfall (Figure 6.9 a) and the two SBPPs (Figure 6.9 b- e). Visual inspection of the precipitation patterns in conjunction with the quantitative statistics (indicated in each panel) showed good agreement between the SBPPs and the gauged rain data. The two bias-adjusted SBPPs (Figure 6.9 d & e) is very similar to the gauged rainfall data. Figure 6.9 also reveals that the SBPPs with no bias-adjustment indicate a tendency to overestimate the extreme rainfall events with biases of 10.41% & 26.39% at daily scale for TRMM and WaterBase products, respectively. However, TRMM product is in good agreement with the gauged rain more than WaterBase product. After bias adjustment, TRMM (bias=0.00%) and WasterBase (bias=0.04%), the overestimation is considerably reduced signifying good agreement.

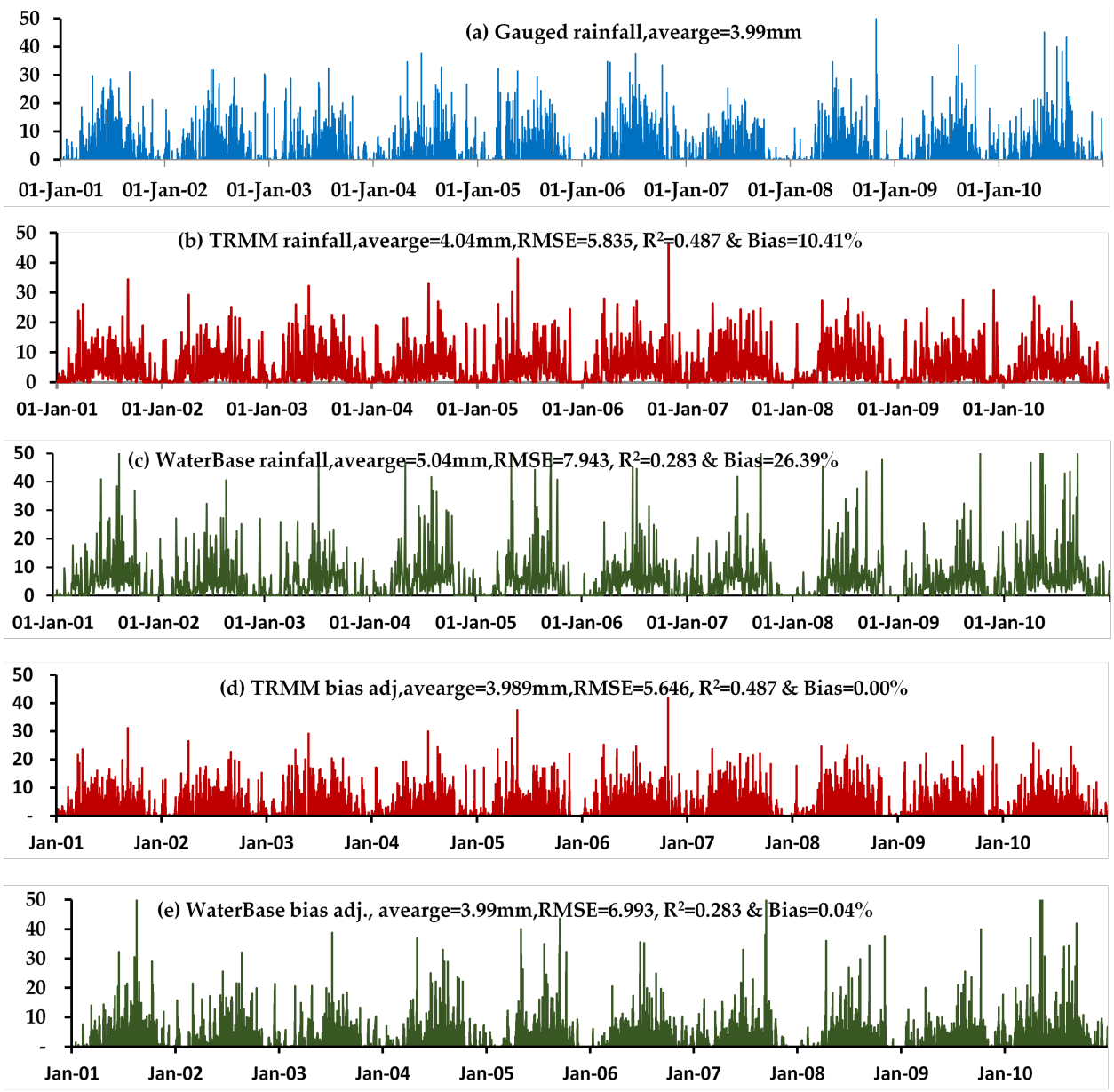

Figure 6.9: Basin-averaged precipitation products of (a) Gauged, (b) TRMM, (c) WaterBase, (d) TRMM bias adj. and (e) WaterBase bias adj.

6.4.4.2 Evaluation of simulated Stream flows

In this section, the effect the two SBPPs streamflow simulations was evaluated. The model was calibrated with 15 years of gauged rain data (1986- 2000) by simple trial and error adjustment of grouped key parameters [195] matching with the observed streamflow and then validated with 10 years of gauged rainfall data (2001- 2010) as explained earlier. This approach of the calibration procedure is commonly used by the hydrological community particularly for gauged basins [302]. Then after, replacing the gauged rain forcing file with precipitation data of TRMM and WaterBase for the same validation period (2001-2010), simulations of the daily streamflow time series were carried out. Simulations were carried out using the model parameters calibrated by gauged rain data during the calibration period from 1986 to 2000. Thus, the daily streamflow hydrographs generated from the individual daily SBPPs and gauged rainfall input are compared with streamflow observations in Figure 6.11.

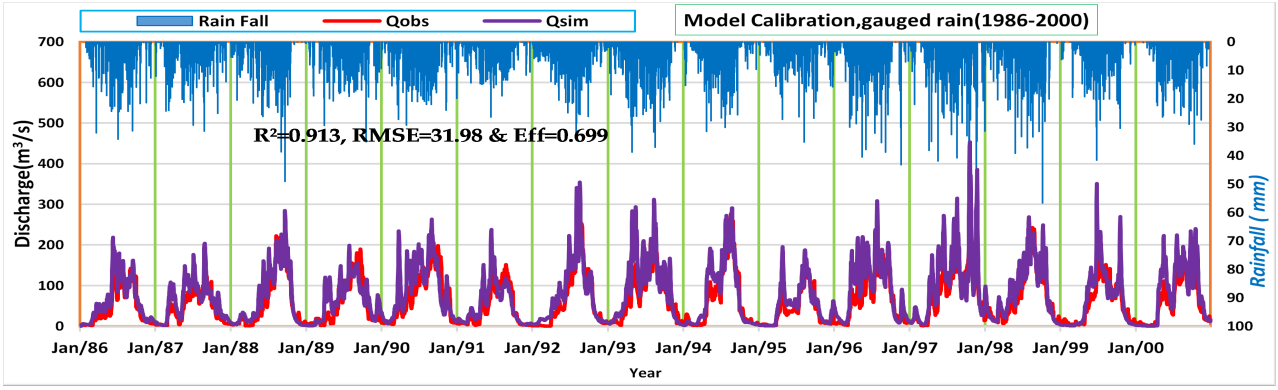

Figure 6.10: Comparison of simulated & observed stream flows for calibration period (1986-2000)

Table 6.4: The statistical comparisons of the three precipitation products (bias-unadjusted)

Precipitation Products	Precipitation input			Simulated stream flow		
	R^2	RMSE	Bias (%)	R^2	RMSE	NS
Gauged	-	-	-	0.899	28.58	0.669
TRMM	0.487	5.853	10.41	0.753	40.37	0.339
WaterBase	0.283	7.943	26.39	0.752	60.51	-0.486

While the WaterBase product largely missed the higher peak flows, the TRMM product more or less adequately captured most of the peak flows. The statistical comparisons of the three precipitation products (Gauged /TRMM/WaterBase) show that the streamflow simulations forced by gauged rain data had better value of the statistical metrics than those based on TRMM and WaterBase precipitation products in the validation period (Table 6.4). Interestingly, the TRMM rainfall based simulations had similar, but slightly worse performance than the gauged rainfall-forced streamflow predictions in the validation period.

Visual examination of the hydrographs (Figure 6.11 b- e) indicates that the SBPPs result in reasonable capture of the magnitude and time of extreme flows. Nonetheless, if the SBPPs are not bias-adjusted (as indicated in Figure 6.11 b & c as well as Figure 6.12), there is substantial overestimation of peak flows outspreading to the recession limbs. Table 6.4 compares the statistical performance for input precipitation and the subsequent streamflow during validation period (2001-2010). Performance measures in Table 6.4 along with streamflow hydrographs, displayed in Figure 6.11 b & c, indicate that the overestimation of stream flow is more significant for WaterBase than for TRMM with streamflow Biases of 26.39% and 10.41%, respectively. Moreover, the TRMM-based stream flow presents better NS and lower RMSE scores than Waterbase, but worse R^2 as compared to Gauged rainfall. In general, the overall results indicate that the bias-unadjusted SBPPs lead to considerable overestimation (high Bias and high RMSE) of streamflow forecast over wet months (June-September) and underestimation of streamflow prediction over few dry months (January & February).

On the other hand, the stream flows generated from bias-adjusted SBPPs (TRMM-adj and WaterBase-adj) suitably capture the streamflow magnitude and their timings (Figure 6.11 d & e as well as Figure 6.13). Table 6.5 provides the statistical matrices for the three precipitation products and the resulting streamflow predictions for bias – adjusted precipitation products. The simulated stream flows from gauged rainfall input offer the highest R^2 (R^2=0.899) at catchment's outlet followed

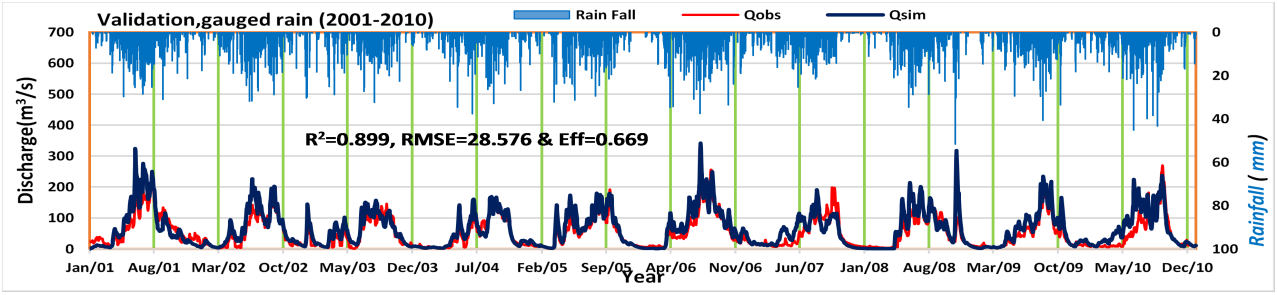

(a) Gauged rainfall

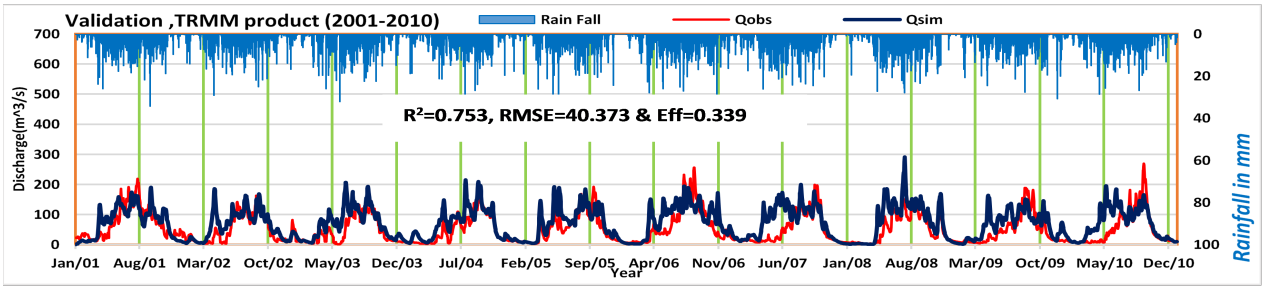

(b) TRMM3B42 precipitation product

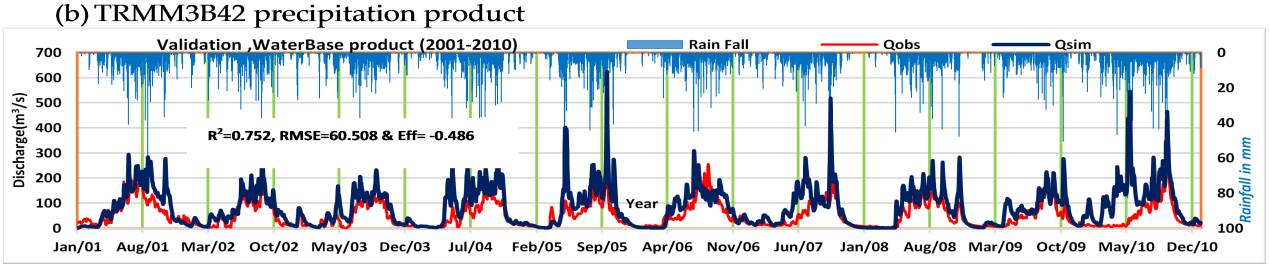

(c) WaterBase precipitation product

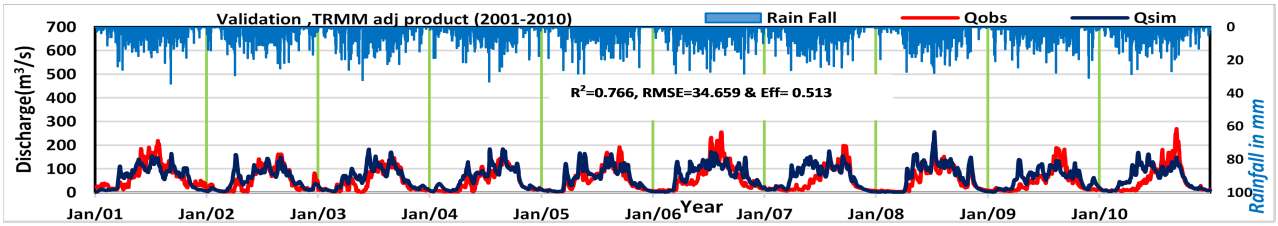

(d) TRMM bias adj. precipitation product

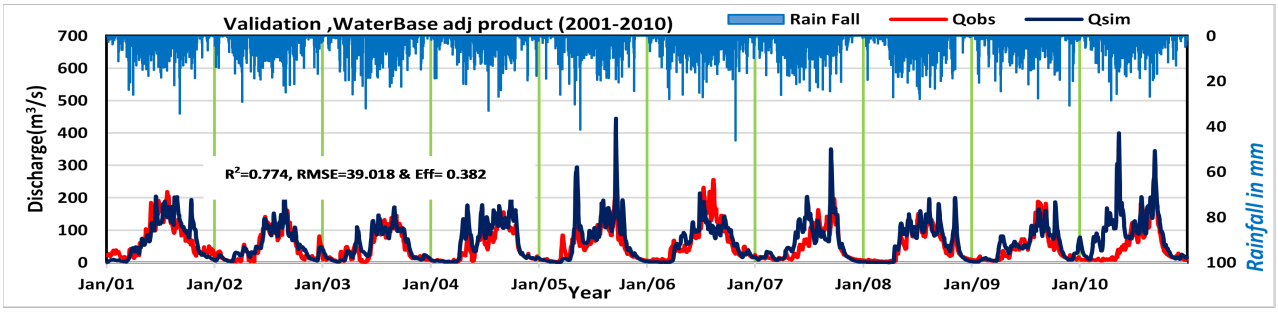

(e) WaterBase bias adj. precipitation product

Figure 6.11: Comparison of simulated & observed hydrographs for validation period (2001-2010): (a) Gauged rainfall,(b) TRMM, (c) WaterBase, (d) TRMM-adj and (e) WaterBase-adj

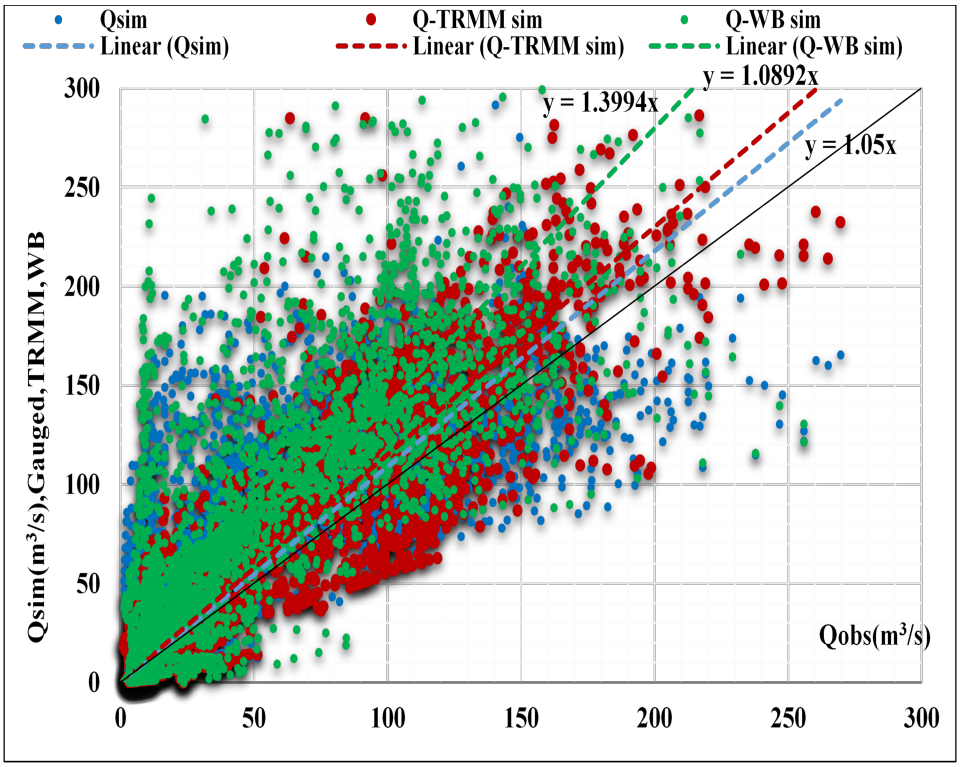

Figure 6.12: Comparisons of simulated and observed stream flows (2001-2010): Bias–unadjusted

Table 6.5: The statistical comparisons of the three precipitation products (bias-adjusted)

Precipitation Products	Precipitation input			Simulated stream flow		
	R^2	RMSE	Bias (%)	R^2	RMSE	NS
Gauged	-	-	-	0.899	28.58	0.669
TRMM	0.487	5.646	0.00	0.766	34.659	0.513
WaterBase	0.283	6.993	0.04	0.774	39.018	0.382

by WateBase - adj (R^2 = 0.774) and TRMM - adj (R^2 = 0.766). Table 6.5 also indicates that by using the bias-adjusted SBPPS in the PyTOPKAPI modeling, the RMSE of predicted stream flow was reduced, the NS & R^2 have improved compared to the bias-unadjusted case. This shows that bias-adjustment can be vital to improve the performance of the SBPPs in streamflow modeling. Though, all streamflow simulations are meaningfully improved after the bias-adjustment and captured almost all of the peak flows, comparatively, the simulation based on TRMM product has shown better agreement (Table 6.5) than that of WaterBase product. The overall results demonstrate that the simulated streamflow using the gauged rainfall is better than those acquired from other products including bias-adjusted ones.

6.4.5 Conclusion and Recommendations

Stream flow information is vital for peak flood estimation. Such information can be obtained either through ground-based monitoring station or by streamflow modelling. Precipitation data is the key "input" to stream flow modelling. The SBPPs are the viable alternative sources of precipitation data, particularly for developing countries like Ethiopia with poor or nonexistent ground based streamflow measurements. Over a Gilgel Ghibe basin, 10 years of two SBPPs (TRMM,

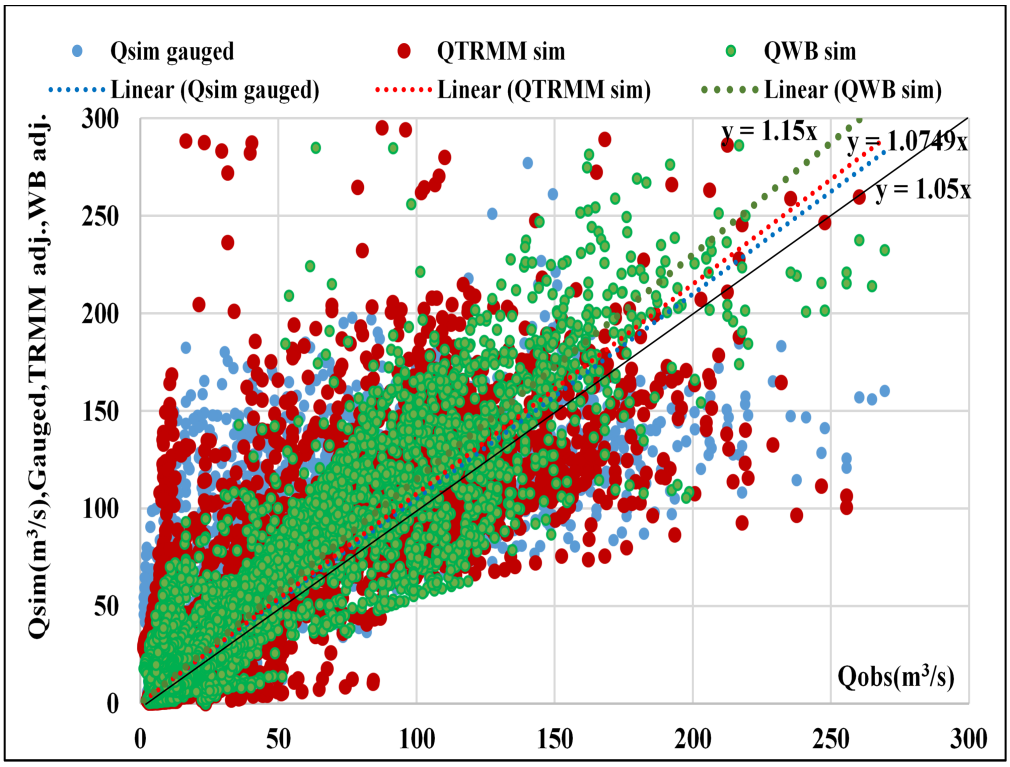

Figure 6.13: Comparisons of simulated and observed stream flows (2001-2010): Bias–adjusted

and Waterbase) were used for stream flow modeling. These products were then introduced to the PyTOPKAPI model to generate stream flows at daily time scale and the results were compared with streamflow observations at Gilgel Ghibe Nr, Assendabo gauging station with the help of four statistical tools (Bias, R^2, NS and RMSE). The results indicate that the bias-adjusted SBPPs agree well with gauged rainfall compared to bias-unadjusted ones. The SBPPs with no bias-adjustment tend to overestimate (high Bias and high RMSE) extreme precipitation events and the corresponding simulated streamflow outputs, particularly during wet months (June-September) and underestimate the streamflow prediction over few dry months (January and February). It was finally concluded that the general streamflow patterns were well captured at daily time scale from SBPPs after bias adjustment. However, the overall results demonstrate that the simulated streamflow using the gauged rainfall is better than those acquired from SBPPs including bias-adjusted ones.

Despite their global coverage, SBPPs are not universally combined with operative hydrological modeling in Ethiopia primarily because there is no evidence on the reliability of the SBPPs at basin scale. Thus, evaluation of reliability of different SBPPs should be conducted constantly to evaluate the applicability of these products for stream-flow modeling in data sparse areas in Ethiopia. Therefore, efforts in making use of the best quality SBPP for streamflow modelling in Ethiopia should be a major effort of the future.

Chapter 7

Evaluation of Various Methods of Flood Frequency Analysis for Ethiopian Rivers

7.1 Introduction

Hydrological systems are influenced by extreme events such as peak floods. The magnitudes of such events are inversely related with their frequencies of occurrences, very high events happening less repeatedly than moderate ones. The frequency analysis of the flood series is thus vital for several engineering applications: for design of dams, bridges, culverts, and flood mitigating arrangements; to demarcate flood plains areas and find out the consequence of high floods on the flood plain areas [58]. The aim is to correlate the magnitude of peak floods to their frequencies of occurrences (return periods) by means of probability functions. The flood data that are to be utilized should be cautiously chosen such that the supposition of independence is fulfilled. This is often attained by choosing the annual maximum discharge data being examined with the expectation that succeeding recorded data from year to year will be independent. Generally, a peak flood event is defined to have happened if a random flood variable X is greater than or equal to some level X_T. The recurrence interval τ is the time between the happenings of $X > X_T$. The return-period T of the event $X > X_T$ is the predictable value of τ, E(τ), its mean value measured over a very large number of incidences. The probability p of the occurrence of an event $X > X_T$ in any flood record may be related to the return-period by E(τ) = T = 1/p. Hence, the probability of occurrence of a flood event in any record is the inverse of its return-period, i.e., P($X > X_T$) = 1/T [58, 204].

Assessing flood frequency methodologies and finding the peak flood are the ultimate objectives for hydrological investigation [6]. A problem in flood hydrology is the selection of an appropriate method of flood frequency analysis for fitting peak flood series in a region. Many methods of flood frequency analysis and various ways of fitting them are available. In spite of the significant developments made, the selection of an appropriate method of flood frequency analysis for any particular flood records from amongst the alternative methods is still a subject of current research. The most common distributions of flood frequency assessment are Extreme Value Type I (EV1), Log-Pearson Type III (LPIII), Log-Normal (LN), Pearson Type III (PIII), etc. [188, 229, 261]. Similarly, there are many plotting position formulae, the choice of which for fitting the method of flood frequency analysis, has been studied extensively [173]. The plotting position formulae give a quantile-unbiasedness for different distributions [63, 229]. This study attempted to find out the appropriate flood frequency method for fitting the annual maximum discharge data series of two Ethiopian rivers (Awash and Gilgel Ghibe rivers). In order to find the most suitable method of flood frequency analysis, the Probability Plot Correlation Coefficient (PPCC) [87] test was used along

with the Root Mean Square Deviation (RMSD) [3,50] and the Nash-Sutcliffe efficiency coefficient (NS) [154] tests. The PPCC test is more robust and has found numerous applications in flood hydrology [45, 119]. Seven methods of flood frequency analysis were considered for the current study: the recently developed TSPT (Power transformed Normal & Log-transformed Normal), LPIII, EVI, Chow's and Stochastic methods as well as Weibull's plotting position formula to model at-site annual maximum discharge data series with the help of the Plotting Position formulae. This study also summarizes a comparative investigation conducted to find out the best method that represents the statistical characteristics of recorded flood data of the study areas.

7.2 Theoretical background

Hydrological events such as floods are exceptionally complex natural phenomena as they are the resultants of numerous factors and are therefore difficult to model mathematically [259]. For instance, the peak floods in a basin depend on the characteristics of the basin, precipitation and antecedent soil conditions, each them in turn depend upon the group of several other factors which can yield floods [204]. This makes the estimation of the flood peak a very difficult task. The rational method, the empirical methods and the unit hydrographs technique explained in the earlier sections are some of the methods of peak flood estimation. Another approach for prediction of peak flood flows, and also implementable to other hydrologic variables such as precipitation etc., is the statistical technique of frequency analysis [259]. It is highly data dependent and requires good samples of hydrological data of watershed in both time and space. The processing and analysis of the data help to foresee the sustainability of the structure under high flood conditions. Furthermore, in flood frequency analysis, the combinations of numerous factors which can produce floods are probabilistic and are therefore subject to statistical analysis [58]. The main task in this method is to determine a future flood peak related to a given return period on the basis of the past records of the stream flows by means of statistics. This method can be used for estimation of the expected peak floods of a river with a specified frequency, if adequate historical records exist. Furthermore, the predictions will be appropriate only if there has not been a considerable alteration in the regime of the river throughout or after the period of the records [204].

7.3 Methods of flood frequency analysis

Most of the hydrologic variables are assumed to come from a continuous random process, and historical sequences thereof are fitted with some of the common continuous distributions. Thus, the most universally employed frequency assessment functions for forcasting of extreme flood events are as described below [188, 229, 261].

7.3.1 Normal Distribution

The normal frequency distribution also known as "Gaussian distribution" is a symmetrical bell-shaped probability density function (PDF) of continuous random variable and is expressed as [58]:

$$f(x) = \frac{1}{2\sqrt{2\pi}} exp\left(-\frac{(x-\mu)^2}{2\sigma^2}\right) \tag{7.1}$$

The two parameters of the frequency function are the mean, μ, and the standard deviation σ for which X_{bar} and S derived from the sample data are substituted in the above equation. By a simple

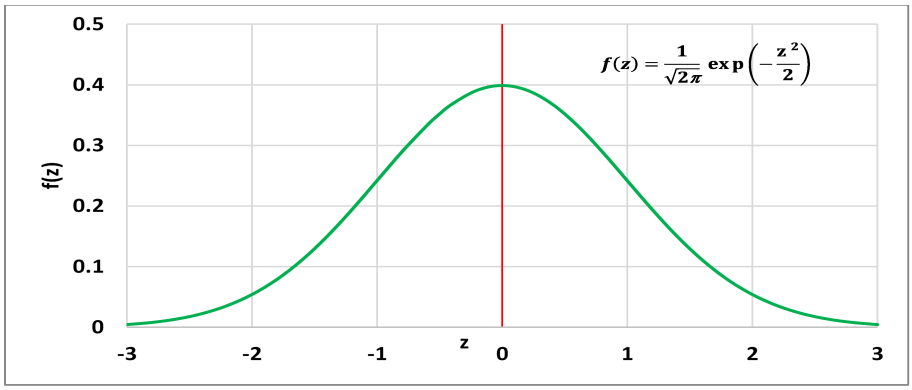

Figure 7.1: The probability density function for the standard normal distribution (μ= 0,σ = 1)

transformation, the distribution can be written as a single parameter function.

Thus, when z = $(x-\mu)/\sigma$, the corresponding standard normal distribution has a probability density function [149]:

$$f(x) = \frac{1}{2\sqrt{2\pi}} exp\left(\frac{-z^2}{2}\right); (-\infty < z < \infty) \tag{7.2}$$

which depends only on the value of the standard variate z . It is normally distributed with unit standard deviation and zero mean. The standard normal cumulative probability function,

$$F(z) = \frac{1}{\sqrt{2\pi}} \int_{-\infty}^{z} \exp(-u^2/2) du \tag{7.3}$$

where u is a dummy variable of integration and has no analytical form. Its values are tabulated in Table 7.3. According to Abramowitz and Stegun [2], these values may also be approximated by the following polynomial [58].

$$B = \frac{1}{2}\left[1 + 0.196854|z| + 0.115194|z|^2 + 0.000344|z|^3 + 0.019527|z|^4\right]^4 \tag{7.4}$$

where |z| is the absolute value of z and the standard normal function has:

F(z) =B for z < 0 and F(z)=1- B for z > 0. The error in F(z) as evaluated by this formula is less than 0.00025 [2, 58].

Table 7.3 is the tabulated form of the area under the standard normal curve which can be used in all the normal distributions functions after standardizing the variables.

7.3.2 Log-normal (LN) distribution

Many hydrologic variables may also show a noticeable right skewness, partly owing to the influence of natural occurrences with values larger than zero or some other lower boundary, and unrestrained hypothetically in its upper values. In such case, the frequencies will not follow the normal distribution function, and instead, variables fortunately are functionally normal and their log-transformed values follow a normal distribution [62]. The LN distribution is especially useful because the transformation opens the extensive body of theoretical and applied uses of the normal distribution. It may be either two-parameter or three-parameter as described below.

7.3.2.1 Two – parameter LN distribution

When the log-transformed, $y = ln(x)$ of the variables is normally distributed, the distribution of the variables is said to be two-parameter logarithmic normally distributed in such a way that its PDF can be expressed by:-

$$f(x) = \frac{1}{x\sigma_y\sqrt{2\pi}} exp\left(-\frac{(ln(x)-\mu_y)^2}{(2\sigma_y)^2/2}\right) \tag{7.5}$$

where, ${\sigma_y}^2$ and μ_y are the variance and the mean and of the log-transformed variables (x) and x is bounded at zero from below.

7.3.2.2 Three - parameter LN distribution

This represents the normal frequency function of the logarithms of the reduced variables (x-a) where 'a' is the lower boundary of the distribution estimated by trial and error and its PDF can be given by;

$$f(x) = \frac{1}{(x-a)\sigma_y\sqrt{2\pi}} exp\left(-\frac{(ln(x-a)-\mu_y)^2}{(2\sigma_y)^2/2}\right) \tag{7.6}$$

where, μ_y and ${\sigma_y}^2$ are the mean and the variance of the reduced variable (x-a).

7.3.3 Log-Pearson type III (LPIII) distribution

This is a distinct case of Gamma distribution and is more beneficial and has been extensively implemented as a standard method of flood frequency analysis [254]. This distribution is broadly used in USA for projects of the US Government. Bulletin 17B endorses the usage of the method-of-moments (MoM) to fit a Pearson type III distribution to the logarithms of the flood information, thus giving a LPIII method to model the recorded streamflow data [78, 254]. In this, the variable is primary converted into base 10 logarithmic form (Z= log(x)) and the converted data is then fitted to the distribution. Using this Z-series, for any recurrence interval T;

$$Z_T = Z_{bar} + K_z * \sigma_z \tag{7.7}$$

where K_Z = a frequency factor (as given in Table 7.1) which is a function of return period (T) and the skew coefficient (Cs), σ_z= the standard deviation of the Z variate of the sample and are given as:

$$\sigma_z = \sqrt{\frac{\sum(Z - Z_{bar})^2}{N-1}} \tag{7.8}$$

$$Cs = \frac{N(\sum(Z - Z_{bar})^3}{(N-1)(N-2)(\sigma_Z^3)} \tag{7.9}$$

where, Z_{bar} is the mean of the Z value and N is the sample size.

After obtaining Z_T by equation 7.7, the respective value of X_T in the original data is obtained as:

$$X_T = antilog(Z_T) = 10^{Z_T} \tag{7.10}$$

Sometimes, the coefficient of skewness, Cs, is fine-tuned to account for the size of the sample by means of the succeeding relation proposed by Hazen(1930) [259]:

Table 7.1: Kz = f (Cs,T) for use in LPIII distribution [58]

Cs	Recurrence Interval T in years							Cs	Recurrence Interval T in years						
	2	10	25	50	100	200	1000		2	10	25	50	100	200	1000
3.0	-0.40	1.18	2.28	3.15	3.05	4.97	7.25	0.1	-0.02	1.29	1.76	2.11	2.40	2.67	3.24
2.5	-0.36	1.25	2.26	3.05	3.85	4.65	6.60	0.0	0.00	1.28	1.75	2.05	2.33	2.58	3.09
2.2	-0.33	1.28	2.24	2.97	3.71	4.44	6.20	-0.1	0.02	1.27	1.72	2.00	2.25	2.48	2.95
2.0	-0.31	1.30	2.22	2.91	3.61	4.30	5.91	-0.2	0.03	1.26	1.68	2.95	2.18	2.39	2.81
1.8	-0.28	1.32	2.19	2.85	3.50	4.15	5.66	-0.3	0.05	1.25	1.64	1.89	2.10	2.29	2.68
1.6	-0.25	1.33	2.16	2.78	3.39	3.99	5.36	-0.4	0.07	1.23	1.61	1.83	2.03	2.20	2.54
1.4	-0.23	1.34	2.13	2.71	3.27	3.83	5.11	-0.5	0.08	1.22	1.57	1.78	1.96	2.11	2.40
1.2	-0.20	1.34	2.09	2.63	3.15	3.66	4.82	-0.6	0.99	1.20	1.53	1.72	1.88	2.02	2.28
1.0	-0.16	1.34	2.04	2.54	3.02	3.49	4.54	-0.7	0.12	1.18	1.49	1.66	1.81	1.93	2.15
0.9	-0.15	1.34	2.18	2.50	2.96	3.40	4.40	-0.8	0.13	1.17	1.45	1.61	1.73	1.84	2.04
0.8	-0.13	1.34	2.00	2.45	2.89	3.31	4.25	-0.9	0.15	1.15	1.41	1.55	1.66	1.75	1.91
0.7	-0.12	1.33	1.97	2.41	2.82	2.22	4.11	-1.0	0.16	1.13	1.37	1.49	1.59	1.66	1.88
0.6	-0.10	1.33	1.94	2.36	2.76	3.13	3.96	-1.4	0.23	1.04	1.20	1.27	1.32	1.35	1.47
0.5	-0.08	1.32	1.91	2.31	2.69	3.04	3.82	-1.8	0.28	0.95	1.04	1.07	1.09	1.10	1.13
0.4	-0.07	1.32	1.88	2.26	2.62	2.95	3.67	-2.2	0.33	0.84	0.89	0.90	0.91	0.91	0.91
0.3	-0.05	1.31	1.85	2.21	2.54	2.86	3.53	-3.0	0.39	0.66	0.67	0.67	0.67	0.67	0.67
0.2	-0.03	1.30	1.82	2.16	2.47	2.76	3.38								

$$C\hat{}S = Cs(1 + 8.5)/N \tag{7.11}$$

where $C\hat{}S$ = fine-tuned coefficient of skewness. However, the standard procedure for use of LPIII distribution adopted by US water Resources Council does not incorporate this fine-tuning for skewness. When the skew is zero i.e., Cs =0, the LPIII method reduces to LN method [58,259].

7.3.4 Extreme Value Type I (EVI) Distribution

This method was initially presented by Gumbel in 1941 and is generally known as Gumbel's distribution [58]. This is the one broadly used PDF for extreme events in hydro-meteorological studies for estimating the probability of exceedance of the hydrologic events (flood peaks).

Gumbel [58] defined a flood as the maximum of the 365 day-to-day flows and the yearly flood series creates a series of the maximum stream flow values. According to Gumbel's philosophy of extreme events, the probability of an event of magnitude X_o being equaled or exceeded (the probability of exceedance) is given by [149,204,259]:

$$P(X \geq X_o) = 1 - e^{-e^{-Y}} \tag{7.12}$$

This implies that the probability of an event of value X_o not being equaled or exceeded (probability of non-occurrence) is given by:

$P(X < X_o) = e^{-e^{-Y}}$; where: Y = a dimensionless variable given by: $Y = (X - u)/\sigma$; $u = x_{bar} - \gamma * \alpha$; γ =0.5772 (Euler 's constant); $\alpha = \frac{\sqrt{6}}{\pi}\sigma$; x_{bar} and σ are the mean and the standard deviation of the variate x, respectively

Thus,

$$Y = (1.2825/\sigma)(X - X_{bar}) + 0.5772 \tag{7.13}$$

The probability of occurrence of a flood in any year (with a return-period T-year), the probability of exceedance [204], is given by: **p=1/T**. That is,

$$p = 1 - e^{-e^{-y}} = 1/T \tag{7.14}$$

Table 7.2: Reduced mean (Y_n) and Reduced Standard Deviation (S_n) for EVI distribution (N=Sample Size) [259]

N	Yn	Sn	N	Yn	Sn	N	Yn	Sn	N	Yn	Sn	N	Yn	Sn
10	0.4925	0.9496	29	0.5353	1.1086	47	0.5473	1.1557	65	0.5535	1.1803	83	0.5574	1.1959
11	0.4996	0.9676	30	0.5362	1.1124	48	0.5477	1.1574	66	0.5538	1.1814	84	0.5576	1.1967
12	0.5035	0.9833	31	0.5371	1.1159	49	0.5481	1.159	67	0.554	1.1824	85	0.5578	1.1973
13	0.507	0.9971	32	0.538	1.1193	50	0.5485	1.1607	68	0.5543	1.1834	86	0.558	1.198
14	0.51	1.0095	33	0.5388	1.1226	51	0.5489	1.1623	69	0.5545	1.1844	87	0.5581	1.1987
15	0.5128	1.0206	34	0.5396	1.1255	52	0.5493	1.1658	70	0.5548	1.1854	88	0.5583	1.1994
16	0.5157	1.0316	35	0.5402	1.1285	53	0.5497	1.1658	71	0.555	1.1863	89	0.5585	1.2001
17	0.5181	1.0411	36	0.541	1.1313	54	0.5501	1.1667	72	0.5552	1.1873	90	0.5586	1.2007
18	0.5202	1.0493	37	0.5418	1.1339	55	0.5504	1.1681	73	0.5555	1.1881	91	0.5587	1.2013
19	0.522	1.0565	38	0.5424	1.1363	56	0.5508	1.1696	74	0.5557	1890	92	0.5589	1.202
20	0.5236	1.0628	39	0.543	1.1388	57	0.5511	1.1708	75	0.5559	1.1898	93	0.5591	1.2026
21	1.5236	1.0696	40	0.5436	1.1413	58	0.5515	1.1721	76	0.5561	1.1906	94	0.5592	1.2032
22	0.5268	1.0754	41	0.5442	1.1436	59	0.5518	1.1734	77	0.5563	1.1915	95	0.5593	1.2038
23	0.5283	1.0811	42	0.5448	1.1458	60	0.5521	1.1747	78	0.5565	1.1923	96	0.5595	1.2044
24	0.5296	1.0864	43	0.5453	1.148	61	0.5524	1.1759	79	0.5567	1.193	97	0.5596	1.2049
25	0.5309	1.0915	44	0.5458	1.1499	62	0.5527	1.177	80	0.5569	1.1938	98	0.5598	1.2055
26	0.532	1.0961	45	0.5463	1.1519	63	0.553	1.1782	81	0.557	1.1945	99	0.5599	1.206
27	0.5332	1.1004	46	0.5468	1.5389	64	0.5533	1.1793	82	0.5572	1.1953	100	0.56	1.2065
28	0.5343	1.1047												

In actual usage, the magnitude of X for a specified probability (p) is essential, and hence, equation 7.14 is rearranged as; Yp = - ln (- ln (1 - p))

Noticing that the return-period **T= 1/p** and defining Y_T as the value of Y (generally called the reduced variate) for a specified T.

$$Y_T = -ln[ln(T/(T-1))] \tag{7.15}$$

Now, rearranging equation 7.13, the value of the variate X having a return period T is given by:

$$X_T = X_{bar} + K_T * \sigma_x \tag{7.16}$$

where: $K_T = (Y_T - 0.5772)/1.2825$

Equation 7.16 is main Gumbel's equation and is utilizable to an unlimited sample size (N$\rightarrow \infty$), where K_T is known as the frequency factor. Since the practical annual maximum discharge data series has finite length of records, Equation 7.16 is modified to account for finite sample size, as:-

$$X_T = X_{bar} + K_T * \sigma_{n-1} \tag{7.17}$$

where, K_T (frequency factor) = $(Y_T - Y_n)/S_n$ and σ_{n-1} (sample std.dev.) = $\frac{\sqrt{\sum (X-X_{bar})^2}}{(N-1)}$

Here, S_n and Y_n are reduced standarad deviation and reduced mean (both are the functions of the sample size N as given in Table 7.2) with their maximum values of 1.2825 and 0.5772 at $N \rightarrow \infty$, respectively.

This EVI method is used in the following steps [259] to approximate the flood magnitude related to a specified return period based on the yearly maximum discharge data series.

1. Gather the streamflow data and define the sample size, N.
2. Determine X_{bar} and σ_{n-1} for the given data using annual maximum flood variate (X).
3. Determine Y_n and S_n corresponding to the given N from Table 7.2.

4. Determine Y_T corresponding to the given T by Y_T = - ln (ln (T/(T-1)))
5. Determine the frequency factor K_T by K_T = (Y_T-Y_n)/S_N
6. Determine the required X_T appropriate to the given T by X_T = X_{bar} + K_T* σ_{n-1}

To find out if the specified data follow the assumed EVI distribution, the magnitude of X_T for some return-periods $T < N$ are computed with the use of EVI distribution and plotted as X_T versus T on Gumbel's probability paper. If this graphical plot of X_T versus T results a straight line, the data will follow the assumed EVI distribution. Moreover, EVI distribution has a character which offers T=2.33 years for the mean of the yearly flood series if N is very big. Thus, the magnitude of a flood with T=2.33 years is called the average yearly flood and it is an obligatory point [259] within which the line indicating variation of X_T with T should pass [204].

An alternative way of calculating the magnitudes of extreme flood events for a given T (return period) is by using the frequency factor (K_T) in the frequency factor equation, $X_T = \mu + K_T * \sigma$. The frequency factor equation was proposed by Chow in 1951, and is practicable to several probability functions used in hydrological frequency assessment [58]. For a specified distribution, a K-T relationship may be found using the K values and the corresponding T values. This relationship can be expressed analytically or may be presented in tabular form. The theoretical K-T relationships for several probability functions that are commonly used in hydrologic frequency analysis are now described.

It is known that the variable X_T of a hydrological event may be signified as the mean μ plus the departure ΔX_T of the variable from the mean, i.e, $X_T = \mu + \Delta X_T$. The departure is taken as equal to the product of the standard deviation σ and K_T, that is, $\Delta X_T = K_T * \sigma$. That is to say the departure ΔX_T and K_T are functions of T and the type of probability function used in the assessment. The above equation may therefore be expressed as $X_T = \mu + K_T * \sigma$, which may be approximated by $X_T = X_{bar} + K_T * S$. The case when the data to be assessed is $Y = log(X)$, then the same procedure is implemented to the logarithmic transformed data, with the use of $Y_T = Y_{bar} + K_T * S_y$ and the needed maginitude of X_T is obtained by using the antilogarithim of Y_T.

Thus, K_T can be expressed as $K_T = (X_T - \mu)/\sigma$. For normal distribution, this is identical with the standard normal variate Z. The maginitude of Z corresponding to an exceedance probability of p (i.e., p =1/T) is determined by obtaining the value of a transitional parameter, "w" using:
$w = [ln(1/p^2)]^{(\frac{1}{2})}$; $(0 < p \leq 0.5)$, then calculating K_T or z using the expression:

$$K_T = z = w - \frac{(2.515517 + 0.802853w + 0.010328w^2)}{(1 + 1.432788w + 0.189269w^2 + 0.001308w^3)} \tag{7.18}$$

When p > 0.5, (1— p) is replaced for p in above expression and the value of z determined is given a minus sign. The error in this technique is not more than 0.00045 in z [2]. For the LN distribution, the same procedure applies except that it is implemented to the log-transformed variables. For the EVI distribution, the expression shown in equation 7.19 is used.

$$K_T = -\frac{\sqrt{6}}{\pi}(0.5772 + ln[ln(T/(T-1))]) \tag{7.19}$$

For LPIII distribution, the first step is to take the logarithms of the hydrologic data, y = log(x). Usually, logarithms to base 10 are used. The mean Y_{bar}, the standard deviation S_y, and the coefficient of skewness C_s are found for the logarithmic transformed data. The K_T factor in this case

depends on T and C_s . When the skew coefficient $C_s = 0$, K_T = the standard normal variate Z. Where as when the skew coefficient $C_s \neq 0$, K_T is estimated by Kite formula [58] as;

$$K_T = z + (z^2 - 1)k + \frac{1}{3}(z^3 - 6z)k^2 - (z^2 - 1)k^3 + zk^4 + \frac{1}{3}k^5 : where, k = C_s/6 \quad (7.20)$$

$$z = w - \left(\frac{2.515517+0.802853w+0.010328w^2}{1+1.432788w+0.189269w^2+0.001308w^3}\right); w = [ln(1/p^2)]^{\frac{1}{2}} \text{ for } (0 < p \leq 0.5)$$

But, when p > 0.5, (1— p) is replaced for p in the above expression and the value of z determined is given a minus sign.

In addition to all the methods presented in previous sections, there are also some other methods with which peak floods corresponding to certain return period can be predicted. These are as given below.

7.3.5 Ven. Te. Chow's Method

This method is a modification of EVI distribution using the frequency factor [204]. According to Chow, the annual peak flood that would be equaled or exceeded in T years is given by:

$$Q_T = a + b * Y_T \quad (7.21)$$

$$Y_T = -log(log(T/(T-1))) \quad (7.22)$$

where, a and b are the parameters approximated from the observed data of sample size N by the moments method and T in this case is also the return-period of a specified magnitude of flood.

Using the least squares method :

$$\sum Q_T = a * N + b * \sum Y_T \quad (7.23)$$

$$\sum Q_T * Y_T = a * \sum Y_T * N + b * \sum (Y_T) * (Y_T) \quad (7.24)$$

By arranging the annual maximum discharge data in descending order of magnitude and then giving rank for each of them, the two parameters a and b can be acquired by solving the two linear equations given in equation (7.23 and 7.24). Here, if the annual flood peak has got a rank M, with the help of the Weibull's Plotting Position formula [204], the return period will be;

$$T = (N + 1)/M \quad (7.25)$$

where, N is the data size and M is the rank of the descending ordered data.

7.3.6 Stochastic Method

Unlike the above method, this approach considers the effect of time on annual flood estimation. The following formula was developed by means of poisson's probability law and the theory of the sum of random variable so as to estimate Q_T [204].

$$Q_T = Q_{min} + 2.3(Q_{bar} - Q_{min}) * log((Nf/N) * T) \quad (7.26)$$

where, Q_{min} = the minimum value of recorded flood peaks, Nf = the number of flood magnitudes counting only one time for repeated flood peaks, N = the total number of recorded floods, T = return period in years for which Q_T is to be determined, and Q_{bar}= the mean of recorded peak floods.

7.3.7 Two-Step Power Transformation (TSPT) Technique

This is a promising technique for estimation of flood-peak corresponding to a given return period [164]. In this method, the observed flood data are converted through a suitable power transformation function [162, 164] such that the transformed series would show a normal distribution, and then it is wholly defined by the mean and standard deviation. This technique uses the Box-Cox transformations approach. The Box- Cox transformations are all families of a class of the exponential transformations that raise numbers to an exponent (power). Such transformations basically standardize a specific data, eradicating the need to haphazardly attempt several conversions to find out the best normalizing option. The technique helps researchers easily find the optimum standardizing conversion for each variable [134]. It is very suitable to use because of the low number of distribution parameters, i.e., the mean and the standard deviation. It has been found that true normalization of skewed data can be achieved by this two-step power transformation technique [112]. This particular study aims to find out, through application in a number of gauging stations of two Ethiopian rivers, whether this method is capable of normalizing the skewed flood series. Then after, the method could be used for flood frequency analysis.

The Box-Cox transformation equations employed for normalizing the skewed data is [44,134,164]:

$$Y_i = \begin{cases} \frac{(X_i^{\lambda}-1)}{\lambda}, \text{if } \lambda \neq 0 \\ \log(X_i), \text{if } \lambda = 0 \end{cases} \tag{7.27}$$

where; X_i = the i^{th} original data series, Y_i = the i^{th} power transformed data series, and λ= the parameter of power transformation.

If the transformed values are actually normally distributed, the skewness and the kurtosis will be equal to zero and three, respectively [162]. With a suitable value of λ, the skewness of the observed flood data can be reduced to zero or nearly zero and thus the histogram becomes symmetrical about the vertical axis passing through the mean. This transformed histogram may be truly normal only when kurtosis also becomes equal to three. When kurtosis is not equal to three, the histogram may be either peaky (Leptokurtic) or flat (platy kurtic). Thus, correction for kurtosis is envisaged through another transformation in this two-step transformation approach in that the two limbs of the transformed histograms obtained after Box-Cox power transformation in the first step are equally stretched or compacted according to the following modulus transformation [112];

$$t_i = (|Y_i - Y_{bar}|)^{\gamma} \tag{7.28}$$

where, γ is the parameter of two-step power transformation and is positive, t_i is the two-step power transformed data series and is given the same sign as $(Y_i - Y_{bar})$, and Y_{bar} is the mean of the power transformed data series.

With an appropriate value of γ , the condition of kurtosis equal to three (3) may be achieved [112]. In the above transformation, it is evident that when $\gamma \to 0$, the kurtosis of the transformed t- series tends to be 1, and when $\gamma \to \infty$, the kurtosis of the transformed t-series tends to be ∞. For $\gamma = 1$, the kurtosis of the t-series will be the same as that of the Y-series (obtained after Box-Cox power transformation). Therefore, if kurtosis of Y-series is more than three, γ will be between 1 and 0 and if kurtosis of Y- series is less than three, γ will be more than 1. With the help of the iterative algorithm developed (Figure 7.2), the value of λ and γ are obtained such that both the skewness and kurtosis of the converted series are nearly zero and three, respectively.

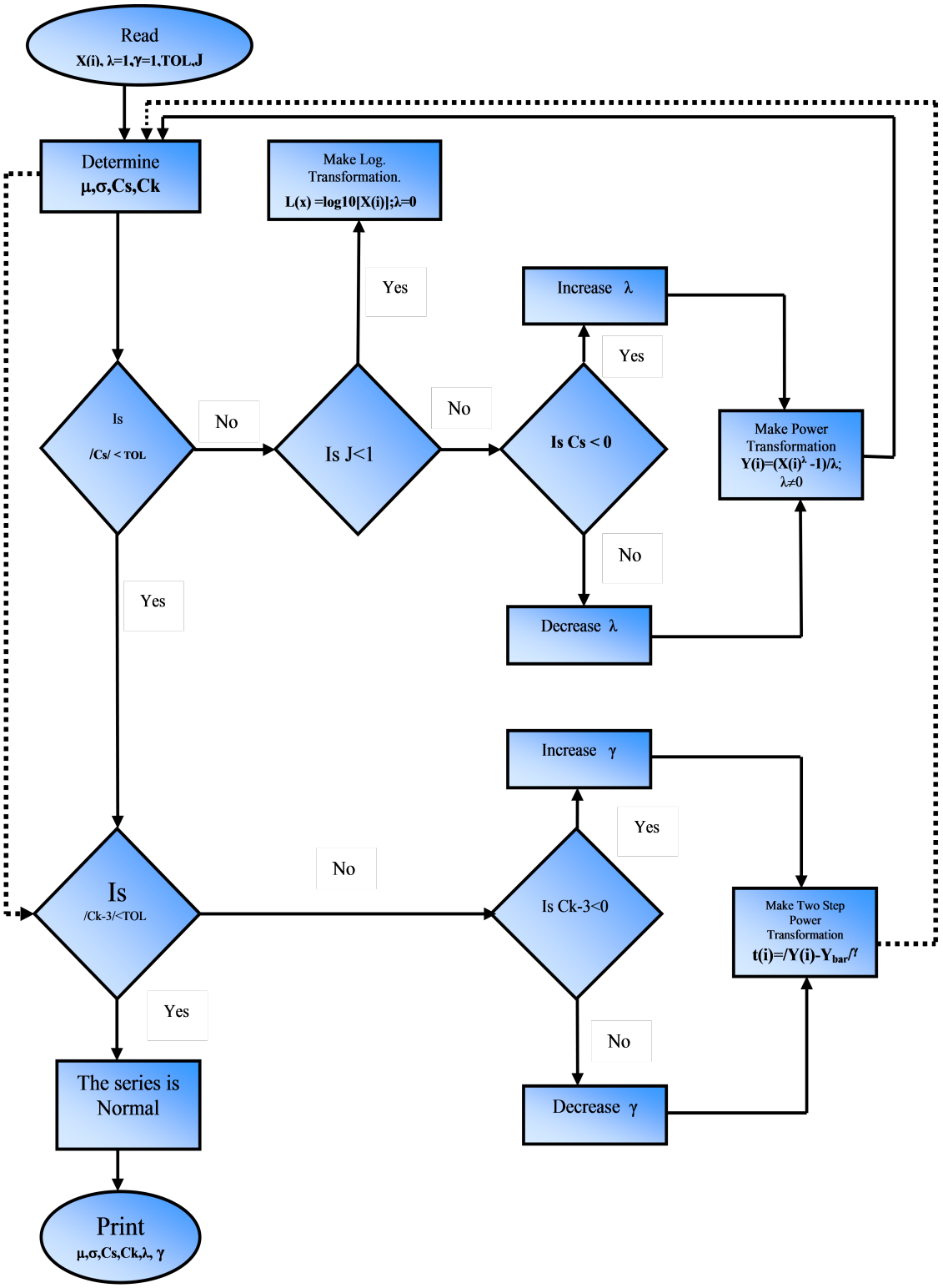

Figure 7.2: Algorithm for determination of λ and γ in TSPT method of flood frequency analysis.

Table 7.3: Cumulative probability of the standard normal function [58, 107]

z	0	1	2	3	4	5	6	7	8
0	0.5	0.504	0.508	0.512	0.516	0.5199	0.5239	0.5279	0.5319
0.1	0.5398	0.5438	0.5478	0.5517	0.5557	0.5596	0.5636	0.5675	0.5714
0.2	0.5793	0.5832	0.5871	0.591	0.5948	0.5987	0.6026	0.6064	0.6103
0.3	0.6179	0.6217	0.6255	0.6293	0.6331	0.6368	0.6406	0.6443	0.648
0.4	0.6554	0.6591	0.6628	0.6664	0.67	0.6736	0.6772	0.6808	0.6844
0.5	0.6915	0.695	0.6985	0.7019	0.7054	0.7088	0.7123	0.7157	0.719
0.6	0.7257	0.7291	0.7324	0.7357	0.7389	0.7422	0.7454	0.7486	0.7517
0.7	0.758	0.7611	0.7642	0.7673	0.7704	0.7734	0.7764	0.7794	0.7823
0.8	0.7881	0.791	0.7939	0.7967	0.7995	0.8023	0.8051	0.8078	0.8106
0.9	0.8159	0.8186	0.8212	0.8238	0.8264	0.8289	0.8315	0.834	0.8365
1	0.8413	0.8438	0.8461	0.8485	0.8508	0.8531	0.8554	0.8577	0.8599
1.1	0.8643	0.8665	0.8686	0.8708	0.8729	0.8749	0.877	0.879	0.881
1.2	0.8849	0.8869	0.8888	0.8907	0.8925	0.8944	0.8962	0.898	0.8997
1.3	0.9032	0.9049	0.9066	0.9082	0.9099	0.9115	0.9131	0.9147	0.9162
1.4	0.9192	0.9207	0.9222	0.9236	0.9251	0.9265	0.9279	0.9292	0.9306
1.5	0.9332	0.9345	0.9357	0.937	0.9382	0.9394	0.9406	0.9418	0.9429
1.6	0.9452	0.9463	0.9474	0.9484	0.9495	0.9505	0.9515	0.9525	0.9535
1.7	0.9554	0.9564	0.9573	0.9582	0.9591	0.9599	0.9608	0.9616	0.9625
1.8	0.9641	0.9649	0.9656	0.9664	0.9671	0.9678	0.9686	0.9693	0.9699
1.9	0.9713	0.9719	0.9726	0.9732	0.9738	0.9744	0.975	0.9756	0.9761
2	0.9772	0.9778	0.9783	0.9788	0.9793	0.9798	0.9803	0.9808	0.9812
2.1	0.9821	0.9826	0.983	0.9834	0.9838	0.9842	0.9846	0.985	0.9854
2.2	0.9861	0.9864	0.9868	0.9871	0.9875	0.9878	0.9881	0.9884	0.9887
2.3	0.9893	0.9896	0.9898	0.9901	0.9904	0.9906	0.9909	0.9911	0.9913
2.4	0.9918	0.992	0.9922	0.9925	0.9927	0.9929	0.9931	0.9932	0.9934
2.5	0.9938	0.994	0.9941	0.9943	0.9945	0.9946	0.9948	0.9949	0.9951
2.6	0.9953	0.9955	0.9956	0.9957	0.9959	0.996	0.9961	0.9962	0.9963
2.7	0.9965	0.9966	0.9967	0.9968	0.9969	0.997	0.9971	0.9972	0.9973
2.8	0.9974	0.9975	0.9976	0.9977	0.9977	0.9978	0.9979	0.9979	0.998
2.9	0.9981	0.9982	0.9982	0.9983	0.9984	0.9984	0.9985	0.9985	0.9986
3	0.9987	0.9987	0.9987	0.9988	0.9988	0.9989	0.9989	0.9989	0.999
3.1	0.999	0.9991	0.9991	0.9991	0.9992	0.9992	0.9992	0.9992	0.9993
3.2	0.9993	0.9993	0.9994	0.9994	0.9994	0.9994	0.9994	0.9995	0.9995
3.3	0.9995	0.9995	0.9995	0.9996	0.9996	0.9996	0.9996	0.9996	0.9996
3.4	0.9997	0.9997	0.9997	0.9997	0.9997	0.9997	0.9997	0.9997	0.9997

When a TSPT transformed t-series with normal distribution is obtained, the flood peak of a particular return period can be calculate by the equation 7.29 [112]:

$$t_p = t_{bar} + K_p * \sigma_t \tag{7.29}$$

where t_{bar} = the mean TSPT t-series, σ_t = the standard deviation of the TSPT t-series, K_p= standard normal deviate corresponding to the given return period and is taken from Table 7.3 and t_p = the value corresponding to p^{th} return period in TSPT transformed series.

The value corresponding to t_p in the original flood data series X_p , may be obtained by using the equation 7.30.

$$X_p = (Y_p^{\lambda} + 1.0)^{(1.0/\lambda)} \tag{7.30}$$

where, $Y_p = Y_p' + Y_{bar}$ = value corresponding to p^{th} return period in power transformed series and $Y_p' = (|t_p|)^{(1.0/\gamma)}$. Y_P' is given the same sign as that of t_p.

7.4 Analysis, Results and Discussions

7.4.1 Introduction

Many probability distributions are available for analysis of a given flood data series. The most commonly used methods of flood frequency analysis are EV1, LPIII, LN, Pearson Type III, etc. [188, 229, 261]. Similarly, there are many plotting formulae, as summarized in Table 7.4, the choice of which for fitting the method of flood frequency assessment, have been discussed in numerous studies [173]. The plotting position formulae give a quantile-unbiasedness for different distributions [229]. This study attempted to find out the best and appropriate flood frequency method for fitting the annual maximum discharge data series of two Ethiopian rivers (Awash and Gilgel Ghibe rivers). In order to find out the most suitable method of flood frequency assessment, the PPCC [87], the RMSD [3, 50] and the NS [154] tests were used. Seven methods of flood frequency analysis were considered for the current study: the TSPT (Power transformed Normal & Log-transformed Normal), LPIII, EVI, Chow's and Stochastic methods as well as the Weibull's Plotting Position formula to model at-site annual maximum discharge data with the help of the appropriate plotting position formulae. Plotting position denotes to the probability value allocated to each part of data to be plotted. Numerous plotting position formulae have been proposed for the determination of plotting positions, most of which are empirical [58]. Many of the plotting position formulae needed for fitting the method of the flood frequency analysis can be formulated in a universal form as [63, 142, 173, 305];

$$F_i = \frac{(i-\alpha)}{(n+1-2\alpha)} \tag{7.31}$$

where F_i is the probability of plotting, i is the rank in ordered data with i = 1 (for the biggest observed maginitude in the sample) and α is the plotting position parameter giving approximately unbiased plotting positions. The value of α determines how well the calculated plotting positions fit a given theoretical distribution.

Table 7.4: Various Plotting Position Formulae [63, 142, 173, 229]

SN	Authors/Proponent	α	Plotting position formula	Parent Distribution
1	California	-	i/n	All distributions
2	Weibull(1939)	0	i/(n+1)	All distributions
3	Chegodajev(1955)	0.3	(i-0.3)/(n+0.4)	Pearson III distribution
4	Beard(1943)	0.31	(i-0.31)/(n+0.38)	Normal distribution
5	Median	0.3175	(i-0.3175)/(n+0.365)	Normal distribution
6	Tukey(1962)	0.33	(i-1/3)/(n+1/3)	Normal distribution
7	Blom(1958)	0.375	(i-3/8)/(n+1/4)	Normal &LPIII distributions
8	Cunnane(1977)	0.4	(i-0.4)/(n+0.2)	All distributions
9	Gringorton(1963)	0.44	(i-0.44)/(n+0.12)	Gumbel(EVI),Exponential, GEV
10	Foster (1936)	0.5	(i-0.5)/n	Gumbel(EVI) distribution
11	Hazen (1914)	0.5	(i-0.5)/n	Gumbel(EVI) distribution
12	Nguyen et.al (1989)	-	(i-0.42)/(n+0.3y+0.05)	Pearson III distribution

In this study, following the recommendations of Cunnane [63], the appropriate plotting position formula for fitting the flood frequency methodologies were determined [173]; in which the Grin gorten formula (α = 0.44) was used for fitting the EVI distribution [285], and the Blom formula (α = 0.375) for the TSPT (power & log transformed normal) and LPIII distributions along with Weibull (α = 0) plotting position formula [173, 286] .

7.4.2 Goodness-of-fit (GOF) Tests

7.4.2.1 Probability Plot Correlation Coefficient (PPCC) Test

This is a simple but powerful GOF test developed by Filliben [87]. It is the product moment coefficient of correlation between the order statistic means and the ordered data for each assumed frequency methodology [12, 286]. It gives the relationship between the fitted quantiles obtained by a plotting position and the corresponding ordered data. This test is based on probability-plot and correlation coefficient [173]. The application of the procedure for frequency assessment of hydrological data was examined by Vogel [285]; Vogel and Kroll [286]; Vogel and McMartin [287]; and Fuladipanah Mehdi and Jorabloo Mehdi [173]. Thus, the competence of a fitted flood frequency methodology could possibly be assessed with the technique of the PPCC test that is principally the linearity measure of the probability plot [87] which is a graphical plot of the i^{th} order statistic of the data sample y_i against the non exceedance probability plotting position of the i^{th} order statistic obtained from the assumed standardized distribution. The i^{th} order statistic can be acquired by arranging recorded data from the least (i = 1) to the biggest (i = n) value, then y_i is equal to the i^{th} biggest value [286]. This test uses the correlation **r** between the ordered data and the corresponding fitted quantiles $(y)_{pi} = F_{p_i}^{-1}$, obtained with the use of the plotting position p_i for each y_i. This test was also utilized by Vogel and Kroll [286] to detect the best fit of numerous distributions to the observed data. If y_i denotes the observed i^{th} largest observations, w_i the fitted quantiles at the i^{th} plotting position, $\overline{y}$ the mean value of the ordered data and $\overline{w}$ the fitted quantiles' mean value, then the PPCC test statistic [140] is given by (Equation 7.32).

$$r = \frac{\sum_{i=1}^{n}(y_i - \overline{y})(w_i - \overline{w})}{[\sum_{i=1}^{n}(y_i - \overline{y})^2(w_i - \overline{w})^2]^{0.5}} \tag{7.32}$$

where n is data size.

If the data sample to be assessed is truly drawn from the population of the hypothesized distribution, it is anticipated that the correlation coefficient will be close to one. A value of the PPCC near one indicates that the sample data might have come from the fitted statistical function. This test statistic should also be associated with the critical value of PPCC at an appropriate significant level. The critical values of PPCC test statistic have been found for normal and EVI distribution by Vogel [285], for the Weibull, and the uniform distributions by Vogel and Kroll [286], for the LPIII distribution by Vogel and McMartin [287]. Accordingly, the critical PPCC test statistic values were determined for each station and are given in Table 7.12. If the calculated PPCC test statistic is greater than the critical PPCC value at a specified significance level, we cannot reject the null hypothesis that the data came from a population with a hypothesized distribution (in our case a normal distribution), i.e, we should reject the hypothesized distribution if the observed value, **r**, is smaller than the critical one.

7.4.2.2 Root-Mean-Square-Deviation, RMSD

A regularly used technique for evaluating the GOF of a distribution is the RMSD. The method was utlized for ranking candidate flood frequency methodologies [140, 229]. The RMSD is determined [140] by:

$$RMSD = \left[\frac{1}{n}\sum_{i=1}^{n}(y_i - w_i)^2\right]^{0.5} \tag{7.33}$$

where n is the data size, y_i and w_i are the i^{th} observed and quantile values, respectively.

Non-dimension forms of the RMSD are helpful since one often wants to associate RMSD with dissimilar units. Normalizing the RMSD further assists the comparison between datasets. This value is commonly referred to as the normalized root-mean-square deviation (NRMSD), and often expressed as a percentage, where lower values indicate less residual variance. This is performed by two approaches: normalizing the RMSD to the observed data range (maximum value- minimum value), or normalizing to the average of the observed data, i.e,

$$NRMSD = \begin{cases} \left(\frac{RMSD}{X_{obs,max} - X_{obs,min}}\right) \\ OR \\ \left(\frac{RMSD}{X_{mean}}\right) \end{cases} \tag{7.34}$$

When normalizing by the mean of the observed data, the term coefficient of variation of the RMSD, CV(RMSD) is used to avoid ambiguity. In this study, CV (RMSD) was adopted.

7.4.2.3 NS efficiency

The NS efficiency is usually used to evaluate the forcasting efficiency of hydrologic models [154]. It can also be employed to define the correctness of model outputs. It measures the effectiveness of the model by relating the Goodness-Of-Fit of the simulated data to the recorded data. It is expressed as:

$$NS = 1 - \frac{\sum_{i=1}^{n}(X_{obs,i} - X_{model})^2}{\sum_{i=1}^{n}(X_{obs,i} - X_{bar,obs})^2} \tag{7.35}$$

where X_{obs} is recorded data and X_{model} is modeled values @ i^{th} event.

NS efficiency can vary from -∞ to 1. An NS = 1 shows a perfect match between model values and observations. Principally, the closer the NS is to 1, the better the model fit.

7.4.3 Application to annual maximum discharge data

The annual maximum discharge data series of 14 flow recording stations of two Ethiopian rivers (8 in Awash River and 6 in Gilgel Ghibe River) obtained from Ministry of Water, Irrigation and Electricity in Ethiopia was used for this study. These data are given in Tables A.4.1 and A.4.2. The characteristics of the flow gauging stations is also presented in Table 7.5, in which the stream flow records are available for the period from 1960 to 2013 (25 to 54 years) for Awash River and from 1975-2013 (23 to 38 years) for Gilgel Ghibe River.

Table 7.5: Characteristics of the flow gauging stations used in the analysis.

SN	River catchment	Gauging Station	Coordinates		Drainage area(km^2)	Record legnth	Duration (Years)
			Lat.	Long.			
1	Awash	Akaki	$8^0$53'N	$38^0$47'E	884	1981-2005	25
2	Awash	Berga Nr. Addis Alem	$9^0$01'N	$38^0$21'E	249	1975-2012	38
3	Awash	Bello Nr. Guder	$8^0$52'N	$37^0$40'E	165	1960-2013	54
4	Awash	Holota Nr. Holota	$9^0$05'N	$38^0$31'E	119	1975-2009	35
5	Awash	Awash below Koka dam	$8^0$28'N	$39^0$10'E	11219	1970-2010	41
6	Awash	Awash @ Melka Kuntire	$8^0$42'N	$38^0$36'E	4456	1966-2012	47
7	Awash	Mojo @ mojo village	$8^0$36'N	$39^0$05'E	1496	1968-2012	45
8	Awash	Teji Nr. Asgory	$8^0$49'N	38022'E	663	1975-2012	38
9	Gilgel Ghibe	GilgelGhibe Nr.Asendabo	$7^0$45'N	$37^0$11'E	2943	1984-2013	30
10	Gilgel Ghibe	Ghibe Nr Seka	$7^0$36'N	$36^0$45'E	294	1984-2013	30
11	Gilgel Ghibe	Awiatu Nr, Babu	$7^0$40'N	$36^0$50'E	88	1988-2010	23
12	Gilgel Ghibe	Kito Nr Jimma	$7^0$42'N	$36^0$50'E	85	1982-2010	29
13	Gilgel Ghibe	Awaitu At Jimma	$7^0$41'N	$36^0$50'E	72	1982-2010	29
14	Gilgel Ghibe	Bidru Awana Nr Sokuru	$7^0$25'N	$37^0$24'E	41	1981-2010	30

The analysis started with computations of the return periods of observed flows by means of the commonly used Weibull's plotting position formula [112].Several plotting position formulae are available; but then the technique in all of such cases is to arrange the data in increasing or decreasing order of magnitude and then to assign order number M to the ranked values. By far, the most efficient plotting position formula for unspecified distributions and one now commonly used for most sample data is the Weibull's plotting position formula and is given as [64, 204, 241]:

$$P = M/(N+1) \tag{7.36}$$

And **T=1/P**, in which case P is the estimated probability, i.e., the relative frequency of values being equal to or higher than the ranked value, T is the obvious return period and M is ranked from the highest to the lowest. Moreover, this plotting position formula was also used in Chow's flood estimation method.

Thus, the annual maximum discharge data series of the 14 stations are ordered in descending magnitude, ranked and then the corresponding return periods were computed with the help of Weibull's plotting position formula. Using the annual maximum discharge data so arranged and the corresponding return periods calculated, the best fit frequency curves were drawn through these data points for each station on semi-log papers and were then extrapolated for peak floods of higher return periods to use for comparison with the results of Chow's, Stochastic, LPIII, LN, EVI & TSPT methods. An exhaustive analysis of the annual maximum discharge data series of those 14 stations by TSPT method was also carried out with the view to select a suitable method of flood frequency analysis for Ethiopia. To do so, firstly the Box-Cox transformation parameters (the values of λ and γ that make both the skewness and kurtosis of the transformed data series zero and three, respectively) were estimated by developing the python scripts according to the iterative algorithm given in Figure 7.2 and the final values of these parameters are given in Table 7.6. Using values of the parameters so obtained, the accuracy [162] and suitability of TSPT method for flood frequency analysis along with other methods was studied.

Table 7.6: The Box-Cox λ and γ with the corresponding skew ness & kurtosis for the stations of Awash and Gilgel Ghibe catchments

SN	River catchment	Gauging Station	Years of record(N)	λ	γ	Skewness coefficient	Kurtosis
1	Awash	Akaki	25	0.295	2.233	0.0007	2.9993
2	Awash	Berga Nr. Addis Alem	38	-0.244	2.573	0.0007	2.9995
3	Awash	Bello Nr. Guder	54	-1.005	1.240	0.0018	2.9993
4	Awash	Holota Nr. Holota	35	1.417	4.852	-0.0005	2.9996
5	Awash	Awash below Koka dam	41	-0.345	1.955	0.0042	3.0044
6	Awash	Awash @ Melka Kuntire	47	-0.410	2.200	0.0034	2.997
7	Awash	Mojo @ mojo village	45	0.166	3.858	0.0008	2.9994
8	Awash	Teji Nr. Asgory	38	0.691	1.751	0.0001	3.0000
9	Gilgel Ghibe	GilgelGhibe Nr.Asendabo	30	-0.438	7.130	0.0008	2.9999
10	Gilgel Ghibe	Ghibe Nr Seka	30	-1.337	1.628	0.0006	2.9992
11	Gilgel Ghibe	Awiatu Nr, Babu	23	-0.299	3.170	0.0005	3.0008
12	Gilgel Ghibe	Kito Nr Jimma	29	-1.410	4.862	0.0006	2.9993
13	Gilgel Ghibe	Awaitu At Jimma	29	0.085	2.535	-0.0041	3.0006
14	Gilgel Ghibe	Bidru Awana Nr Sokuru	30	-0.450	2.470	-0.0001	2.9987

7.4.4 Normality Tests for TSPT Technique

The importance of normal distribution is undeniable since it is an underlying assumption of numerous statistical processes [212]. If the assumption of normality is violated, interpretation and inference may not be reliable or valid. Therefore, it is vital to check this assumption before proceeding to any statistical processes. One of the normality testing methods is the numerical methods which include the skewness and kurtosis coefficients of the data and they are considered as the useful tool for checking the normality of the data [212]. Even though the numerical methods can assist as the beneficial tool for checking the normality of the data, they are still not enough to offer a convincing evidence that the normal assumption holds. Thus, to support the numerical methods, more normality testing procedures (the formal normality testing and the graphical normality testing methods) should also be conducted before making any decision about the normality of the data. With this perception, in this study the efficacy of the TSPT technique for transforming the data to approximately follow a normal distribution was tested by utilizing a series of normality tests. Here, the tests are the measure of goodness of fit that help check whether the converted data is reasonably good fit to the normal distribution at 5% significance level (α=0.05) or a 95% confidence level. Failing to fit the normality test permits us to ratify with 95% confidence that the data may not fit the normal distribution. Passing to fit the normality test indicates that the data can be considered to be normally distributed.

A number of the formal normality testing methods are available in the literature. However, the commonly used ones are Chi-Square, Kolmogorov-Smirnov (K-S), Shapiro-Wilk, and Anderson-Darling [212] and these tests were employed for this study. In addition, the easiest graphical method, the normal probability plot was also utilized. The normal probability plot is the most generally used and the effective indicative tool for assessing the normality of data [212]. These tests are defined for the hypothesis:

- Ho: The data follow a normal distribution (no difference between the data and normal data).
- Ha: The data do not follow the normal distribution.

A descriptive summary of the normality tests applied to the TSPT technique and the results obtained are given hereunder.

7.4.4.1 Chi-Square Test

The Chi-square test [249] is used to examine if a sample data came from a particular distribution (normal distribution in our case). The chi-square GOF test is employed to the data put into classes, i.e, binned data, in which a measure of the difference between the recorded and anticipated number of observations in k defined bins (class intervals) is assessed by the expression given below [188]:

$$\chi^2 = \sum_{i=1}^{k} \frac{(O_i - E_i)^2}{E_i} \tag{7.37}$$

where O_i is the recorded and E_i are the expected frequencies for bin i, respectively.
The anticipated frequency is calculated by:

$$E_i = N * F(Y_u - F(Y_l)) \tag{7.38}$$

where F is the CDF for the distribution being evaluated, Y_u is the upper limit for class i, Y_l is the lower limit for class i, and N is the data size.

The computed χ^2 values are compared with the critical values $\chi^2_{\alpha-k}$ @ a specified α significance level and a degree of freedom (k-1-number of parameters) to make a decision. In this analysis, the data was binned into ten bins and the number of parameters is taken as two (the mean and standard deviation) which gives 7 degrees of freedom.

If the test statistic is found within the upper critical χ^2 and the lower critical χ^2 values, we do not reject the null hypothesis. Rather, we can conclude that the data fits reasonably to the normal distribution.

7.4.4.2 Kolmogorov-Smirnov (K-S) Test

In this case, the GOF of an observed distribution function P(x) to a hypothetical distribution function F(x) is assessed using the maximum deviation between the two [177, 188, 212]:

$$D = Max|F(x) - P(x)| \tag{7.39}$$

Depending on the sample size and the significance level (α), the maximum deviance D_n value is compared with the critical tabulated value $D_{n,\alpha}$ to evaluate the goodness-of-fit [81]. If $D_n < D_{n,\alpha}$, we accept that the data fits reasonably to the normal distribution [186].

7.4.4.3 Shapiro-Wilk Test

We used the original approach to perform the Shapiro-Wilk (SW) Test [231]. In this case, the basic steps used for normality test is as follows:

- Rearrange the data in ascending order so that $x_1 \leq \ldots \leq x_n$, Calculate SS as follows:

$$SS = \sum_{i=1}^{n} (X_i - X_{bar})^2 \tag{7.40}$$

- If n is an even number, use m to be equal to n/2, while if n is an odd number, use m to be equal to (n–1)/2; and then calculate b as follows, taking the a_i weights from the Table 5 in

the Shapiro-Wilk Tables based on the value of n. Note that if n is odd, the median data value is not used in the calculation of b.

$$b = \sum_{i=1}^{m} a_i (x_{n+1-i} - x_i) \tag{7.41}$$

- Determine the test statistic, $W = \frac{b^2}{SS}$
- Find the corresponding value in the Table 6 of the Shapiro-Wilk Tables for a given value of n that is closest to W, interpolating if necessary. This is the value of p of the test.

We retain the null hypo thesis that the data are distributed normally if p-value > α(=0.05).
For example, suppose $W = 0.975$ and n = 10. Based on Table 6 of the Shapiro-Wilk Tables, the p-value for the test is somewhere between 0.90 (W =0 .972) and 0.95 (W = 0.978).

7.4.4.4 Anderson-Darling (AD) test

This test [255] is likewise employed to evaluate the sample data for fitting the hypothesized distribution. It is similar to but slightly modified form KS test and offers more weight to the tails than does the KS test. This technique, though having exceptional theoretical properties, has a serious inaccuracy when implemented as it is sigificantly affected by ties in the data, i.e, when equal values occur more than once in the data. The test will usually reject the data as non-normal, irrespective of how well the data are distributed normally, when numerous ties exist. In spite of this, it can be used for general normality testing.

Test Statistic: The AD test measure can be expressed as:

$$AD = -N - \frac{1}{N}\left(\sum_{i=1}^{n}(2i-1)[ln(F(Y_i)) + ln(1 - F(Y_{N+1-i}))]\right) \tag{7.42}$$

This formula needs to be modified to account for sample size and for normal distribution [255] as follows:

$$AD^* = AD\left(1 + \frac{0.75}{N} + \frac{2.25}{N^2}\right) \tag{7.43}$$

where N is sample size, F is the CDF for normal distribution, Y_i is the ordered data and AD* is modified AD test statistic.

This AD test statistic is then related with an appropriate critical value, which is found based on a particular distribution that is being evaluated. The critical values can be in the forms of tabulated values and formulas [255, 256] for a few specific probability fuctions (EVI, Normal, Log-normal, Weibull, etc.).

Like other normality tests, when the calculated p-value is greater than 0.05 or when the AD test measure is less than the corresponding critical value of the AD for normal distribution, we cannot reject the null hypothesis in that the data are distributed normally [207, 227, 255, 256].

Accordingly; therefore, the TSPT method was tested for normality by the above GOF tests (χ^2, K-S, Shapiro-Wilk and AD). The summarized results are given in Tables 7.7 and 7.8.

Table 7.7: Summarized results of the normality test for stations in Awash catchment

Station		Akaki	Berga Nr. Addis Alem	Bello Nr. Guder	Holota Nr. Holota	Awash below koka dam	Awash @ melka kuntire	Mojo @ mojo village	TEJI Nr. AS-GORY
Sample size (n)		25	38	54	35	41	47	45	38
Mean		13.8	1.67	1.6	80.38	2.39	2.43	8.37	29.09
Std. deviation		3.14	0.19	0.11	27.35	0.12	0.15	1.33	8.08
(α)		0.05	0.05	0.05	0.05	0.05	0.05	0.05	0.05
Chi-square	Upper critical χ^2	14.07	14.07	14.07	14.07	14.07	14.07	14.07	14.07
	Calculated χ^2	11.03	3.3	6.71	8.21	13.56	14.25	11.65	7.66
	Lower Critical χ^2	2.167	2.167	2.167	2.167	2.167	2.167	2.167	2.167
	p-value	0.27	0.95	0.67	0.51	0.14	0.114	0.23	0.57
K-S	D_n calculated	0.16	0.07	0.09	0.10	0.10	0.07	0.08	0.11
	$D_n, \alpha = 0.05$	0.27	0.22	0.19	0.23	0.20	0.20	0.20	0.22
Shapiro-Wilk	b	15.08	1.02	0.05	156.88	0.78	0.24	8.76	48.35
	SS	236.86	1.06	0.00	25436	0.63	0.06	80.09	2413
	w	0.96	0.98	0.98	0.97	0.96	0.96	0.96	0.97
	p-value	0.45	0.66	0.65	0.48	0.14	0.193	0.18	0.46
Anderson-Darling	AD test	0.48	0.28	1.26	0.37	0.63	0.4	0.46	0.45
	AD* test	0.50	0.29	1.28	0.38	0.64	0.4	0.47	0.46
	p-value	0.211	0.626	0.003	0.4	0.096	0.353	0.244	0.264

Table 7.8: Summarized results of the normality test for stations in Gilgel Ghibe catchment

Station		Ghibe Nr.Asendabo	GHIBE NR SEKA	Awiatu Nr Babu	KITO NR JIMMA	AWAITU AT JIMMA	BIDRU AWANA NR Sokoru
Sample size (n)		30	30	23	29	29	30
Mean		2.05	0.73	2.03	0.53	2.58	1.36
Std. deviation		0.03	0.02	0.23	0.08	0.92	0.19
(α)		0.05	0.05	0.05	0.05	0.05	0.05
Chi-square	Upper critical χ^2	14.07	14.07	14.07	14.07	14.07	14.07
	Calculated χ^2	8.25	12.88	8.58	7.17	13.40	12.08
	Lower Critical χ^2	2.167	2.167	2.167	2.167	2.167	2.167
	p-value	0.51	0.17	0.48	0.62	0.15	0.21
K-S	D_n calculated	0.09	0.21	0.11	0.11	0.22	0.12
	$D_n, \alpha = 0.05$	0.24	0.24	0.28	0.25	0.25	0.24
Shapiro-Wilk	b	0.15	0.02	1.08	0.41	4.63	0.99
	SS	0.02	0.00	1.20	0.18	23.91	1.02
	w	0.94	0.93	0.96	0.92	0.90	0.96
	p-value	0.15	0.08	0.49	0.05	0.06	0.39
Anderson-Darling	AD test	0.42	1.22	0.33	0.28	0.90	0.52
	AD* test	0.43	1.25	0.34	0.28	0.93	0.54
	p-value	0.310	0.003	0.502	0.629	0.018	0.168

From Tables 7.7 and 7.8, it can be observed that since (1) the calculated Chi-Square (χ^2) value at each station was within the upper and the lower critical Chi-Square (χ^2) values or the observed p-value was greater than alpha ($\alpha = 0.05$), (2) the calculated $D_n < D_{n,\alpha}$ for all stations by K-S test, (3) the observed p-values were greater than alpha ($\alpha = 0.05$) for all the stations by SW test, and (4) the calculated p-values were greater than alpha ($\alpha = 0.05$) for all the stations by Anderson-Darling test except at three stations (Bello Nr. Guder, Ghibe Nr. Seka and Awetu at Jimma that might be affected by the existence of ties in the data series), all the power transformed data are reasonably

good fit with the normal distribution at all stations and we cannot reject the null hypothesis that the transformed data are normally distributed.

Furthermore, as explained earlier, the tests could also be justified by the graphical normal probability plot [87] indicated in Figure 7.3. It is a graphical tool to assess if the observed data fits a normal distribution. In this case, the transformed data were ranked from the largest (m = 1) to the smallest (m = n); Blom plotting position formula $[p = (m - \frac{3}{8})/(n+)]$ was assigned to the ranked data; the standard normal variable z corresponding to the plotting position (p) was calculated by NORMSINV(p) in Excel and finally the plot of the data against z is the Normal probability plot. That is, the data were fitted to the normal distribution in that the data points formed nearly a straight line.

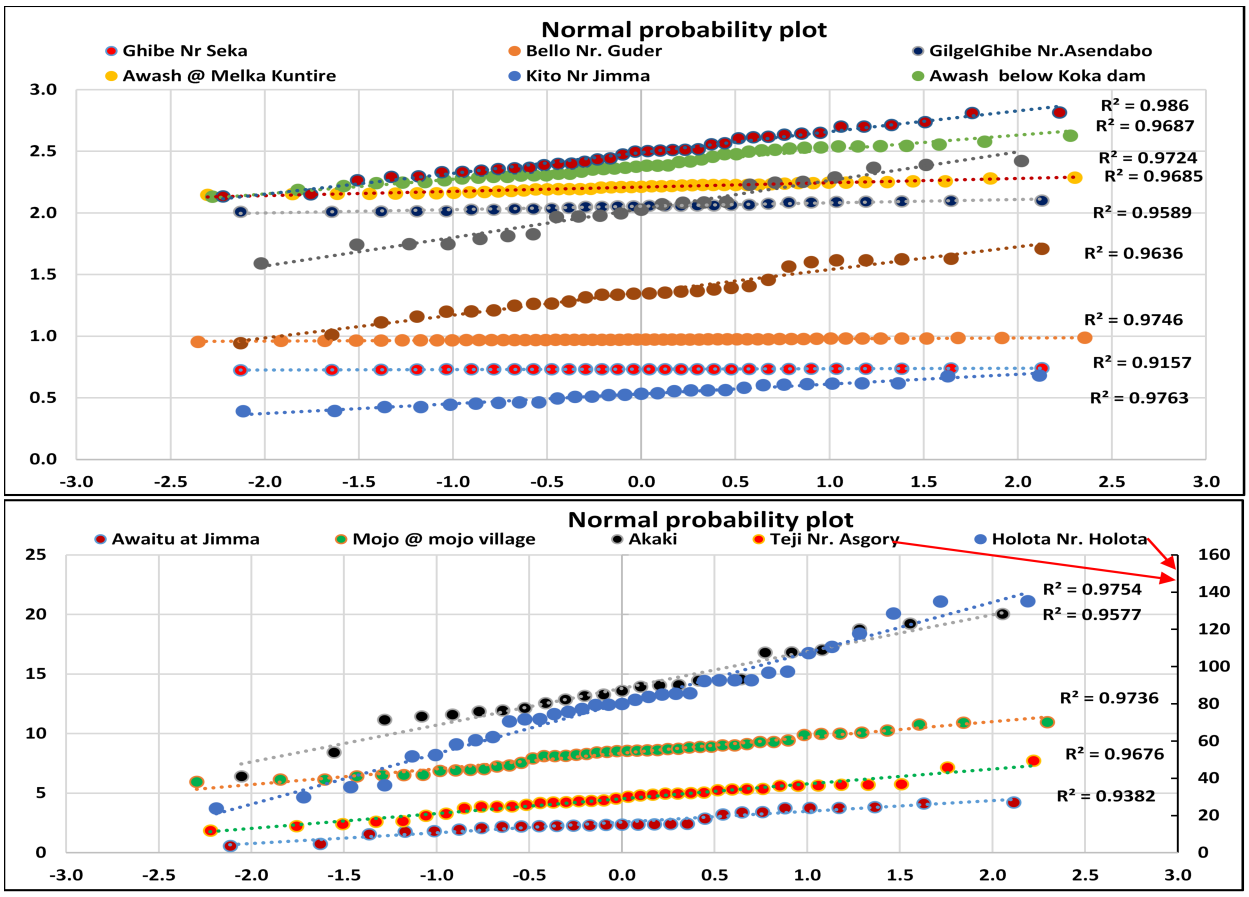

Figure 7.3: Normal probability plot for all stations

Thus, the above analyses pointed out that the data were successfully transformed by the TSPT technique to approximately fit the normal distribution. Consequently, the flood magnitudes for different return periods (2, 10, 50, 100, 200, 500, and 1000 years) were calculated by all the seven methods (Weibull's Plotting position formula, Chow's, Stochastic, LPIII, EVI & TSPT (power transformed normal & log transformed normal) methods at each station separately. These are summarized in Tables 7.9 and 7.10 for comparison. Additionally, using the findings in Tables 7.9 and 7.10, flood frequency curves were plotted on semi log paper for all the 14 stations and are given in figures 7.4, 7.5 and 7.6 for further comparison.

Table 7.9: Summary of estimated peak floods of different return periods by all the seven methods for the stations of Awash catchment

SN	Station	Method	Flood (m3/s) of a given return period (years)						
			2	10	50	100	200	500	1000
1	Akaki	Plotting position	227.04	539.93	852.82	987.58	1122.33	1300.47	1435.22
		Chow	250.88	523.13	761.82	862.72	963.26	1095.9	1196.15
		Stochastic	201.39	584.12	966.86	1131.69	1296.53	1514.42	1679.26
		LP-III	248.56	491.94	664.56	726.06	781.44	846.45	890.18
		LN	229.53	527.74	871.66	1040.52	1223.55	1489.01	1708.87
		EV1	249.75	400.56	576.76	658.5	742.92	857.88	946.91
		TSPT	284.9	572.37	678.01	792.98	877.63	989.54	1074.19
2	Berga Nr. Addis Alem	Plotting position	44.42	87.66	130.91	149.54	168.17	192.79	211.41
		Chow	47.86	85.96	119.36	133.48	147.54	166.1	180.13
		Stochastic	41.85	91.89	141.93	163.48	185.03	213.52	235.07
		LP-III	46.07	82.44	120.26	138.08	157.06	184.13	206.27
		LN	46.83	81.68	114.21	128.55	143.25	163.33	179.07
		EV1	47.77	68.44	92.59	103.79	115.37	131.12	143.32
		TSPT	50.03	92.66	108.15	125.19	137.71	154.25	166.77
3	Bello Nr. Guder	Plotting position	37.39	59.09	80.79	90.14	99.48	111.84	121.18
		Chow	39.2	58.16	74.77	81.8	88.8	98.03	105.01
		Stochastic	35.31	65.31	95.31	108.23	121.15	138.23	151.15
		LP-III	38.02	55.93	75.73	85.45	96.07	111.71	124.9
		LN	39.47	55.15	67.47	72.45	77.32	83.67	88.43
		EV1	39.13	49.54	61.7	67.35	73.17	81.11	87.26
		TSPT	46.18	78.45	110.72	124.62	138.52	156.89	170.79
4	Holota Nr. Holota	Plotting position	26.28	37.9	49.53	54.54	59.54	66.16	71.17
		Chow	27.13	38.07	47.67	51.72	55.76	61.09	65.12
		Stochastic	23.26	48.78	74.3	85.3	96.29	110.82	121.81
		LP-III	28.58	37.03	40.52	41.43	42.11	44.29	45.66
		LN	27.18	38.96	48.41	52.27	56.07	61.04	64.79
		EV1	27.07	33.22	40.42	43.75	47.2	51.89	55.53
		TSPT	32.52	39.22	40.25	40.53	42.88	44.67	46.03
5	Awash below koka dam	Plotting position	147.96	399.29	650.62	758.86	867.11	1010.19	1118.44
		Chow	168.67	386.53	577.54	658.29	738.74	844.88	925.1
		Stochastic	144.87	377.59	610.32	710.55	810.77	943.27	1043.5
		LP-III	144.67	364.69	680.31	858.33	1067.94	1402.19	1705.78
		LN	150.44	357.13	601.3	722.68	855.1	1048.48	1209.66
		EV1	167.57	288.93	430.74	496.51	564.46	656.97	728.62
		TSPT	176.07	488.39	725.81	832.93	940.65	1095.52	1230.33
6	Awash @ melka kuntire	Plotting position	252.72	438.39	624.05	704.01	783.97	889.68	969.64
		Chow	267.75	432.67	577.26	638.38	699.28	779.63	840.36
		Stochastic	243.71	451.98	660.25	749.95	839.64	958.22	1047.91
		LP-III	262.78	419.08	570.91	640.03	712.31	813.45	894.7
		LN	267.19	415.24	541.64	594.89	648.19	719.22	773.63
		EV1	267.33	356.84	461.42	509.93	560.04	628.27	681.11
		TSPT	345.87	577.1	681.55	719.41	753.48	796.94	830.58
7	Mojo @ mojo village	Plotting position	174.94	373.43	571.92	657.41	742.9	855.9	941.39
		Chow	194.99	379.33	540.93	609.25	677.33	767.13	835
		Stochastic	166.49	407.63	648.76	752.61	856.46	993.75	1097.60
		LP-III	186.75	372.43	550.38	628.91	709.12	818.05	902.8
		LN	183.68	376.76	580.9	676.79	778.35	922.06	1038.41
		EV1	194.6	294.3	410.79	464.82	520.64	596.64	655.5
		TSPT	255.05	423.9	466.27	532.84	578.32	638.45	683.93
8	TEJI Nr. ASGORY	Plotting position	75.22	129.25	183.29	206.56	229.83	260.59	283.87
		Chow	79.33	129.01	172.56	190.97	209.31	233.52	251.81
		Stochastic	65.78	160.83	255.87	296.8	337.73	391.84	432.77
		LP-III	82.53	126.24	150.3	157.83	164.17	181.04	192.62
		LN	77.71	133.46	184.88	207.42	230.44	261.78	286.27
		EV1	79.14	106.53	138.53	153.38	168.71	189.59	205.76
		TSPT	86.85	131.72	148.55	166.51	179.8	197.36	210.65

Table 7.10: Summary of estimated peak floods of different return periods by all the seven methods for the stations of Gilgel Ghibe catchment

SN	Station	Method	Flood (m3/s) of a given return period (years)						
			2	10	50	100	200	500	1000
1	GILGEL GHIBE NR. ASENDABO	Plotting position	179.11	280.61	382.1	425.81	469.52	527.31	571.02
		Chow	186.47	275.38	353.33	386.28	419.12	462.43	495.17
		Stochastic	173.39	286.42	399.45	448.13	496.81	561.16	609.84
		LP-III	186.2	269.71	341.87	372.64	403.69	445.49	477.83
		LN	187.77	268.38	332.84	359.12	384.97	418.8	444.29
		EV1	186.57	236.2	294.19	321.08	348.87	386.7	416
		TSPT	244.53	301.64	312.16	334.49	349.05	368.3	382.86
2	GHIBE NR SEKA	Plotting position	18.41	26.22	34.03	37.39	40.75	45.2	48.56
		Chow	19.03	25.74	31.61	34.1	36.57	39.84	42.3
		Stochastic	17.65	28.02	38.39	42.85	47.31	53.21	57.68
		LP-III	18.57	24.97	32.08	35.57	39.36	44.93	49.62
		LN	19.26	24.7	28.7	30.27	31.77	33.69	35.11
		EV1	18.98	22.85	27.37	29.47	31.64	34.59	36.87
		TSPT	18.8	27.25	31.95	33.87	35.8	38.39	40.41
3	AWAITU NR, Babu	Plotting position	23.32	58.79	94.27	109.55	124.83	145.02	160.30
		Chow	26.59	57.15	83.94	95.27	106.55	121.44	132.7
		Stochastic	22.48	54.63	86.77	100.61	114.46	132.75	146.6
		LP-III	23.21	52.95	91.39	111.8	135.02	170.64	201.82
		LN	23.9	52.11	83.35	98.38	114.5	137.61	156.55
		EV1	25.88	42.86	62.7	71.91	81.41	94.36	104.38
		TSPT	20.92	60.54	72.97	88.71	99.92	114.74	125.95
4	KITO NR JIMMA	Plotting position	2.74	6.02	9.30	10.71	12.12	13.98	15.39
		Chow	3.01	5.76	8.16	9.18	10.2	11.53	12.54
		Stochastic	2.80	5.19	7.57	8.60	9.63	10.99	12.02
		LP-III	2.68	5.15	9.2	11.74	14.95	20.55	26.13
		LN	2.94	5.04	6.98	7.83	8.69	9.87	10.8
		EV1	2.97	4.64	6.58	7.48	8.41	9.68	10.67
		TSPT	3.50	6.30	7.61	8.74	9.63	10.8	11.69
5	AWAITU AT JIMMA	Plotting position	10.44	29.12	47.81	55.86	63.9	74.54	82.59
		Chow	11.91	28.07	42.24	48.23	54.2	62.07	68.03
		Stochastic	9.78	28.45	47.12	55.16	63.2	73.83	81.87
		LP-III	10.41	26.91	46.11	55.44	65.44	79.75	91.41
		LN	10.19	27.32	49.49	61.04	73.95	93.31	109.84
		EV1	11.82	20.9	31.51	36.43	41.52	48.44	53.80
		TSPT	13.25	30	36.21	42.91	47.85	54.38	59.33
6	BIDRU AWANA NR SOKURU	Plotting position	8.32	19.04	29.75	34.37	38.98	45.08	49.7
		Chow	9.17	18.4	26.50	29.92	33.33	37.83	41.23
		Stochastic	7.98	18.53	29.07	33.61	38.16	44.16	48.7
		LP-III	8.34	17.24	28.86	35.12	42.34	53.59	63.6
		LN	8.72	16.88	25.12	28.91	32.87	38.41	42.84
		EV1	12.13	17.93	24.71	27.85	31.1	35.52	38.95
		TSPT	9.19	19.35	24.42	28.55	31.83	36.16	39.44

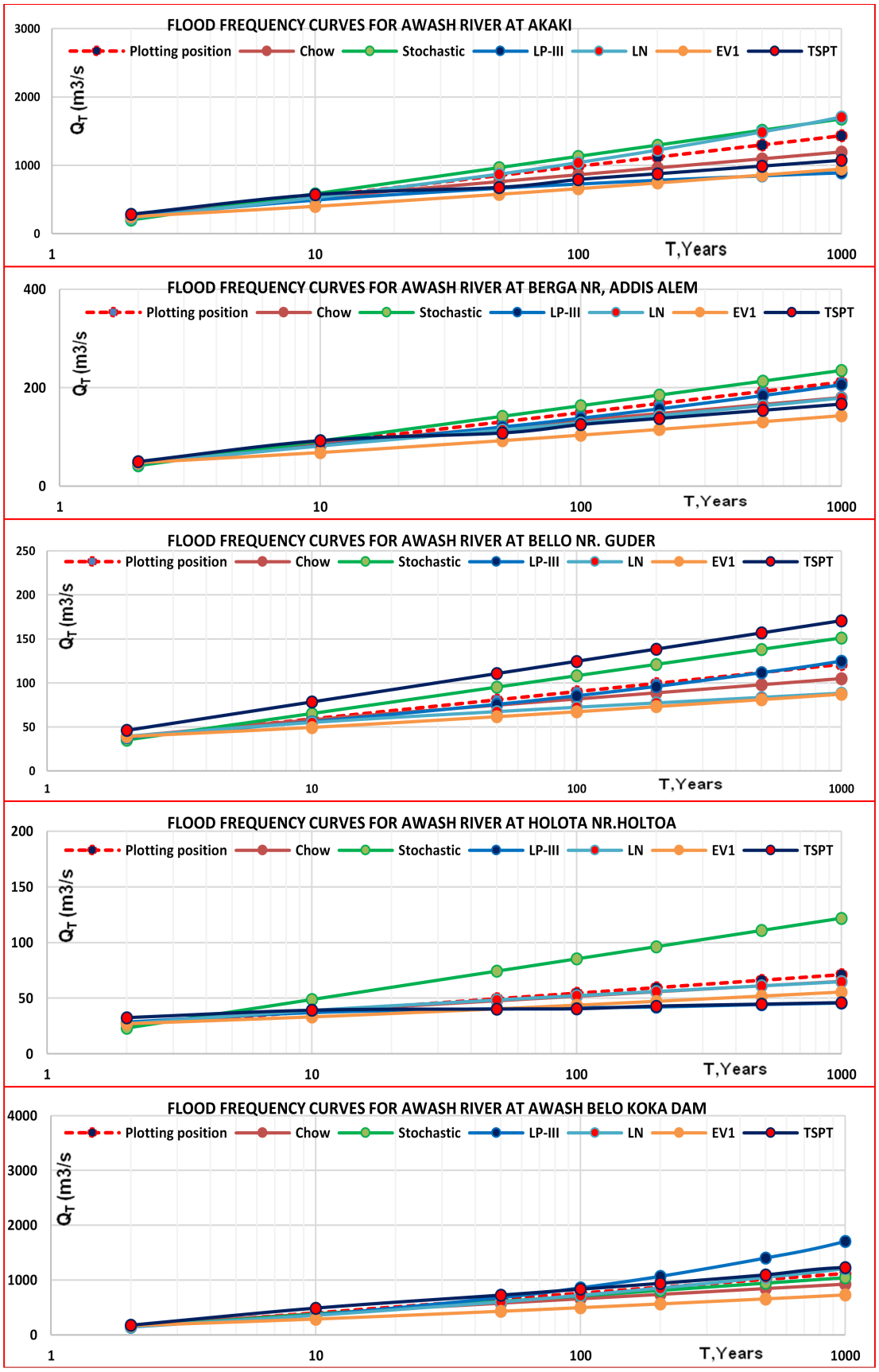

Figure 7.4: Flood frequency furves at the gauging stations of the two rivers -(Plate 1)

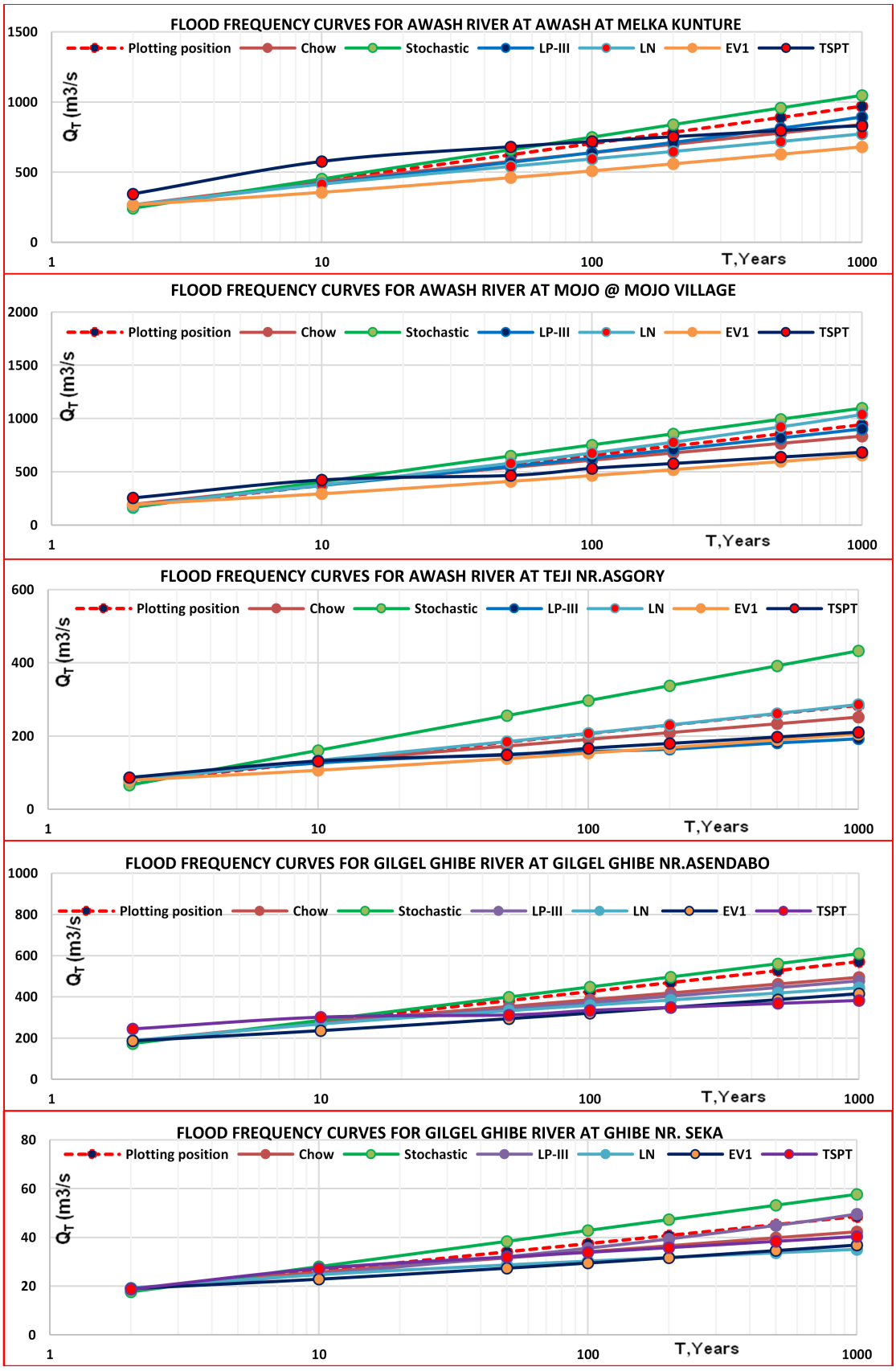

Figure 7.5: Flood frequency curves at the gauging stations of the two rivers -(Plate 2)

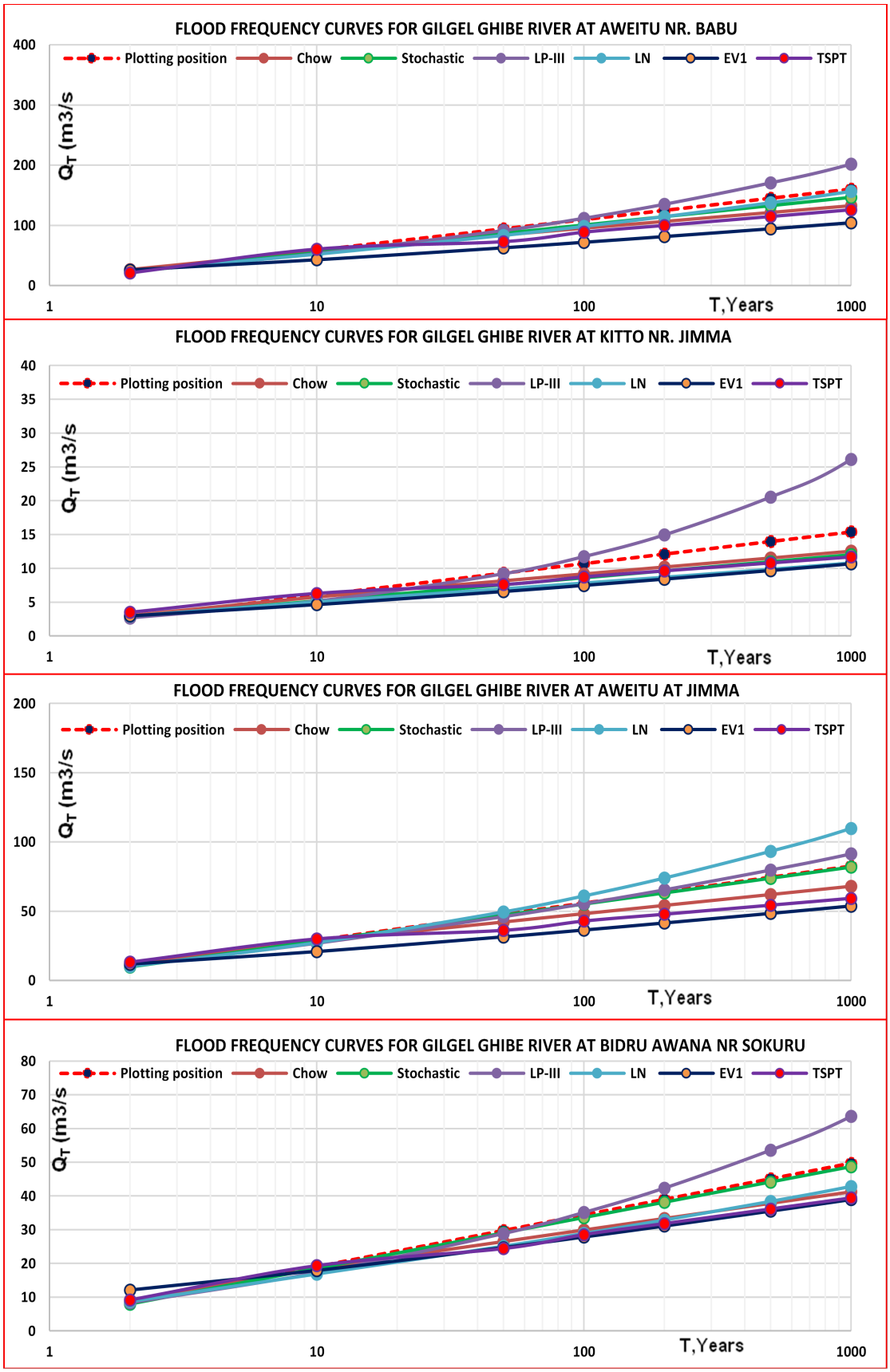

Figure 7.6: Flood frequency curves at the gauging stations of the two rivers -(Plate 3)

It has been observed that (from Figures 7.4, 7.5 and 7.6; and Tables 7.9 and 7.10), the values obtained by TSPT method agree better with those of the other methods. Especially, the peak flood

values of lower return periods obtained by TSPT method are similar with the results of the other methods at all the stations. However, the results obtained by TSPT method were found slightly different from those obtained by other methods for higher return periods. The summaried results of the evaluation is given in the Table 7.11.

Table 7.11: Comparison of TSPT method with other methods of flood frequency analysis at all stations.

SN	River Basin	Gauging Station	Peak flood value estimated by TSPT method agrees better with	Than
1	Awash	Akaki	Chow's, LPIII & EVI	LN & Stochastic
2	Awash	Berga Nr. Addis Alem	Chow's, LN & EV	LPIII & Stochastic
3	Awash	Bello Nr. Guder	Stochastic,& LPIII	LN, Chow's, & EVI
4	Awash	Holota Nr. Holota	Chow's, LPIII, LN & EVI	Stochastic
5	Awash	Awash below Koka dam	Chow's, Stochastic, LN & EVI	LPIII
6	Awash	Awash @ Melka Kuntire	Chow's, LPIII, LN & EVI	Stochastic
7	Awash	Mojo @ mojo village	Chow's, LPIII & EVI	LN & Stochastic
8	Awash	Teji Nr. Asgory	Chow's, LPIII, LN & EVI	Stochastic
9	Gilgel Ghibe	GilgelGhibe Nr.Asendabo	Chow's, LPIII,LN & EVI	Stochastic
10	Gilgel Ghibe	Ghibe Nr Seka	Chow's,LN & EVI	LPIII & Stochastic
11	Gilgel Ghibe	Awiatu Nr, Babu	Chow's, Stochastic, ,LN & EVI	LPIII
12	Gilgel Ghibe	Kito Nr Jimma	Chow's, Stochastic,, LN & EVI	LPIII
13	Gilgel Ghibe	Awaitu At Jimma	Chow's, Stochastic, & EVI	LN & LPIII
14	Gilgel Ghibe	Bidru Awana Nr Sokuru	Chow's, Stochastic, LN & EVI	LPIII

An additional statistical analysis of the annual maximum discharge data series [Tables A.4.1 and A.4.2] at all the stations of the two rivers was carried out to check the reliability, accuracy [162] and suitability of the flood frequency methodologies considered in this study. In this regard, all the methods of flood frequency analysis were fitted to the data with the help of the appropriate plotting position formulae and tested for goodness of fit. Applying the GOF tests (PPCC, RMSD and NS) to fit the flood frequency methodologies to the observed data, the results are given in Tables 7.13 & 7.14 for all the 14 stations. The critical PPCC values @ 5% significant level were also determined for all the methods with the use of the fitted plotting position formula at all stations & are shown in Table 7.12. In this case, the 5% critical magnitudes of PPCC test statistic for LPIII were calculated by: $r_{0.05} = exp[3.77 - 0.0290\gamma^2 - 0.000670n]n^{(0.105\gamma - 0.758)}$ for $|\gamma| \leq 5$ as given by Vogel and Kroll [286], where γ is skewness coefficient.

Table 7.12: The [$r_{5\%}$ critical values of the PPCC test static for TSPT, EVI, LPIII, Chow's, Weibull's (W2) plotting position and Stochastic methods]

Station	Akaki	Berga Nr. Addis Alem	Bello Nr. Guder	Holota Nr. Holota	Awash below koka dam	Awash @ melka kuntire	Mojo @ Mojo village
Sample size (n)	25	38	54	35	41	47	45
Normal,logNormal [87]	0.959	0.970	0.977	0.969	0.972	0.975	0.974
EVI [285]	0.947	0.959	0.967	0.957	0.961	0.964	0.963
Chow,W2,Stochastic [286]	0.947	0.959	0.967	0.957	0.961	0.964	0.963
LPIII [286]	0.983	0.981	0.982	0.994	0.982	0.987	0.991
Station	TEJI Nr.Asgory	Ghibe Nr Asendabo	Ghibe Nr Seka	Awiatu Nr Babu	Kito at Jimma	Awaitu at Jimma	BidruAwana Nr Sekoru
Sample size (n)	38	30	30	23	29	29	30
Normal,logNormal [87]	0.970	0.964	0.964	0.956	0.963	0.963	0.964
EVI [285]	0.959	0.953	0.953	0.944	0.952	0.952	0.953
Chow,W2,Stochastic [286]	0.959	0.953	0.953	0.944	0.952	0.952	0.953
LPIII [286]	0.993	0.969	0.890	0.923	0.841	0.977	0.953

Table 7.13: Summary of the results GOF test for the flood frequency methodologies at the stations of Awash catchment

SN	Station	Method	PPCC	RMSD	$Q_{obs,av}$	NS	NRMSD	Rank by NRMSD	r0.05
1	Akaki	Plotting position	0.982	30.519	274.627	0.964	0.11	2	0.947
		Chow	0.975	36.1038	274.627	0.9502	0.13	4	0.947
		Stochastic	0.982	49.149	274.627	0.908	0.18	6	0.947
		LP-III	0.978	54.604	274.627	0.886	0.2	7	0.983
		LN	0.927	0.139	2.439	0.747	0.06	1	0.959
		EV1	0.956	41.756	274.627	0.933	0.15	5	0.947
		TSPT	0.978	1.639	13.797	0.716	0.12	3	0.959
2	Berga Nr. Addis Alem	Plotting position	0.992	3.011	51.421	0.983	0.06	3	0.959
		Chow	0.988	3.5295	51.421	0.977	0.07	5	0.959
		Stochastic	0.992	4.934	51.421	0.955	0.1	7	0.959
		LP-III	0.99	3.276	51.421	0.98	0.06	4	0.981
		LN	0.993	0.023	1.711	0.985	0.01	1	0.97
		EV1	0.978	4.27	51.421	0.966	0.08	6	0.959
		TSPT	0.994	0.065	2.49	0.847	0.03	2	0.97
3	Bello Nr. Guder	Plotting position	0.989	1.754	41.048	0.979	0.04	3	0.967
		Chow	0.972	2.8141	41.048	0.9457	0.07	6	0.967
		Stochastic	0.929	6.964	41.048	0.667	0.17	7	0.967
		LP-III	0.99	1.811	41.048	0.977	0.04	4	0.982
		LN	0.969	0.028	1.613	0.939	0.02	2	0.977
		EV1	0.957	2.77	41.048	0.947	0.07	5	0.967
		TSPT	0.987	0.001	0.974	0.95	0	1	0.977
4	Holota Nr. Holota	Plotting position	0.894	3.071	28.14	0.8	0.11	5	0.957
		Chow	0.954	2.056	28.14	0.9104	0.07	3	0.957
		Stochastic	0.894	8.002	28.14	-0.357	0.28	7	0.957
		LP-III	0.983	1.277	28.14	0.965	0.05	2	0.994
		LN	0.944	0.04	1.449	0.891	0.03	1	0.969
		EV1	0.898	2.428	28.14	0.875	0.09	4	0.957
		TSPT	0.988	22.618	80.382	0.296	0.28	6	0.969
5	Awash below koka dam	Plotting position	0.982	26.274	189.405	0.964	0.14	3	0.961
		Chow	0.961	38.3928	189.405	0.9231	0.2	5	0.961
		Stochastic	0.814	81.703	189.405	0.652	0.43	7	0.961
		LP-III	0.977	30.079	189.405	0.953	0.16	4	0.982
		LN	0.983	0.055	2.277	0.964	0.02	2	0.972
		EV1	0.936	38.769	189.405	0.922	0.2	6	0.961
		TSPT	0.985	0.024	2.393	0.96	0.01	1	0.972
6	Awash @ melka kuntire	Plotting position	0.984	18.503	283.565	0.977	0.07	6	0.964
		Chow	0.985	17.5752	283.565	0.9795	0.06	4	0.964
		Stochastic	0.882	53.823	283.565	0.725	0.19	7	0.964
		LP-III	0.991	14.299	283.565	0.981	0.05	3	0.987
		LN	0.989	0.022	2.453	0.977	0.01	2	0.975
		EV1	0.977	18.372	283.565	0.968	0.06	5	0.964
		TSPT	0.987	0.01	2.21	0.914	0	1	0.975
7	Mojo @ mojo village	Plotting position	0.982	22.32	212.636	0.962	0.1	6	0.963
		Chow	0.989	16.9149	212.636	0.978	0.08	2	0.963
		Stochastic	0.751	88.06	212.636	0.405	0.41	7	0.963
		LP-III	0.986	18.845	212.636	0.974	0.09	3	0.991
		LN	0.986	0.041	2.328	0.977	0.02	1	0.974
		EV1	0.975	21.247	212.636	0.965	0.1	5	0.963
		TSPT	0.988	0.771	8.375	0.658	0.09	4	0.974
8	TEJI Nr. ASGORY	Plotting position	0.935	10.94	83.971	0.874	0.13	6	0.959
		Chow	0.973	7.1724	83.971	0.9458	0.09	3	0.959
		Stochastic	0.935	24.604	83.971	0.362	0.29	7	0.959
		LP-III	0.976	6.778	83.971	0.952	0.08	2	0.993
		LN	0.957	0.053	1.924	0.915	0.03	1	0.97
		EV1	0.947	7.997	83.971	0.933	0.1	4	0.959
		TSPT	0.983	2.939	29.088	0.864	0.1	5	0.97

Table 7.14: Summary of the results GOF test for the flood frequency methodologies at the stations of Gilgel Ghibe catchment

SN	Station	Method	PPCC	RMSD	$Q_{obs,av}$	NS	NRMSD	Rank by NRMSD	r0.05
1	GILGEL GHIBE NR. ASENDABO	Plotting position	0.968	13.62	195.019	0.937	0.07	6	0.953
		Chow	0.984	9.642	195.019	0.969	0.049	3	0.953
		Stochastic	0.968	15.387	195.019	0.92	0.079	7	0.953
		LP-III	0.98	10.764	195.019	0.961	0.055	4	0.969
		LN	0.984	0.022	2.274	0.966	0.01	2	0.964
		EV1	0.978	13.604	195.019	0.938	0.07	5	0.953
		TSPT	0.981	0.018	2.054	0.571	0.009	1	0.964
2	GHIBE NR SEKA	Plotting position	0.955	1.263	19.638	0.912	0.064	4	0.953
		Chow	0.932	1.543	19.638	0.868	0.079	6	0.953
		Stochastic	0.955	1.868	19.638	0.807	0.095	7	0.953
		LP-III	0.968	1.101	19.638	0.933	0.056	3	0.89
		LN	0.931	0.03	1.285	0.866	0.024	2	0.964
		EV1	0.947	1.536	19.638	0.869	0.078	5	0.953
		TSPT	0.954	0.002	0.734	0.728	0.002	1	0.964
3	AWAITU NR BABU	Plotting position	0.989	2.671	28.634	0.978	0.093	3	0.944
		Chow	0.974	4.153	28.634	0.947	0.145	6	0.944
		Stochastic	0.989	3.423	28.634	0.964	0.12	4	0.944
		LP-III	0.976	3.917	28.634	0.953	0.137	5	0.923
		LN	0.985	0.046	1.378	0.968	0.034	1	0.956
		EV1	0.974	4.986	28.634	0.923	0.174	7	0.944
		TSPT	0.985	0.096	2.032	0.826	0.047	2	0.956
4	KITO NR JIMMA	Plotting position	0.932	0.659	3.255	0.869	0.202	4	0.952
		Chow	0.889	0.834	3.255	0.79	0.256	6	0.952
		Stochastic	0.932	0.808	3.255	0.803	0.248	5	0.952
		LP-III	0.967	0.513	3.254	0.92	0.158	3	0.841
		LN	0.942	0.06	0.468	0.887	0.129	2	0.963
		EV1	0.905	0.862	3.255	0.775	0.265	7	0.952
		TSPT	0.989	0.047	0.532	0.644	0.088	1	0.963
5	AWAITU AT JIMMA	Plotting position	0.974	2.254	13.353	0.948	0.169	2	0.952
		Chow	0.958	2.839	13.353	0.918	0.213	6	0.952
		Stochastic	0.974	2.349	13.353	0.944	0.176	3	0.952
		LP-III	0.963	2.674	13.353	0.927	0.2	5	0.977
		LN	0.965	0.086	1.008	0.931	0.086	1	0.963
		EV1	0.959	3.228	13.353	0.894	0.242	7	0.952
		TSPT	0.969	0.508	2.579	0.687	0.197	4	0.963
6	BIDRU AWANA NR SOKURU	Plotting position	0.973	1.322	10	0.947	0.132	3	0.953
		Chow	0.953	1.737	10	0.908	0.174	6	0.953
		Stochastic	0.973	1.374	10	0.942	0.137	4	0.953
		LP-III	0.968	1.451	10	0.936	0.145	5	0.953
		LN	0.972	0.052	0.941	0.945	0.055	1	0.964
		EV1	0.958	1.933	10	0.886	0.193	7	0.953
		TSPT	0.982	0.092	1.356	0.75	0.068	2	0.964

7.4.5 Comparison of the flood frequency methodologies

The seven flood frequency methodologies used for this study were ranked based on the findings of GOF (PPCC, RMSD and NS) tests in Tables 7.13 & 7.14 at each site. A summary of ranking is given in Table 7.15, in which each method was assigned a ranking scale of 1 up to 7 with 1 being for the best fitting flood frequency methodology and 7 for the worst fitting one.

Table 7.15: Ranking of the methods of flood frequency assessment using the result of NRMSD GOF criteria

GOF Criteria	Method	Number of stations Receiving Weight							Total of Ranks	Rank
		1	2	3	4	5	6	7		
NRMSD	LN	8	6	0	0	0	0	0	20	1
	TSPT	6	3	1	2	1	1	0	34	2
	LP-III	0	2	4	4	3	1	0	53	3
	Plotting position	0	2	5	2	1	4	0	56	4
	Chow	0	1	3	2	2	5	1	66	5
	EV1	0	0	0	2	6	2	4	78	6
	Stochastic	0	0	1	2	1	1	9	85	7

Furthermore, the ranking was refined using the critical PPCC values @ 5% significant level indicated in Table 7.12. Figures 7.7 & 7.8 show the plot of the PPCC and the $r_{5\%}$ values for all the flood frequency methodologies at all stations.

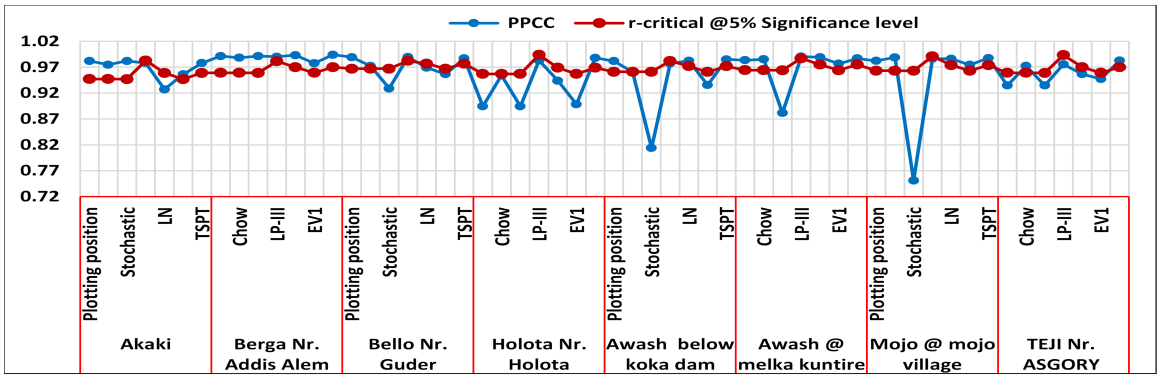

Figure 7.7: Plot of the PPCC and the $r_{5\%}$ critical values for all methods at the stations of Awash catchment

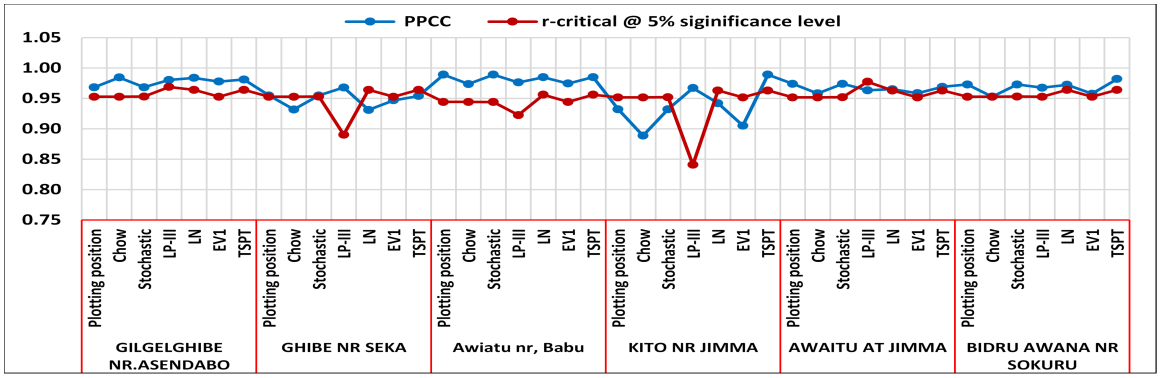

Figure 7.8: Plot of the PPCC and the $r_{5\%}$ critical values for all methods at the stations of Gilgel Ghibe catchment

Figures 7.7 & 7.8 show that some of the flood frequency methodologies fall in rejection zone at the respective 5% critical value of PPCC test statistic at few stations. Stochastic method was rejected at six stations, LPIII at 5 stations, LN & EVI at 4 stations each, Plotting position & Chow's method at 2 stations each for Awash River. Similarly, Chow's, LN & EVI methods were rejected at 2 stations

each; and plotting position, LPIII, Stochastic & TSPT were rejected at one station each for Gilgil Ghibe River. Thus, refining the ranking based upon the 5% critical PPCC test statistic values, the ranking summary is given in Table 7.16. In this case, each method was assigned a weightage ranking scale of 7 to 1 with 7 being for the best fitting method and 1 for the poorest fitting method.

Table 7.16: Ranking summary of the methods of flood frequency analysis based on the PPCC GOF criteria

GOF Criteria	Method	Number of stations Receiving Weight							Total of Ranks	Rank
		7	6	5	4	3	2	1		
PPCC	TSPT	5	3	1	2	1	1	0	71	1
	LN	5	3	0	0	0	0	0	53	2
	Plotting position	0	2	5	1	0	3	0	47	3
	Chow	0	1	2	2	1	4	0	35	4
	LP-III	0	0	3	3	2	0	0	33	5
	EV1	0	0	0	0	4	1	3	17	6
	Stochastic	0	0	0	2	1	1	3	16	7

7.4.6 Flood frequency analysis with PyTOPKAPI model-simulated flow data

In this section, analysis of the flood frequencies was carried out using the PyTOPKAPI model simulated streamflow data. In flood frequency investigation, the usual procedure is to determine the frequencies of flood flows that comprises of fitting of the observed streamflow records to the standard probability functions. However, this technique only works for catchments that have long observed stream flows to warrant the statistical analysis. If streamflow records are not available at all or are too short for flood frequency analysis, a hydrological model like PyTOPKAPI model can be a valuable tool to generate stream flows from the catchments from which the required flood quantiles can be computed. In this study, as indicated in Chapter 5, the PyTOPKAPI model was used to simulate stream flows from the two Ethiopian case study catchments at "Ghibe Nr.Asendabo" and "Mojo @ Mojo village" gauging stations. The rainfall data used for thse simulations were the the respective gauged rainfall data for stydy catchments. Consequently, 25 years (1986-2010) and 15 years (1999-2013) daily stream flows were generated from Gilgel Ghibe and Mojo catchments, respectively. Next, the annual maximum discharge data series were determined from the simulated stream flows for the catchments and are shown in Table 7.17.

Table 7.17: The annual maximum discharge data series obtained from the simulated stream flows.

Gilgel Ghibe River	Year	1986	1987	1988	1989	1990	1991	1992	1993	1994	1995
	Q (m^3/s)	166.48	167.86	225.02	154.02	216.41	186.47	287.70	247.95	243.53	154.30
	Year	1996	1997	1998	1999	2000	2001	2002	2003	2004	2005
	Q (m^3/s)	249.24	356.11	213.46	280.07	194.50	259.68	182.81	123.80	143.30	154.94
	Year	2006	2007	2008	2009	2010					
	Q (m^3/s)	278.84	154.86	239.86	196.45	206.87					
MOJO River	Year	1999	2000	2001	2002	2003	2004	2005	2006	2007	2008
	Q (m^3/s)	449.37	213.87	116.7	116.21	397.18	252.07	253.57	198.96	139.47	423.87
	Year	2009	2010	2011	2012	2013					
	Q (m^3/s)	127.81	254.41	130.35	309.55	294.56					

Based on the computed annual maximum streamflow data series of the catchments, analysis of the flood frequencies was conducted for both the study catchments. In this case, all the seven flood frequency methodologies were fitted to the simulated annual maximum streamflow data series, with the help of the corresponding plotting position formula. As indicated in section 7.4.2, three GOF tests (PPCC, RMSD and NS) were used for detection of the best fit method. The results of

the GOF tests were presented in Table 7.18. The $r_{5\%}$ critical values for PPCC test statistic were also determined for all the methods and are shown in Table 7.18 and were then plotted in Figure 7.9 indicating that all the flood frequency methodologies considered fall in acceptable zone at the respective $r_{5\%}$ critical value of the PPCC test statistic.

Table 7.18: Summary of the results GOF tests for the simulated stream flows.

River	Simulation period (years)	Method	PPCC	RMSD	Qobav	NS	r-@ 5% sigif. level	NRMSD	Rank by NRMSD
Gilgel Ghibe	1986-2010	Plotting position	0.972	15.23	211.38	0.946	0.947	0.072	6
		Chow	0.973	10.11	211.38	0.825	0.947	0.048	3
		Stochastic	0.991	27.30	211.38	0.980	0.947	0.129	7
		LP-III	0.991	9.09	176.15	0.987	0.952	0.052	4
		LN	0.992	0.02	1.926	0.991	0.959	0.008	2
		EV1	0.990	13.93	211.38	0.961	0.947	0.066	5
		TSPT	0.925	0.02	3.14	0.925	0.959	0.006	1
Mojo	1999-2013	Plotting position	0.970	26.46	245.20	0.941	0.928	0.108	3
		Chow	0.980	50.18	245.20	0.788	0.928	0.205	6
		Stochastic	0.970	49.37	245.20	0.795	0.928	0.201	5
		LP-III	0.972	25.65	245.20	0.945	0.766	0.105	2
		LN	0.971	0.034	1.17	0.998	0.939	0.029	1
		EV1	0.973	34.25	245.20	0.901	0.927	0.140	4
		TSPT	0.940	1.45	6.57	0.688	0.939	0.220	7

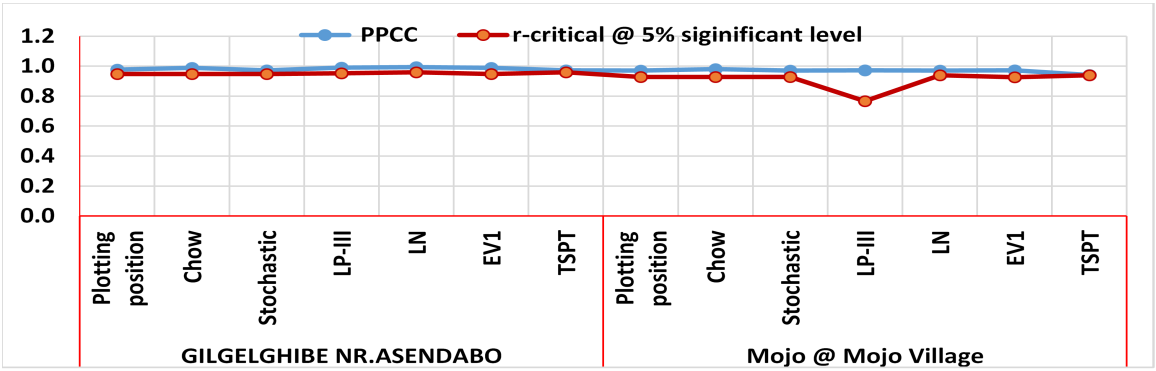

Figure 7.9: Plot of the PPCC and the $r_{5\%}$ critical values for the two catchments.

From Table 7.18, it can be observed that the TSPT method was the best fit for Gilgel Ghibe catchment. Likewise, the LN method was the best fit for Mojo catchment. These results agreed with those of the observed stream flows (see section 7.4.5). The overall ranking of the analysis based upon the GOF tests was also shown in Table 7.18.

Then after, the flood values of different return periods were then computed by all the flood frequency methodologies considered in this study. The results are presented in Table 7.19 and Figures 7.10 and 7.11 and were then compared with those of the observed stream flows as indicated in Figures 7.12 and 7.13.

Table 7.19: Estimated floods peaks of different return period for Gilgel Ghibe and Mojo rivers.

River	Method	Flood (m^3/s) of a given return period (years)						
		2	10	50	100	200	500	1000
GILGEL GHIBE	Plotting position	196	300	404	449	494	7554	599
	Chow	203	296	378	413	447	493	527
	Stochastic	184	325	466	527	587	667	728
	LPIII	204	286	353	380	407	443	470
	LN	205	286	349	375	400	432	457
	EV1	203	254	313	341	369	408	438
	TSPT	202	250	332	355	383	420	448
MOJO	Plotting position	214	440	665	762	858	987	1084
	Chow	230	427	600	673	745	841	914
	Stochastic	206	413	620	710	799	917	1006
	LP-III	222	406	581	659	739	848	935
	LN	221	407	586	667	751	867	958
	EV1	229	339	468	527	589	673	738
	TSPT	369	430	491	517	543	578	604

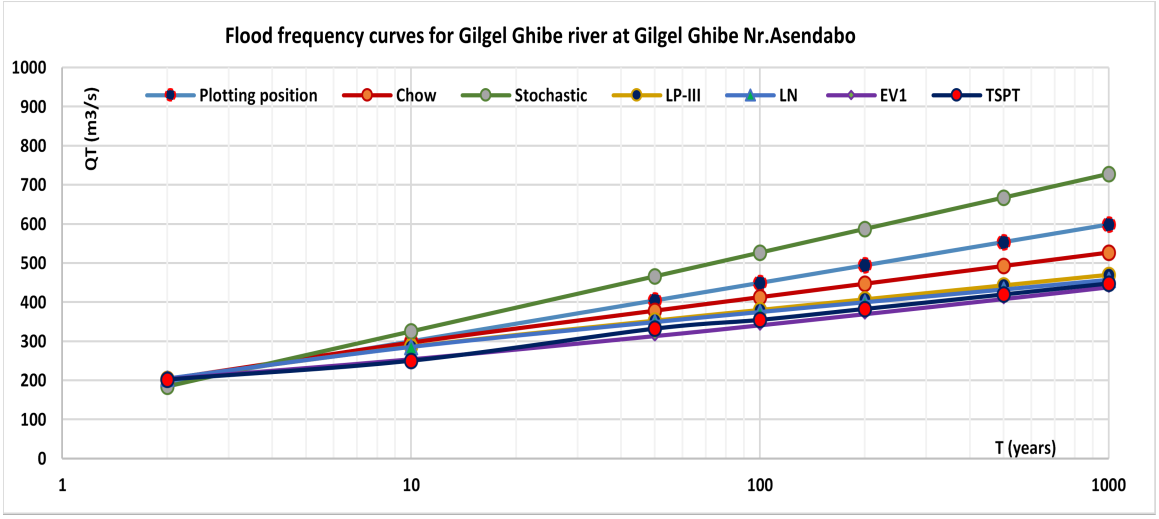

Figure 7.10: Flood frequency curves for Gilgel Ghibe river based on the simulated stream flows.

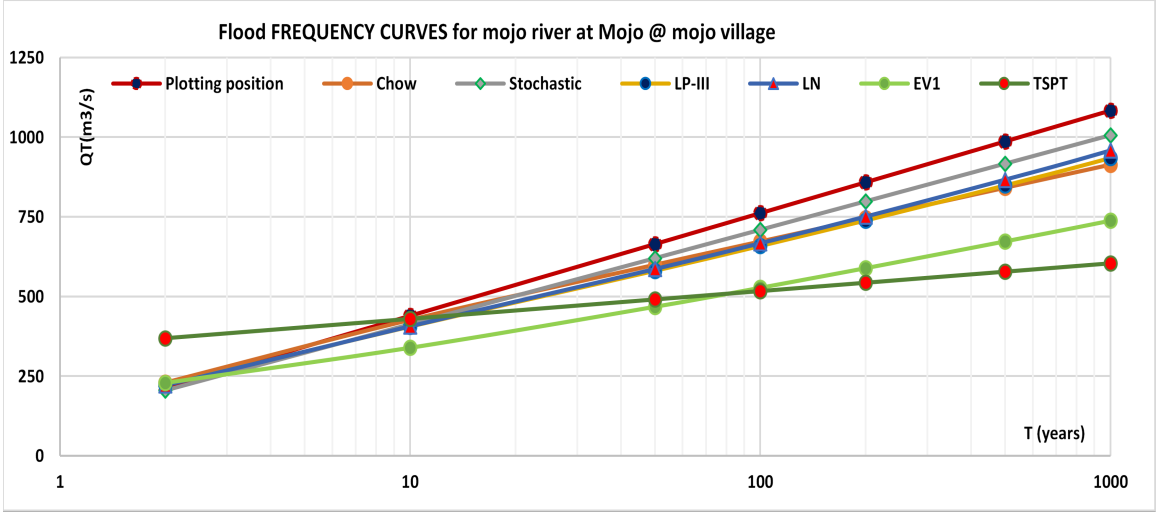

Figure 7.11: Flood frequency curves for Mojo river based on the simulated stream flows.

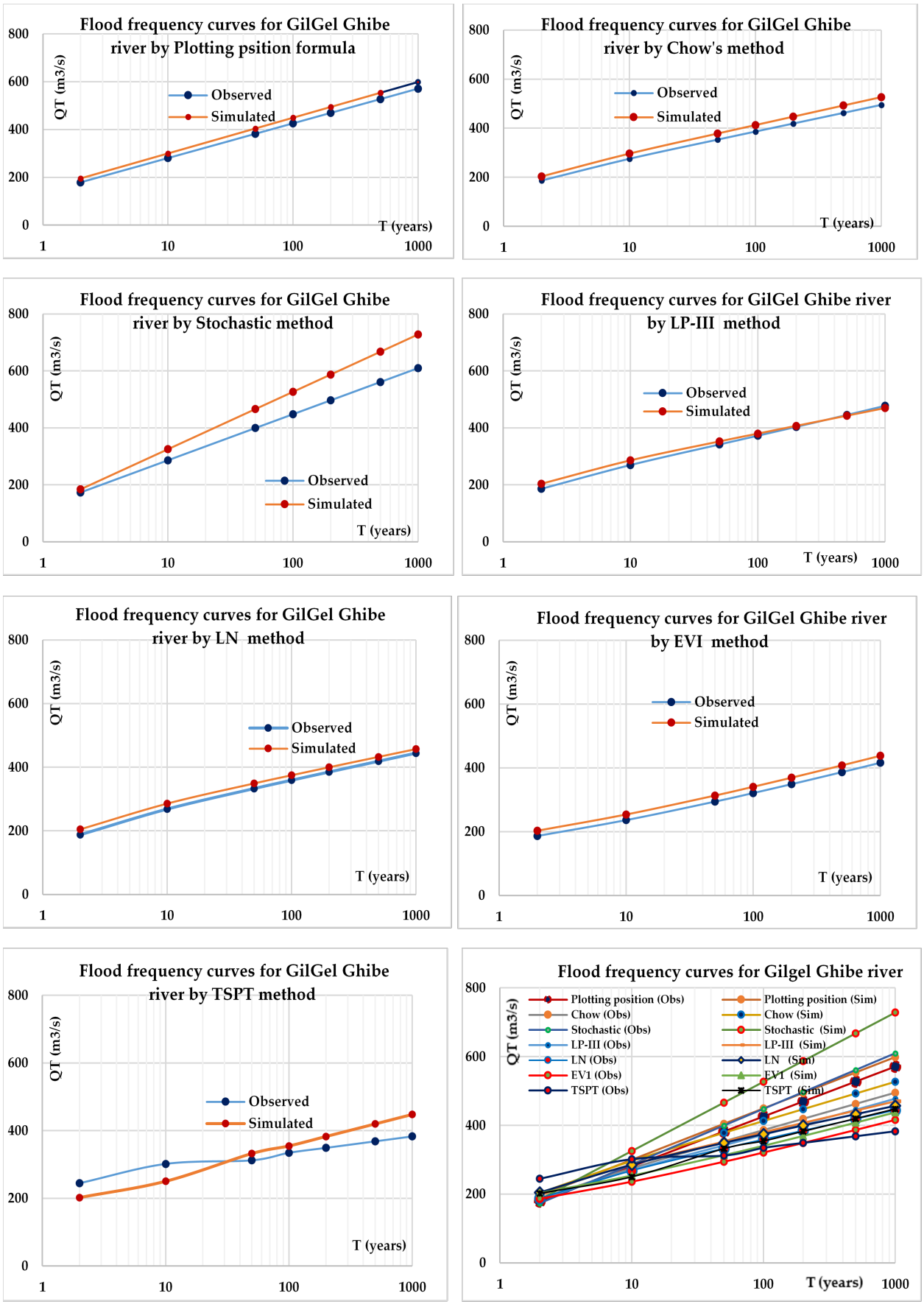

Figure 7.12: Comparison of the flood frequencies based on observed and simulated stream flows for Gilgel Ghibe river.

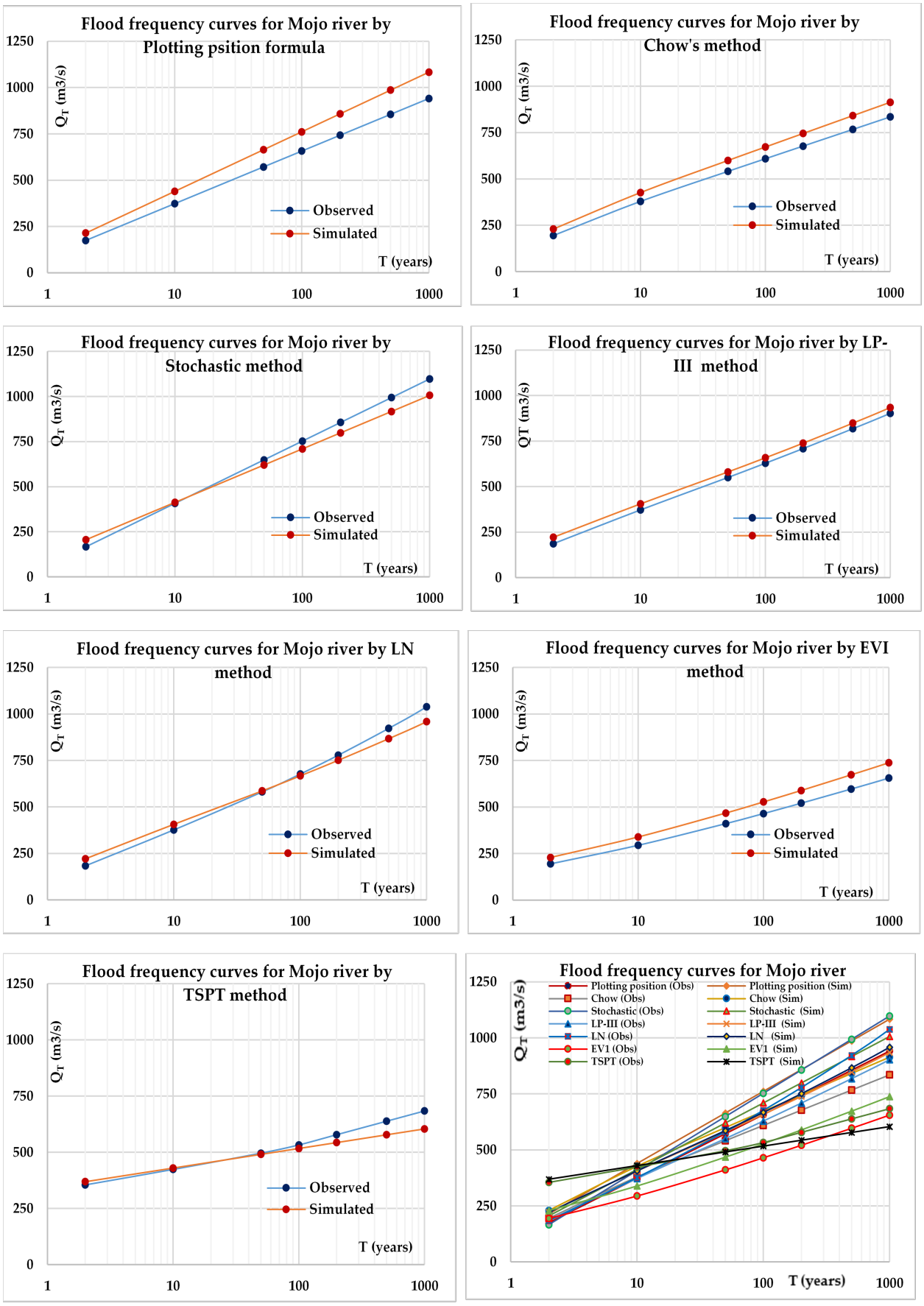

Figure 7.13: Comparison of the flood frequencies based on observed and simulated stream flows for Mojo river.

Comparison of the results of PyTOPKAPI model simulation-based flood frequency analysis with that of the statistical (traditional) frequency assessment of observed stream flow data showed that, for a specified return period, a flood quantile based on the simulated stream flows agreed with that of the corresponding observed discharges for Gilgel Ghibe catchment. This is clearly shown in Figure 7.12. For Mojo river, however, the PyTOPKAPI model simulation-based flood frequency assessment produced slightly lower values flood quantiles of higher return periods by TSPT, LN and the Stochastic methods when compared with the corresponding observed discharges (Figure 7.13). Other than these, all the frequency methodologies showed good agreement of simulation-based flood quantiles compared with the corresponding observed ones. In general, it was found that simulation-based flood frequency analysis showed good agreement with the corresponding observed stream flows for the study catchments.

7.4.7 Summary of the Results

The annual maximum discharge data series of 14 selected stations of two Ethiopian rivers were analyzed by the TSPT (power transformed normal & log transformed normal) method together with Weibull's Plotting Position formula, Chow's, Stochastic, LPIII, & EVI methods to examine the relative efficiency of the methods for flood frequency analysis. The TSPT method uses the Box-Cox transformation approach for converting the data to follow normal distribution. In this TSPT technique, the data were successfully transformed to approximately follow normal distribution. This was confirmed by the GOF tests (Chi-square, K-S, Shapiro-Wilk, Anderson-Darling, and QQ plot) flood applied. Then after, the flood frequency methodologies considered were tested on the recorded annual maximum discharge data series at all stations to detect the best fit method that represents the statistical characteristics of the observed data. In this case, three additional GOF tests (PPCC, RMSD and NS) were employed. The findings of these GOF tests were indicated in Tables 7.13 & 7.14. The overall refined result of the ranking (Table 7.16) based upon the GOF tests showed that TSPT technique, Weibull's Plotting position, and Chow's method gave better fits than LPIII, EVI and Stochatic methods.

The analysis also indicated that (1) EVI method, as recommended by Tadesse et al. [261], is not a satisfactory solution for flood frequency analysis in Ethiopia, (2) Webull's plotting position formula and Chow's method gave fairly good fit to the data but not the best, (3) the Stochastic method was not found to be the best appropriate for flood frequency analysis in Ethiopia. It seems that the stochastic method could not fit the observed skewness of flood-data in Ethiopia. In general, it was observed that the TSPT method was the best fit, followed by Weibull's plotting position formula, Chow's, LPIII, EVI and Stochastic methods, in decreasing order of their effectiveness for the study catchments.

In addition, analysis of the flood frequencies was carried out using the annual maximum discharge data of the PyTOPKAPI model-simulated stream flows from Gilgel Ghibe and Mojo catchments. The results were compared with those of the recorded stream flows. It was then found that the PyTOPKAPI model-simulation based flood frequency analysis gave flood quantiles that were in good agreement with the corresponding observed stream flows for the two study catchmets.

7.5 Conclusion and Recommendations

Many methods are available for estimation of peak floods. The empirical methods, the rational formula, the unit hydrograph method and the statistical method of flood frequency studies are some of them. However, each technique has its own limitations and assumptions being applied to

the real world. For example, the flood frequency analysis, which starts with the treatment of raw flood data and finally determines the frequency or the probability of a certain flood value, requires sufficiently long data. On the other hand, in flood frequency analysis, identification of the true statistical distributions for flood data series continues to be major challenges facing engineers and hydrologists. Because, none of the common probability distributions can best describe the true inherent variability of flood peak occurrences. A probability model fitted through the observed flood data may provide an accurate estimate of flood peak of a given return period. But this is computationally a difficult task.

Due to these reasons, it was realized that there is a possibility of finding a standard probability distribution for fitting the flood data series of a particular location. This can be achieved by transforming the observed flood data through a suitable power transformation function (Two-Step-Power-Transformation/TSPT) such that the transformed flood data series follows normal distribution.

With this concept, the Box-Cox transformations approach was used for converting a recorded flood series to approximately follow normal distribution. Python scripts was developed and utilized to determine the Box-Cox transformations parameters (λ and γ that make both the skewness and kurtosis of the transformed data series zero and three, respectively). In this TSPT technique, the data series were successfully transformed to follow normal distribution. This was confirmed by the GOF (Chi-square, K-S, Shapiro-Wilk, Anderson-Darling, and QQ plot) tests applied. Then after, the TSPT technique and other flood frequency methodologies (LPIII, EVI,Chow's, Stochastic methods and Weibull's plotting position formula) were tested on flood data series of 14 stations of the two Ethiopian rivers to examine the relative efficiency of the methods in predicting a peak flood of a given return period. Statistical GOF tests based on PPCC, RMSD and NS tests were applied for detection of the best fit method to the observed flood data series. The results showed that the estimated values of floods of smaller return periods by all the methods are quite close. However, the results obtained by TSPT method were found slightly different from those obtained by other methods for higher return periods. But, the overall GOF analyses indicated that the TSPT technique was the best fit for flood frequency analysis in the study regions. Weibull's plotting position formula and Chow's method also gave good fit but not the best. EVI and Stochastic methods may not be the satisfactory solution for flood frequency analysis for study areas. Hence, the TSPT method can be one of the appropriate methods of flood frequency analysis for Ethiopian rivers.

Furthermore, analysis of the flood frequencies was carried out using the PyTOPKAPI model simulated flow data of the two case study catchments. The results of the analysis were then compared with those of the corresponding observed stream flows. The overall output of the comparisons revealed that PyTOPKAPI model simulation-based flood frequency analysis produced flood quantiles that were in agreement with the corresponding observed stream flows for the two study catchments. Finally, it was concluded that PyTOPKAPI model simulation-based flood frequency analysis can also be an appropriate method for peak flood estimation and flood freuency analysis for Ethiopian rivers.

Chapter 8

Conclusions and Recommendations

8.1 Introduction

Extreme flood events have become more destructive in some parts of Ethiopia. Hydrologists and engineers should help decision makers to mitigate the effects of these extreme flood events. Thus, accurate estimates of the magnitudes and the frequencies of floods are vital for effective flood risk management. This section therefore summarizes the overall findings of the study and gives some recommendations for future study. In this study, a broad overview of the practical and the current design flood estimation methods in Ethiopia along with the international ones was conducted. The results revealed very large gaps between flood researches and the current design flood practices in Ethiopia. Trend analysis of the hydro-meteorological data of the study catchment was also carried out. The results showed temperature and rainfall increase for the future periods which has an impact on the streamflow from the catchment. The PyTOPKAPI model was utilized to simulate streamflow from gauged and ungauged Ethiopian catchments. This is the first attempt to implement the model in Ethiopia. The results indicated that the general streamflow patterns were well captured. In addition, the various flood frequency methodologies were evaluated on two Ethiopian (Gilgel Ghibe and Awash) rivers. The aim was to determine an appropriate method that best represents the statistical characteristics of recorded flood data. An appropriate method was selected and then tested for its applicability in Ethiopia for flood frequency analysis using the data of the two rivers. Furthermore, analysis of flood frequencies was conducted using the PyTOPKAPI model-simulated flows from the two case study (Gilgel Ghibe and Mojo) Ethiopian catchments. The results of the evaluation were then compared with those of the corresponding observed stream flows. The overall output of the comparisons revealed that PyTOPKAPI simulation based flood frequency analysis produced flood quantiles that are in good agreement with the corresponding observed stream flows for the study catchments. The findings of this study are summaried hereunder.

8.2 Summary of results

8.2.1 Review of design flood estimation methods in Ethiopia

This addresses the current methods of design flood estimation in Ethiopia along with the international ones, provides recommendations and clarifies the future direction about design flood estimation method in Ethiopia. It was then concluded that further research works are required to improve the estimates of design flood in Ethiopia by making use of longer recorded data and improved information currently available.

Thus, based the findings of the review, comprehensive recommendations have been made for further research needs to design flood estimation in Ethiopia as indicated in Conclusions and Recommendations section 2.2.5 of Chapter 2.

8.2.2 Review of the practical Implementation of (Py)TOPKAPI model

This review presents the summarized practical implementation of the (Py)TOPKAPI model in numerous catchments of the world. This highlights the capability of the model for use in stream flow simulation in gauged catchments and enlightens its applicability to model ungauged catchments. Being the first attempt to implement the model in Ethiopia, it also creates better awareness to apply the model on Ethiopian catchments. It has therefore provided a further understanding of the model and its application to a research and operational hydrological processes. This review indicated that the model is a promising tool for scientific and research hydrology. Nonetheless, good skills and experience on calibrating the model allows obtaining better model efficiency in applying in ungauged catchments.

8.2.3 Historical trends of hydro-meteorological data

The importance of trend analysis of hydro-meteorological data for the proper water resources planning and management was envisaged, especially for flood frequency analysis and peak flood estimation. This section then summarizes the trend changes of the hydro-meteorological data in Gilgel Ghibe catchment. Daily rainfall, temperature and steam flow data of the stations in the catchment were considered for detection of the variability and the changes in trend using non-parametric Mann-Kendall test. The outcomes indicated an increasing tendency in rainfall and temperature in the study area. The analysis also showed a decreasing tendency of stream flows (at about 0.007% per year) at the outlet of the catchment. In general, the analysis specified insignificant trend changes of the hydro-metrological data of the study catchment. Similar results could possibly be obtained for the other catchment/basin (Mojo).

8.2.4 PyTOPKAPI model Application in Ethiopia

This discusses summary of the PyTOPKAPI model application in gauged catchments for stream flow modeling in Ethiopia. In this case, the preparation of the model input files, the setting up of the model, model calibration & validation, and its performance evaluation were conducted. Applied on the Gilgel Ghibe catchment ($2901km^2$, in Omo-Ghibe River Basin) and Mojo catchment ($1476km^2$, in Awash River Basin) at a 24-hour time-step with a limited adjustment of the model-parameters and low computation times, it was observed that the model showed good performance in modelling the river discharges of the study catchments. This has provided a significant knowledge and an understanding of the model being applied. Finally, it can be concluded that the model is a promising hydrological tool for modelling the river behaviour of a catchment with the following:

- Because of its simplicity, its parsimonious parameterization and the direct physical linkage between the catchment data and the model parameters, it is an easy to use.
- The option to have predictions in ungauged inner parts of the basin is one of the benefits of the model.
- Its ability to replicate stream flows in ungauged basins, by means of the parameters value obtainable in literature is another benefit of the model.

- Because it is "physically based", the parameters can be assigned according to field data obtained from in-situ measurements or remotely sensed data or from literature.
- The configuration of the model is based on the connection of independent cell entities that allows the easy addition of external flows or some other hydrological processes that might alter the hydrological response of the catchment.

8.2.5 PyTOPKAPI Application in ungauged catchments

Hydrological processes of a given region are often understood through studying river basins for which sophisticated rainfall-runoff models are required to assess climatic and hydro meteorological conditions, as they impact the sustainability of water resources as well as water availability. These rainfall-runoff models are powerful tools used in various water resources applications for simulating stream flows. This section presents the application of the PyTOPKAPI model on ungauged catchment by testing its suitability for simulating flows from Gilgel Ghibe (2943km^2) catchment in Ethiopia. To generate reliable stream flows, models generally need to be calibrated, which typically relies on the availability of reliable stream flow time series. However, it may be difficult to calibrate the model in such ungauged catchments by conventional calibration procedure. Efforts are made to investigate the use of runoff ratio formula proposed by Schreiber as an alternative to conventional model calibration procedure. This approach seems to be a new method proposed in this work as an alternative model calibration procedure for streamflow simulation from ungauged catchments. Runoff ratio is the (time averaged) ratio of volume of runoff to volume of rainfall in a catchment. It illustrates the average excess rainfall for a catchment. Consequently, the runoff ratios were computed from the simulated stream flows and the rainfall data of the study catchments. The model was then calibrated by comparing the simulated runoff ratio with that predicted by the Schreiber formula. The calibrated PyTOPKAPI model generated a realistic daily streamflow time series over the catchments. The results suggest that the PyTOPKAPI model, with this simplified calibration approach, can produce acceptable streamflow simulations from ungauged catchments. In summary, it was concluded that PyTOPKAPI can be used for simulating stream flows from ungauged catchments for water resources applications and flood prediction in developing countries.

8.2.6 Application of PyTOPKAPI model with remotely sensed rainfall data

In many developing countries like Ethiopia, ground-based hydrological monitoring networks are either sparse or nonexistent. These situations restrict these regions to manage their water resources and hamper early flood-warning systems resulting in massive socioeconomic damages. In such cases, satellite remote sensing could be a suitable way or even the only way to acquire such information for data-scarce areas. This section then summarizes the usage of remotely sensed rainfall data for streamflow modelling with case study in Gilgel Ghibe basin in Ethiopia. Ten years (2001-2010) data of two satellite-based precipitation products (SBPP), TRMM & WaterBase, were used. These products were then introduced to PyTOPKAPI model to generate stream flows at daily time-scale. The results were compared with streamflow observations at Gilgel Ghibe Nr, Assendabo gauging station of the catchment. Four statistical tools (Bias, R^2, NS and RMSE) were used for comparisons of the results. The study reveals that the SBPPs result in reasonable capture of streamflow discharge including extreme cases and their timings. However, these products have shown overestimation of stream flows extending to the recession limb over wet months (June-September) that led to overestimation of the flood magnitudes and underestimation of streamflow prediction over few dry months (January and February). With this, the paper (1) presents the efficacy of the PyTOPKAPI model for use in stream flow modeling and consequently peak flood estimation for Ethiopian catchments, (2) provides a further understanding of the model and its

application for reproducing the river behavior of a catchment in Ethiopia, and (3) explores the usage and applications of satellite-based precipitation products in streamflow modeling in Ethiopia. In general, it was concluded that remote sensing contributes valuable information to streamflow estimation.

8.2.7 Evaluation of Flood Frequency Methodologies for Ethiopian Rivers

Accurate estimates of the magnitudes and the frequencies of floods are vital for water resources applications. This section presents the evaluation of the various methods of flood frequency analysis for modeling at-site annual maximum discharge data series in Ethiopia. The aim is to determine the method that best signifies the statistical character of recorded flood data. In this study, the annual maximum discharge data series from 14 stations of two Ethiopian rivers (6 in Gilgel Ghibe and 8 in Awash) with 23 to 54 years of records were used. Seven methods of flood frequency analysis (TSPT [Power & Log], LPIII, EVI, Chow's Stochastic methods and Weibull's plotting position formula) were considered. In this case, the suitability of Two-Step-Power-Transformation (TSPT) technique for flood frequency analysis was firstly studied. The Box-Cox transformation approach was used for converting the observed data series to follow a normal distribution. Python script was developed and utilized to determine the Box-Cox transformation parameters. In this TSPT technique, the data were successfully transformed to follow a normal distribution. This was confirmed by the Goodness-Of-Fit tests (Chi-square, Kolmogorov– Smirnov, Shapiro-Wilk and Anderson-Darling tests as well as QQ-plot) applied. Then after, all the seven methods of flood frequency analysis considered were fitted to the observed annual maximum discharge data to detect the best fit method. Comparison of the results were made based upon the probability plot correlation coefficient (PPCC), the root mean square deviation (RMSD) and Nash-Sutcliffe coefficient (NS) in fit. The comparison results indicated that the TSPT method was the best that signified the statistical characteristics of recorded data of the study areas. It was also found that the Weibull's plotting position formula was the next best fit, followed by Chow's, LPIII, EVI and Stochastic methods, in decreasing order of their efficiencies.

Moreover, analysis of the flood frequencies was carried out using the PyTOPKAPI model-simulated streamflow data of the two (Gilgel Ghibe and Mojo) case study Ethiopian catchments and the results were then compared with those of the corresponding recorded stream flows. It was observed that PyTOPKAPI model simulation-based flood frequency analysis produced flood quantiles that were in good agreement with the corresponding observed stream flows for the study catchments.

Finally, it was concluded that PyTOPKAPI model can also be one of the appropriate methods to use for flood frequency analysis and peak flood estimation in Ethiopia.

8.3 Contributions

The following are the key contributions of this study.

1. The review of the practical design flood estimation methods in Ethiopia provides the broad overview of the current design flood estimation methodologies in Ethiopia along with the international design flood estimation techniques. It also provides recommendations and clarifies future directions for design flood estimation methods in Ethiopia.

2. The critical review of the (Py)TOPKAPI hydrological modelling presents a summarized practical implementation of the model in numerous catchments of the world. It highlights the suitability of the model for use in stream flow simulation in gauged catchments and enlightens its applicability to ungauged catchments. Being the first attempt to implement the model in Ethiopia, it also creates better awareness to apply the model on Ethiopian catchments.

3. The use of PyTOPKAPI model in this study would provide a further understanding and a better visualization of the catchment hydrologic processes. The model was applied on the Gilgel Ghibe catchment (Omo-Gibe basin) and Mojo catchment (Awash basin) for streamflow modeling and peak flood estimation. The outputs of the model could ultimately help decision makers and planners make better decisions regarding water resources planning and management.

4. Hydro-meteorological data trend analysis has been conducted. The results of the analysis can be used as an indicative to prescribe the trend changes for studies to be conducted in the basin in the future. This is so important that if there might be some change in trend in the future that will ultimately have an impact on stream flows in the catchmets, which in turn could be the main input for flood frequency analysis.

5. The two parameters of flood frequency assessment are the flood peak and its return period. The evaluation of the several flood frequency methodologies was done to select the best fit method for Ethiopian rivers. In this case, the method of flood frequency assessment in Ethiopia would be more generally standardized. With this, a particular return period design flood would be estimated more accurately. The result of this particular study can be a guideline for design flood estimation and flood risk management in Ethiopia.

8.4 Recommendations for Further Work

1. Future studies should examine the impact of land cover alterations on stream flows as well as sediment quantity. The land cover change may contribute to streamflow variations. To obtain better results, the performance of other hydrologic models should also be explored.

2. The PyTOPKAPI model should also be applied on other Ethiopian catchments to further test the suitability of the model to reproduce the catchment response in Ethiopia.

3. The satellite precipitation products (SBPPs) are not universally combined with operative hydrological modelling in Ethiopia essentially owing to not having appropriate evidence on the reliability of the products at basin scale. Evaluating the reliability of different SBPPs should be conducted constantly to evaluate applicability of the products for stream flow modelling in data sparse areas.

4. The possibility of using the PyTOPKAPI model together with the Schreiber run-off ratio formula for application to ungauged catchments was examined. The results suggest the approach can produce satisfactory streamflow predictions from ungauged catchments for water resources applications and flood predictions in developing countries. Further refinement of the approach is recommended by implementing and testing it on additional catchments.

5. The approach of PyTOPKAPI model-simulation based flood frequency analysis may produce better results than the alternative traditional approaches. Further refinement of this approach should be another objective of the future.

6. It was found that the TSPT technique has the capability of normalizing efficiently a skewed flood distribution and can be used for flood frequency analysis. Further evaluation of the suitability of the technique for flood frequency analysis using the hydrologic data of other catchments should be the major work of the future.

7. Obtaining adequate and good quality data is still a major problem in Ethiopia. Hence, the concerned organizations responsible for data collection and handling shall give proper attention to the data management

References

[1] Abdurahman, M. A., Coldewey, W. G., Mohn, R., Werner, J., Awulachew, S. B., Kruse, B. & Klemme, O. (2008). Use of adaptable empirical equations for Potential Evapotranspiration estimation and Soil Moisture Balance approaches for estimating actual Evapotranspiration. International Water Management Institute IWMI, P.O.Box 5689, Addis Ababa, ETHIOPIA.

[2] Abramowitz, M. & Stegun, I.A. (1965). Handbook of Mathematical Functions. Dover, New York.

[3] Adeboye, O. B. & Alatise, M. O. (2007). Performance of Probability Distributions and Plotting Positions in Estimating the Flood of River Osun at Apoje Sub-basin, Nigeria. Agricultural Engineering International: the CIGR Ejournal,Vol. IX.

[4] Africa Climate Change Resilience Alliance (ACCRA) report (2011). Climate trends in Ethiopia: Summary of ACCRA research in three sites; available at http://community.eldis.org/accra/.

[5] Ahmad, W., Fatima, A., Awan, U. K. & Anwar, A. (2014). Analysis of long term meteorological trends in the middle and lower Indus Basin of Pakistan—A nonparametric statistical approach. Global and Planetary Change 122, 282-291.

[6] Ahn, J., Cho, W., Kim, T., Shin, H. & Heo, J.-H. (2014). Flood Frequency Analysis for the Annual Peak Flows Simulated by an Event-Based Rainfall-Runoff Model in an Urban Drainage Basin. Water 2014 6, 3841-3863.

[7] Alain Pietroniro, A. & Prowse, T. D. (2002). Applications of remote sensing in hydrology. Hydrol. Process 16, 1537-1541.

[8] Alexander, W. (2001). Flood risk reduction measures: Incorporating flood hydrology for Southern Africa, Pretoria: University of Pretoria, Department of Civil and Biosystems Engineering.

[9] Alexander, W. (2002). Statistical analysis of Extreme Floods. Journal of the South African Institution of Civil Engineering, 44(1), 20-25.

[10] Almazroui, M. (2011). Calibration of TRMM rainfall climatology over Saudi Arabia during 1998–2009. Atmospheric Research 99, 400-414.

[11] Amengual, A., Diomede, T., Marsigli, C., Martın, A., Morgillo, A., Romero, R., Papetti, P. & Alonso, S. (2008). A hydrometeorological model intercomparison as a tool to quantify the forecast uncertainty in a medium size basin. Natural Hazards Earth System Sciences 8, 819-838.

[12] Amirataee, B. & Montaseri, M. (2013). Evaluation Of L-Moment and PPCC Method to determine the best regional distribution of monthly rainfall data: case study northwest of Iran. Journal of Urban and Environmental Engineering 7(2), 247-252.

[13] Ampadu, B., Chappell, N. A. & Kasei, R. A. (2007). Rainfall-river flow modelling approaches: Making a choice of data-based mechanistic modelling approach for data limited catchments: A review, Lancaster Environment Centre, Lancaster University, LA1 4YQ, United Kingdom.

[14] Ampitiyawatta, A. D. & Guo, S. (2009). Precipitation Trends in the Kalu Ganga Basin in Sri Lanka. The Journal of Agricultural Science 4 (1), 10-18.

[15] Anghileri, D. , Pianosi, F., & Soncini-Sessa, R. (2014). Trend detection in seasonal data: from hydrology to water resources. Journal of Hydrology 511, 171-179.

[16] Ardaya, A. B. (2012). Flood forecasting modeling for the Búzi river basin in Mozambique. Thesis of Master of Science, Cologne University of Applied Sciences.

[17] Arora, K. & Sigh, V. P. (1989). A comparative evaluation of the estimators of the log Pearson type(LP) 3 distribution. J. Hydrol. 105, 19-37.

[18] Arora, V. K. (2002). The use of the aridity index to assess climate change effect on annual runoff. J. Hydrol. 265, 164-177.

[19] Asante, K. O., Artan, G. A., Pervez, S., Bandaragoda C. & Verdin, J. P. (2008). Technical Manual for the Geospatial Stream Flow Model (GeoSFM). U.S. Geological Survey Open-File Report 2007-1441, 65 p.

[20] Awulachew, S. B., yilma, A. D., Loulseged, M., Loiskandl, W., Ayana, M. & Alamirew, T. (2007). Water Resources and Irrigation Development in Ethiopia, Working Paper 123. (Ed International Water Management Institute). Addis Ababa, Ethiopia.

[21] Ayalew, L, (2009). Analyzing the effects of historical and recent floods on channel pattern and the environment in the Lower Omo basin of Ethiopia using satellite images and GIS. Environmental Geology 58(8), 1713-1726.

[22] Azeze, M. (2004). Development of Synthetic Unit Hydrographs for Watersheds in the Upper Awash and Upper Tekeze Basins. M.Sc. Thesis (Civil Engineering), Addis Ababa University.

[23] Badgley, G., Fisher, J. B., Jiménez, C., Tu, K. P. & Vinukollu, R. (2015). On Uncertainty in Global Terrestrial Evapotranspiration Estimates from Choice of Input Forcing Datasets. Journal of Hydrometeorology 16(4), 1449-1455.

[24] Bari, S. H., Rahman, M. T. U., Hoque, M. A. & Hussain, M. M. (2016). Analysis of seasonal and annual rainfall trends in the northern region of Bangladesh. Atmospheric Research 176-177, 148 - 158.

[25] Bashar, K. E. & Zaki, A. F. (2005). SMA Based Continuous Hydrologic Simulation of the Blue Nile. UNESCO Chair in Water Resources, Khartoum, Sudan; UNESCO Cairo Office, Cairo, Egypt.

[26] Bates, B.C., Z.W. Kundzewicz, S. Wu and J.P. Palutikof, Eds., 2008: Climate Change and Water. Technical Paper of the Intergovernmental Panel on Climate Change, IPCC Secretariat, Geneva, 210 pp.

[27] Behrangi, A., Khakbaz, B., Jaw, T. C., AghaKouchak, A., Hsu, K. & Sorooshian, S. (2011). Hydrologic evaluation of satellite precipitation products over a mid-size basin. Journal of Hydrology 397, 225-237.

[28] Ben Aissia, M. A., Chebana, F., Ouarda, T. B. M. J., Roy, L., Bruneau, P. & Barbet, M. (2014). Dependence evolution of hydrological characteristics, applied to floods in a climate change context in Quebec. Journal of Hydrology 519, 148-163.

[29] Berhanu, B. & Ayalew, S. (2013). Background report: Hydro-meteorological trends, FAO and Ministries of Water and Energy, and Agriculture of FDRE. 54, Addis Ababa, Ethiopia.

[30] Berhanu, B., Melesse, A. M. & Seleshi, Y. (2013). GIS-based hydrological zones and soil geo-database of Ethiopia. Catena 104, 21-31.

[31] Berhanu, B., Seleshi, Y., Demisse, S. S. & Melesse, A. M. (2015). Flow Regime Classification and Hydrological Characterization: A Case Study of Ethiopian Rivers. Water 2015 7, 3149-3165.

[32] Beven, K. J. (2000). Uniqueness of place and process representations in hydrological modelling. Hydrol. Earth Syst. Sci. 4, 203-213.

[33] Beven, K. J. (2001). How far can we go in distributed hydrological modelling?. Hydrology and Earth System Sciences 5(1), 1-12.

[34] Beven, K. J. (2007). Towards integrated environmental models of everywhere:uncertainty,data and modelling as well as a learning process. Hydrology and Earth System Sciences 11(1), 460-467.

[35] Biondi, D., Freni, G., Iacobellis, V., Mascaro, G. & Montanari, A. (2012). Validation of hydrological models: Conceptual basis, methodological approaches and a proposal for a code of practice. Physics and Chemistry of the Earth, Parts A/B/C 42-44, 70-76.

[36] Birsan, M.V. (2013). Application of a distributed physically-based hydrological model on the upper river basin of Someşul Mare (Northern Romania),Meteo Romania (National Meteorological Administration). Romanian Reports in Physics 65 (4),1469-1478.

[37] Blaney, H. F. & Criddle , W. D. (1962). Determining consumptive use and irrigation water requirements. USDA Technical Bulletin 1275, US Department of Agriculture, Beltsville. https://en.wikipedia.org/wiki/Blaney%E2%80%93Criddle_equation

[38] Bledring, S. (2002). Multi-criteria validation of a precipitation-runoff model. Journal of Hydrology 257, 189-211.

[39] Blöschl, G. (2013). Runoff prediction in ungauged basins: synthesis across processes, places and scales. Cambridge University Press.

[40] Bobée & Ashkar (1991). The gamma family and derived distributions applied in hydrology. Water Resources Publications- Science ; available at http://books.google.co.za/books?id=gdpPAQAAIAAJ

[41] Botai, C. M., Botai, J. O., Muchuru, S. & Ngwana, I. (2015). Hydrometeorological Research in South Africa: A Review. Water 2015 7, 1580-1594.

[42] Boughton, W. & Droop, O. (2003). Continuous simulation for design flood estimation—a review. Environmental Modelling & Software 18(4), 309-318.

[43] Bourdin, D. R., Sean W. Fleming & Roland B. Stull (2012). Streamflow Modelling: A Primer on Applications, Approaches and Challenges. Atmosphere-Ocean 50(4), 507-536.

[44] Box, G. E. P. & Cox, D. R. (1964). An analysis of transformations. J. Royal Statistical Soc., Ser. B 26, 211-252.

[45] Bulu, A. & Onoz, B. (1997). Frequency analysis of low flows by the PPCC test in Turkey; FRIEND '97 — Regional Hydrology: Concepts and Models for Sustainable Water Resource Management. (Proceedings of the Postojna, Slovenia, Conference, September-October Î997) IAHS Pubj. no. 246.

[46] Burn, D. H. & Elnur, M. A. H. (2002). Detection of hydrologic trends and variability. Journal of Hydrology 255(1), 107-122.

[47] Campbell, G. S. (1985). Soil physics with basic: Transport models for soil plant systems, Elsevier Science, New York.

[48] Capriolo, A. D. & Scarpati, O. E. (2012). Extreme Hydrologic Events in North Area of Buenos Aires Province (Argentina). International Scholarly Research Network ISRN Meteorology 2012(Article ID 415081).

[49] Castellarin, A. (2012). Review of applied Statistical methods for flood frequency analysis in Europe. Centre for Ecology & Hydrology , FloodFrqCOSt Action Es0901, Italy.

[50] Chai, T. & Draxler, R. R. (2014). Root mean square error (RMSE) or mean absolute error (MAE)? – Arguments against avoiding RMSE in the literature. Geoscientific Model Development 7 (3), 1247-1250.

[51] Chakraborty, S., Pandey, R. P., Chaube, U. C. & Mishra, S. K. (2013). Trend and variability analysis of rainfall series at Seonath River Basin, Chhattisgarh (India). Int. Journal of Applied Sciences and Engineering Research 2(4), 425-434.

[52] Chatterjee, S., Khan, A., Akbari, H. & Wang, Y. (2016). Monotonic trends in spatio-temporal distribution and concentration of monsoon precipitation (1901–2002), West Bengal. India Atmospheric Research 182, 54-75.

[53] Chen, J., Wu, X., Finlayson, B. L., Webber, M., Wei, T., Li, M. & Chen, Z. (2014). Variability and trend in the hydrology of the Yangtze River, China: Annual precipitation and runoff. Journal of Hydrology 513, 403-412.

[54] Chetty, K. & Smithers, J. (2005). Continuous simulation modelling for design flood estimation in South Africa: Preliminary investigations in the Thukela catchment. Physics and Chemistry of the Earth, Parts A/B/C 30(11-16), 634-638.

[55] Chiew, F. & Siriwardena, L. (2005). User Guide for first full release of TREND version 1.0.2; for Catchment Hydrology;available at www.toolkit.net.au/trend.

[56] Xu, C. (1999). Operational testing of a water balance model for predicting climate change impacts. Agricultural and Forest Meteorology 98-99 (1999), 295-304.

[57] Chong-yu Xu (2002). Textbook of Hydrologic Models (Lärobok i Avrinningsmodeller) (edition 2002). Uppsala University Department of Earth Sciences Hydrology.

[58] Chow, V. T., R.Maidment, D. & W.Mays, L. (1988). Applied Hydrology, McGraw-Hill, USA.

[59] Ciarapica and Todini (2002). TOPKAPI: A model for the representation of the rainfall-runoff process at different scales. Hydrological Processes 16, 207-229.

[60] Coccia, G., Mazzetti, C., Ortiz, E. A. & Todini, E. (2009). Application of the TOPKAPI model within the DMIP 2 Project(pdf), University of Bologna, ProGea Srl, Bologna, Italy.

[61] Cort J. Willmott, Steven G. Ackleson, Roberte E. Davis, Johannes J. Feddema, Katherine M. Klink, David R. Legates, James O'Donnel, & Clinton M.Rowe (1985). Statistics for the Evaluation and Comparison of Models. Journal of Geophysical Research 90 (5), 8995-9005

[62] Crow, E. L. and Shimizu, K. (Ed.) (1988). Lognormal Distributions: Theory and Applications. Dekker, New York.

[63] Cunnane, C. (1978). Unbiased plotting positions—A review. Journal of Hydrology 37, 205-222.

[64] Dalrymple, T. (1960). Flood-Frequency Analyses. Geological Survey Water-Supply Paper, 1543-A.

[65] Demissie, M. (2008). Regional Flood Frequency Analysis Upstream of Awash subbasin (Upstream of Koka). M.Sc. Thesis (Engineering), Addis Ababa University.

[66] Demissie, T. A. (2013). Climate change impact on stream flow and simulated sediment yield to Gilgel Gibe 1 hydropower reservoir and the effectiveness of Best Management Practices. Thesis of Doctor of Engineering (Dr.Ing.), Rostock University.

[67] Demissie, T. A., Saathoff, F., Seleshi, Y. & Gebissa, A. (2013a). Trends of Hydro-Meteorological Data and Impact of Climate Change on the Stream flow of Gilgel Gibe 1 River Basin-Ethiopia. International Journal of Current Research, 5(10), 2988-2993.

[68] Demissie, T. A., Saathoff, F., Seleshi, Y. & Gebissa, A. (2013b). Evaluating the Effectiveness of Best Management Practices in Gilgel Gibe Basin Watershed—Ethiopia. Journal of Civil Engineering and Architecture, 7(10),1240-1252.

[69] Di Baldassarre, G., Laio, F. & Montanari, A. (2009). Design flood estimation using model selection criteria. Physics and Chemistry of the Earth, Parts A/B/C, 34(10-12), 606-611.

[70] Dindang, A., Taat, A , Beng, P. E, Mohd Alwi, A., Mandai, A. A., Mat Adam, S. F., Othman, F. S., Awang Bima, D. N. & Lah, D. (2013). Statistical and Trend Analysis of Rainfall Data in Kuching, Sarawak from 1968-2010, Research pubilication No.6/2013.

[71] Dinku, T., P., Ceccato , Grover-Kopec, E., Lemma, M., Connor, S. J. & Ropelewski, C. F.(2007). Validation of satellite rainfall products over East Africa's complex topography. International Journal of Remote Sensing 28(7), 1503-1526.

[72] Dixon, H., Lawler, D. M., Shamseldin, A. Y. & Webster, P. (2006). The effect of record length on the analysis of river flow trends in Wales and central England, Climate Variability and change—Hydrological Impacts (Proceedings of the Fifth FRIEND World Conference held at Havana, Cuba, November 2006), 490-495.

[73] Dooge, J. C. I. (1992). Sensitivity of runoff to climate change: a Hortonian approach. Bull. Am. Meteorol. Soc. 73(12), 2013-2024.

[74] Du , S., Gu , H., Wen, J., Chen, K. & Rompaey, A. V. (2015). Detecting Flood Variations in Shanghai over 1949–2009 with Mann-Kendall Tests and a Newspaper-Based Database. Water 2015, 7, 1808-1824

[75] Duan, R., Fedler, C. B. & Borrelli, J. (2012). Comparison of Methods to Estimate Saturated Hydraulic Conductivity in Texas Soils with Grass. Journal of Irrigation and Drainage Engineering 138 (4), 322-327.

[76] Duan, Z. & Bastiaanssen, W. G. M. (2013). First results from Version 7 TRMM 3B43 precipitation product in combination with a new downscaling–calibration procedure. Remote Sensing of Environment 131, 1-13.

[77] Duncan, J. M. A., Biggs, E. M., Dash, J., & Atkinson, P. M. (2013). Spatio-temporal trends in precipitation and their implications for water resources management in climate-sensitive Nepal. Applied Geography 43, 138-146.

[78] England Jr., J.F., Cohn, T.A., Faber, B.A., Stedinger, J.R., Thomas Jr., W.O., Veilleux, A.G., Kiang, J.E., and Mason, R.R. (2015). Guidelines for Determining Flood Flow Frequency – Bulletin 17C: U.S. Geological Survey Techniques and Methods 4–BXX, XXX p., at http://dx.doi.org/10.3133/tm4–BXX/.

[79] ERA Manual (2013). Drainage Design Manual: Ethiopian Road Authority (ERA), Addis Ababa, Ethiopia.

[80] Ethiopian CSA (2013). Population Sensus report, Centeral Statistical Agency (CSA), Addis Ababa, Ethiopia.

[81] Facchinetti, S. (2009). A procedure to find exact critical values of Kolmogorov-Smirnov test Statistica Applicata -Italian. Journal of Applied Statistics 21 (3-4), 337.

[82] FAO Irrigation and Drainage Paper (1977). FAO Irrigation and Drainage Paper 24-Guidelines for Predicting Crop Water Requirements. 154: Food and Agriculture Organization of the United Nations, Rome 1977.

[83] FAO Irrigation and Drainage Paper No. 56 (2006). FAO Irrigation and Drainage Paper - Crop Evapotranspiration (guidelines for computing crop water requirements). FAO, Water Resources, Development and Management Service Rome, Italy.

[84] FAO/IIASA/ISRIC/ISS-CAS/JRC (2009). Harmonized World So il Database (version 1.1). FAO, Rome, Italy and IIASA, Laxenburg, Austria.

[85] Fatoyinbo, B. S. (2017). Rainfall-Runoff Modelling in Ungauged Catchments Using PyTOPKAPI: A Case Study of Mhlanga Catchment. M.Sc. Thesis, University of KwaZulu-Natal.

[86] Fentahun, T. & Gashaw, T. (2014). Analysis of rainfall and temperature data to determine climate change in Dilla Zuria District, Southern Ethiopia. Civil and Environmental Research 6(7), 39-43.

[87] Filliben, J. J. (1975). The Probability Plot Correlation Coefficient Test for Normality. Technometrics 17(1), 111-117.

[88] Fleig, A. K. & Wilison, D. (2013). The Natural Hazards Project - 5, Flood and Surface Water Flooding, Flood estimation in small catchments. Norwegian Water Resources and Energy Directorate. Norway, Report no. 60 – 2013.

[89] Fotakis, D., Sidiropoulos, E. & Loukas, A. (2014). Integration of a Hydrological Model within a Geographical Information System: Application to a Forest Watershed. Water 6(3), 500-516.

[90] Fraedrich, K. & Sielmann, F. (2011). An Equation of State for Land Surface Climates. International Journal of Bifurcation and Chaos 21(12) 3577 -3587.

[91] Fraedrich, K. (2010). A Parsimonious Stochastic Water Reservoir: Schreiber's 1904 Equation American Meteorological Society 11 575-578.

[92] Fraedrich, K., Sielmann, F., Cai, D., Zhang, L. & Zhu, X. (2015). Validation of an Ideal Rainfall-Runoff Chain in a GCM Environment. Water Resour Manage 29, 313-324.

[93] Gadoa, T. A., & Nguyen, V. -T. -V. (2016). An at-site flood estimation method in the context of nonstationarity II. Statistical analysis of floods in Quebec. Journal of Hydrology 335, 722-736.

[94] Gao, G, Chen, D., Xu, C. & Simelton, E. (2007). Trend of estimated actual evapotranspiration over China during 1960–2002. Journal of Geophysical Research 112 (D11120) 1-8

[95] Garg, S.K.(1998). Hydrology and water resources Engineering. Kanna Publishers, Nath Market Nai Sarak Delhi-110006, Delhi.

[96] Gashaw, W. and Legesse, D. (2008). Flood Hazard and Risk Assessment Using GIS and Remote Sensing in Fogera Woreda, Northwest Ethiopia. A Report. Addis Ababa, Ethiopia.

[97] Gebeyehu, A. (1989). Regional Flood Frequency Analysis. Hydraulics Laboratory, Royal Institute of Technology, Stockholm, Sweden.

[98] Gedefa, T. (2009). Regional Flood Frequency analysis for upper Omo-Gibe subbasin. M.Sc. Thesis, Addis Ababa University.

[99] Gericke, O. J. & Du Plessis, J. A. (2011). Evaluation of critical storm duration rainfall estimates used in flood hydrology in South Africa. Water SA 37(4), 453-470.

[100] Gericke, O. J. & Smithers, J. C. (2014). Review of methods used to estimate catchment response time for the purpose of peak discharge estimation. Hydrological Sciences Journal 59(11), 1935-1971.

[101] GLCC (2008). Global Land Cover Characterization, "United States Geological Survey (USGS)", Global Land Cover Characteristics Data Base version 1.2 , http://edcdaac.usgs.gov/glcc/globdoc1_2.php .

[102] Gleyzer, A., Denisyuk, M., Rimmer, A & Salingar, Y. (2004). A fast recursive Gis algorithm for computing Strahler stream order in braided and non-braided networks. Journal of the American Water Resources Association 40(4), 937-946.

[103] González-Zeas, D., Garrote, L., Iglesias, A. & Sordo-Ward, A. (2012). Improving runoff estimates from regional climate models: a performance analysis in Spain. Hydrology and Earth System Sciences 16(6), 1709-1723.

[104] Görgens, A. (2007). Joint Peak-Volume (JPV) Design Flood Hydrographs for South Africa. (241 pp): WRC Report No. 1420/3/07. Water Research Commission, Pretoria, RSA.

[105] Gourley, J. J., & Vieux, B. E. (2005). A Method for Evaluating the Accuracy of Quantitative Precipitation Estimates from a Hydrologic Modeling Perspective. American Meteorological Society 6, 115-133.

[106] Goyal, M. K. (2014). Statistical Analysis of Long Term Trends of Rainfall During 1901–2002 at Assam, India. Water Resour Manage 28 1501-1515.

[107] Grant, E. L.& Leavenworth, R. S. (1972). Statistical Quality and Control, Table A, p.643, McGraw-Hill, New York.

[108] Green, W.H. and G. Ampt. (1911). Studies of soil physics, part I – the flow of air and water through soils. J. Ag. Sci. 4, 1-24.

[109] Griffis, V. W., Stedinger, J. R. & Cohn, T. A. (2004). Log Pearson type 3 quantile estimators with regional skew information and low outlier adjustments. Water Resources Research 40(7), 1-17.

[110] GTP annual Report of FDRE (2014). Federal Democratic Republic of Ethiopia, Growth and Transformation Plan, Annual Progress Report for F.Y. 2012/13, Addis Ababa, Ethiopia.

[111] Guo, S. L. (1990). A Discussion On Unbiased Plotting Positions For The General Extreme Value Distribution. Journal of Hydrology 121 33-44.

[112] Gupta, D. K., Asthana, B. N. & Bhargawa, A. N. (1986). Estimation of Design Flood In International symposium on flood frequency and risk analysis, 101-112 (Ed V. P.SINGH). Louisiana State University, Baton Rouge, USA.

[113] Gupta, H. V., Kling, H., Yilmaz, K. K. & Martinez, G. F. (2009). Decomposition of the mean squared error and NSE performance criteria: Implications for improving hydrological modelling. Journal of Hydrology 377(1-2), 80-91.

[114] Haktanir, T. & Horlacher, H. B. (1993). Evaluation of various distributions for flood frequency analysis. Hydrological Sciences -Journal- des Sciences Hydrologiques 1, 15-32.

[115] Hamed, K. H. (2008). Trend detection in hydrologic data: The Mann–Kendall trend test under the scaling hypothesis. Journal of Hydrology 349(34), 350- 363.

[116] Harmonized World Soil Database(HWSD), available at:http://webarchive.iiasa.ac.at/Research/LUC/External-World-soil-database/HTML/HWSD_Data.html?sb=4

[117] Heathman, G. C. & Larose, M. (2009). Influence of Scale on SWAT Model Calibration for Streamflow. United States Department of Agriculture, National Soil Erosion Laboratory, West Lafayette, USA. 2747-2753

[118] Helsel, D. R., Mueller, D. K. & Slack, J. R. (2006). Computer program for the Kendall family of trend tests. U.S. Geological Survey Scientific Investigations Report 2005–5275, 4 p.

[119] Heo, J.-H., Kho, Y. W., Shin, H., Kim, S., & Kim, T. (2008). Regression equations of probability plot correlation coefficient test statistics from several probability distributions. Journal of Hydrology 355, 1- 15.

[120] Hirsch, R. M. & Slack. J. R. (1984). A nonparametric trend test for seasonal data with serial dependence. Water Resources Research 20(6), 727-732.

[121] Hua, J., Liang, Z. & Yu, Z. (2003). A Modified Rational Formula for Flood Design in Small Basins. Journal of The American Water Resources Association, 1017-1025.

[122] Huffman, G. J., Adler, R. F., Bolvin, D. T., Gu G, Nelkin E.J, Bowman K.P, Hong Y , Stocker E.F & Wolff D.B (2007). The TRMM Multi-satellite Precipitation Analysis: Quasi-global, multi-year, combined-sensor precipitation estimates at fine scale . J. Hydrometeor 8, 38-55.

[123] Husain, A. (2012). Estimation of Design Flood for Kol Dam and Rampur in Satluj River Basin. International Journal of Emerging Technology and Advanced Engineering 2(8) 163-166.

[124] Hussein, A. K. (2014). Best Distribution and Plotting Positions of Annual Rainfall in the Catchment of Holy Karbala in Iraq. Journal of Babylon University/Engineering Sciences/ 22(4), 894-906.

[125] Immerzeel , W.W. , Rutten, M.M. & Droogers, P. (2009). Spatial downscaling of TRMM precipitation using vegetative response on the Iberian Peninsula. Remote Sensing of Environment 113, 362-370.

[126] IPCC (2001). Climate Change 2001: Impacs, Adaptations and Vulnerability, UK.

[127] IPCC (2007). Climate Change 2007: Impacts, Adaptation and vulnerability, In Physics and Chemistry of the Earth, Parts A/B/C, Published for the Intergovernmental Panel on Climate Change, London.

[128] Islam, M. N. & Uyeda, H. (2007). Use of TRMM in determining the climatic characteristics of rainfall over Bangladesh. Remote Sensing of Environment 108, 264-276.

[129] Jabro, J. D. (1992). “Estimation of saturated hydraulic conductivity of soils from particle size distribution and bulk density data.”. Trans. ASABE, 35(2), 557-560.

[130] James R. Jones , John S. Schwartz , Kelsey N. Ellis, Jon M. Hathaway & Curtis M. Jawdy (2015). Temporal variability of precipitation in the Upper Tennessee Valley. Journal of Hydrology: Regional Studies 3, 125-138.

[131] Jarvis A., Reuter, H. I., Nelson, A. & Guevara, E. (2008a). Hole-filled seamless SRTM data V4, International Centre for Tropical Agriculture (CIAT), available at http://srtm.csi.cgiar.org

[132] Jarvis, A., Reuter, H. I., Nelson, A. & Guevara, E.(2008b). Hole-filled SRTM for the globe Version 4, available from the CGIAR-CSI SRTM 90m Database at (http://srtm.csi.cgiar.org

[133] Jarvis, A., Rubiano, J., Nelson, A., Farrow, A. & Mulligan, M. (2004). Practical use of SRTM data in the tropics – Comparisons with digital elevation models generated from cartographic data. Working Document no. 198. International Centre for Tropical Agriculture (CIAT), Cali, Colombia, AA6713.

[134] Jason W. Osborne (2010). Practical Assessment, Research & Evaluation. A peer-reviewed electronic journal 15 (12), 1-9

[135] Jeon, J.-H., Lim, K.J. & Engel, B. A. (2014). Regional Calibration of SCS-CN L-THIA Model: Application for Ungauged Basins. Water 6(5), 1339-1359.

[136] Jha, M. K. (2011). Evaluating Hydrologic Response of an Agricultural Watershed for Watershed Analysis. Water 3(4), 604-617.

[137] Jones, D. H. (1994). Statistical Methods: Book review. Journal of Educational and Behavioral Statistics 19(3), 304-307.

[138] Kalayci, E. & Kalayc, S. (2014). Trend analysis of streamflow in Turkey. Journal of Hydrology 289, 128-144.

[139] Kamruzzaman, M., Shahriar, M. & Beecham, S. (2014). Assessment of Short Term Rainfall and Stream Flows in South Australia. Water 6(11), 3528-3544.

[140] Karim, M. A. & Chowdhury, J. U. (1995). A comparison of four distributions used in flood frequency analysis in Bangladesh. Hydrological Sciences Journal 40(1), 55-66.

[141] Kefyalew (2003). Integrated Flood Management: The Case of Ethiopia. WMO/GWP Associated Programme on Flood Management. Addis Ababa, Ethopia. 15p.

[142] Kim, S., Shin, H., Kim, T. & Heo, J.-H. (2010). Derivation of the Probability Plot Correlation Coefficient Test Statistics for the Generalized Logistic Distribution. International Workshop Advances in Statistical Hydrology, May 23-25 (2010), Taormina, Italy.

[143] Kim, U. & Kaluarachchi, J. J. (2008). Application of parameter estimation and regionalization methodologies to ungauged basins of the Upper Blue Nile River Basin, Ethiopia. Journal of Hydrology 362(1-2), 39-56.

[144] Kim, U., Kaluarachchi J. J. & Smakhtin, V. U. (2008). Climate change impacts on hydrology and water resources of the Upper Blue Nile River Basin, Ethiopia. Colombo, Sri Lanka: International Water Management Institute. 27p (IWMI Research Report 126)

[145] Kite, G. W. & Pietroniro, A. (1996). Remote sensing applications in hydrological modelling. Hydrological Sciences Journal 41 (4), 563-591.

[146] Kjeldsen, T. R., Stewart, E. J., Packman, J. C., Folwell, S. S. & Bayliss, A. C. (2005). Revitalisation of the FSR/FEH rainfall runoff method, Joint Defra/EA. Flood and Coastal Erosion Risk Management R&D Programme. RD Technical Report FD1913/TR.

[147] Konz, M. (2009). The TOPKAPI model as a basis for the APUNCH Hydrological Modelling Framework, PhD-retreat.

[148] Kothyari, U. C., Singh, V. P. & Aravamuthan, V. (1997). An Investigation of Changes in Rainfall and Temperature Regimes of the Ganga Basin in India. Water Resources Management 11, 17-34.

[149] Kottegoda, N. T. & Rosso, R. (2008). Applied Statistics for Civil and Environmental Engineers-Second Edition. Blackwell Publishing Ltd, United Kingdom.

[150] Koutroulis, A. G., Tsanis, I. K., Daliakopoulos, I. N. & Jacob, D. (2013). Impact of climate change on water resources status: A case study for Crete Island, Greece. Journal of Hydrology 479, 146-158.

[151] Krause, P. , Boyle., D. P. & Base, F. (2005). Comparison of different efficiency criteria for hydrological model assessment. Advances in Geosciences 5, 89-97.

[152] Lastoria, B. (2008). Hydrological processes on the land surface: A survey of modelling approaches. FORALPS Technical Report, 9. Università degli Studi di Trento, Dipartimento di Ingegneria Civile e Ambientale, Trento, Italy, 56 pp.

[153] Leavesley, G. H., Lichty, R. W., Troutma, B. M. & Saindon, L. G. (1983). Precipitation-runoff modeling system : User's manual. US Geological Survey Water Investigation Report, 83–4238.

[154] Legates, D. R., Gregory J. & McCabe Jr. (1999). Evaluating the use of "goodness-of-fit" measures in hydrologic and hydroclimatic model validation. Water Resources Research 35 (1), 233-241.

[155] Ling, H., Xu, H. & Fu, J. (2013). Temporal and Spatial Variation in Regional Climate and its Impact on Runoff in Xinjiang, China. Water Resour Manage 27, 381-399.

[156] Liu , Z., Martina, M. L. V. & Todini, E. (2005). Flood forecasting using fully distributed model:Application of TOPKAPI model to Upper Xixian catchment. Hydrology and Earth System Sciences 9(4): 347-364.

[157] Liu and Todini (2002). The TOPKAPI model. Department of Earth and Geo-Environmental Sciences, University of Bologna, Italy.

[158] Liu, X. T., Liu, Q., Fu, Y. F. & Li, R. (2014). Daytime precipitation identification scheme based on multiple cloud parameters retrieved from visible and in-frared measurements. Science China: Earth Sciences 57, 2112-2124.

[159] Liu, Y., Sang, Y.-F., Li, X., Hu, J. & Liang, K. (2017). Long-Term Streamflow Forecasting Based on Relevance Vector Machine Model. Water 2017 9, 9.

[160] Liu, Z. & Todini, E. (2002). Towards a comprehensive physically-based rainfall-runoff model. Hydrology and Earth System Sciences 6(5), 859-881.

[161] Liu, Z. -Y., Tan, B.-Q., Tao, X. & Xie, Z.-H. (2008). Application of a Distributed Hydrologic Model to Flood Forecasting in Catchments of Different Conditions. Journal of Hydrol. Engineering, 13, 378-384.

[162] Loganathan, G. V., Kuo, C. Y. & McCormick, T. C. (1985). Frequency Analysis of Low Flows . Nordic Hydrology 16, 105-128.

[163] Ludwig, W., Serrat, P., Cesmat, L. & Garcia-Esteves, J. (2004). Evaluating the impact of the recent temperature increase on the hydrology of the Têt River (Southern France). Journal of Hydrology 289, 204-221.

[164] Lye, L. (1993). A technique for selecting the Box-Cox transformation in flood frequency analysis. Can. J. Civ. Eng. 20, 760-766

[165] Machiwal, D. & Jha, M. K. (2006). Time series analysis of hydrologic data for water resources planning and management: a review. J. Hydrol. Hydromech 54 (3), 237-257.

[166] Maidment (1993). Handbook of Hydrology, McGraw-Hill, USA.

[167] Major Rivers of Ethiopia, available at: http://www.ethiovisit.com/major-rivers-of-ethiopia/34/.

[168] Martina, M. L. V., Todini, E. & Liu, Z. (2011). Preserving the dominant physical processes in a lumped Hydrological model. Journal of Hydrology 399 (2011), 121–131.

[169] Mathevet, T., Michel, C., Andréassian, V. & Perrin, C. (2006). A bounded version of the Nash-Sutcliffe criterion for better model assessment on large sets of basins. Large Sample Basin Experiments for Hydrological Model Parameterization: Results of the Model Parameter Experiment-MOPEX. IAHS Publ. 307, 2006: EDF-DTG, 21, Avenue de l'Europe, BP 41, F-38040 Grenoble cedex 09, France

[170] McSweeney, C., New, M. & Lizcano, G. (2008). UNDP Climate Change Country Profiles: Ethiopia (http://country-profiles.geog.ox.ac.uk/index.html?country=Ethiopia&d1=Reports)

[171] McSweeney, C., New, M., Lizcano, G. & Lu, X. (2010). The UNDP Climate Change Country Profiles: Improving the Accessibility of Observed and Projected Climate Information for Studies of Climate Change in Developing Countries. American Meteorological Society BAMS Feb. 2010, 157-166.

[172] Meals, D. W., Spooner, J., Dressing, S. A. & Harcum, J. B. (2011). Statistical analysis for monotonic trends, Tech Notes 6,November 2011. Developed for U.S. Environmental Protection Agency by Tetra Tech, Inc., Fairfax, VA, 23 p.

[173] Mehdi, F. & Mehdi, J. (2011). Determination of Plotting Position Formula for the Normal, Log-Normal, Pearson(III), Log-Pearson(III) and Gumbel Distributional Hypotheses Using The Probability Plot Correlation Coefficient Test. World Applied Sciences Journal 15 (8), 1181-1185.

[174] Mekonnen, Z. Z. (2008). Development of Flood Forecasting Model in Middle Awash River Basin of Ethiopia, International Centre for Water Hazard and Risk Management (ICHARM-Japan) and Ministry of Water Resources (Ethiopia).

[175] Minasny, B. & McBratney, A. B. (2000). Evaluation and development of hydraulic conductivity pedotransfer functions for Australian soil. Aust. J. Soil Res. 38, 906-926.

[176] Mkhandi, S. H., Kachroo, R. K. & Gunasekara, T. A. G. (2000). Flood frequency analysis of southern Africa: II-Identification of regional distributions. Hydrological Sciences-]'ournal-des Sciences Hydrologiques 45(3), 449-464.

[177] Molin P. & Abdi H. (1998). New Tables and numerical approximation for the Kolmogorov- mirnov/Lillierfors/Van Soest test of normality. Technical report, University of Bourgogne; available at www.utd.edu/\T1\guillemotrightherve/MolinAbdi1998-LillieforsTechReport.pdf

[178] Moriasi, D. N., Arnold, J. G., Liew, M. W. V., Bingner, R. L., Harmel, D. & Veith, L. (2007). Model Evaluation Guidelines for Systematic Quantification of Accuracy in Watershed Simulations. American Society of Agricultural and Biological Engineers 50(3), 885900.

[179] MoWR (2002). Integrated water and land management research and capacity building priorities for Ethiopia. In Physics and Chemistry of the Earth, Parts A/B/C, Proceedings of a MoWR/EARO/IWMI/ILRI international workshop held at ILRI, Addis Ababa, Ethiopia.

[180] Mualem, Y. (1976). A new model for predicting the hydraulic conductivity of unsaturated porous media. Water Resour. Res. 12, 513-522.

[181] Nalley, D., Adamowski, J., Khalil, B. & Ozga-Zielinski, B. (2013). Trend detection in surface air temperature in Ontario and Quebec, Canada during 1967- 2006 using the discrete wavelet transform. Atmospheric Research 132-133, 375 - 398.

[182] Narayanan, P. , Basistha, A., Sarkar, S. & Kamna, S. (2013). Trend analysis and ARIMA modelling of pre-monsoon rainfall data for western India Comptes Rendus Geoscience 345 (1), 22 - 27.

[183] Nasher, N. M. R. & Uddin, M. N. (2013). Maximum and minimum Temperature Trends variation over the northern and southern part of Bangeladesh. J. Environ. Sci. & Natural Resources 6(2), 83-88.

[184] Nash-Sutcliffe model efficiency coefficient-Wikipedia(the free encyclopedia), available at :https://en.wikipedia.org/wiki/Nash\T1\textendashSutcliffe_model_efficiency_coefficient/.

[185] Negash, F. (2012). Managing Water for Inclusive and Sustainable Growth in Ethiopia: Key Challenges and Priorities. Report, Addis Ababa, Ethiopia.

[186] O'Connor, P. D. T. & Kleyner, A. (2012). Kolmogorov -Smirnov Tables in Practical Reliability Engineering, Fifth Edition, John Wiley & Sons, Ltd.

[187] Ogunlela, A. O., Adewale, P. O. & Adamowski, J. F. (2012). Developing Design Storm Hydrographs for Small Tropical Catchments with Limited Data. Ethiopian Journal of Environmental Studies and Management 5(4).

[188] Opere, A. O., Mkhandi, S. & Willems, P. (2006). At site flood frequency analysis for the Nile Equatorial basins. Physics and Chemistry of the Earth, Parts A/B/C 31(15-16), 919-927.

[189] Papalexiou, S. M., Koutsoyiannis, D. & Makropoulos, C. (2013). How extreme is extreme? An assessment of daily rainfall distribution tails. Hydrology and Earth System Sciences 17(2), 851-862.

[190] Parmentier, B., Dooge, J. C. I & Bruen, M. (2003). Root Selection Methods in flood analysis. Hydrology and Earth System Sciences 7(2), 151-161

[191] Pechlivanidis, I.G. , Jackson, B. M., Mcintyre, N. R., & Wheater, H.S. (2011). Catchment Scale Hydrological Modelling: A Review of Model Types, Calibration Approaches and Uncertainty Analysis Methods In The Context of Recent Developments in Technology and Applications. Global NEST Journal, 13 (3), 193-214.

[192] Pegram, G. & Parak, M. (2004). A review of the regional maximum flood and rational formula using geomorphological information and observed floods. Water SA 30 (3), 37-392.

[193] Pegram, G.G.S & Parak, M. (2006). The rational formula from the run-hydrograph. Water SA 32 (2), 163-180.

[194] Pegram, G. (2010). SAFeWater: Soil moisture estimation from remote sensing in RSA, Secience and technology , RSA.

[195] Pegram, G., Sinclair, S., Vischel, T. & Nxumalo, N. (2010). Soil Moisture from Satellites: Daily Maps Over RSA for Flash Flood Forecasting, Drought Monitoring, Catchment Management & Agriculture. Water Research Commission WRC Report No. 1683110 ISBN 978-1(WRC-1683).

[196] Pegram, G., Vischel, T., Sinclair, S., Wagner, W.& Bartsch, A. (2007). Comparison of soil moisture fields estimated by catchment modelling and remote sensing: a case study in South Africa. Hydrol. Earth Syst. Sci., 4,2273–2306.

[197] Peng, D., Li, Z. & Liu, Z. (2008). Numerical algorithm of distributed TOPKAPI model and its application. Water Science and Engineering, 1(4),14-21.

[198] Potential evapotranspiration by Thornthwaite method (Online thornthwaite and others); available at: http://ponce.sdsu.edu/onlinethornthwaite.php.

[199] Pradhan, M. P. & Ghose, M. K. (2012). Automatic Association of Stream Order for Vector Hydrograph using Spiral Traversal Technique. Journal of Computer Engineering 1 (5), 09-12.

[200] ProGea s.r.l. (2003). The Generla skeleton about the TOPKAPI model, segreteria@progea.net, via Don Bedetti, 20,40129 Bologna (ITALY).

[201] Python computer programming: http://www.python.org/.

[202] Rabba, Z. A., Fatoyinbo , B. S. and Stretch, D.D. (2018). Applications of PyTOPKAPI model to ungauged catchments. Water SA3464.(Accepted for publication).

[203] Ragettli, S. & Pellicciotti, F. (2012). Calibration of a physically based, spatially distributed hydrological model in a glacierized basin: On the use of knowledge from glaciometeorological processes to constrain model parameters. Water Resources Research 48,W03509.

[204] Raghunath, H. M. (2006). Hydrology text, Principles-Analysis-Design (2nd Edition). New Age International (P) Limited, New Delhi - 110002.

[205] Rahman, A., Weinmann, P.E., Hoang, T.M.T.& Laurenson, E.M. (2002). Monte Carlo simulation of flood frequency curves from Rainfall. Journal of Hydrology 256, 196-210.

[206] Rahman, A., Hoang, T.M.T., Weinman, P.E. & Laurenson, E.M. (1998). Joint probability approach to Design flood estiamation- A review:Cooperative research centre for Catchment hydrology.

[207] Rahman, M., Pearson, L. M. & Heien, H. C. (2006). A Modified Anderson-Darling Test for Uniformity. Bull. Malays. Math. Sci. Soc. (2) 29 (1), 11 -16.

[208] Rango, A. (1994). Application of remote sensing methods to hydrology and water resources. Hydrological Sciences Journal 39 (4), 309-320.

[209] Rashid , M. M., Beecham, S., & Chowdhury, R. K. (2015). Assessment of trends in point rainfall using Continuous Wavelet Transforms Advances in Water Resources 82: 1-15.

[210] Rawls, W., Brakensiek, D. & Saxton, K. (1982). Estimation of soil water properties. Trans. of the ASAE,25(5), 1316-1320 and 1328.

[211] Rawls, W. J., Brakensiek, D. L. & Soni, B. (1983). Agricultural management effects on soil water processes: Soil water retention and Green Ampt parameters. Trans. ASAE, 26, 1747-1752.

[212] Razali, N. M. & Wah, Y. W. (2011). Power comparisons of Shapiro-Wilk, Kolmmogorov-Smirnov, Lillifors and AndersonDarling Tests. Journal of Statistical Modelling and Analystics 2(1), 21-33.

[213] Reis, D. S. & Stedinger, J. R. (2005). Bayesian MCMC flood frequency analysis with historical information. Journal of Hydrology 313(1-2), 97-116.

[214] Report of Flood Disaster in Ethiopia (2006). Joint Government and Humanitarian Partners Flash Appeal for the 2006 Flood Disaster in Ethiopia, Addis Ababa, Ethiopia.

[215] Ries III, K. G. (2007). The national streamflow statistics program: A computer program for estimating streamflow statistics for ungaged sites. U.S. Geological Survey Techniques and Methods 4-A6, 37 p.

[216] Rogger, M., Kohl, B., Pirkl, H., Viglione, A., Komma, J., Kirnbauer, R., Merz, R. & Blöschl, G. (2012). Runoff models and flood frequency statistics for design flood estimation in Austria – Do they tell a consistent story? .Journal of Hydrology 456-457, 30-43.

[217] S A Drainage Manual (2006). Drainage Manual,5^{th} edition-fully Revised: The South African National Roads Agency Limited, Peritoria.

[218] Saeidifarzad, B., Nourani, V., Aalami, M. & Chau, K.-W. (2014). Multi-Site Calibration of Linear Reservoir Based Geomorphologic Rainfall-Runoff Models. Water 6(9), 2690-2716.

[219] Salas, J. D. & Obeysekera, J. (2014). Revisiting the Concepts of Return Period and Risk for Nonstationary Hydrologic Extreme Events. Journal of Hydrologic Engineering 19(3), 554-568.

[220] Sanborn, S. C. & Bledsoe, B. P. (2006). Predicting streamflow regime metrics for ungauged streamsin Colorado, Washington, and Oregon. Journal of Hydrology 325(1-4), 241-261.

[221] SANRAL (2007). South African National Road Agenct Limitted (SANRAL), annual Report.

[222] Saxton, K. E. & Rawls, W. J. (2006). Soil Water Characteristic Estimates by Texture and Organic Matter for Hydrologic Solutions. Soil Science Society of America Journal 70(5), 1569.

[223] Saxton, K. E., W. J. Rawls, J. S. Romberger & R. I. Papendick (1986). Estimating generalized soil water characteristics from texture. Soil Sci. Soc. Amer. J. 50, 1031-1036.

[224] Sayyad, K. S. (2014). The trend of seasonal and annual precipitation stations Orumieh lake basin using the Mann Kendall. Researcher 6(5), 1-4.

[225] Schaefli, B. & Gupta, H. V. (2007). How Do We Communicate Model Performance? Do Nash values have value?. Hydrological Processes. DOI: 10.1002/hyp.6825

[226] Scheel, M. L. M., Rohrer, M., Huggel, Ch., Santos Villar, D. , Silvestre, E. & Huffman, G. J. (2011). Evaluation of TRMM Multi-satellite Precipitation Analysis (TMPA) performance in the Central Andes region and its dependency on spatial and temporal resolution. Hydrol. Earth Syst. Sci. 15, 2649-2663.

[227] Scholz, F. W. & Stephens, M. A. (1987). K-Sample Anderson-Darling Tests . Journal of the American Statistical Association 82(399), 918-924.

[228] Schwab, G.O., Fangmeier, D.D., Elliot, W.J., and Frevert, R.K. (1993). Soil and Water Conservation Engineering. 4th edition. John Wiley and Sons, Inc., New York.

[229] Shabri, A. (2002). A Comparison of Plotting Formulas for the Pearson type III Distribution. Jurnal Teknologi, 36 (C), 61-74.

[230] Shang, H., Yan, J., Gebremichael, M. & Ayalew, S. M. (2011). Trend analysis of extreme precipitation in the Northwestern Highlands of Ethiopia with a case study of Debre Markos. Hydrology and Earth System Sceinces 15, 1937-1944.

[231] Shapiro, S. S. & Wilk, M. B. (1965). An analysis-of-variance test for normality (Complete Samples). Biometrika 52, 591-611.

[232] Sharma, C. S., Panda, S. N., Pradhan, R. P., Singh, A. & Kawamura, A. (2016). Precipitation and temperature changes in eastern India by multiple trend detection methods. Atmospheric Research 180, 211-225.

[233] Shiu, C.-J., Liu, S. C., Fu, C., Dai, A. & Sun, Y. (2012). How much do precipitation extremes change in a warming climate? Geophysical Research Letters 39 (L17707), 1-5.

[234] Sileshi, Y. (2005). Engineering Hydrology , Addis Ababa, Ethiopia, unpublished.

[235] Simard, R. & L'Ecuyer, P. (2011). Computing the Two-Sided Kolmogorov-Smirnov Distribution. Journal of Statistical Software 39(11), 1-18.

[236] Sinclair, S. & Pegram, G. G. S. (2010). A comparison of ASCAT and modelled soil moisture over South Africa, using TOPKAPI in land surface mode. Hydrology and Earth System Sciences 14, 613-626.

[237] Sinclair, S. & Pegram, G. (2011). PyTOPKAPI - an open source hydrological model used to estimate Soil Moisture in near real time over South Africa for flood potential & drought monitoring and remote sensing model inter-comparison, European Geosciences Union general Assembly, Vienna.

[238] Sinclair, S. & Pegram, G.G.S. (2012). A sensitivity assessment of the TOPKAPI model with an added infiltration module. Journal of Hydrology 479, 100-112.

[239] Sinclair, S. & Pegram, G. G. S. (2013a). PyTOPKAPI – an Open-Source Implementation of the TOPKAPI Hydrological Model,Civil Engineering, University of Kwazulu-Natal and Pegram and Associates, Durban, South Africa.

[240] Sinclair, S. & Pegram, G. (2013b). HYLARSMET: A Hydrologically Consistent Land Surface Model for Soil Moisture and Evapotranspiration Modelling over Southern Africa using Remote Sensing and Meteorological Data. Technical report, Water Research Commission Report No. 2024/1/13, Water Research Commission, Pretoria, South Africa.

[241] Singh, K. P. & Nakashima, M. (1981). A New Methodology for Flood Frequency Analysis With Objective of Detection and Modification af Outliers/Inliers State Water Survey Division, Surface Water Section, Illinois Institute of Natural Resources (SWS Contract Report 272)

[242] Singh, V. P., & Woolhiser, D. A. (2002). Mathematical Modeling of Watershed Hydrology J. Hydrol. Eng. 7(4), 270-292.

[243] Smal, R. (2012). Evaluation of the Catchment Parameter (CAPA) and Midgley and Pitman (MIPI) empirical design flood estimation methods. M.Sc. Thesis(Civil Engineering), University of Stellenbosch.

[244] Smettem, K. R. J., Oliver, Y. M., Heng, L. K., Bristow, K. L. & Ford, E. J. (1999). "Obtaining soil hydraulic properties for water balance and leaching models from survey data. 1. Water retention.". Aust. J. Agric. Res. 50 (2), 283-289.

[245] Smith, L. C.(1997). Satellite Remote Sensing of River inundation Area, Stage, and Discharge: A Review . Hydrological Processes 11, 1427-1439.

[246] Smithers, J. C. (2012). Methods for design flood estimation in South Africa. Water SA 38(4), 633-646.

[247] Smithers, J. C. & Schulze, R. E. (2002). Design Rainfall and Flood Estimation in South Africa, S A Water Research Commission. WRC Project No: K5/1060.

[248] Smithers, J. C., Chetty, K. T., Frezghi, M. S., Knoesen, D. M. & Tewolde, M. H. (2013). Development and assessment of a daily time-step continuous simulation modelling approach for design flood estimation at ungauged locations: ACRU model and Thukela Catchment case study. Water SA 39(4), 467-476.

[249] Snedecor, G. W. & Cochran, W. G. (1989). Statistical Methods, Eighth Edition. Iowa State University Press.

[250] Sobieraj, J. A., H. Elsenbeer & R. A. Vertessy (2001). Pedotransfer functions for estimating saturated hydraulic conductivity: Implications for modeling storm flow generation. J. Hydrol. 251, 202-220.

[251] Some'e, B. S., Ezani, A. & Tabari, H. (2012). Spatiotemporal trends and change point of precipitation in Iran. Atmospheric Research 113, 1-12.

[252] Sonali, P. & Kumar, D. N. (2013). Review of trend detection methods and their application to detect temperature changes in India. Journal of Hydrology 476, 212-227.

[253] SRTM DEM: http://srtm.csi.cgiar.org.

[254] Stedinger, J. R. & Griffi, V. W. (2008). Flood Frequency Analysis in the United States: Time to Update. Journal of Hydrologic Engineering © ASCE / April 2008 / 199-204.

[255] Stephens, M. A. (1974). EDF statistics for goodness-of-fit and some comparisons. J. Am. Statist. Assoc. 69, 730-737.

[256] Stephens, M. A. (1979). The Anderson-Darling Statistic-Technical Report No. 39. Department Of Statistics, Stanford University, Stanford, California.

[257] Stolte, J., Freijer, J.I., Bouten, W. , Dirksen, C., Halbertsma,J.M., Van Dam, J.C., van Den Berg, J.A., Veerman, G.J. & Wosten, J.H.M. (1994). Comparison of six methods to determine unsaturated soil hydraulic conductivity. Soil Sci. Soc. Am. J. 58, 1596-1603.

[258] Strupczewski, W. G., Singh, V. P. & Weglarczyk, S. (2001). Impulse response of a linear diffusion analogy model as a flood frequency probability density function. Hydrological Sciences-Journal des Sciences Hydrologiques 46(5), 761-780.

[259] Subramanya, K. (1998). Engineering Hydrology. Tata McGrawhill Publishing Company Limited, New Delhi.

[260] Suhaila, J., Deni, S. M., Zin, W. Z. W. & Jemain, A. A. (2010). Trends in Peninsular Malaysia Rainfall Data during the Southwest Monsoon and Northeast Monsoon Seasons: 1975–2004. Sains Malaysiana 39(4), 533-542.

[261] Tadesse, L, Sonbol, M. A. & Willems, P. (2005). At-Site and Regional Flood Frequency Analysis Of The Upper Awash Sub – Basin in the Ethiopian Plateau. Water Resources Research Institute, National Water Research Center 3, 1-15

[262] Tan, M. L., Latif, AB, Pohl, C. & Duan, Z. (2014). Streamflow modelling by remote sensing: A contribution to digital Earth. Earth and Environmental Science 18(012060): 1-6.

[263] Tapiador, F. J., Machado, L. A. T., Angelis, C. F., Salio, P., Kidd, C., Huffman, G. J. & Castro, M. d. (2012). Global precipitation measurement: Methods, datasets and applications. Atmospheric Research 104-105, 70-97.

[264] Technical Release 20 (TR-20). Computer Program for Project Formulation Hydrology, The Hydrology Unit and the Technology Development Support Staff, Soil Conservation Service.

[265] Technical Release 55 (TR-55). Urban Hydrology for Small Watersheds: Resources Conservation Service, Conservation Engineering Division.

[266] Tesfaye, B. (2011). Predicting Discharge at Ungauged Catchments Using Rainfall-Runoff Model (Case study: Omo-Gibe River Basin). M.Sc Thesis, Addis Ababa University.

[267] The HWSD attribute database, avaiable at http://www.fao.org/soils-portal/soil-survey/soil-maps-and-databases/harmonized-world-soil-database-v12/en/

[268] Thornthwaite, C. W. & Mather, J. R. (1955). The Water Balance: Centerton, N.J., Laboratory of Climatology, Publications in Climatology,8(1), 1-104.

[269] Salmi, T., Määttä, A., Anttila, P., Ruoho-Airola, T. & Amnell, T. (2002). Detecting trends of annual values of atmospheric pollutants by the Mann-Kendall test and Sen's slope estimates –the Excel template application MAKESENS.31, 1-35: Finnish Meteorological Institute, Helsinki, Finland.

[270] Todini, E. (2007). Hydrological catchment modeling: past, present and future. Hydrology & Earth System Sceinces 11(1), 468-482.

[271] Todini, E. (2007b). A mass conservative and water storage consistent variable parameter Muskingum-Cunge approach. Hydrol. Earth Syst. Sci. 11, 1645-1659.

[272] Todini, E. (2011). History and perspectives of hydrological catchment modelling. Hydrology Research 42(2–3),73-85.

[273] TR-20 (2004). WinTR-20 User Guide. USA.

[274] TRMM 3B42RT product: avaiable at http://gdata1.sci.gsfc.nasa.gov/daac-bin/G3/gui.cgi?instance_id=TRMM_3B42RT

[275] Trucano, T. G., Swiler, L. P., Igusa, T., Oberkampf, W. L. & Pilch, M. (2006). Calibration, validation, and sensitivity analysis: What's what. Reliability Engineering & System Safety 91(10-11), 1331-1357.

[276] USGS Land Use/Land Cover System Legend (Modified Level 2); available at : http://edc2.usgs.gov/glcc/globdoc1_2.php.

[277] Van der Spuy, D., & Rademeyer, P. F. (2010). Flood frequency estimation methods as applied in the Department of Water Affairs: Department of Water Affairs. Pretoria, South Africa.

[278] Van Liew, M. W. & Garbrecht, J. (2003). Hydrologic simulation of the Little Washita River Experimental Watershed using SWAT. Journal of the American Water Resources Association 39(2), 413-426.

[279] Veiga, V. B., Hassan, Q. K. & He, J. (2015). Development of Flow Forecasting Models in the Bow River at Calgary, Alberta, Canada. Water 2015 7, 99-115.

[280] Vieux, B. E., Cui, Z. & Gaur, A. (2004). Evaluation of a physics-based distributed hydrologic model for flood forecasting. Journal of Hydrology 298(1-4), 155-177.

[281] Vis, M., Knight, R., Pool, S., Wolfe, W. & Seibert, J. (2015). Model Calibration Criteria for Estimating Ecological Flow Characteristics. Water 2015 7, 2358-2381.

[282] Vischel, T. , Pegram,,G. G. S., Sinclair, S., Wagner, W. & Bartsch, A. (2008). Comparison of soil moisture fields estimated by catchment modelling and remote sensing: a case study in South Africa. Hydrology and Earth System Sciences 12, 751-767.

[283] Vischel, T., Pegram, G., Sinclair, S. & Parak, M. (2008). Implementation of the TOPKAPI model in South Africa: Initial results from the Liebenbergsvlei catchment. Water SA 34, 331-342.

[284] Viviroli, D., Mittelbach, H., Gurtz, J. & Weingartner, R. (2009). Continuous simulation for flood estimation in ungauged mesoscale catchments of Switzerland – Part II: Parameter regionalisation and flood estimation results. Journal of Hydrology 377(1-2), 208-225.

[285] Vogel, R. M. (1986). The Probability Plot Correlation Coefficient Test for the Normal, Lognormal, and Gumbel Distributional Hypotheses. Water Resources Research 22(4), 587-590.

[286] Vogel, R. M. & Kroll, C. N. (1989). Low-flow frequency analysis using probability-plot correlation coefficients. Journal of Water Resources Planning and Management 115(3), 338-357.

[287] Vogel, R. M. & McMartin, D. E. (1991). Probability plot goodness-of-fit and skewness estimation procedures for the Pearson type 3 distribution. Water Resources Res. 27(12), 3149-3158.

[288] Vogel, R. M. & Wilson, I. (1996). Probability distribution of annual maxi-mum, mean and minimum stream flows in the United States. J. Hydrol. Eng. 1(2), 69-76.

[289] W R Report of Ethiopia (2006). Managing Water Resources of Ethiopia to Maximize Sustainable Growth, Addis Ababa, Ethiopia.

[290] Wagner, W., Lemoine, G. & Rott, H. (1999). A method for estimating soil moisture from ERS scatterometer and soil data. Remote Sensing of Environent 70, 191-207.

[291] WaterBase Web site: http://www.waterbase.org/download_data.html

[292] Wigmosta, M. S., Vail, L. W. & Lettenmaier, D. P. (1994). A distributed hydrologyvegetation model for complex terrain. Water Resources Research 30 (6), 1665-1679.

[293] Willems P., Sonbol M., Abdo G., Mkhandi S., Opere A., Tadesse L., Abdel Motaleb M., Farid S., Zaki A. & Al-Weshah R. (2009). Regional Flood Frequency Analysis in the Nile Basin.Hydraulics Laboratory, K.U.Leuven, B-3001, Belgium.

[294] Willmott, C. J. & Matsuura, K. (2006). On the use of dimensioned measures of error to evaluate the performance of spatial interpolators. International Journal of Geographical Information Science 20(1), 89-102.

[295] Wilson, D. (2014). Evaluation of the methods used by NVE for flood frequency estimation, ppt presentation: NVE.

[296] Wilson, D., Hisdal, H. & Lawrence, D. (2010). Has stream flow changed in the Nordic countries? – Recent trends and comparisons to hydrological projections. Journal of Hydrology (394), 334-346.

[297] Wilson, D., Fleig, A. K., Hisdal, H. , Pettersson, L.-E., & Holmqvist, E. (2011). A review of NVE's flood frequency estimation procedures: Norwegian Water Resources and Energy Directorate.

[298] Woo, M.-k & Thorne, R. (2003). Comment on 'Detection of hydrologic trends and variability' by Burn, D.H. and Hag Elnur, M.A., 2002, Journal of Hydrology 255, 107–122. Journal of Hydrology 277(1-2), 150 - 160.

[299] Wu, M.-C. & Lin, G.-F. (2015). An Hourly Streamflow Forecasting Model Coupled with an Enforced Learning Strategy. Water 2015 7, 5876-5895.

[300] XU, Z. X., CHEN, Y. N. & LI, J. Y. (2004). Impact of Climate Change onWater Resources in the Tarim River Basin. Water Resources Management 18 , 439-458.

[301] Xu, Z. X., Takeuchia, K. & Ishidairaa, H. (2003). Monotonic trend and step changes in Japanese precipitation. Journal of Hydrology 279, 144-150.

[302] Xue, X., Hong, Y., Limaye, A. S., Gourley, J. J., Huffman, G. J., Khan, S. I., Dorji, C. & Chen, S. (2013). Statistical and hydrological evaluation of TRMM-based Multi-satellite Precipitation Analysis over the Wangchu Basin of Bhutan: Are the latest satellite precipitation products 3B42V7 ready for use in ungauged basins? . Journal of Hydrology 499, 91-99.

[303] Yahaya, A. S, Yee, C. S., Ramli, N. A. & Ahmad, F. (2012). Determination of the Best Probability Plotting Position for Predicting Parameters of the Weibull Distribution. International Journal of Applied Science and Technology 2(3), 106-111.

[304] Yirefu, S. M. (2010). Regional Flood Frequency Analysis Upstream of Awash with the confluence of Kesem River. M. Sc. Thesis (Engineering), Addis Ababa University.

[305] Yu, G. H. & Huang, C. C. (1999). A distribution free plotting position. Stochastic Environ. Res. and Risk Assess 15, 462-476.

[306] Yue, S. & Chunyuanwang (2004). The Mann-Kendall Test Modified by Effective Sample Size to Detect Trend in Serially Correlated Hydrological Series. Water Resources Management 18, 201-218.

[307] Yue , S., Pilon, P. & Cavadias, G. (2002). Power of the Mann–Kendall and Spearman's rho tests for detecting monotonic trends in hydrological series. Journal of Hydrology 249 (1-4), 254-271.

[308] Zelenáková, M., Purcz, P., Poórová, Z., Alkhalaf, I., Hlavatá, H. & Manuela Portela, M. (2016). Monthly Trends of Precipitation in Gauging Stations in Slovakia. Procedia Engineering 162, 106-111.

[309] Zhang, Q., Liu, C., Xu, C.-y., Xu, Y. & Jiang, T. (2006). Observed trends of annual maximum water level and streamflow during past 130 years in the Yangtze River basin, China. Journal of Hydrology 324, 255-265.

[310] Zhang, Z., Dehoff, A. D., Pody, R. D. & Balay, J. W. (2010). Detection of Streamflow Change in the Susquehanna River Basin. Water Resour Manage 24, 1947-1964.

[311] Zhao, G., Tian, P., Mu, X., Jiao, J., Wang, F. & Gao, P. (2014). Quantifying the impact of climate variability and human activities on streamflow in the middle reaches of the Yellow River basin, China. Journal of Hydrology 519 387-398.

[312] Zhao, J., Huang, Q., Chang, J., Liu, D., Huang, S., & Shi, X. (2015). Analysis of temporal and spatial trends of hydro-climatic variables in the Wei River Basin. Environmental Research 139, 55- 64.

[313] Zhao, N., Yu, F., Li, C., Wang, H., Liu, J. & Mu, W. (2014). Investigation of Rainfall-Runoff Processes and Soil Moisture Dynamics in Grassland Plots under Simulated Rainfall Conditions. Water 6(9), 2671-2689.

[314] Zhuorana, D., Liping, Z. & Lingcheng, L. (2012). The Extreme Precipitation Change Characteristics of the Source Area of the Middle Route of South-North Water Transfer Project. Procedia Engineering 28, 569-573.

Appendix

Rainfall,Temperatures and Streamflow Data

A.1 Rainfall data of the stations in Gilgel Ghibe catchment

Table A.1.1: Monthly Rainfall (mm) at Jimma station (1984-2014).

Year	Jan	Feb	Mar	Apr	May	Jun	Jul	Aug	Sep	Oct	Nov	Dec
1984	23.9	8.9	32.2	82.8	196.5	183.1	353.4	466.0	231.1	9.5	138.2	49.7
1985	25.1	19.5	77.4	147.2	203.3	150.5	267.6	168.2	127.6	63.1	49.9	11.9
1986	0.0	48.2	81.7	114.8	150.7	256.1	232.5	133.8	163.1	88.6	13.9	47.4
1987	26.4	88.5	157.7	59.8	187.7	204.3	185.5	180.0	135.8	116.4	45.6	51.9
1988	81.3	59.0	30.9	87.1	181.8	165.1	184.6	294.0	291.9	171.9	1.5	0.0
1989	27.8	46.8	138.2	178.9	102.2	178.6	232.0	213.3	204.1	106.8	28.3	161.3
1990	24.6	46.0	132.9	56.0	193.6	320.1	279.6	280.2	244.6	22.9	92.5	18.7
1991	79.4	80.9	61.9	169.0	109.5	222.8	199.7	244.3	139.5	50.7	7.8	78.1
1992	28.4	56.4	55.9	161.7	143.5	287.0	212.2	356.0	175.2	180.0	69.7	35.6
1993	78.7	80.8	119.7	236.7	237.1	224.7	188.7	262.6	171.0	174.1	3.0	0.3
1994	0.9	28.2	96.5	153.4	212.5	274.4	255.4	159.2	177.1	11.1	18.1	10.5
1995	8.2	17.2	74.0	192.8	115.2	163.2	181.0	216.4	141.1	48.5	30.0	126.1
1996	40.8	23.4	135.5	203.1	174.8	196.5	231.5	91.0	248.1	23.9	93.1	40.4
1997	66.0	0.0	68.7	178.0	274.6	236.9	122.4	256.0	148.1	336.7	243.2	36.1
1998	102.5	22.4	96.5	93.2	183.6	222.6	248.4	306.7	199.9	200.7	46.5	1.4
1999	29.8	0.7	82.4	71.8	213.7	175.0	136.1	102.3	130.9	197.8	1.3	2.0
2000	0.0	1.0	39.3	194.7	237.7	153.7	265.9	158.7	255.2	244.0	46.8	24.9
2001	16.2	12.9	85.9	116.8	341.2	299.4	312.3	160.8	183.4	162.9	75.8	3.8
2002	68.9	5.0	91.2	89.7	137.3	241.6	149.7	234.9	165.3	79.6	8.1	138.4
2003	28.7	61.3	86.9	111.3	12.2	272.2	186.7	150.9	238.9	91.7	29.9	14.6
2004	51.0	28.4	46.1	130.9	161.9	128.4	216.3	219.4	201.0	133.2	67.3	84.2
2005	44.5	0.5	193.8	141.4	173.8	177.2	273.5	227.8	229.1	68.3	29.7	0.0
2006	15.8	77.1	181.8	110.3	211.5	207.4	327.2	240.2	169.9	91.1	127.6	100.2
2007	37.5	51.0	104.1	121.6	196.1	142.6	247.4	177.0	256.2	50.8	5.9	0.0
2008	34.0	12.3	39.4	112.7	249.0	238.2	209.8	236.8	133.4	186.1	92.9	6.3
2009	63.0	29.5	79.8	96.8	243.6	160.3	149.6	304.7	209.4	92.2	78.4	67.7
2010	27.3	88.4	67.4	101.4	192.9	394.7	181.3	203.5	186.5	37.0	96.2	10.5
2011	24.1	7.5	39.3	151.2	192.9	311.2	189.9	192.1	269.5	10.3	104.9	26.0
2012	2.1	1.8	55.8	154.5	118.7	335.0	223.9	132.7	250.5	32.8	77.4	57.7
2013	34.9	50.9	58.6	94.2	132.7	193.3	151.5	255.2	183.3	56.7	114.7	1.0
2014	17.8	16.8	115.3	507.7	458.6	117.4	271.3	265.6	337.0	144.2	18.6	17.7

Table A.1.2: Monthly Rainfall (mm) at Limu-Genet station (1984-2014).

Year	Jan	Feb	Mar	Apr	May	Jun	Jul	Aug	Sep	Oct	Nov	Dec
1984	16.1	0.0	52.7	63.2	284.1	412.5	277.7	359.8	188.5	26.9	69.7	18.0
1985	11.1	9.7	27.4	216.5	168.2	395.6	464.8	317.8	249.6	133.5	16.2	18.5
1986	0.0	68.5	66.9	104.7	152.6	288.3	394.2	283.7	368.0	124.9	10.6	54.5
1987	0.0	84.5	37.2	54.3	123.8	306.0	322.1	219.6	246.7	199.3	26.5	31.5
1988	49.5	51.5	46.4	63.8	300.5	279.8	324.3	317.7	298.0	212.2	20.9	0.0
1989	15.2	23.4	106.5	168.5	121.7	185.4	254.1	280.5	210.7	99.0	7.6	143.9
1990	16.9	80.7	213.2	120.1	116.7	264.4	278.1	409.2	267.3	52.3	58.3	4.7
1991	50.8	45.3	96.5	128.0	221.1	270.9	353.8	292.7	189.9	57.0	6.1	61.5
1992	40.2	82.3	90.4	173.3	173.2	213.4	322.7	334.3	278.2	242.9	79.6	6.8
1993	27.3	35.4	78.3	250.6	241.1	394.0	228.0	300.6	252.1	262.9	24.8	0.0
1994	8.9	3.7	62.0	76.0	284.3	172.6	413.4	285.8	200.2	49.3	10.1	10.2
1995	0.1	22.5	66.0	178.6	188.4	106.0	104.2	230.8	147.0	86.1	30.0	99.7
1996	49.0	6.4	106.1	182.8	256.9	352.1	424.9	246.3	200.9	33.0	77.3	4.6
1997	59.0	1.7	53.1	261.6	277.7	322.4	231.0	201.6	239.5	367.1	131.1	37.6
1998	11.4	37.4	77.8	95.2	164.8	320.1	303.1	268.5	202.0	312.5	46.0	0.0
1999	2.5	0.0	29.3	67.7	233.3	215.2	258.4	260.8	225.0	302.4	3.0	1.2
2000	0.0	0.2	14.3	181.7	363.7	165.6	228.5	188.7	258.0	168.5	80.0	16.6
2001	11.7	24.8	140.9	107.4	238.0	238.3	327.6	257.6	306.3	228.8	25.4	37.3
2002	41.5	20.5	86.4	60.9	178.6	278.0	174.0	300.8	257.3	38.9	3.7	95.2
2003	11.0	36.2	112.0	126.0	25.8	310.3	370.5	299.9	283.8	52.3	19.4	19.9
2004	27.8	15.3	69.8	74.2	123.7	277.6	255.4	240.2	308.7	125.1	74.9	42.2
2005	32.6	0.0	130.5	123.1	229.6	265.1	300.6	319.4	346.6	221.8	32.9	0.0
2006	23.5	14.7	156.6	47.6	111.2	434.6	394.4	352.3	292.6	204.3	25.1	123.9
2007	20.4	26.5	96.8	108.8	213.1	221.6	314.9	320.3	225.8	186.8	5.8	0.0
2008	44.8	28.9	48.7	102.1	201.6	193.7	173.0	192.7	117.2	155.7	62.1	24.6
2009	37.9	41.5	63.9	149.8	159.0	258.1	390.9	215.2	317.0	182.9	1.5	51.7
2010	21.1	53.8	122.4	73.9	509.9	322.5	411.2	268.6	156.0	46.9	90.1	27.6
2011	37.5	25.4	48.6	130.2	160.6	246.9	158.5	160.1	216.5	27.5	96.5	38.9
2012	8.5	7.0	50.9	160.6	157.9	264.3	183.2	207.2	242.2	43.9	76.4	62.0
2013	45.4	57.1	62.7	88.7	190.3	341.7	206.6	535.7	316.8	61.3	103.6	0.0
2014	32.9	26.8	104.0	390.2	354.4	103.0	407.4	294.2	265.7	125.1	33.5	3.4

Table A.1.3: Monthly Rainfall (mm) at Sekoru station(1984-2014).

year	Jan	Feb	Mar	Apr	May	Jun	Jul	Aug	Sep	Oct	Nov	Dec
1984	2.6	7.0	19.2	15.3	300.8	412.4	269.6	213.4	179.9	13.0	13.5	21.0
1985	29.1	2.1	28.4	135.6	184.2	144.5	250.5	353.6	44.0	36.7	7.9	6.2
1986	5.2	71.5	85.4	78.7	177.0	398.7	219.6	192.0	281.3	44.1	0.0	47.5
1987	43.6	38.9	58.2	113.5	122.5	229.0	169.8	311.1	193.4	69.5	0.2	35.8
1988	20.1	73.1	47.6	100.3	92.7	184.1	276.2	272.3	251.7	130.3	13.7	0.4
1989	82.8	54.5	150.4	144.6	62.8	190.4	241.2	257.0	125.3	65.1	41.8	175.4
1990	1.4	106.0	68.1	103.0	105.1	273.1	255.3	232.4	167.5	12.2	5.2	3.0
1991	21.0	70.5	133.9	63.5	114.8	227.7	289.8	232.8	93.5	18.0	2.3	27.5
1992	77.7	89.3	49.5	94.2	157.2	264.7	258.0	312.9	141.1	90.4	87.3	13.8
1993	13.8	116.2	56.8	246.1	180.4	191.5	157.7	309.7	183.5	185.8	1.4	0.0
1994	0.0	0.0	71.1	143.7	189.5	222.6	243.4	166.0	150.4	0.0	0.0	0.0
1995	5.8	12.9	62.2	165.1	182.5	122.3	155.3	167.1	183.4	39.9	0.0	66.2
1996	61.9	4.9	194.2	172.3	213.2	244.6	314.4	209.0	150.8	37.8	12.0	2.4
1997	50.3	1.3	62.0	177.1	158.8	122.6	181.9	211.2	131.6	275.0	96.0	14.3
1998	46.6	62.1	61.9	111.6	187.0	285.0	299.0	207.9	197.1	111.5	28.0	0.2
1999	9.1	0.0	38.2	65.9	179.3	276.4	264.6	156.8	182.1	135.4	0.0	0.0
2000	0.0	0.0	18.6	149.6	123.7	132.4	150.2	187.6	165.9	162.4	34.4	12.5
2001	24.8	1.8	117.1	75.8	195.7	222.0	217.0	194.8	218.0	102.7	0.9	0.3
2002	89.9	6.7	43.1	54.2	59.0	153.7	268.6	205.8	152.3	8.9	0.0	48.3
2003	37.9	51.0	63.3	124.3	28.0	232.1	238.9	147.5	151.3	12.5	61.9	48.8
2004	49.0	26.2	37.3	149.6	63.1	130.3	181.8	279.0	152.4	82.1	17.2	23.0
2005	39.9	1.4	118.6	96.6	229.6	175.6	237.1	116.2	124.1	102.2	33.9	0.0
2006	12.0	26.0	132.2	81.5	121.5	191.9	239.2	230.3	165.4	114.7	43.6	45.6
2007	56.7	26.7	119.6	105.9	135.5	283.6	343.2	209.5	273.3	46.3	0.0	0.0
2008	53.3	2.2	23.8	103.6	263.6	169.3	249.6	239.4	184.0	102.6	109.3	27.0
2009	80.9	49.1	24.4	85.8	52.6	179.7	181.3	255.0	195.5	70.9	11.7	55.9
2010	47.0	78.3	182.9	148.4	230.2	242.4	262.0	194.3	198.3	56.2	112.5	31.0
2011	43.9	28.1	58.4	164.8	204.4	316.9	201.6	203.7	277.2	30.8	120.7	45.7
2012	0.0	0.0	67.3	78.6	64.0	339.5	233.9	170.4	261.5	1.5	9.6	75.9
2013	54.2	69.4	76.7	110.6	147.2	167.0	264.4	225.0	211.8	75.0	130.1	0.2
2014	33.5	50.6	130.6	169.7	189.1	183.0	290.5	301.2	121.5	158.1	38.7	1.2

Table A.1.4: Monthly Rainfall (mm) at Asendabo station (1984-2014).

year	Jan	Feb	Mar	Apr	May	Jun	Jul	Aug	Sep	Oct	Nov	Dec
1984	9.6	8.7	19.7	16.9	107.9	92.6	144.1	146.1	111.6	4.9	29.0	17.9
1985	10.0	38.6	55.4	145.1	185.4	86.8	235.6	161.2	78.2	42.3	14.3	4.7
1986	6.2	72.9	95.3	71.7	134.9	201.1	186.3	218.1	105.6	34.3	3.2	27.4
1987	22.1	82.9	124.4	39.5	200.7	209.5	146.6	167.6	55.0	75.2	0.0	8.9
1988	27.0	73.8	35.1	72.2	67.8	205.6	224.8	232.2	254.2	79.1	0.0	0.0
1989	25.0	78.2	130.6	102.0	118.3	109.0	198.2	234.8	76.2	108.9	4.6	69.6
1990	20.3	89.6	94.7	117.9	64.3	210.3	194.4	222.4	109.0	8.7	26.0	25.4
1991	0.6	54.3	88.9	25.3	152.3	216.1	197.7	206.1	113.0	58.1	8.0	22.7
1992	19.8	29.6	99.0	54.4	123.1	223.7	126.5	345.8	106.2	65.7	21.6	12.8
1993	33.3	97.6	84.0	197.6	132.5	231.8	178.4	136.9	113.3	144.1	10.0	0.0
1994	21.0	5.9	88.7	160.0	113.2	257.4	190.6	303.1	132.3	7.0	13.5	29.0
1995	9.4	34.4	55.9	98.6	98.1	111.4	214.6	115.0	76.5	8.4	9.2	116.5
1996	38.7	54.1	164.6	198.0	143.4	207.8	192.6	201.7	143.3	8.7	27.4	0.0
1997	38.6	0.0	29.4	153.1	138.0	202.3	237.7	203.8	108.9	249.6	146.6	10.8
1998	54.6	59.2	60.5	83.6	130.3	217.1	218.9	199.7	169.9	87.1	26.8	0.0
1999	23.5	0.0	51.8	71.1	168.9	226.6	296.4	145.1	76.3	103.3	1.9	0.3
2000	0.0	0.2	5.6	119.5	113.8	157.4	149.9	144.2	157.3	86.7	34.6	3.0
2001	30.8	22.0	103.5	162.2	242.6	261.6	197.0	235.9	91.1	121.1	8.3	5.6
2002	37.4	18.7	124.6	73.9	110.7	162.2	169.5	158.4	86.9	8.3	5.1	103.6
2003	27.2	91.5	209.3	88.3	35.8	204.5	203.9	145.2	19.4	29.7	19.4	30.8
2004	45.2	7.7	72.4	118.2	67.4	216.5	205.9	267.3	127.0	52.1	28.1	39.6
2005	29.9	1.9	97.6	166.4	185.3	99.9	175.2	135.4	176.8	66.9	13.9	0.0
2006	7.4	23.7	176.2	115.8	119.2	212.1	287.2	183.1	69.4	120.0	37.1	24.9
2007	48.6	45.4	99.6	94.3	75.5	159.0	211.8	188.7	185.3	10.9	1.7	0.0
2008	10.3	31.5	51.8	141.8	226.2	157.6	205.3	179.7	143.6	136.8	63.9	33.2
2009	28.1	33.6	117.8	99.1	50.6	154.8	161.6	287.5	119.5	84.7	9.2	87.0
2010	31.7	52.8	103.2	131.8	162.6	158.5	204.5	208.2	160.5	10.8	18.3	34.1
2011	26.0	31.5	107.7	124.9	136.6	157.0	207.6	197.1	142.5	71.7	24.0	29.9
2012	0.0	36.4	109.4	117.9	75.4	232.7	213.0	207.4	228.4	8.0	10.8	5.8
2013	15.5	38.5	98.3	118.3	121.1	240.9	264.3	294.9	181.6	69.3	6.4	9.6
2014	6.2	37.4	98.0	122.3	128.8	137.7	209.4	229.1	162.7	68.8	22.1	33.3

Table A.1.5: Monthly Rainfall (mm) at Busa station (1991-2014).

year	Jan	Feb	Mar	Apr	May	Jun	Jul	Aug	Sep	Oct	Nov	Dec
1991	42.0	31.5	100.5	137.6	161.5	255.9	257.5	254.0	139.2	116.1	26.6	47.3
1992	80.4	58.8	136.9	194.8	171.6	220.3	242.3	297.6	141.9	84.5	21.7	0.0
1993	10.0	85.0	95.6	139.0	182.5	373.3	348.0	311.7	142.4	117.2	6.7	0.0
1994	4.5	6.7	137.0	141.1	161.1	283.3	325.0	269.6	115.6	2.2	14.3	0.0
1995	7.0	52.7	55.1	141.4	94.9	211.3	164.7	183.8	123.6	17.3	16.7	108.0
1996	84.6	12.8	220.1	193.1	176.4	257.9	298.0	139.9	97.8	62.1	23.3	13.8
1997	46.1	0.0	63.5	141.6	165.7	221.4	161.9	206.0	169.6	334.4	129.8	70.6
1998	78.7	36.0	50.5	69.6	196.5	211.3	255.3	437.1	126.2	170.6	0.0	0.0
1999	24.7	0.0	45.6	80.4	143.7	268.7	264.9	186.2	196.5	140.7	0.0	0.0
2000	2.1	0.0	10.8	142.5	251.9	195.6	159.7	258.0	169.2	133.6	12.2	10.7
2001	5.8	3.2	182.3	202.3	163.8	203.8	266.8	194.0	140.3	76.5	33.6	0.0
2002	55.6	11.5	102.4	76.7	130.9	174.8	158.3	136.0	122.7	0.7	1.6	25.4
2003	24.4	56.0	46.8	106.4	38.7	225.4	350.3	419.3	176.5	47.9	31.1	15.3
2004	64.0	15.5	46.1	141.4	183.0	341.0	348.1	217.6	143.2	163.6	80.0	3.7
2005	32.5	0.0	143.8	131.7	234.6	305.4	270.8	247.1	149.9	127.8	86.1	0.0
2006	11.3	122.9	159.5	106.0	93.6	235.7	297.2	246.6	183.3	177.4	16.5	26.3
2007	36.0	37.4	143.4	92.7	125.8	204.2	345.1	195.6	208.5	22.0	0.0	0.0
2008	27.6	26.1	92.2	123.4	155.0	243.8	264.5	238.1	160.2	108.5	32.6	10.2
2009	29.0	30.8	104.4	125.0	85.5	141.3	251.1	8.6	161.7	93.7	32.6	10.2
2010	26.7	151.0	172.4	267.9	197.5	241.8	267.9	273.7	181.4	90.6	35.2	10.1
2011	35.0	37.5	104.8	112.9	130.9	234.0	285.7	213.6	163.2	92.7	35.1	11.4
2012	31.4	55.0	113.6	136.8	139.2	242.3	299.4	146.0	81.9	10.5	7.2	3.2
2013	32.8	52.7	120.8	137.6	150.7	243.4	291.3	205.1	106.3	91.6	39.8	9.0
2014	0.0	47.2	55.4	39.4	90.7	100.3	159.8	196.2	161.3	90.4	0.0	0.0

Table A.1.6: Monthly Rainfall (mm) at Dimtu station (1991-2014).

year	Jan	Feb	Mar	Apr	May	Jun	Jul	Aug	Sep	Oct	Nov	Dec
1984	5.1	4.9	28.7	33.1	210.9	240.3	213.9	259.7	104.2	2.9	19.3	14.3
1985	26.5	5.4	67.5	143.2	143.2	147.4	149.8	183.2	137.5	37.5	10.8	3.8
1986	10.4	101.4	84.7	100.7	124.1	194.4	304.7	202.1	160.4	40.2	0.9	14.3
1987	27.8	85.3	168.6	75.6	193.4	282.6	211.5	213.2	98.3	39.6	1.4	3.7
1988	23.6	59.1	26.0	48.1	42.7	110.8	333.7	181.2	178.2	57.2	0.0	0.4
1989	33.5	58.6	162.2	100.9	110.4	160.8	315.3	137.7	137.9	58.1	8.9	193.9
1990	21.2	52.5	89.6	83.6	137.5	189.4	254.8	196.2	136.1	39.3	6.9	38.4
1991	23.8	60.4	99.8	92.0	125.2	180.9	261.6	185.6	141.4	45.3	4.8	42.4
1992	23.4	69.5	105.1	83.5	122.2	186.5	280.3	186.0	142.0	46.6	3.8	48.9
1993	25.5	64.2	108.6	80.6	121.9	185.2	276.2	183.3	139.0	47.7	4.3	54.6
1994	25.2	60.7	98.5	81.5	110.0	168.9	287.0	178.3	145.8	49.0	4.8	63.1
1995	25.4	61.0	110.6	87.0	121.2	178.6	279.2	177.9	140.4	47.7	5.6	73.5
1996	24.1	61.4	102.0	84.7	123.0	181.6	273.2	184.5	140.8	45.9	5.0	53.5
1997	24.6	62.9	104.1	84.9	120.6	180.3	276.2	182.6	141.6	47.0	4.7	56.0
1998	24.7	63.3	104.8	83.7	119.8	180.2	278.7	182.1	141.6	47.3	4.7	58.3
1999	24.9	62.2	104.8	83.7	119.4	179.1	278.4	181.5	141.5	47.4	4.9	59.8
2000	1.9	0.0	19.8	211.8	196.4	281.2	309.6	494.0	172.6	144.7	45.2	7.8
2001	28.1	30.7	252.8	235.2	333.7	356.7	498.5	507.7	280.1	100.5	20.9	4.4
2002	31.5	31.8	282.0	300.6	238.2	280.5	265.0	355.0	202.6	56.5	12.7	40.0
2003	49.2	17.5	50.3	166.6	188.0	243.0	172.2	202.3	221.0	126.7	52.7	39.5
2004	49.7	0.0	114.9	88.8	96.9	218.0	178.4	347.8	230.4	89.8	10.9	34.2
2005	18.2	1.0	83.8	124.2	179.7	171.8	165.4	134.7	184.9	42.6	20.9	0.0
2006	11.0	21.7	115.4	70.5	63.6	198.8	271.7	293.9	80.6	62.8	33.3	54.4
2007	51.0	32.0	77.0	150.6	151.0	193.0	338.7	373.0	304.3	39.9	0.0	0.0
2008	35.1	17.3	120.6	150.2	152.9	217.5	231.9	284.5	204.0	69.7	21.8	28.0
2009	35.7	14.9	93.7	102.4	141.9	343.3	296.9	367.1	163.4	103.2	23.3	59.4
2010	25.0	69.6	128.5	99.8	166.6	231.3	329.9	227.0	183.9	11.9	15.1	37.3
2011	29.3	26.1	103.2	116.3	142.6	226.0	272.4	280.0	186.8	156.9	5.6	68.2
2012	31.2	30.3	106.4	115.0	136.4	235.0	290.3	304.2	187.2	74.1	16.5	41.2
2013	34.6	31.7	104.9	122.4	148.6	234.8	364.3	347.6	234.2	115.4	34.7	39.0
2014	29.5	31.7	109.5	117.7	148.2	248.0	297.6	301.7	193.2	88.5	415.3	4.2

Table A.1.7: Monthly Rainfall (mm) at Cheka station (1987-2014).

year	Jan	Feb	Mar	Apr	May	Jun	Jul	Aug	Sep	Oct	Nov	Dec
1987	42.7	80.5	91.9	159.9	141.1	252.5	281.2	315.6	212.2	58.5	21.4	0.4
1988	65.5	107.7	43.8	91.7	85.3	196.6	275.8	259.0	249.7	105.3	0.0	0.0
1989	83.0	49.1	101.5	170.4	118.2	171.0	241.8	231.4	173.1	76.7	13.3	14.5
1990	0.4	112.7	86.1	136.7	135.4	228.3	149.5	246.2	174.1	22.5	4.0	19.5
1991	12.7	73.7	105.7	10.2	143.2	259.9	303.0	459.4	141.9	0.9	0.4	23.5
1992	92.3	223.3	97.6	103.4	79.3	439.5	670.4	719.4	406.7	70.4	23.6	11.4
1993	48.8	57.0	43.1	233.3	203.6	236.3	226.8	198.7	153.8	188.1	10.8	1.6
1994	1.6	15.8	69.1	154.4	252.1	322.7	267.9	249.4	195.3	0.8	5.9	0.0
1995	4.9	49.1	47.5	229.6	141.9	103.1	166.8	204.8	162.5	42.8	8.3	46.1
1996	75.1	36.4	233.1	309.5	111.1	315.0	228.8	271.7	252.4	19.4	27.7	0.0
1997	69.1	0.0	29.3	185.8	179.4	255.9	298.1	224.0	70.7	268.9	12.3	14.1
1998	67.4	42.2	104.4	90.4	161.4	199.7	484.5	271.3	256.7	346.2	36.7	0.0
1999	15.4	0.0	41.6	108.9	175.0	172.3	279.1	331.2	291.0	213.5	0.0	0.0
2000	0.0	0.0	52.6	308.3	255.0	302.9	115.9	234.3	111.8	114.2	6.8	0.0
2001	37.3	20.1	99.4	204.5	299.7	234.3	321.7	202.3	104.7	87.8	0.0	0.0
2002	32.8	0.0	56.3	81.5	82.1	151.9	248.1	255.5	126.4	12.1	0.0	94.1
2003	66.9	73.5	57.7	132.7	5.8	255.6	330.9	254.8	94.8	5.9	50.3	48.8
2004	38.7	1.9	18.0	89.5	143.6	155.4	350.5	514.1	212.4	44.2	0.0	28.7
2005	22.0	4.9	109.1	86.8	181.5	165.2	253.9	200.9	207.0	74.9	6.5	0.0
2006	4.2	20.6	186.6	101.2	99.7	200.5	215.0	77.9	95.8	89.9	12.5	18.9
2007	37.7	92.1	78.2	28.3	104.4	143.5	147.1	160.6	199.3	25.3	12.1	18.0
2008	36.8	38.7	84.4	151.9	58.8	163.9	182.9	161.0	141.3	84.3	6.6	46.3
2009	38.4	39.8	82.7	153.0	154.7	228.4	287.8	273.2	183.8	100.3	13.3	17.6
2010	70.3	72.4	113.6	152.3	222.8	166.8	185.3	137.9	233.9	12.4	21.6	18.8
2011	34.3	27.2	84.4	151.0	150.4	210.6	261.2	242.9	169.1	95.7	12.4	20.8
2012	0.0	30.7	87.2	150.9	148.6	200.9	220.4	164.0	171.5	28.7	11.6	31.3
2013	40.4	29.4	89.5	85.5	144.0	181.0	261.9	238.4	171.9	99.7	13.7	20.4
2014	35.7	29.0	80.3	106.2	150.5	127.0	261.4	231.6	166.9	100.3	12.7	22.3

Table A.1.8: Monthly Rainfall (mm) at Kumbi station (1984-2014).

year	Jan	Feb	Mar	Apr	May	Jun	Jul	Aug	Sep	Oct	Nov	Dec
1984	6.7	10.6	32.5	5.9	284.0	253.1	189.4	133.5	74.4	0.0	8.0	15.3
1985	21.3	3.5	38.1	89.7	167.0	271.0	283.3	375.0	164.7	12.6	4.4	0.2
1986	0.0	72.5	74.7	72.8	181.2	220.2	277.9	110.9	105.5	15.6	0.0	15.2
1987	1.4	55.8	174.7	33.9	170.0	126.5	134.1	231.7	63.6	54.9	28.5	37.5
1988	45.9	78.2	15.1	45.2	63.9	255.5	579.7	329.4	279.2	205.1	0.0	0.0
1989	7.6	47.7	115.2	126.1	95.5	158.3	245.7	282.2	163.6	61.0	2.7	63.7
1990	25.7	92.9	110.5	71.4	41.5	117.6	246.2	227.0	101.2	30.8	16.2	0.0
1991	40.4	36.1	69.9	33.9	154.8	195.7	269.2	270.7	75.6	10.8	0.0	48.8
1992	49.2	0.0	128.7	96.5	26.0	208.9	186.0	114.5	43.0	99.3	16.2	15.1
1993	22.2	21.3	25.0	207.3	182.7	239.5	228.3	155.9	198.1	183.8	0.0	0.0
1994	0.2	0.0	83.1	83.8	158.4	127.5	365.7	228.5	127.2	2.4	4.2	0.0
1995	0.0	47.4	19.4	166.6	99.0	332.2	252.9	121.4	119.3	10.0	0.0	73.5
1996	60.2	12.7	208.2	124.3	171.9	216.9	311.4	210.1	96.0	23.7	32.7	2.5
1997	63.3	0.0	53.8	141.6	93.4	162.6	170.1	159.1	97.1	219.0	35.2	0.9
1998	80.7	63.6	96.3	87.5	115.6	284.3	314.7	250.2	128.1	177.6	2.1	0.0
1999	11.7	0.0	37.1	92.4	150.2	296.7	224.5	190.0	111.3	116.9	2.1	0.0
2000	0.0	0.0	0.0	89.5	126.6	178.0	225.8	322.1	120.2	55.1	30.4	17.3
2001	26.4	11.2	119.8	71.7	184.9	333.9	390.1	182.0	112.4	26.0	8.2	22.1
2002	24.2	72.2	43.0	85.0	67.6	374.8	263.4	127.3	54.1	9.7	0.0	18.8
2003	22.9	42.8	116.9	141.4	115.5	192.1	284.9	167.7	63.1	0.0	18.0	59.7
2004	25.2	0.0	0.0	61.9	6.0	310.1	262.8	314.3	80.0	7.0	3.5	4.0
2005	35.9	2.4	119.8	103.7	49.4	238.1	266.4	202.7	101.8	64.8	11.3	17.5
2006	1.2	25.7	0.0	65.9	83.4	158.4	267.7	201.1	101.8	67.1	10.9	18.7
2007	36.1	20.0	30.0	27.7	156.0	161.4	245.7	196.5	103.6	70.8	11.7	0.0
2008	27.3	21.3	63.5	103.4	117.4	240.4	271.6	201.9	107.6	68.9	11.3	15.7
2009	27.7	21.3	66.1	71.3	63.1	138.4	280.1	206.1	183.2	142.8	12.1	16.7
2010	29.5	73.2	144.7	111.3	148.2	297.4	252.5	264.5	525.0	18.2	12.0	99.1
2011	31.5	24.4	73.3	91.9	109.9	238.9	268.8	213.0	132.4	71.2	13.4	19.5
2012	0.0	25.2	64.3	89.7	105.8	240.4	265.9	213.2	134.8	74.3	12.1	251.0
2013	0.0	26.9	65.0	86.3	106.6	245.5	190.8	272.1	88.0	73.0	10.6	0.0
2014	6.0	20.0	62.9	86.2	192.3	65.5	264.1	218.3	4.9	57.7	1.6	37.3

Table A.1.9: Monthly Rainfall (mm) at Meteso station (1984-2014).

Year	Jan	Feb	Mar	Apr	May	Jun	Jul	Aug	Sep	Oct	Nov	Dec
1984	0.0	1.1	48.0	59.5	156.2	136.7	175.6	218.7	168.6	35.9	111.5	68.9
1985	22.4	15.4	96.6	248.7	130.4	294.4	198.9	269.5	160.2	91.3	31.7	18.4
1986	3.9	69.1	117.0	89.5	104.5	246.3	177.8	246.1	205.7	107.1	8.9	72.3
1987	24.0	163.2	95.4	70.0	275.4	204.9	130.3	219.1	150.9	179.2	11.8	33.3
1988	96.0	107.4	45.9	128.1	106.6	174.0	293.6	402.1	383.2	179.4	1.2	2.2
1989	49.2	95.7	113.1	179.3	169.4	146.3	240.3	222.7	156.2	100.5	14.7	167.7
1990	12.3	118.5	149.1	137.0	188.7	298.7	232.3	181.2	277.3	34.6	124.8	27.5
1991	62.3	118.8	358.9	160.8	164.1	219.3	263.5	258.1	161.4	46.7	22.7	76.5
1992	77.0	187.8	68.6	240.0	331.3	328.3	372.2	352.4	295.3	241.5	23.1	50.7
1993	83.5	81.6	85.8	331.9	162.7	323.0	424.3	315.4	327.9	239.2	36.7	2.7
1994	26.9	14.3	124.2	110.5	254.5	237.2	296.6	212.2	135.8	22.5	45.2	18.9
1995	1.5	55.3	85.5	300.3	155.5	197.5	322.4	253.5	223.0	27.4	8.5	75.7
1996	70.9	76.3	270.7	179.2	191.3	237.5	300.5	180.8	152.8	68.4	96.5	9.9
1997	99.2	4.0	92.1	95.1	267.0	236.7	241.2	334.5	148.1	394.6	250.9	45.0
1998	72.8	34.6	73.1	103.1	60.6	92.3	222.0	136.3	99.9	124.9	53.7	47.7
1999	12.4	1.8	78.7	100.5	142.9	97.1	292.0	256.9	99.2	170.2	20.8	5.6
2000	3.6	5.9	34.6	228.7	191.9	170.7	189.4	257.2	98.3	182.2	54.3	27.6
2001	21.6	35.3	160.1	165.8	201.3	233.2	387.5	287.4	107.3	114.3	11.9	13.6
2002	38.7	32.6	125.6	134.5	130.9	258.0	264.2	247.8	123.3	111.4	16.7	141.6
2003	93.7	38.8	210.5	135.8	64.5	239.4	274.7	279.7	187.9	22.4	84.6	22.1
2004	57.0	10.7	109.3	184.0	162.4	202.8	172.3	335.2	181.7	125.3	44.3	80.2
2005	41.3	29.5	207.5	162.7	223.8	161.4	317.2	233.0	258.3	102.9	12.1	0.7
2006	53.4	17.8	242.5	88.5	146.3	172.5	373.2	296.5	269.0	151.7	64.6	94.7
2007	70.1	71.3	124.0	179.3	140.5	221.3	345.0	260.0	257.6	57.1	22.3	0.0
2008	46.5	27.8	124.2	148.3	146.5	184.9	283.8	259.0	168.3	116.2	38.5	43.4
2009	43.8	27.2	129.3	152.8	155.1	194.1	289.9	271.3	175.1	115.4	37.0	42.9
2010	49.8	40.8	149.2	117.6	302.1	129.2	318.4	330.8	425.4	68.2	48.1	57.3
2011	51.6	33.2	145.8	146.9	167.3	199.7	302.6	280.1	215.4	98.5	38.0	49.7
2012	54.6	33.0	144.4	145.0	163.9	333.6	248.8	290.4	280.5	96.9	40.6	53.3
2013	56.2	33.0	146.3	146.1	167.2	203.9	292.6	283.6	241.9	95.5	43.0	44.4
2014	52.4	32.4	139.8	147.1	177.5	200.3	294.4	401.5	210.3	102.8	38.9	46.7

Table A.1.10: Monthly Rainfall (mm) at Dedo Sheki station (1984-2014).

Year	Jan	Feb	Mar	Apr	May	Jun	Jul	Aug	Sep	Oct	Nov	Dec
1984	0.0	14.4	46.6	155.1	297.7	372.3	227.5	325.0	163.7	11.2	70.2	51.7
1985	31.4	21.8	101.0	274.5	332.4	182.2	162.7	328.3	269.0	70.2	94.1	20.5
1986	12.5	74.9	83.9	55.2	127.9	273.8	277.7	192.8	158.4	127.6	10.9	66.0
1987	28.7	132.4	109.1	56.7	346.5	216.3	156.1	288.2	114.5	162.8	16.5	49.0
1988	73.7	96.5	48.7	120.1	82.7	173.3	325.9	454.5	231.7	90.5	0.0	0.0
1989	86.6	50.6	205.9	284.0	135.2	240.0	345.4	379.7	206.9	163.0	10.0	120.0
1990	66.0	113.1	176.1	61.1	218.0	253.0	247.0	281.1	392.0	29.0	118.2	21.9
1991	34.8	37.9	127.4	222.8	203.4	307.6	361.2	296.8	83.2	47.3	72.6	21.8
1992	34.4	35.3	134.7	211.0	220.7	316.7	318.4	581.6	497.0	429.3	63.3	19.2
1993	33.4	144.3	109.9	277.0	211.8	297.1	421.0	256.5	282.6	197.2	65.8	0.0
1994	1.3	18.4	152.6	260.4	249.2	290.1	599.9	380.6	271.7	4.2	31.3	20.0
1995	11.1	38.6	67.4	382.2	233.8	230.0	342.0	151.2	196.9	35.0	19.6	90.6
1996	29.5	32.4	207.8	199.9	256.8	447.1	437.6	535.6	328.9	22.4	54.5	1.5
1997	63.0	0.0	355.8	414.3	327.6	360.8	215.0	311.3	152.0	331.7	248.8	30.7
1998	86.5	20.5	83.0	237.1	96.1	307.6	327.3	299.3	217.6	208.1	39.3	0.0
1999	26.2	0.0	69.7	205.1	230.1	219.9	352.6	160.5	458.9	87.6	3.2	0.3
2000	0.0	2.4	8.9	241.3	241.5	208.2	338.3	291.6	262.7	288.6	76.5	16.6
2001	23.9	10.4	148.0	172.1	276.1	434.9	410.7	170.2	147.6	97.9	173.8	0.0
2002	10.6	30.6	85.8	40.7	112.3	259.4	192.4	165.2	181.5	60.4	18.5	31.2
2003	63.5	98.3	155.0	131.4	43.4	259.9	316.9	254.1	273.6	37.2	62.9	0.2
2004	68.7	61.3	78.1	123.8	144.8	367.7	423.3	300.1	234.1	143.2	85.9	104.1
2005	29.5	2.3	228.8	104.5	270.5	264.0	327.7	378.3	283.3	128.8	41.4	0.0
2006	25.7	44.7	170.7	216.5	181.1	212.5	463.4	232.1	181.3	100.3	69.7	28.1
2007	30.5	43.6	90.9	155.3	166.8	199.3	343.3	264.4	184.6	84.0	3.9	29.8
2008	37.6	43.2	144.2	215.1	216.7	308.0	378.7	312.4	272.3	131.3	73.5	24.5
2009	35.9	39.1	142.3	224.1	216.6	311.2	386.5	314.2	265.3	137.3	70.9	24.6
2010	36.0	39.1	143.1	224.2	217.4	311.4	387.9	315.2	276.0	142.6	70.8	24.8
2011	10.9	17.5	123.2	144.8	284.4	304.0	176.0	226.8	229.2	37.8	120.0	10.3
2012	0.0	24.8	43.3	75.3	103.7	382.8	224.5	171.8	179.4	31.9	104.7	32.1
2013	0.0	19.2	0.0	164.5	111.9	152.3	168.9	131.7	112.6	17.4	31.8	29.8
2014	68.7	31.1	134.0	193.5	205.8	312.4	345.4	284.4	249.5	117.0	79.4	22.9

Table A.1.11: Monthly Rainfall (mm) at Seka station (1984-2014).

Year	Jan	Feb	Mar	Apr	May	Jun	Jul	Aug	Sep	Oct	Nov	Dec
1984	12.7	7.6	81.1	82.3	204.6	304.3	272.5	193.4	136.2	112.7	33.2	33.2
1985	28.5	58.8	174.2	211.8	227.2	267.9	259.1	131.5	82.7	69.3	32.3	39.6
1986	3.1	91.4	93.1	88.5	169.7	361.0	187.3	216.5	207.2	49.9	29.1	55.7
1987	27.7	81.6	182.9	115.1	163.5	278.2	107.2	269.5	146.3	93.1	11.0	17.6
1988	37.5	101.0	25.3	90.6	158.9	235.7	168.3	241.5	244.9	162.5	0.0	4.4
1989	37.0	51.1	167.6	219.7	70.3	118.8	245.6	201.3	122.1	149.4	33.9	153.6
1990	31.1	65.3	120.7	181.9	132.4	173.8	210.1	305.2	237.0	110	35.3	34.1
1991	104.8	105.7	44.6	167.1	142.2	145.3	137.8	250.2	168.9	70.7	7.4	106.9
1992	27.6	155.5	58.6	87.2	219.3	208.5	291.0	280.3	321.1	267.1	121.3	62.1
1993	34.6	81.3	88.2	258.5	302.6	297.0	183.5	186.2	150.9	211.8	30.5	20.0
1994	34.5	22.0	86.6	70.0	206.7	160.0	213.9	147.1	214.2	19.9	88.2	3.2
1995	10.4	42.3	91.1	199.4	143.2	124.3	129.2	244.7	141.4	107.1	55.3	131.1
1996	34.8	27.8	33.7	226.4	262.3	257.0	237.9	199.9	267.8	432.1	106.2	110.5
1997	17.0	71.6	221.1	261.9	197.2	198.6	92.0	216.3	273.0	320.9	433.1	54.8
1998	36.9	159.8	8.1	211.0	206.9	146.0	193.6	286.6	387.8	449.0	454.6	12.4
1999	0.0	24.6	0.0	9.5	286.5	334.8	325.8	234.8	416.8	223.7	0.0	0.8
2000	1.0	23.3	72.8	204.7	496.0	455.0	205.2	243.1	282.3	244.2	162.3	13.1
2001	25.0	268.4	284.6	213.1	98.0	259.2	227.3	162.2	179.5	124.4	25.5	23.1
2002	63.1	14.3	99.0	95.4	167.5	238.9	147.6	140.1	186.0	75.5	47.2	118.8
2003	63.5	27.6	127.3	153.3	33.1	263.9	268.1	168.3	164.6	60.1	43.3	62.6
2004	35.1	42.8	63.2	125.1	107.4	137.3	207.0	192.2	109.7	90.1	37.8	37.9
2005	52.3	9.6	130.6	64.5	108.5	107.6	179.9	146.4	186.1	130.3	25.7	0.0
2006	13.5	45.5	115.8	82.2	158.2	186.8	208.4	226.7	154.1	107.4	122.8	72.7
2007	30.7	68.8	112.3	142.1	185.9	232.8	205.5	201.7	234.0	182.6	135.2	39.6
2008	32.1	68.5	101.4	130.1	184.8	236.2	216.8	200.2	230.1	168.7	105.4	38.1
2009	31.6	59.3	110.7	122.0	182.6	245.3	219.2	191.6	214.3	140.7	70.5	40.7
2010	34.8	62.8	121.8	133.2	172.2	236.3	208.5	187.2	194.1	132.4	77.6	44.7
2011	10.6	5.5	74.1	154.9	222.7	157.9	345.9	429.7	110.6	76.5	68.4	7.1
2012	0.0	40.5	105.6	120.3	152.3	216.7	463.2	379.6	340.3	12.0	39.8	0.0
2013	30.4	43.1	106.3	130.8	308.0	335.1	474.2	380.8	301.3	110.1	5.7	34.3
2014	41.5	19.4	236.3	129.1	261.3	359.2	231.6	269.4	467.6	152.1	66.2	19.3

Table A.1.12: Monthly Rainfall (mm) at Yebu station (1984-2014).

Year	Jan	Feb	Mar	Apr	May	Jun	Jul	Aug	Sep	Oct	Nov	Dec
1984	6.8	16.0	40.5	204.6	261.2	289.7	283.1	218.8	231.3	13.0	140.8	34.8
1985	17.4	12.9	49.1	197.5	217.1	218.1	224.6	248.9	194.9	51.7	23.8	11.4
1986	0.5	78.0	90.1	140.4	105.4	296.0	329.4	144.6	217.8	101.6	73.7	43.4
1987	20.5	89.2	232.0	59.1	217.1	172.0	173.0	257.5	195.7	171.2	52.1	39.1
1988	43.6	108.7	39.9	49.7	213.1	234.5	349.5	294.8	371.8	273.9	4.1	3.9
1989	13.7	59.0	136.3	156.8	92.4	209.0	228.8	198.9	148.4	188.5	33.4	131.5
1990	3.0	98.4	456.7	161.6	469.6	282.4	181.0	400.9	400.3	146.2	259.5	14.0
1991	103.8	68.1	37.7	204.3	223.7	355.1	170.4	270.7	151.1	63.4	5.4	59.3
1992	116.5	64.5	78.1	215.0	319.2	204.9	408.1	384.3	201.6	81.3	10.8	36.3
1993	46.4	80.0	238.8	337.7	439.0	281.1	374.7	421.5	363.0	187.3	44.1	57.4
1994	188.4	35.8	146.6	174.4	409.0	287.6	543.8	524.0	140.8	43.2	61.1	7.0
1995	2.5	45.8	126.9	376.4	101.2	58.3	106.8	356.2	140.9	140.3	26.7	107.6
1996	51.6	35.6	318.5	321.1	315.6	322.3	480.0	328.3	326.2	60.7	207.2	42.2
1997	184.4	12.2	207.1	306.0	202.8	362.2	311.9	563.6	160.1	516.0	403.9	129.6
1998	96.9	12.4	205.3	157.4	235.7	223.7	342.4	396.0	309.2	396.4	63.0	0.0
1999	23.1	0.0	64.3	135.2	247.3	351.5	380.6	219.5	172.5	354.6	17.0	38.8
2000	0.0	6.5	46.3	192.3	447.5	224.3	412.1	441.6	253.4	458.5	121.2	59.2
2001	13.2	38.8	155.6	164.5	359.8	394.1	414.2	198.4	146.6	94.4	50.6	21.7
2002	115.8	7.7	99.1	128.7	216.0	488.0	253.8	339.2	194.9	114.5	54.9	213.8
2003	39.2	56.2	91.1	176.7	53.3	391.9	241.1	192.7	226.3	69.7	8.5	22.2
2004	33.1	18.6	47.9	164.8	131.4	253.5	310.5	308.9	222.0	116.0	93.6	49.1
2005	31.7	6.1	179.1	171.2	191.8	164.0	186.0	257.0	262.5	105.2	63.3	0.0
2006	25.3	43.0	145.0	71.3	199.0	246.6	447.4	343.6	248.8	210.2	80.2	52.7
2007	43.3	74.3	73.5	74.7	242.0	97.4	283.6	333	61.4	47.1	16.2	8.7
2008	33.5	19.7	26.1	161.9	296.9	219.7	208.6	323.9	151.5	243.3	57.1	47.9
2009	93.8	15.2	70.5	100.5	88.4	210.5	178.1	293.2	265.0	185.7	41.4	71.7
2010	7.6	87.6	106.1	83.7	225.0	264.4	243.5	297.5	193.5	128.8	57.5	30.0
2011	82.1	1.3	134.6	84.0	145.0	121.7	314.9	323.0	209.6	180.8	74.2	52.8
2012	4.5	1.6	25.2	94.1	78.8	212.9	316.5	217.1	212.5	186.7	77.6	52.4
2013	18.6	12.1	13.0	11.7	186.0	245.2	318.4	345.3	275.0	120.8	61.3	53.2
2014	54.4	26.5	114.1	157.5	218.6	323.0	298.9	313.5	208.6	188.6	81.8	53.0

A.2 Temperature data of the stations in Gilgel Ghibe catchment

Table A.2.1: Mean Annual Temperatures data (^oc).

Year	Mean annual Temperatures (oc)																	
	Asendabo			Dedo Sheki			Jimma			Limu Genet			Sekoru			Yebu		
	Max	Min	Aver.	Max	Min	Aver.	Max	Min	Aver.	Max	Min	Aver.	Max	Min	Aver.	Max	Min	Aver.
1984	35.2	0.9	18.1	27.5	2.0	14.8	33.5	0.0	16.8				35.0	8.5	21.8	32.0	9.5	20.8
1985	34.1	3.0	18.6	27.8	1.4	14.6	33.0	0.5	16.8				35.7	4.0	19.9	30.2	10.0	20.1
1986	32.4	1.0	16.7	26.2	9.0	17.6	31.6	1.0	16.3				31.5	8.0	19.8	29.0	10.3	19.7
1987	32.0	1.2	16.6	26.0	5.0	15.5	31.6	-2.0	14.8	31.0	7.2	19.1	32.8	6.5	19.7	30.3	11.0	20.7
1988	32.4	3.4	17.9	27.4	7.5	17.5	32.5	-1.0	15.8	32.0	6.0	19.0	30.7	9.1	19.9	30.7	10.3	20.5
1989	30.2	5.0	17.6	25.0	8.0	16.5	31.8	1.9	16.9	31.0	7.6	19.3	29.5	9.9	19.7	31.5	10.3	20.9
1990	31.0	4.0	17.5	25.0	7.1	16.1	30.6	1.5	16.1	30.2	7.9	19.1	29.5	10.2	19.9	28.5	11.0	19.8
1991	32.4	0.0	16.2	25.4	7.9	16.7	31.5	0.0	15.8	32.0	7.4	19.7	31.3	10.8	21.1	28.0	10.1	19.1
1992	30.8	5.0	17.9	25.0	8.5	16.8	32.0	1.8	16.9	30.5	7.8	19.2	31.6	10.7	21.2	27.7	10.5	19.1
1993	38.5	4.0	21.3	25.2	8.3	16.7	31.5	-1.0	15.3	30.5	7.7	19.1	30.6	10.8	20.7	28.7	11.0	19.9
1994	35.2	5.1	20.2	27.4	8.7	18.1	32.6	-1.3	15.7	31.0	7.6	19.3	31.0	10.8	20.9	29.1	11.0	20.1
1995	32.7	5.2	19.0	27.4	10.0	18.7	34.0	0.8	17.4	30.7	7.7	19.2	31.1	10.8	21.0	32.5	7.5	20.0
1996	32.0	4.4	18.2	27.0	10.0	18.5	32.1	1.2	16.7	30.7	7.7	19.2	31.1	8.4	19.8	32.9	9.0	21.0
1997	32.6	1.8	17.2	27.2	1.0	14.1	33.8	-0.1	16.9	30.8	7.7	19.2	31.1	4.0	17.6	33.0	9.7	21.4
1998	32.7	5.0	18.9	26.4	8.5	17.5	33.0	0.5	16.8	31.5	7.5	19.5	31.0	7.5	19.3	32.0	9.5	20.8
1999	32.6	0.8	16.7	27.2	0.0	13.6	34.0	-1.2	16.4	32.5	7.8	20.2	31.4	6.0	18.7	31.5	8.5	20.0
2000	33.0	3.6	18.3	31.6	1.5	16.6	35.0	-0.6	17.2	33.5	6.5	20.0	31.8	8.0	19.9	32.7	1.2	17.0
2001	32.6	5.2	18.9	27.6	1.0	14.3	34.0	3.0	18.5	32.2	9.0	20.6	31.8	6.0	18.9	33.5	5.5	19.5
2002	32.5	1.0	16.8	27.0	8.0	17.5	33.5	2.0	17.8	33.2	8.5	20.9	31.6	7.2	19.4	32.5	6.4	19.5
2003	32.2	0.8	16.5	28.8	8.0	18.4	33.5	0.4	17.0	33.5	8.5	21.0	32.4	7.6	20.0	33.5	9.0	21.3
2004	32.2	1.2	16.7	27.4	6.0	16.7	33.0	1.0	17.0	32.5	8.5	20.5	31.7	9.6	20.7	33.5	9.0	21.3
2005	34.6	3.2	18.9	29.6	6.0	17.8	33.8	0.4	17.1	34.0	6.8	20.4	33.0	8.0	20.5	35.0	10.0	22.5
2006	32.6	5.2	18.9	27.0	6.6	16.8	33.0	2.8	17.9	33.0	6.0	19.5	32.2	7.0	19.6	32.5	9.5	21.0
2007	33.0	0.5	16.8	27.8	7.4	17.6	33.4	-1.5	16.0	32.0	7.5	19.8	31.7	7.0	19.4	32.4	10.1	21.3
2008	33.2	3.2	18.2	27.6	7.2	17.4	34.5	1.0	17.8	32.5	7.3	19.9	32.0	8.0	20.0	32.6	10.0	21.3
2009	33.0	0.3	16.7	27.7	7.0	17.4	32.8	2.3	17.6	33.0	9.0	21.0	32.3	9.0	20.7	32.5	9.6	21.1
2010	33.0	2.8	17.9	27.7	6.9	17.3	35.0	2.5	18.8	32.0	8.3	20.2	31.5	8.4	20.0	31.0	11.5	21.3
2011	32.6	4.0	18.3	30.0	0.5	15.3	37.6	0.0	18.8	32.8	6.3	19.5	31.3	9.3	20.3	32.6	0.0	16.3
2012	32.7	0.2	16.4	29.0	1.0	15.0	35.0	-0.6	17.2	33.5	8.6	21.1	37.5	7.0	22.3	32.6	9.9	21.3
2013	32.7	0.8	16.7	27.6	6.8	17.2	35.3	1.8	18.6	39.5	8.5	24.0	32.5	9.0	20.7	32.5	11.0	21.7
2014	32.7	1.8	17.2	28.0	6.7	17.4	34.2	3.2	18.7	33.0	8.5	20.8	31.0	9.4	20.2	32.7	10.1	21.4

Table A.2.2: Mean Monthly Temperatures data(^oc),(1984-2014).

Year	Mean annual Temperatures (oc)																	
	Asendabo			Dedo Sheki			Jimma			Limu Genet			Sekoru			Yebu		
	Max	Min	Aver.	Max	Min	Aver.	Max	Min	Aver.	Max	Min	Aver.	Max	Min	Aver.	Max	Min	Aver.
Jan	31	5.3	18.2	24.7	9.4	17.1	31	2.5	16.8	30.5	9.1	19.8	29.6	10.5	20	29.6	10.4	20
Feb	31.8	7.7	19.8	26.9	9.5	18.2	32.4	3.9	18.1	29.9	10.3	20.1	31	11.2	21.1	30.9	11.5	21.2
Mar	32.3	9.2	20.7	26.8	9.4	18.1	32.6	6.1	19.3	31.8	11.3	21.5	31.2	11.2	21.2	31.2	11.1	21.2
Apr	31.4	9.9	20.7	25.9	8.9	17.4	31.7	8.6	20.2	29.9	12	20.9	30.8	10.9	20.8	30.2	11.7	21
May	30.4	10.8	20.6	25.4	9.7	17.6	31	9.9	20.4	30	12.2	21.1	29.9	11.2	20.5	29.3	11.4	20.4
Jun	28.5	10.7	19.6	24.1	9.1	16.6	28.8	11.1	19.9	25.5	10.2	17.8	27.5	10.4	19	27.8	11.3	19.5
Jul	26.9	11	19	22.9	9.1	16	27.9	11	19.4	25.1	11.5	18.3	25.8	10.5	18.1	26.4	11	18.7
Aug	26.8	10.7	18.8	23.1	9.1	16.1	27.8	11.4	19.6	26.7	11.4	19	25.5	10.4	18	26.6	11.1	18.9
Sep	27.4	9.8	18.6	23.5	8.9	16.2	28.2	10.9	19.6	27.2	11	19.1	26.3	10.2	18.2	27.2	11.2	19.2
Oct	28.5	6.7	17.6	24.4	9.4	16.9	28.1	6.5	17.3	28	9.9	19	27.3	10.3	18.8	27.9	10.6	19.3
Nov	29.4	4.6	17	25.2	9.4	17.3	29.4	4.1	16.7	28.7	8.6	18.6	28	9.9	18.9	28.6	10.8	19.7
Dec	30.1	4.5	17.3	25.7	8.2	17	29.8	2.6	16.2	29.8	8.1	18.9	28.4	9.6	19	28.9	10.7	19.8

A.3 Discharge data of the stations in Gilgel Ghibe catchment

Table A.3.1: Monthly discharge (m^3/s) at Gilgel Ghibe Nr. Assendabo station (1984-2013).

Year	Jan	Feb	Mar	Apr	May	Jun	Jul	Aug	Sep	Oct	Nov	Dec
1984	15.53	6.21	3.95	6.26	15.47	77.44	143.86	152.88	128.33	32.15	14.56	10.51
1985	4.22	3.05	1.98	9.24	24.39	60.05	121.80	193.10	150.22	60.54	20.95	9.92
1986	3.51	4.26	6.59	5.92	7.22	56.32	122.73	115.79	142.58	54.34	16.92	11.59
1987	5.39	3.61	12.35	9.07	26.27	68.22	94.24	100.59	126.46	58.40	25.13	10.63
1988	6.53	6.85	2.73	2.39	5.69	17.70	92.28	258.55	202.33	156.45	33.82	12.21
1989	7.85	8.26	5.81	34.60	18.84	44.93	86.13	126.58	128.60	68.51	24.65	28.26
1990	13.48	10.66	15.89	14.69	26.91	80.07	150.88	125.71	199.44	296.47	153.91	15.67
1991	10.31	8.68	12.17	7.31	17.36	57.03	110.88	186.91	139.64	33.41	5.08	4.31
1992	1.05	2.33	0.22	2.12	19.65	69.56	141.23	310.40	196.18	123.42	32.81	12.78
1993	11.99	17.47	7.36	33.35	87.94	128.46	211.58	196.84	139.17	99.74	54.72	16.79
1994	8.51	5.25	7.14	8.22	35.32	116.09	215.92	278.40	206.19	44.93	18.62	9.61
1995	5.34	5.03	4.16	13.30	19.42	24.99	74.42	107.12	129.49	30.87	13.11	10.22
1996	10.61	7.81	8.12	8.32	70.99	149.34	140.00	204.89	148.70	76.55	28.41	14.63
1997	15.69	20.67	4.00	28.18	43.13	115.98	115.53	173.31	118.54	220.19	229.29	88.36
1998	45.30	26.60	26.85	19.31	34.23	49.56	140.52	285.05	164.28	140.10	56.22	24.61
1999	17.52	9.61	11.96	9.91	27.14	58.21	130.31	177.95	97.52	118.82	42.58	18.03
2000	10.41	6.06	3.90	11.91	32.58	48.79	103.03	135.54	143.78	123.57	59.79	25.16
2001	37.56	38.61	40.42	39.26	59.84	110.77	192.48	174.44	126.89	81.63	48.75	82.15
2002	16.02	9.63	11.84	15.94	11.68	48.62	94.59	125.10	100.27	35.87	20.86	20.65
2003	17.41	8.64	14.75	16.39	9.40	39.79	132.58	139.41	154.87	50.40	20.86	16.21
2004	9.14	7.38	9.51	11.43	33.91	53.85	94.80	124.71	123.82	115.88	27.82	20.20
2005	12.23	7.72	26.23	17.39	67.10	53.85	108.98	169.08	192.43	89.16	27.28	13.04
2006	11.43	12.23	14.30	20.20	25.18	61.40	218.94	255.70	145.85	78.24	49.87	39.80
2007	24.67	29.44	15.60	33.91	49.22	72.97	133.76	163.17	198.68	148.69	23.14	11.82
2008	9.89	7.72	4.55	13.88	28.89	60.00	113.28	152.50	119.39	63.51	101.39	19.25
2009	20.20	14.73	10.65	16.49	15.60	25.18	72.22	164.15	119.39	100.56	24.16	24.16
2010	13.88	10.65	13.46	17.85	55.19	123.82	182.15	177.08	269.54	90.76	21.65	29.44
2011	13.04	9.51	11.04	11.04	29.44	75.21	103.06	147.74	179.11	80.54	41.63	14.30
2012	8.07	5.14	5.14	13.04	13.04	70.75	128.31	186.24	170.08	105.58	21.16	15.60
2013	12.23	6.38	13.04	14.73	39.80	70.75	108.98	198.68	176.08	137.45	29.44	17.39

Table A.3.2: Monthly discharge (m^3/s) at Ghibe Nr. Seka station (1984-2013).

Year	Jan	Feb	Mar	Apr	May	Jun	Jul	Aug	Sep	Oct	Nov	Dec
1984	1.32	0.95	0.79	0.87	1.24	5.97	14.17	15.13	12.08	4.04	3.64	1.92
1985	1.02	0.77	0.65	1.59	3.08	10.72	15.98	17.49	14.35	5.16	2.75	1.58
1986	0.87	1.04	1.59	1.46	1.80	9.81	12.71	13.49	18.66	6.97	2.80	1.82
1987	1.11	1.05	2.45	1.71	4.27	11.32	16.26	15.70	18.19	9.38	4.15	2.32
1988	1.82	1.79	1.19	0.92	2.21	6.08	16.85	21.40	21.33	20.41	4.05	1.77
1989	1.30	1.29	1.17	2.13	1.85	5.45	16.21	16.51	15.18	7.87	3.39	5.52
1990	2.42	2.29	3.61	3.68	5.02	12.41	15.91	23.05	23.08	9.84	3.87	2.18
1991	1.82	1.46	1.26	1.97	3.39	8.52	14.57	18.64	17.07	5.29	2.46	2.00
1992	1.53	1.67	1.27	1.59	4.25	11.48	18.61	17.36	18.31	14.48	4.40	2.75
1993	2.36	1.97	1.27	3.46	13.13	15.60	23.21	16.32	15.84	10.25	4.87	2.25
1994	1.59	1.03	1.14	1.07	3.25	15.22	19.98	19.95	19.17	4.46	2.48	1.35
1995	0.80	0.68	0.65	3.09	4.08	6.21	11.25	13.18	14.55	6.41	3.07	3.34
1996	1.54	1.53	1.53	1.73	1.82	16.97	14.19	16.62	18.73	7.96	3.68	2.26
1997	1.71	0.97	1.30	3.09	4.74	13.49	12.14	14.38	9.44	17.90	17.78	7.85
1998	4.95	2.66	3.96	2.17	3.64	7.94	11.75	17.56	12.09	16.09	5.07	2.28
1999	1.48	0.86	1.01	1.20	3.44	5.89	11.69	13.19	9.52	9.75	3.44	2.36
2000	1.03	1.57	0.54	1.95	5.83	9.20	19.25	18.43	19.33	23.65	5.78	2.65
2001	4.40	4.48	4.41	4.11	5.44	13.92	24.19	16.15	10.89	14.11	6.45	4.69
2002	2.05	0.96	1.12	1.54	0.93	8.37	11.51	17.69	16.40	5.18	2.35	2.68
2003	1.38	1.06	1.29	2.38	1.17	14.69	21.11	16.44	21.29	3.85	2.17	1.34
2004	0.96	0.61	0.67	2.87	2.69	4.76	15.41	29.19	27.84	27.18	2.33	1.51
2005	0.61	0.14	1.99	4.99	13.67	12.33	21.08	25.23	35.29	11.68	4.65	2.87
2006	2.33	2.69	2.87	2.25	4.13	10.29	16.27	17.87	17.67	11.00	4.35	2.70
2007	1.78	1.48	1.68	2.32	4.26	10.49	16.37	17.99	17.92	11.31	4.38	2.73
2008	1.81	1.51	1.73	2.35	4.32	10.47	16.39	18.02	18.08	11.59	4.45	2.78
2009	1.85	1.53	1.73	2.39	4.43	10.50	16.55	18.22	18.05	11.80	4.53	2.83
2010	1.89	1.56	1.70	2.42	4.44	10.47	16.57	18.34	18.05	11.91	4.55	2.85
2011	1.89	1.55	1.72	2.49	4.54	10.67	16.55	18.20	17.90	11.53	4.57	2.90
2012	1.92	1.56	1.75	2.50	4.66	10.90	16.57	18.27	18.02	11.69	4.62	2.78
2013	1.90	1.52	1.66	2.45	4.65	10.84	16.60	18.06	17.79	11.78	4.66	2.81

Table A.3.3: Monthly discharge (m^3/s) at Aweitu Nr. Babu station (1988-2010).

Year	Jan	Feb	Mar	Apr	May	Jun	Jul	Aug	Sep	Oct	Nov	Dec
1988	0.92	0.76	1.15	1.51	4.11	17.50	13.54	41.16	20.21	6.86	2.61	2.03
1989	1.51	1.34	1.68	2.28	5.22	22.40	13.72	26.43	23.86	6.23	4.35	5.43
1990	1.34	0.99	2.07	1.97	1.59	8.57	11.11	46.96	20.36	6.89	0.92	0.70
1991	0.43	0.36	0.55	0.92	2.28	33.96	18.21	65.34	21.45	8.07	0.81	0.30
1992	0.39	0.36	0.30	0.86	7.34	5.05	11.11	25.91	15.17	6.23	4.35	1.68
1993	0.81	0.70	0.55	0.60	9.65	42.01	27.51	23.36	23.86	6.45	4.19	4.19
1994	0.84	0.36	0.51	4.22	2.75	14.43	30.34	73.25	20.98	11.11	1.59	0.24
1995	0.30	0.33	0.60	9.37	4.19	3.57	3.87	10.80	11.11	20.77	14.82	2.04
1996	0.91	0.43	1.10	1.84	3.28	9.35	13.29	39.21	25.91	6.66	4.19	1.68
1997	1.19	0.51	0.51	4.52	6.45	22.87	26.43	22.87	15.54	60.68	40.59	9.65
1998	0.96	0.52	2.78	1.15	2.34	4.01	7.91	11.82	10.99	8.25	8.27	1.39
1999	0.86	0.44	0.73	0.61	1.66	6.10	9.80	12.91	7.56	7.48	6.21	4.24
2000	0.61	0.26	0.39	1.08	2.67	4.42	9.01	12.47	14.03	12.69	6.21	2.89
2001	1.23	1.00	1.75	1.15	2.89	7.56	13.58	9.78	11.40	10.78	3.62	1.15
2002	1.15	0.39	1.23	0.73	2.67	7.73	7.21	8.64	8.09	2.03	0.86	1.31
2003	1.23	0.49	0.93	2.24	0.44	4.70	9.39	11.82	9.59	4.42	6.09	2.29
2004	0.86	0.54	0.99	2.06	3.50	12.60	13.30	26.04	15.30	10.92	6.45	2.42
2005	0.86	0.53	0.98	2.09	3.47	12.31	13.28	25.15	15.01	11.16	6.68	2.45
2006	0.82	0.48	0.94	2.08	3.36	11.72	1.54	1.68	1.56	11.45	6.82	2.27
2007	0.79	0.45	0.87	2.09	3.47	11.91	12.69	22.41	13.38	11.71	7.16	2.36
2008	0.81	0.46	0.89	2.16	3.54	10.61	12.37	19.89	12.91	11.93	7.54	2.49
2009	0.84	0.47	0.93	2.23	3.31	10.94	12.44	19.54	12.78	12.26	7.72	2.53
2010	0.84	0.45	0.95	2.33	2.94	9.11	11.56	19.31	12.13	12.61	7.93	2.44

Table A.3.4: Monthly discharge (m^3/s) at Ghibe Nr. Limu Genet station (1984-2010).

Year	Jan	Feb	Mar	Apr	May	Jun	Jul	Aug	Sep	Oct	Nov	Dec
1984	2.74	1.80	1.07	0.95	3.75	30.81	35.72	35.00	31.52	8.00	2.74	2.07
1985	0.83	0.57	0.87	1.94	6.63	26.97	32.00	36.87	34.42	16.62	3.96	2.07
1986	0.87	1.58	1.49	2.40	0.91	19.91	35.15	35.15	44.93	36.21	10.12	1.89
1987	0.80	1.03	2.84	2.17	2.21	15.09	25.20	37.53	37.04	16.55	11.66	4.07
1988	1.31	1.25	1.57	1.86	3.38	11.40	35.89	42.21	41.03	40.19	7.12	2.53
1989	2.12	1.62	1.11	5.15	2.89	10.82	31.84	33.12	39.52	22.04	4.66	9.55
1990	2.99	3.39	4.01	3.14	4.60	16.62	35.40	41.54	42.55	37.86	7.58	3.34
1991	7.52	1.85	2.99	3.55	7.70	15.50	30.88	42.89	38.69	16.76	3.39	2.64
1992	1.58	2.03	2.42	3.42	4.64	13.59	33.50	39.94	40.45	29.21	10.50	4.44
1993	2.07	1.76	1.19	9.80	12.39	43.74	43.48	41.20	39.36	39.94	6.53	4.99
1994	3.54	1.30	1.47	2.42	5.04	18.55	49.67	58.21	51.06	18.74	3.64	2.16
1995	1.33	1.73	2.02	4.59	3.24	10.98	19.40	40.89	51.20	13.81	3.39	2.42
1996	2.13	1.70	1.78	5.06	6.33	21.71	36.52	45.06	52.18	30.01	7.39	3.49
1997	2.59	1.61	1.00	5.98	12.24	46.27	51.90	38.49	29.79	58.50	51.34	29.33
1998	6.61	2.77	3.74	1.58	3.94	9.92	40.13	52.88	50.23	52.88	29.90	4.53
1999	2.33	1.58	1.43	1.51	3.89	22.22	36.99	44.33	45.85	38.80	23.00	9.94
2000	3.41	1.92	1.99	3.53	6.60	25.03	41.38	45.19	44.51	45.05	27.91	11.82
2001	3.74	1.97	2.04	3.15	6.67	25.86	42.60	45.22	42.59	48.81	33.04	13.91
2002	4.02	2.06	2.30	2.44	5.28	9.19	40.27	46.91	45.79	46.39	28.46	10.05
2003	3.38	1.88	1.94	2.66	5.61	6.99	22.67	23.08	39.88	16.24	2.08	1.47
2004	0.83	0.71	0.61	0.71	6.04	16.77	36.73	40.10	43.19	39.12	22.87	9.31
2005	2.99	1.66	1.72	2.24	5.90	14.70	35.57	38.83	42.86	37.64	21.61	8.69
2006	2.80	1.58	1.64	2.01	5.71	11.91	33.81	37.23	42.93	34.85	18.76	7.38
2007	2.50	1.46	1.48	1.91	5.81	12.59	32.20	34.81	42.22	31.96	16.33	6.71
2008	2.28	1.35	1.36	1.72	5.86	13.99	34.58	37.74	42.80	35.89	19.89	8.02
2009	2.64	1.51	1.55	1.97	5.82	13.30	34.04	37.15	42.70	35.09	19.15	7.70
2010	2.56	1.47	1.51	1.90	5.80	12.95	33.66	36.74	42.66	34.45	18.53	7.45

Table A.3.5: Monthly discharge (m^3/s) at Kitto Nr. Jimma station (1982-2010).

Year	Jan	Feb	Mar	Apr	May	Jun	Jul	Aug	Sep	Oct	Nov	Dec
1982	0.27	0.15	0.18	0.27	0.47	0.88	0.97	1.77	1.37	1.57	1.76	1.25
1983	0.87	0.88	0.93	0.90	1.11	0.98	2.00	3.96	2.21	1.82	0.47	1.21
1984	0.54	0.51	0.49	0.60	0.74	3.87	1.40	1.60	1.94	1.35	1.21	1.16
1985	1.07	1.07	1.14	1.43	1.52	1.92	2.31	2.52	3.08	2.41	1.74	1.56
1986	1.28	1.16	1.01	0.90	1.10	2.07	2.75	1.44	1.86	1.41	0.68	0.45
1987	0.33	0.25	0.28	0.25	0.33	0.76	1.78	1.26	1.49	1.19	1.14	1.00
1988	0.98	1.03	1.42	1.36	1.59	2.26	2.78	3.68	4.28	3.65	2.57	1.88
1989	1.77	1.73	1.93	1.93	1.44	1.71	2.46	2.56	2.56	9.82	7.70	3.31
1990	2.56	2.41	2.49	2.12	2.47	2.89	4.08	3.87	3.21	2.37	0.70	0.54
1991	0.26	0.14	0.35	0.71	1.57	1.93	2.28	2.52	2.40	2.58	1.52	1.22
1992	1.08	1.02	1.11	0.71	1.57	2.04	2.43	2.60	2.40	2.58	1.52	1.22
1993	1.01	1.13	1.07	1.35	1.98	2.88	4.20	3.00	2.62	2.42	2.03	1.23
1994	0.98	0.86	0.72	1.19	1.51	2.05	2.79	2.67	2.95	1.89	0.94	0.73
1995	0.72	0.38	0.54	0.90	0.93	0.97	1.37	1.31	1.92	0.98	0.77	0.36
1996	1.08	0.99	1.10	1.17	1.49	1.94	2.69	2.61	2.26	1.52	1.13	0.66
1997	0.53	0.45	0.26	0.45	0.69	0.84	1.59	2.75	2.73	3.09	3.33	8.70
1998	0.97	0.60	0.24	0.23	0.24	0.54	1.14	4.29	1.79	1.48	0.88	0.44
1999	0.23	0.16	0.16	0.26	0.50	0.82	1.01	2.00	1.00	2.10	1.05	0.95
2000	0.98	0.38	0.49	0.85	3.40	1.16	2.39	0.79	1.17	0.64	1.46	1.72
2001	0.84	0.66	0.63	0.79	1.37	1.47	2.18	2.45	2.09	1.86	1.46	1.78
2002	0.45	0.27	0.18	0.26	1.34	1.31	1.41	2.34	2.18	2.05	0.70	0.99
2003	0.55	0.55	0.61	1.00	0.59	1.56	1.60	1.66	2.46	1.33	1.13	1.14
2004	0.70	0.69	0.50	0.69	0.76	1.11	3.03	1.15	1.45	0.47	0.18	0.19
2005	0.12	0.09	0.15	0.08	0.08	0.70	1.36	1.70	3.04	1.47	1.01	0.56
2006	0.60	0.43	0.36	0.51	1.00	1.06	1.74	2.13	1.99	1.61	1.24	1.83
2007	0.60	0.43	0.37	0.52	1.03	1.08	1.76	2.06	1.91	1.44	1.01	1.07
2008	0.56	0.41	0.38	0.55	1.12	1.14	1.83	1.81	1.92	1.44	1.03	1.14
2009	0.60	0.43	0.41	0.58	1.19	1.18	1.92	1.79	2.02	1.37	1.02	1.16
2010	0.56	0.44	0.40	0.55	0.94	1.18	1.87	1.90	2.12	1.45	0.98	1.09

Table A.3.6: Monthly discharge (m^3/s) at Aweitu Nr. Jimma station (1982-2010).

Year	Jan	Feb	Mar	Apr	May	Jun	Jul	Aug	Sep	Oct	Nov	Dec
1982	0.35	0.13	0.03	0.13	1.00	3.43	3.32	5.09	6.17	3.04	1.32	0.37
1983	0.72	0.16	0.24	0.80	1.58	0.13	5.53	7.99	6.30	4.97	0.84	0.42
1984	0.45	0.15	0.08	0.08	0.13	0.80	3.77	5.53	5.47	0.53	0.36	0.36
1985	0.18	0.13	0.18	0.27	0.30	6.44	7.24	7.52	6.90	1.71	0.96	0.11
1986	0.03	0.06	0.08	0.45	0.18	5.47	7.58	7.58	7.85	1.12	0.80	0.57
1987	0.06	0.08	0.57	0.13	0.57	2.46	5.91	7.58	7.72	3.32	1.12	0.64
1988	0.18	0.24	0.24	0.13	0.43	4.84	7.44	8.13	8.27	4.56	1.09	1.25
1989	0.08	0.04	0.37	5.29	1.31	7.22	17.47	8.23	13.96	5.79	1.07	1.85
1990	0.35	0.50	4.16	4.83	10.22	12.16	11.39	12.04	13.37	6.91	2.75	0.36
1991	0.15	0.41	0.97	2.95	13.30	16.42	20.42	17.52	26.45	4.07	0.51	0.32
1992	0.20	0.29	0.17	0.78	5.42	10.11	12.61	19.51	14.19	27.14	3.06	1.29
1993	0.53	1.21	0.60	7.00	20.54	17.73	8.05	5.72	9.15	3.99	1.36	0.26
1994	0.14	0.11	0.11	0.31	7.02	20.91	28.24	23.67	18.91	2.27	2.73	0.56
1995	0.10	0.08	0.15	0.63	1.65	1.84	6.36	7.40	20.33	5.35	0.32	0.33
1996	0.38	0.11	0.51	8.60	17.01	27.01	8.71	10.85	19.13	8.65	0.45	0.23
1997	0.57	0.10	0.88	1.62	5.00	20.07	15.68	4.63	4.75	38.18	19.93	16.53
1998	5.88	0.90	0.51	2.86	11.40	14.86	15.02	35.59	17.58	23.17	5.25	0.35
1999	0.11	0.07	0.11	1.29	3.25	5.09	5.01	8.90	4.83	8.69	1.29	0.26
2000	0.32	0.25	0.25	0.37	0.61	1.13	1.36	2.92	4.37	1.67	1.40	0.60
2001	0.21	0.19	0.19	0.30	0.33	0.83	3.93	3.65	2.39	5.28	0.44	0.20
2002	0.21	0.11	0.16	0.13	0.11	0.50	2.99	6.83	3.04	0.39	0.19	0.21
2003	0.21	0.10	0.16	0.48	0.13	1.32	2.09	0.89	1.35	0.60	0.18	0.12
2004	0.11	0.09	0.09	0.84	1.48	0.30	1.16	1.74	1.30	0.39	0.19	0.14
2005	0.22	0.11	0.13	0.51	1.97	0.89	6.03	3.56	9.16	2.15	0.27	0.15
2006	0.14	0.11	0.37	3.26	4.16	7.90	8.05	9.22	8.93	8.07	2.72	1.64
2007	0.70	0.19	0.29	1.74	3.92	6.81	6.37	8.02	8.10	8.55	2.72	1.73
2008	0.76	0.19	0.31	1.83	4.11	7.22	6.37	8.07	7.08	8.82	2.92	1.85
2009	0.79	0.20	0.29	1.27	3.04	5.58	6.17	7.83	6.07	8.83	3.12	1.98
2010	0.80	0.21	0.24	1.24	2.88	4.37	5.38	8.10	6.18	6.38	1.72	0.77

Table A.3.7: Monthly discharge (m^3/s) at Bulbul Nr. Serbo station (1986-2010).

Year	Jan	Feb	Mar	Apr	May	Jun	Jul	Aug	Sep	Oct	Nov	Dec
1986	3.02	3.42	3.26	3.59	4.01	27.29	34.86	32.17	34.86	16.16	3.10	1.98
1987	1.52	0.80	2.14	1.45	2.14	6.52	18.55	32.37	32.17	11.50	5.73	1.98
1988	0.94	0.87	0.52	0.04	1.08	2.45	32.17	34.86	34.86	34.86	5.99	1.83
1989	0.73	0.80	0.66	3.84	1.98	6.97	34.10	33.89	34.32	12.07	2.37	3.92
1990	2.61	1.90	2.29	1.98	2.06	14.39	25.51	33.46	32.92	15.57	4.09	2.61
1991	2.29	1.56	1.77	2.18	2.25	11.53	29.04	34.86	34.64	4.43	2.29	1.15
1992	1.30	1.01	0.87	1.60	7.06	34.86	33.67	41.19	36.16	22.72	13.03	12.07
1993	1.67	1.90	1.37	2.29	9.53	24.27	34.86	28.24	25.31	24.47	35.73	4.32
1994	1.83	1.43	1.39	2.38	6.34	15.96	34.21	35.94	35.29	20.66	1.82	4.82
1995	0.59	0.72	1.00	6.97	6.31	4.37	4.15	34.74	32.86	17.57	4.59	5.04
1996	1.54	1.32	1.28	3.08	6.30	18.20	27.19	34.99	23.13	8.16	2.27	1.36
1997	1.36	1.10	0.39	1.47	4.08	26.34	36.51	35.19	18.26	36.77	36.77	23.13
1998	3.38	3.45	1.80	1.47	3.31	8.43	26.10	36.77	36.77	34.66	6.14	2.21
1999	43.59	0.81	1.15	1.05	3.11	23.48	36.77	36.77	20.60	40.14	13.23	3.58
2000	1.05	0.59	0.47	1.15	7.47	15.28	18.70	30.93	32.33	21.40	10.24	2.97
2001	1.58	1.15	2.03	2.46	6.31	18.35	39.73	44.14	37.44	19.81	9.59	3.72
2002	1.80	1.41	1.17	0.93	0.53	7.34	34.09	126.00	34.09	1.95	1.14	2.13
2003	0.74	0.87	1.14	0.80	0.38	4.52	65.04	106.77	71.27	20.30	2.52	1.00
2004	0.74	0.43	0.43	0.69	1.77	31.20	69.02	117.91	89.48	99.27	4.26	2.04
2005	1.68	0.74	1.52	0.87	2.95	4.13	21.89	100.32	141.04	111.72	3.88	1.44
2006	1.31	0.92	1.26	1.15	2.39	13.11	45.95	99.03	74.66	50.61	4.28	2.07
2007	1.26	0.87	1.10	0.89	1.60	12.06	47.20	110.01	82.11	56.77	3.21	1.73
2008	1.15	0.77	1.09	0.88	1.82	13.00	49.82	106.81	91.71	67.73	3.63	1.65
2009	1.23	0.75	1.08	0.89	2.10	14.70	46.77	106.81	95.80	77.22	3.85	1.79
2010	1.32	0.81	1.21	0.94	2.17	11.40	42.33	104.60	97.07	72.81	3.77	1.74

Table A.3.8: Monthly discharge (m^3/s) at Bidru Awana Nr. Sekoru station (1981-2010).

Year	Jan	Feb	Mar	Apr	May	Jun	Jul	Aug	Sep	Oct	Nov	Dec
1981	0.03	0.01	0.11	0.09	0.04	0.14	3.16	2.21	3.44	1.72	0.44	0.31
1982	0.30	0.28	0.33	0.54	1.28	3.41	4.33	5.71	4.13	1.71	0.45	0.30
1983	0.09	0.18	0.09	0.18	0.87	4.04	2.49	5.21	2.13	4.66	0.35	0.38
1984	0.92	1.08	0.11	0.09	4.52	0.98	1.29	5.82	2.64	0.32	0.07	0.06
1985	0.04	0.19	0.33	0.66	0.98	6.55	2.21	6.24	3.71	1.77	0.06	0.27
1986	0.09	0.26	0.16	1.62	1.43	6.20	4.37	6.20	6.34	1.32	0.23	0.12
1987	0.06	0.04	0.21	0.10	0.98	1.23	6.02	6.59	3.25	1.14	0.28	0.20
1988	0.11	0.11	0.38	0.17	0.17	0.11	1.89	4.72	4.17	2.60	0.51	0.31
1989	0.90	0.29	0.50	1.71	1.36	3.80	3.00	5.67	4.86	1.20	0.27	0.64
1990	0.45	0.32	0.57	0.36	0.62	1.33	3.25	7.85	1.17	0.54	0.17	0.04
1991	0.02	0.07	0.75	0.23	1.29	1.63	1.19	6.87	2.02	1.98	1.98	0.78
1992	0.26	0.24	0.17	0.24	0.59	8.22	17.60	1.96	10.99	1.56	0.53	0.22
1993	0.18	0.21	0.17	1.44	1.21	1.77	5.94	6.86	9.47	1.15	0.38	0.17
1994	0.12	0.09	0.17	0.20	0.45	1.40	0.98	18.59	2.36	0.38	0.19	0.15
1995	0.24	0.22	0.26	0.57	1.68	0.59	0.84	4.35	8.22	0.36	0.11	0.08
1996	0.31	0.21	0.37	0.68	4.68	5.94	15.53	11.58	14.65	0.84	0.27	0.22
1997	0.22	0.17	0.22	1.29	0.36	8.10	1.82	1.77	4.59	4.85	0.68	0.47
1998	0.36	0.36	0.30	0.47	4.68	0.90	14.82	18.59	8.83	8.58	0.49	0.29
1999	0.16	0.12	0.12	0.12	0.18	0.51	3.33	7.86	0.40	1.86	0.20	0.10
2000	0.08	0.06	0.04	0.16	0.51	0.47	0.33	0.78	9.08	2.57	0.33	0.21
2001	0.21	0.35	0.38	0.40	1.32	6.14	1.02	0.55	19.21	3.33	0.40	0.27
2002	0.05	0.04	0.05	0.05	0.03	0.43	0.36	2.82	3.89	0.09	0.05	0.04
2003	0.03	0.03	0.02	0.53	0.03	1.77	27.36	2.82	10.14	0.07	0.03	0.05
2004	0.05	0.04	0.06	0.76	0.13	0.09	4.43	10.99	6.34	7.98	0.35	0.26
2005	0.24	0.17	0.27	5.94	5.20	0.90	0.64	19.63	3.19	0.78	0.33	0.32
2006	0.12	0.11	0.14	1.14	1.06	1.47	5.35	6.49	7.46	2.38	0.24	0.18
2007	0.11	0.11	0.14	1.28	1.18	1.61	5.64	6.30	8.47	2.46	0.25	0.19
2008	0.12	0.12	0.15	1.44	1.28	1.77	6.40	7.08	8.39	2.44	0.24	0.19
2009	0.10	0.09	0.12	1.59	1.27	1.15	7.17	8.02	6.84	2.32	0.21	0.17
2010	0.11	0.10	0.13	1.81	1.45	1.25	8.14	8.76	7.26	2.63	0.24	0.19

A.4 Annual Maximum (AM) flood data for the stations in Gilgel Ghibe & Upper Awash catchments

Table A.4.1: AM flood (m^3/s) for the stations in Gilgel Ghibe catchment.

Year	Annual maximum Discharge(m^3/s)							
	GILGEL GHIBE NR. ASEND-ABO	GHIBE NR SEKA	Awiatu Nr, Babu	Ghibe Nr. Limu Genet	KITO Nr JIMMA	AWAITU AT JIMMA	BULBUL Nr. SERBO	BIDRU AWANA Nr. SOKURU
1981								3.44
1982					1.77	6.17		5.71
1983					3.96	7.99		5.21
1984	152.88	15.13		35.72	3.87	5.53		5.82
1985	193.10	17.49		36.87	3.08	7.52		6.55
1986	142.58	18.66		44.93	2.75	7.85	34.86	6.34
1987	126.46	18.19		37.53	1.78	7.72	32.37	6.59
1988	258.55	21.40	41.16	42.21	4.28	8.27	34.86	4.72
1989	128.60	16.51	26.43	39.52	9.82	17.47	34.32	5.67
1990	296.47	23.08	46.96	42.55	4.08	13.37	33.46	7.85
1991	186.91	18.64	65.34	42.89	2.58	26.45	34.86	6.87
1992	310.40	18.61	25.91	40.45	2.6	27.14	41.19	17.60
1993	211.58	23.21	42.01	43.74	4.2	20.54	35.73	9.47
1994	278.40	19.98	73.25	58.21	2.95	28.24	35.94	18.59
1995	129.49	14.55	20.77	51.2	1.92	20.33	34.74	8.22
1996	204.89	18.73	39.21	52.18	2.69	27.01	34.99	15.53
1997	229.29	17.90	60.68	58.5	8.7	38.18	36.77	8.10
1998	285.05	17.56	11.82	52.88	4.29	35.59	36.77	18.59
1999	177.95	13.19	12.91	45.85	2.1	8.9	43.59	7.86
2000	143.78	23.65	14.03	45.19	3.4	4.37	32.33	9.08
2001	192.48	24.19	13.58	48.81	2.45	5.28	44.14	19.21
2002	125.10	17.69	8.64	46.91	2.34	6.83	126	3.89
2003	154.87	21.29	11.82	39.88	2.46	2.09	106.77	27.36
2004	124.71	29.19	26.04	43.19	3.03	1.74	117.91	10.99
2005	192.43	35.29	25.15	42.86	3.04	9.16	141.04	19.63
2006	255.70	17.87	11.72	42.93	2.13	9.22	99.03	7.46
2007	198.68	17.99	22.41	42.22	2.06	8.55	110.01	8.47
2008	152.50	18.08	19.89	42.8	1.92	8.81	106.81	8.39
2009	164.15	18.22	19.54	42.7	2.02	8.83	106.81	8.02
2010	269.54	18.34	19.31	42.66	2.12	8.1	104.6	8.76
2011	179.11	18.20						
2012	186.24	18.27						
2013	198.68	18.06						

Table A.4.2: AM flood (m^3/s) for the stations in Upper Awash catchment.

Year	Annual maximum Discharge(m3/s)							
	Awash @ melka kuntire	Akaki	Mojo @ mojo village	Awash below koka dam	Berga Nr. Addis Alem	Holota Nr. Holota	Bello Nr. Guder	TEJI Nr. ASGORY
1960							55.21	
1961							76.67	
1962							47.23	
1963							35.26	
1964							37.29	
1965							34.27	
1966	318.61						83.12	
1967	220.71						60.37	
1968	161.83		68.95				42.35	
1969	314.86		169.23				33.94	
1970	381.87		83.84	134.50			58.45	
1971	309.27		169.23	332.14			33.94	
1972	154.01		62.64	116.17			31.42	
1973	225.40		104.13	85.35			37.99	
1974	314.86		83.07	118.44			44.27	
1975	300.08		119.84	135.12	54.67	27.36	50.38	78.59
1976	278.60		115.38	75.52	84.42	29.33	32.04	74.89
1977	333.87		101.60	177.16	38.03	26.02	43.11	66.14
1978	222.27		78.49	83.51	36.54	31.50	22.39	90.82
1979	203.98		68.95	95.96	36.75	23.83	29.92	93.16
1980	269.90		83.07	91.04	55.92	26.33	38.81	74.27
1981	175.31	201.31	97.03	133.88	90.47	32.45	38.69	112.72
1982	312.55	172.77	99.19	44.64	69.21	32.59	32.67	63.09
1983	378.76	138.72	502.90	284.10	47.71	22.75	55.21	114.12
1984	254.60	189.38	357.27	91.04	31.28	20.97	30.81	66.14
1985	226.97	165.65	372.10	228.38	33.93	21.16	36.60	111.31
1986	192.24	68.78	228.44	71.30	31.40	16.38	37.19	24.85
1987	198.06	36.55	201.20	80.79	21.00	31.39	43.88	38.66
1988	365.49	148.35	256.81	113.92	115.17	31.50	36.60	110.27
1989	169.85	233.77	209.80	200.15	28.87	31.50	27.05	82.28
1990	169.85	277.22	246.36	127.80	46.76	41.02	44.66	77.76
1991	225.40	215.22	344.10	230.12	20.29	35.65	30.81	94.17
1992	186.50	153.07	274.10	85.35	32.08	27.74	28.75	86.22
1993	307.42	573.57	289.03	354.53	48.48	39.63	34.75	95.17
1994	180.86	162.58	274.10	68.84	26.92	28.94	34.60	73.34
1995	167.16	257.98	215.93	353.28	47.22	29.64	33.30	66.81
1996	398.63	615.76	511.19	718.01	113.04	41.03	70.51	101.97
1997	163.15	276.32	206.09	95.96	39.86	14.33	33.65	52.97
1998	347.52	421.52	396.26	290.10	64.27	29.74	59.46	102.99
1999	289.23	693.10	360.22	327.78	70.42	37.26	37.87	110.27
2000	164.06	255.78	219.66	157.28	28.63	27.02	37.47	49.22
2001	258.12	435.34	203.32	104.17	49.15	34.91	39.66	39.74
2002	264.30	219.87	192.96	90.07	48.36	28.31	32.37	31.57
2003	264.30	420.06	234.17	123.06	44.12	23.39	35.25	69.86
2004	230.38	250.47	182.93	62.55	33.17	12.26	34.60	34.94
2005	309.96	282.54	177.07	69.65	35.72	16.08	43.27	92.99
2006	362.34		156.59	312.78	40.81	29.83	54.66	172.17
2007	430.40		132.75	359.12	62.14	28.40	43.64	154.58
2008	435.91		476.64	475.24	63.67	28.27	41.24	76.92
2009	577.36		197.06	54.81	81.13	26.36	43.94	100.61
2010	283.36		232.85	363.75	67.34		37.79	88.95
2011	403.42		207.56	262.77	33.65		27.94	103.45
2012	623.97		171.33	392.30	81.39		35.58	112.93
2013			245.84	161.42			33.73	

A.5 Estimated ETo for parts of Awash and Omo-Ghibe basins by Silesh's regression equation

Table A.5.1: Estimated monthly ETo over parts of Omo-Ghibe Basin (mm/day).

S N	Station	Altitude (m)	Jan	Feb	Mar	Apr	May	Jun	Jul	Aug	Sep	Oct	Nov	Dec
1	Abalti	1938	5.249	3.783	3.795	3.677	3.202	2.765	2.449	2.321	2.758	3.19	3.27	3.344
2	Assendabo	1764	5.266	3.922	3.952	3.798	3.324	2.886	2.553	2.408	2.862	3.277	3.375	3.448
3	Busa	1993	5.243	3.739	3.746	3.638	3.163	2.726	2.416	2.294	2.725	3.162	3.237	3.311
4	Cheka	1934	5.249	3.786	3.799	3.679	3.205	2.767	2.451	2.323	2.76	3.192	3.273	3.346
5	Dimtu	1780	5.264	3.909	3.937	3.787	3.312	2.875	2.544	2.4	2.853	3.269	3.365	3.439
6	Jimma	1718	5.271	3.959	3.993	3.831	3.356	2.919	2.581	2.431	2.89	3.3	3.402	3.476
7	Kumbi	1930	5.249	3.789	3.802	3.682	3.207	2.77	2.454	2.325	2.763	3.194	3.275	3.349
8	Limu Genet	1766	5.266	3.921	3.95	3.797	3.322	2.885	2.552	2.407	2.861	3.276	3.374	3.447
9	Sokoru	1928	5.25	3.791	3.804	3.684	3.209	2.772	2.455	2.326	2.764	3.195	3.276	3.35
10	Wolkite	2000	5.242	3.733	3.739	3.633	3.158	2.721	2.412	2.29	2.721	3.159	3.233	3.307
11	Chida	1659	5.277	4.006	4.046	3.872	3.397	2.96	2.616	2.461	2.925	3.329	3.438	3.511
12	Meteso	2283	5.214	3.507	3.485	3.435	2.96	2.523	2.242	2.149	2.551	3.017	3.063	3.137
13	Hosana	2307	5.212	3.488	3.463	3.418	2.944	2.506	2.227	2.137	2.536	3.005	3.049	3.123

Table A.5.2: Estimated monthly ETo over parts of Awash Basin (mm/day).

S N	Station	Altitude (m)	Jan	Feb	Mar	Apr	May	Jun	Jul	Aug	Sep	Oct	Nov	Dec
1	Abomsa	1630	3.855	4.355	4.618	4.419	4.227	4.358	3.572	3.605	3.785	3.727	3.997	4.01
2	Arba bordede	990	4.239	4.675	5.002	4.931	4.875	5.83	4.852	4.501	4.553	4.256	4.357	4.33
3	Awash Melka	916	4.283	4.712	5.046	4.99	4.985	6	5	4.605	4.642	4.345	4.415	4.367
4	Bofa	1520	3.921	4.41	4.684	4.507	4.313	4.611	3.792	3.759	3.917	3.797	4.045	4.065
5	Hombole	916	4.283	4.712	5.046	4.99	4.985	6	5	4.605	4.642	4.345	4.415	4.367
6	Melka sadi	749	4.383	4.796	5.147	5.124	5.28	6.384	5.334	4.839	4.842	4.584	4.572	4.451
7	Nuraera(SF)	1140	4.149	4.6	4.912	4.811	4.682	5.485	4.552	4.291	4.373	4.099	4.252	4.255
8	Shola Gebeya	2500	3.333	3.92	4.096	3.723	3.74	2.357	1.832	2.387	2.741	3.326	3.712	3.575
9	Sodore	1351	4.022	4.495	4.785	4.642	4.46	4.999	4.13	3.996	4.12	3.918	4.129	4.15
10	Arerit	1800	3.753	4.27	4.516	4.283	4.109	3.967	3.232	3.367	3.581	3.63	3.929	3.925
11	Mojo	1763	3.775	4.289	4.538	4.313	4.133	4.052	3.306	3.419	3.625	3.65	3.943	3.944
12	Nazeret	1622	3.86	4.359	4.623	4.426	4.233	4.376	3.588	3.616	3.795	3.732	4	4.014
13	Awash 40	1097	4.175	4.622	4.938	4.846	4.734	5.584	4.638	4.351	4.425	4.142	4.28	4.277
14	Gewane	568	4.492	4.886	5.255	5.269	5.715	6.8	5.696	5.092	5.059	4.935	4.796	4.541

A.6 Regression equations for estimation of monthly ETo over the Awash & Omo- Ghibe Basins

Where: X is altitude in meters and Y is ETo in mm

	Equation	R^2	t -value	
			Coeff.	Cons.
January	Y = - 0.0006 X + 4.8328	0.71	28.06	-5.48
February	Y = - 0.0005 X + 5.1702	0.70	33.79	-5.75
March	Y = - 0.0006 X + 5.5959	0.72	33.81	-6.46
April	Y = - 0.0008 X + 5.7231	0.76	32.08	-7.58
May	$Y = 35.054\ X^{-0.286}$	0.73	23.09	-6.20
June	Y = - 0.0023 X + 8.1067	0.72	13.95	-7.01
July	Y = - 0.002 X + 6.8319	0.75	16.46	-7.90
August	Y = - 0.0014 X + 5.8871	0.84	23.77	-10.14
September	Y = - 0.0012 X + 5.7409	0.80	23.29	-8.85
October	Y = 28.698 X - 0.2662	0.76	22.62	-5.65
November	Y = 14.348 X - 0.1728	0.75	30.86	-5.42
December	Y = - 0.0005 X + 4.8254	0.70	28.05	-5.53

Figure A.6.1: Monthly ETo and altitude relationships in Awash and Rift Valley Basins.

	Equation	***R^2***	***t - value***	
			Coeff.	***Cons.***
January	Y = - 0.0010 X + 5.4424	0.88	19.24	-4.78
February	Y = - 0.0008 X + 5.3333	0.71	20.94	-5.70
March	Y = - 0.0009 X + 5.5393	0.73	21.40	-6.32
April	Y = - 0.0007 X + 5.0331	0.69	21.65	-5.53
May	Y = - 0.0007 X + 4.5584	0.65	17.39	-4.93
June	Y = - 0.0007 X + 4.1211	0.52	12.45	-3.73
July	Y = - 0.0006 X + 3.6115	0.62	14.53	-4.79
August	Y = - 0.0005 X + 3.2901	0.56	15.18	-4.21
September	Y = - 0.0006 X + 3.9205	0.58	14.78	-4.03
October	Y = - 0.0005 X + 4.1586	0.56	19.96	-4.67
November	Y = - 0.0006 X + 4.4332	0.58	18.92	-4.38
December	Y = - 0.0006 X + 4.5068	0.62	18.71	-4.78

Figure A.6.2: Monthly ETo and altitude relationships in Omo Ghibe Basin.

A.7 Python codes for determination of the Box-Cox Parameters λ & γ in TSPT Technique

```
import pandas as pd
import scipy.stats.stats as st
import numpy as np
x =np.loadtxt('Ghibe@Asendabo.txt')            # 'Ghibe@Asendabo.txt' text file to be analyzed.
L= np.log10(x)
N = len(x)
TOL=0.001
AL=1.0
BL=1.0

print" The series is made normal with the following results"
print" Table of flood frequency analysis by TSPT method"
print"================================================================================="
print("Original data==Log transformed Data====Power transformed data====TSPT Data")
print"================================================================================="

def goto(linenum):
   global line
   line = linenum
line = 1
while True:
   if line == 1:
      if((abs(st.skew(x))<=TOL) and abs((st.kurtosis(x)-3)<=Tol)):goto(177)
      else:
          goto(100)

   if line == 100:
      Z=1
      YY=np.power(x, AL)
      Y=(YY-1)/AL
      A=sum([Y[i] for i in range(N)])
      Ybar=A/N
      if((Z<1) or (AL==0)):goto(203)
      elif((abs(st.skew(Y))<=TOL) and abs(st.kurtosis(Y)-3)<=TOL):goto(177)
      elif (st.skew(Y)<0):
         AL=AL+TOL
         goto(100)
         if(abs(st.skew(Y))<=TOL) or Z>1000000:goto(101)
      elif (st.skew(Y)>0):
         AL=AL-TOL
         goto(100)
         if((st.skew(Y))<=TOL) or Z>1000000:goto(101)

      Z=Z+1
   elif line == 203:
```

(Continued)

```
      if((abs(st.skew(L))<=TOL) and abs(st.kurtosis(L)-3)<=TOL):goto(177)
      else:
        goto(100)
   elif line == 101:

      TT=np.abs(Y-Ybar)**BL

      if(Y[i]<Ybar):
         T=-1*TT
      else:
         T=1*TT
      if (abs(st.kurtosis(T)-3)<=TOL) :goto(177)
      elif(st.kurtosis(T)-3)<0:
         BL=BL+TOL
         goto(101)
      elif(st.kurtosis(T)-3)>0:
         BL=BL-TOL
         goto(101)

   elif line == 177:
      break

for i in range (N):
   if(Y[i]<Ybar):
         T=-1*TT
   else:
         T=1*TT
   print "%10.3f" % x[i],"%20.5f" % L[i],"%20.5f" % Y[i], T[i]
print("_____________________________________________________________________________")
print "      Summary of the results: Number of sample size,   N =","%4.0f" % N
print("=============================================================================")
print "  1.   Original data:     Skew=","%8.4f" % st.skew(x),",   Kurt=","%8.4f" % st.kurtosis(x)
print("_____________________________________________________________________________")
print "  2.   Log.  Transformed data:   Skew=","%8.4f" % st.skew(L),", Kurt=","%8.4f" % st.kurtosis(L)
print("_____________________________________________________________________________")
print "  3.   First Step Power Transformed data:   Skew=","%8.4f" % st.skew(Y),", Kurt=","%8.4f" % st.kurtosis(Y)
print("_____________________________________________________________________________")
print "  4.   Two-Step-Power-Trasformed data :      Kurt=","%8.4f" % st.kurtosis(T)
print("_____________________________________________________________________________")
print("  5.   In general, the values of the Box-Cox normalizing parameters are:")
print "      Box-Cox lambda,λ =","%6.3f" % AL,",            Box-Cox gamma=","%6.3f" % BL
print("_____________________________________________________________________________")
print( "======== ====================THE END!!=================================")
```

A.8 Python codes (main) for running PyTOPKAPI Model

PyTOPKAPI simulating code

After giving the path for the file as indicated below; the scripts are used to run the model. For example, suppose that the path is "cd C:\Users\ASH\pyTOPKAPI_workshop\example_simulation". Then, we have to use the codes as below:

```
cd C:\Users\ASH\pyTOPKAPI_workshop\example_simulation
import pytopkapi
import matplotlib.pyplot as plt
pytopkapi.run('model-simulation.ini')
```

The model will start running (simulating) if all the input files are properly introduced to it.

Then;

```
import h5py
h5file=h5py.File('results/Example_simulation_results.h5')
channel_flows=h5file['Channel/Qc_out'][...]
plt.plot(channel_flows[:,0])
plt.title('stream flow at outlet',fontweight='bold')
plt.ylabel('Flow ($\mathbf{m^3/s}$)')
plt.xlabel('Model time-steps (6hours)')
plt.show()
```

Then;

```
h5file.close()
```

Finally;

```
from pytopkapi.results_analysis import plot_Qsim_Qobs_Rain
plot_Qsim_Qobs_Rain.run('plot-flow-precip.ini')
plt.show()
```

1. Forcing files creating python scripts (rainfields and ET)

   (a) rainfields

```
import h5py
import numpy as np
x=np.loadtxt('rain.txt')
y=np.empty((365,3564))      # 365 is number of days (time) and 3564 is number of
#pixels(grids); they are changeable.
for i in range(3564):
y[:,i]=x
h=h5py.File('rainfields.h5','w')
grp=h.create_group('sample_event')
dset=grp.create_dataset('rainfall',(365,3564),chunks=True,compression="gzip",compressi
on_opts=9,data=y)
h.close()
```

(Continued)

(a) ET

```
import h5py
import numpy as np
x=np.loadtxt('ETo.txt')
y=np.empty((365,3564))      # 365 is number of days (time) and 3564 is number of pixels(grids); they are changeable.
for i in range(3564):
y[:,i]=x
h=h5py.File('ET.h5','w')
grp=h.create_group('sample_event')
dset=grp.create_dataset('ETo',(365,3564),chunks=True,compression="gzip",compressio
n_opts=9,data=y)
h.close()
```

Cell parameter files creation

After giving the path again; the scripts shown below can create the cell parameters. For example, suppose that the path is “cd C:\Users\ASH\pyTOPKAPI_workshop\example_simulation”. Then, we have to use the codes as follows:

```
cd  C:\Users\ASH\pyTOPKAPI_workshop\example_simulation
import pytopkapi
from pytopkapi.parameter_utils import create_file
create_file.run ('create_the_parameter_files/create_file.ini')
```